

**SPICE Circuit Models**  
**for**  
**Semiconductor Lasers**

**A Thesis**

**Presented to the Faculty of**  
**Computer Sciences and Engineering Graduate School of**  
**De Montfort University**  
**in Partial Fulfilment of the Requirements for the Degree of**  
**Doctor of Philosophy**

**by**

**Dr. Jenkins C. H. CHEN**

**陳智雄 博士**

**4. 4. 00**

© 2000 De Montfort University  
All Rights Reserved

# **SPICE Circuit Models for Semiconductor Lasers**

**Dr. Jenkins C. H. CHEN**  
**De Montfort University 2000**

## **Abstract**

The aim of this thesis is to develop a SPICE circuit model for semiconductor lasers, which simultaneously incorporates the effects of the carrier and lattice heating. The objective of this thesis is to perform numerical simulations for the dc, ac and transient responses of this circuit model. The circuit model is transformed from the rate equations that govern the dynamics of carrier density, photon density, electron temperature, hole temperature and lattice temperature in the active region of semiconductor lasers. SPICE codes are exactly developed according to this circuit model. The results from this work should not only demonstrate the capacity and versatility of the SPICE circuits in simulating the complicated carrier and lattice heating processes for semiconductor lasers but eventually lead to the simulations of optoelectronic systems comprising electronic circuits and devices, all by SPICE circuit models.

## BIOGRAPHICAL SKETCH

Dr. Jenkins Chih-Hsiung CHEN (陳智雄, 字 再傳, 以字行) was born on February 14, 1967, in Tainan city, Taiwan (台灣·台南市). He was brought up in An-Ping (安平), a fishing village in Tainan city, where he enjoyed his carefree childhood. He graduated from the Tainan First High School in 1985 (台南一中) and worked for 6 more years before his college education. He graduated from the Department of Information Engineering at Feng-Chia University, in Tai-Chung city (台中市·私立逢甲大學·資訊工程學系), in June 1995. He ranked the first among 157 students in his department and was awarded an honorary member of the Phi Tau Phi Scholastic Honour Society of the Republic of China (中華民國·斐陶斐學會·榮譽會員) in June 1995. Beside his academic achievement, he was very active in extracurricular activities. He was twice elected as a leader of his class (副班代, 班代) and the representative of his department (資訊工程學系·系學會·總幹事). He also had a part-time job running an art magazine and a communication studio (新翰藝訊·雜誌社·社長) (新翰藝術·傳播中心·負責人).

After his graduation, he was offered a studentship in the Information Group of the Department of Applied Mathematics at National Chung-Hsing University in September 1995 (國立中興大學·應用數學系·研究所·資訊組). He only managed to complete the first semester of this master degree before he decided to come to England for his Ph.D. study.

From September 1996, he started his Ph.D. studies in the Department of Electronic and Electrical Engineering, which expanded into the Department of Computer Sciences and Engineering, at De Montfort University, in Leicester, in United Kingdom. He has worked on the SPICE (Simulation Program with Integrated Circuit Emphasis) circuit models for semiconductor lasers under the supervision of Dr. Chin-Yi Tsai.

During the period of his Ph.D., he has been twice elected as the president of Taiwanese Student Society at De Montfort University (1997~1999 年·蝶·夢·風·大學·台灣同學會·會長). Acknowledging his achievement, the Taipei Office in United Kingdom (駐英·台北辦事處) in the June of 1999 has awarded him a certificate of appreciation (感謝狀) for serving the Taiwanese students at De Montfort University.

**This thesis is dedicated to my family,  
the ones who loved and supported me,  
especially to my elder sister Ms. S. H. Chen (陳淑惠)  
and my mother Ms. Y. E. Wang (王月娥)**

## ACKNOWLEDGEMENTS

First of all, I would like to extend my sincere thanks go to my first supervisor, Dr. Chin-Yi Tsai (蔡進譯), for this guidance throughout the course of my Ph.D., particularly in the development of my SPICE circuit models for semiconductor lasers. I am very much in debt for his guidance and help in leading me to understand the field of optoelectronics and his patience in debugging my SPICE codes; this was not an easy task for him. Not only have I benefited from his academic expertise but I am also influenced by his view of history, economics, politics and all the common sense about life. It seems to me that 'thank you' will be never an adequate word to express my appreciation to him.

Secondly, I would like to take this opportunity to thank Professor Malcolm McCormick, who was the Head of Department of Electronic and Electrical Engineering, and now is the Head of Department of Computing Sciences and Engineering and the Head of Graduate School, for serving as my second supervisor. He was very helpful in providing all the necessary facilities for my research work. I am particularly grateful for his authorisation in connecting the computer on my desk to the network. This turned out to be very crucial. Without spending thousands of pounds on the SPICE software, I managed to find the free *MicroSim* PSPICE program on the Internet. Ever since, my work on writing the SPICE codes for my project became feasible. I also wish to thank his secretary, Ms. Sheila Hayto for patiently helping me deal with all the paperwork. I would also like to thank Dr. Richard McMahon from Cambridge University (劍橋大學

) for his serving as an external examiner and his recommendation for this thesis. Moreover, I would also like to thank Dr. Eric Chowanietz serving as my internal examiner and helping with the final minor amendments and corrections.

In addition, I wish to thank other members of Dr. Tsai's research group, Mr. Jason Wu (吳祖因), Ms. Theresa Shih (石芳平) and Mr. Vincent Sung (宋天立) for sharing their knowledge and experiences on their dissertations.

Although they may not directly help my thesis academically, I still wish to thank the friends that I have made in De Montfort: Mr. John Ho (何慶紋·1998~1999年·中華民國旅英同學總會·會長), Mr. Holger Kraus (高學勤·ISA committee at DMU) and Ms. Enya Kuo (郭佳方), Dr. Jeen G. Khor (許仁義) and Dr. Mei-Wei Kweh, M.D. (郭美薇), Mr. Nee-Joo Teh (鄭義儒), Mr. C. K. Tan (陳俊強) and Ms. Jacquie T. C. Chan (陳亭蓁), Mr. Seng-Kwong Chong (鍾成光) and Ms. Kim E. Beh (馬金燕), Ms. Sheanne Lim (林施雁), Ms. Agnes Poon (潘頌恩) and Mr. Michael Zeng (曾偉琴), Ms. Canne Cheng (鄭金梅·DMU Chinese Society·Vice president), Mr. Sammy Chan (陳劍偉), Ms. Judy Tin (田遠君), Ms. Joey Lo (羅祖兒), Mr. Andy Huang (黃議賢), Ms. Annie Zhai (翟瑰芳), Mr. Leislle Chen (陳建勳), Mr. Koko Huang (黃國鑫), Mr. Tony Chen (陳忠哲), Ms. Rae Ngai (魏瑞瑞) and Mr. Rex Shen (沈哲希), Ms. J. L. Wu (吳佳玲), Ms. Rose Chiu (邱薇臻), Ms. Fei-Yu Chuang (莊斐瑜), Ms. Inès Liu (劉秀英), Ms. Connie Poon (潘潔茹) and Mr. Jamie Chen (陳聰明),



Mr. Young Lee (李柏翰) and Ms. Tina Chen (陳憶婷), Ms. Stacey Chiang (江文代), Mr. David Lee (李明達) and Ms. Erin Tu (涂雅齡), Mr. Tse-Ting Chen (陳澤庭) and Ms. Annie Liu (劉淑儀), Ms. Amber Chong (鍾宜靜), Ms. Jade Chan (詹玉禪), Ms. Fiona Fu (傅于芹), Ms. Ayse Oztayla, Ms. Barbara Liu (劉令環), Ms. Lillian Liao (廖纈璜), Ms. Erica Li (李玉珠), Ms. Camay Pan (潘佳美), Ms. Beatrice Liao (廖悅淳), Ms. Feng-Ju Chen (陳豐如), Ms. Audrea Huang (黃靖媚), Mr. Eric Huang (黃慶臺) and Ms. Gianna Lin (林粲菁), Mr. Dennis Su (蘇威年), Ms. Xiao-Wei Yang (楊小薇), Ms. Angela Lee, Ms. Xiao-Ying Tseng (曾小英), Ms. B. Y. Chang (張寶月) and Tina Liu (劉大敏). With their wonderful companionships, my Ph.D. study became even more enjoyable. As the good old saying goes: A friend in need is a friend indeed.

I would like to thank Mr. Q. C. Chen (陳清泉), Mr. C. J. Xu (許聰吉), Mr. Y. L. Lee (李義龍), Mr. Z. H. Lee (李志鴻), Mr. A. Q. Wu (吳安慶), Mr. A. C. Wu (吳安忠) and Ms. H. C. Wang (王惠娟), Mr. J. Z. Ou (歐駿志), Mr. J. X. Chen (陳建興), Mr. R. B. Hong (洪瑞斌), Mr. S. W. Chen (陳勝文), Mr. S. B. Lin (林世彬), Mr. W. L. Xie (謝汶利), Mr. Y. H. Ou (歐陽輝), Mr. S. H. Wu (吳昇皇), Mr. Z. D. Xie (謝正達), Dr. R. B. Chung, M.D. (莊榮彬), Dr. G. H. Huang, M.D. (黃冠華), Dr. S. Y. Feng, M.D. (馮聖堯), Dr. B. Q. Lin, M.D. (林柏青), Dr. H. S. Wang, M.D. (王宏碩), Dr. W. C. Wang, M.D. (王文哲), Mr. S. C. Huang (黃尚質) and Ms. Y. C. Liu (劉玉春), Mr. P. R. Wang (王培戎), Mr. B. W. Liao (廖百偉), Mr. J. Y. Wang (王金源), Mr. Y. Y. Lee (李玉印), Mr. S. B. Huang (黃順彬), Mr. Z. W. Liao (廖志文), Mr. Q. L. Kuo (郭祈良), Mr. R. Y. Xu (許

瑞益), Mr. C. L. Chang (張振倫), Mr. B. H. Chang (張伯宏), Mr. W. S. Huang (黃文昇), Mr. Y. K. Lee (李裕堃), Mr. T. P. Weng (翁宗平), Mr. M. H. Ji (紀孟宏), Mr. R. J. Huang (黃仁傑), Mr. J. H. Gao (高健雄), Mr. Z. C. Chen (陳志成), Mr. S. C. Lai (賴世昌), Mr. Z. C. Lai (賴俊呈) and Ms. F. M. Su (蘇芳妙), Ms. Q. Q. Yeh (葉青青), Ms. Y. F. Tsai (蔡怡芳), Ms. X. Q. Wang (王萱萩), Mr. S. Y. Chang (張世穎), Mr. Z. Z. Yu (于正之), Ms. M. X. Ho (何旻勳), Mr. Z. D. Wu (吳政德), Ms. Y. W. Chang (張憶文), and Mr. Z. B. Yang (楊志斌). I would like to thank three tutors, Ms. Y. Y. Xie (謝玉英), Ms. D. M. Liu (劉端妹) and Ms. K. C. Qi (齊克勤), of Xi-Men primary school (安平·西門國小). I wish to thank two tutors, Mr. W. H. Ho (何文雄) and Mr. J. H. Chen (陳俊雄), of An-Ping Junior High School (安平·安平國中). I want to thank my tutor, Mr. S. C. Wang (王淑成), of Xin-Hua Senior High School (台南縣·新化高中). I also like to thank two tutors, Mr. X. H. Cheng (鄭新雄) and Mr. D. F. Tsai (蔡丁福), of Tainan First Senior High School (台南一中). I thank the Associated Professor Y. P. Chu (朱延平) and friends of the graduate school of Applied Mathematics of National Chung-Hsing University. I also like to thank lecturers Mr. C. B. Lin (林財寶), Ms. Teresa Zhao (趙淑倬) and Ms. P. L. Lee (李寶玲), Associated Professors H. Y. Xu (徐弘洋) and G. G. Lin (林國貴), Professor A. C. Liu (劉安之·the Principal of Feng-Chia University) and all the classmates of the Department of Information Engineering of Feng-Chia University for their enduring friendship in all the past years.

I feel very sad without the last chance to thank Mr. Q. H. Lin in person (林清和, 字 建忠, 以字行). He died in the July of 1999 when I

was busy with my thesis; I am very sorry for not saying my last goodbye to him in person. He had acted as a saviour for me when I had a personal health problem. In addition, he taught me numerous wisdoms that I never learnt in the school. How sad that I cannot say this to him in person! I also want to thank his son, Mr. J. F. Lin (林錦富), for his kindness of helping with the paper work.

I wish to thank Mr. J. Z. Wang (王金忠), Mr. Z. H. Chen (陳住和), Mr. D. M. Chang (張丁謀), Mr. F. C. Chang (張福成), Mr. D. J. Yun (雲大家), Mr. D. K. Lee (李德綱) and Ms. S. H. Chen (陳淑惠), for they had been very helpful when I was doing business with them. I would also like to thank my uncle, Mr. Z. H. Wang (王正雄), and Mr. R. R. Zeng (曾仁榮) for helping me in my studies when I was at Tainan First High School. I also like to thank my cousin and my cousin-in-law, Ms. L. L. Tung (董莉莉) and Mr. Y. B. Lee (李義寶), for helping me whenever I had a technical difficulty when dealing with my own computer. I also wish to thank my cousin and cousin-in-law, Ms. B. R. Chong (鍾璧如) and Mr. X. N. Lu (魯信南), for their concern for my personal health in all these years. I want to thank my cousins, Mr. M. C. Chen (陳敏誠) and Mr. M. X. Chen (陳敏祥), for their warm caring and concern about my elder sister and the air delivery of parcels from Taiwan.

I also want to take this opportunity to express my gratitude to those who have helped me in all the past years. Without their help, I cannot accomplish my education in Taiwan, not to mention coming to UK and achieving my Ph.D. degree. I wish to thank my uncle, Dr. W. L. Chen,

M.D. (陳文龍), who has helped my family through our financial difficulties. He was the patron of my university education. I appreciate his generosity in financially helping all the young members of our family. I would like to thank Mr. R. T. Tsai (蔡瑞添) and Ms. W. Wu (吳薇), Mr. S. Y. Chen (陳山永) and Ms. Y. Wei (魏英) who treat me as their own child. I am very impressed by their willingness to give me a helping hand when I was in difficulty.

Finally, I would like to thank all the members in my family. Without their help, my Ph.D. study in UK would have been almost impossible. I would like to thank my brother, Mr. Z. K. Chen (陳志剛), for he was one of my childhood playmates. I would like to thank my second sister and my brother-in-law, Ms. H. Z. Chen (陳惠珠) and Mr. Q. L. Chang (張清良). I must say t how much I have enjoyed working with my brother-in-law in my extracurricular activities, such as running a magazine, promoting arts and hosting press conferences. I do not know how to express my gratitude for my second sister. She looked after me just like my mother when I was in Tai-Chung during my college education. I also like to thank my elder sister, Ms. S. H. Chen (陳淑惠), for all her everlasting efforts in taking care of my grandmother for all these years. Actually, she has given me a perfect example of what a decent and respectable person should be. Personally, I very much admire her working spirit, her filial piety and her strong personality. I thank my father and mother, Mr. S. Z. Chen (陳水柱) and Ms. Y. E. Wang (王月娥), for their endless endeavours in raising a family of four children.

Last but not least, I would like to dedicate my thesis and all my work in UK to my dearest mother. She was, is and will always be the most important person in my life, shaping how I was, how I am and how I will be. She has worked very hard all her life by herself in supporting our family without any help from others. Sometimes, I just wonder how anyone in this world can take her hardship without any tear, anger or complaint. To me, she has always been a very wonderful audience and a fantastic counsellor, and she has given me innumerable advice and words of wisdom. If I ever become an honest person, I will thank the discipline that she has taught me. If I ever become a patient person, I will thank the personal paragon that she has set for me. If I ever achieve anything in my life, I will thank all the sacrifices that she has made for me. If I ever know the meaning of love, I will thank all the love that she has given to me. I love you, mom!

# TABLE OF CONTENTS

<b>CHAPTER 1</b>	<b>INTRODUCTION.....</b>	<b>1</b>
1.1	Background.....	1
1.2	Semiconductor Lasers.....	4
1.3	Existing Models for Semiconductor Lasers.....	6
1.4	Literature Review – SPICE Circuit Models for Semiconductor Lasers.....	11
1.5	Heating Models for Semiconductor Lasers.....	13
1.6	The Weaknesses in Previous Circuit Models and the Carrier Heating in SPICE Circuit Models for Semiconductor Lasers.....	15
1.7	Methodologies for Incorporating the Carrier Heating into the SPICE Circuit Model.....	18
1.8	SPICE Circuit Models.....	20
1.9	The Aim and Objectives of the Thesis.....	21

<b>CHAPTER 2</b>	<b>RATE EQUATIONS FOR SEMICONDUCTOR LASERS.....</b>	<b>26</b>
2.1	Rate Equations.....	26
2.2	Parameters for Carrier Processes.....	38
2.3	Parameters for Photon Processes.....	55
2.4	Parameters for Carrier Heating Processes.....	65
2.5	Parameters for Lattice Heating Processes.....	75
<b>CHAPTER 3</b>	<b>TRANSFORMING THE RATE EQUATIONS INTO THE SPICE CIRCUIT MODEL.....</b>	<b>77</b>
3.1	The Derivations of Circuit Models from Rate Equations.....	77
3.2	The Representations of Circuit Models by SPICE Codes.....	93
<b>CHAPTER 4</b>	<b>SPICE SIMULATION RESULTS AND DISCUSSIONS.....</b>	<b>97</b>
4.1	Introduction.....	97
4.2	SPICE Circuit Model without Carrier and Lattice Heating.....	100

4.3	SPICE Circuit Model with Lattice Heating .....	104
4.4	SPICE Circuit Model with Carrier and Lattice Heating.....	118
<b>CHAPTER 5 CONCLUSION AND SUGGESTIONS FOR FUTURE WORK.....</b>		<b>135</b>
5.1	Summary of Previous Work and this Thesis.....	135
5.2	The Achievements of the Thesis.....	138
5.3	Suggestions for Future Work.....	141
<b>REFERENCES.....</b>		<b>146</b>
<b>APPENDIX A: GETTING START WITH PSPICE.....</b>		<b>151</b>
A.1	Downloading the PSPICE.....	151
A.2	Installing the PSPICE.....	151
A.3	Running a PSPICE program.....	152
<b>APPENDIX B: SUMMARY OF THE PSPICE SYNTAXES.....</b>		<b>153</b>
<b>APPENDIX C: SPICE CODES OF THIS THESIS.....</b>		<b>158</b>



C.1	SPICE Circuit Model without Carrier and Lattice Heating.....	158
C.2	SPICE Circuit Model with Lattice Heating but without Carrier Heating.....	160
C.3	SPICE Circuit Model with Lattice Heating but without Carrier Heating but with the addition of the Temperature-Sensitive Leakage Current and Auger process.....	164
C.4	SPICE Circuit Model with Carrier and Lattice Heating.....	169
<b>APPENDIX D: PARAMETERS FOR THE SPICE MODELS.....</b>		<b>175</b>
<b>LIST OF PUBLICATIONS.....</b>		<b>178</b>

## LIST OF FIGURES

Fig. 1.1	Schematic diagram of a semiconductor laser.....	5
Fig. 1.2	Comparisons of the complexity among three numerical methods, the Monte Carlo analysis, partial differential equation or balance equation, and ordinary differential equation or rate equation.....	9
Fig. 1.3	Schematic diagram of energy transfer in semiconductor lasers.....	14
Fig. 1.4	Schematic diagram of downloading, installing, creating, compiling, probing and plotting relating to a PSPICE program.....	22
Fig. 2.1	Rate equations for semiconductor lasers.....	27
Fig. 2.2	Rate equation for the change rate of the carrier density.....	29
Fig. 2.3	Rate equation for the change rate of the photon density.....	30
Fig. 2.4	Rate equation for the change rate of the electron temperature.....	31
Fig. 2.5	Rate equation for the change rate of the hole temperature.....	32
Fig. 2.6	Rate equation for the change rate of the lattice temperature in the active region.....	33
Fig. 2.7	Schematic diagram of the carrier distributed at (a) low carrier density and (b) high carrier density.....	39
Fig. 2.8	Schematic diagram of the injection current.....	43
Fig. 2.9	Schematic diagram of the leakage currents (lateral and transverse directions).....	44
Fig. 2.10	Schematic diagram illustrating the volume of the active region.....	47

Fig. 2.11	(a) SRH (interband) (b) intraband carrier energy relaxation via emitting phonons.....	50
Fig. 2.12	Schematic diagram of spontaneous emission.....	52
Fig. 2.13	Schematic diagram of Auger recombinations.....	54
Fig. 2.14	Schematic diagram of stimulated emission.....	57
Fig. 2.15	Schematic diagram of spectral hole burning.....	59
Fig. 2.16	Schematic diagram of the optical confinement factor.....	62
Fig. 2.17	Schematic diagram of free-carrier-absorption.....	64
Fig. 2.18	Schematic diagram of the coupling coefficient for spontaneous emission.....	66
Fig. 2.19	Schematic diagram of carrier energy relaxation in the injection heating process.....	68
Fig. 3.1	Schematic diagram of transformation from rate equations to circuit models.....	78
Fig. 3.2	The percentage error as a function of the separation of the quasi-Fermi energies between electrons and holes modelled by a $p$ - $n$ diode.....	83
Fig. 3.3	SPICE circuit model with carrier and lattice heating.....	96
Fig. 4.1	SPICE circuit model without carrier and lattice heating.....	101
Fig. 4.2	Transient response of a semiconductor laser with different carrier lifetimes $\tau_n$ (in the unit of second).....	103
Fig. 4.3	AC response of a semiconductor laser with different differential gains $g_n$ (in the unit of $m^2$ ).....	105
Fig. 4.4	AC response of a semiconductor laser with different cavity lengths $L_z$ (in the unit of m).....	106
Fig. 4.5	AC response of a semiconductor laser with different nonlinear gain coefficients $\varepsilon$ (in the unit of $m^3$ ).....	107

Fig. 4.6	SPICE circuit model with lattice heating.....	109
Fig. 4.7	L-I relationship of a semiconductor laser simulated with the effect of the lattice heating but without carrier heating for different thermal conduction times $\tau_{\kappa}$ (in the unit of second).....	110
Fig. 4.8	Lattice temperature as a function of the input current for different thermal conduction times $\tau_{\kappa}$ (in the unit of second).....	111
Fig. 4.9	SPICE circuit model with lattice heating including the temperature-sensitive leakage current and Auger process.....	113
Fig. 4.10	L-I relationship of a semiconductor laser simulated with the temperature-dependent feature of the leakage current and Auger process for different thermal conduction times $\tau_{\kappa}$ (in the unit of second).....	114
Fig. 4.11	L-I relationship of a semiconductor laser simulated with the temperature-dependent feature of the leakage current and the Auger process for different heat-sink temperatures $T_{HS}$ (in the unit of Kelvin).....	116
Fig. 4.12	Comparison of the experimental and simulated L-I relationship for different heat-sink temperatures in a quantum-well laser. (Xu group).....	117
Fig. 4.13	Schematic diagrams of lattice heating under different conditions: (a) no current injection; (b) low current injection; and (c) high current injection.....	119
Fig. 4.14	L-I relationship for different electron-lattice energy relaxation times $\tau_{e-L}$ (in the unit of second).....	124

Fig. 4.15	Electron temperature as a function of the input current for different electron-lattice energy relaxation times $\tau_{e-L}$ (in the unit of second).....	125
Fig. 4.16	Hole temperature as a function of the input current for different electron-lattice energy relaxation times $\tau_{e-L}$ (in the unit of second).....	126
Fig. 4.17	Lattice temperature as a function of the input current for different electron-lattice energy relaxation times $\tau_{e-L}$ (in the unit of second).....	127
Fig. 4.18	Transient response of the output light for different electron-lattice energy relaxation times $\tau_{e-L}$ (in the unit of second).....	128
Fig. 4.19	Transient response of the electron temperature for different electron-lattice energy relaxation times $\tau_{e-L}$ (in the unit of second).....	129
Fig. 4.20	Transient response of the hole temperature for different electron-lattice energy relaxation times $\tau_{e-L}$ (in the unit of second).....	130
Fig. 4.21	Transient response of the electron temperature for different electron-hole energy relaxation times $\tau_{h-L}$ (in the unit of second).....	133
Fig. 4.22	Transient response of the hole temperature for different electron-hole energy relaxation times $\tau_{h-L}$ (in the unit of second).....	134
Fig. 5.1	Schematic diagram of the Ebers-Moll circuit model.....	139
Fig. 5.2	Schematic diagram of the Gummel-Poon circuit model.....	140

# CHAPTER 1

## INTRODUCTION

### 1.1 Background

Traditionally, the physical properties of semiconductor lasers have been satisfactorily explained by rate equations. In fact, the rate equations for carrier density and photon density have become a 'textbook' standard to describe many static and dynamic properties of semiconductor lasers. Such rate-equation approach certainly implies that the spatial distributions of physical quantities can either be neglected or averaged. Taking account of this assumption, it has been proved that such rate equations can characterise many physical properties of semiconductor lasers. However, for some devices such as laser diodes working at high frequencies, the simplified approach may not be applicable or acceptable.

In addition, a laser diode is seldom used as a 'stand-alone' device. It is always used with other electronic devices. Since most of the electronic devices have their own circuit models developed for simulation purposes, it can be anticipated that developing circuit models for semiconductor lasers is desirable. As a result, moving from the rate equation representing of semiconductor lasers to circuit models is becoming a demanding task but has great practical potential.

Developing circuit models for semiconductor lasers certainly has many advantages if they can then be used alongside other circuit models for design purposes. Computer-aided design (CAD) tools are gradually

becoming indispensable for designing electronic processes, devices, circuits and systems, and in achieving the goal of electronic design automation (EDA) [1]. With thousands or even millions of transistors in a single chip, it is almost impossible to design electronic circuits or electronic systems using analytical methods without the help of CAD simulations. In a comparative manner, it is thus predictable that CAD tools for optoelectronic devices and systems will become critically important in the future. Through numerous efforts over more than three decades, CAD tools for electronic processes, devices, circuits and systems have been well developed. Several simulation packages have been commercialised, for example, SUPREM for processes, MEDICI and ATLAS for devices. Some of the simulation languages have become industrial standards, such as SPICE for analogue circuits [2]-[6], and VHDL or Verilog for digital circuits. Despite such success, it is surprising to find that the development of CAD tools for optoelectronic devices or systems is still not fully explored and as yet, no standard associated with them has emerged.

Generally, compared to their electronic counterparts, developing CAD tools for optoelectronic devices and systems is still in its infancy and currently lacks a commonly accepted standard. As a result, the approach to develop any simulation tool is either by establishing a new one or accommodating the well-established ones. For optoelectronic devices, especially optical transmitters, receivers converting electronic and optical signals, used in conjunction with other electronic devices, the latter seems a viable choice. Especially, for semiconductor lasers used in fibre optic communication systems as electronic driving circuits provide their electronic signals. As SPICE circuit simulation is widely used to design the driving circuits of semiconductor lasers, it is logical to develop SPICE

circuit models for these devices. This has the advantage of using established software tools in an integrated systems approach.

Unlike electronic devices that are usually characterised by current and voltage, while optoelectronic devices are normally characterised by light intensity and current. Since light intensity cannot be represented by any physical circuit quantities, modelling optoelectronic devices by SPICE circuit model is certainly not physically transparent and should be implemented with caution. Nevertheless, if the circuit model is well constructed to take account of the realistic physical models and sufficiently represents the physical properties of the optoelectronic device, it will certainly bring great benefit for designing the optoelectronic module working within an electronic system such as optical transmitter and receiver. This approach avoids modelling optoelectronic devices by stand-alone tools or languages

Although the tools for electronic design automation have been highly developed and become almost indispensable in designing and optimising the electronic devices, circuits and systems [1][7], commercialised design tools for semiconductor lasers or optoelectronic devices in general, is still in its infancy. In addition, integrating the optoelectronic simulation programs and tools into existing electronic ones is an important task that has not received the deserved attention. This provides the motivation for undertaking the work of this thesis.



## 1.2 Semiconductor Lasers

The first step in developing any theoretical model or any circuit model for semiconductor lasers is to understand their basic structure and working principles. In this section, a brief introduction on semiconductor lasers is given.

Semiconductor lasers are one of the most important groups of devices in optoelectronic systems [8]-[11]. When a current is injected into the device, which emits lasing light and provide the function of converting electrical signals into coherent light signals. The basic structure of a semiconductor laser is shown as Fig. 1.1. Basically, a semiconductor laser is composed of three parts, the  $p$ -type region, active region ( $i$  is used to denote the intrinsic material) and  $n$ -type region. For example, a semiconductor laser can have  $p\text{-Al}_x\text{Ga}_{1-x}\text{As}$  as the  $p$ -type region,  $i\text{-GaAs}$  as the active region, and  $n\text{-Al}_x\text{Ga}_{1-x}\text{As}$  as the  $n$ -type region. Normally, two cleaved mirrors in which the sharp refractive index difference between the crystal and the surrounding air, acting as the reflectors surround the active region. When a current is applied to the laser, the hole current is injected from the  $p$ -type region and the electron current is injected from the  $n$ -type region respectively, into the active  $i$ -region. Some of the carriers, that is, holes and electrons, may combine in the active region and produce photons (that is, by a radiative recombination such as spontaneous emission or stimulated emission), while some carriers may recombine non-radiatively (such as by Shockley-Read-Hall recombination or Auger recombination). The active region, usually intrinsic type (that is, without intentional doping), provides a platform for electrons and holes to recombine and produce photon, (that is, generate light.)

The first working semiconductor laser was demonstrated in 1962. Since then, enormous progresses have been made in both experimental and theoretical work to understand and optimise the physical properties and the characteristics of semiconductor lasers. However, the physical and theoretical models for characterising the physical properties of semiconductor lasers are still under development. Some of the physical properties, for example, frequency chirp [12] and physical parameters such as nonlinear gain coefficient [13] of semiconductor lasers are still not fully understood.

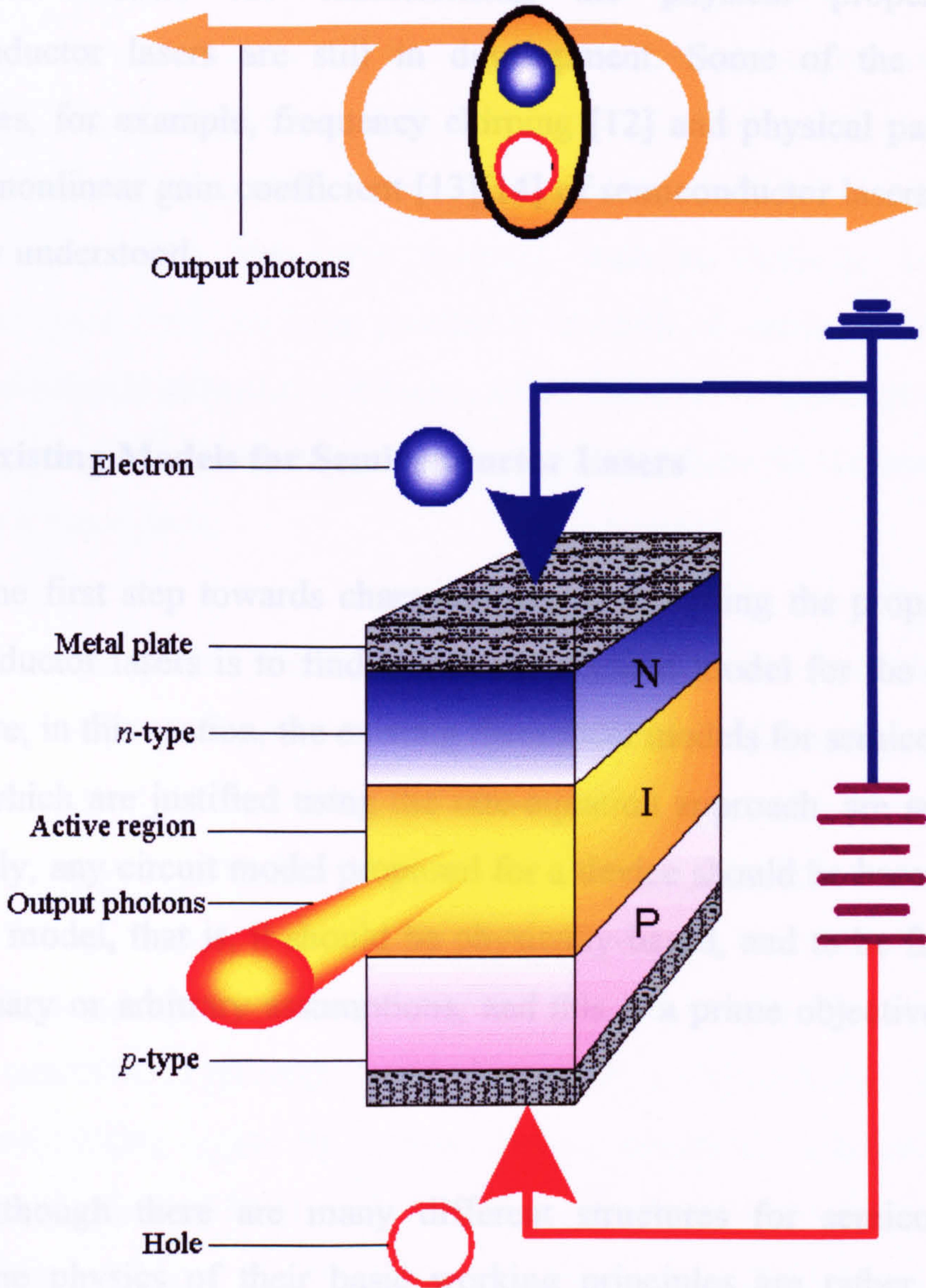


Fig. 1.1. Schematic diagram of a semiconductor laser.

The first working semiconductor laser was demonstrated in 1962. Since then, enormous progresses have been made in both experimental and theoretical work to understand and optimise the physical properties and the characteristics of semiconductor lasers. However, the physical and theoretical models for characterising the physical properties of semiconductor lasers are still in development. Some of the physical properties, for example, frequency chirping [12] and physical parameters such as nonlinear gain coefficient [13][14] of semiconductor lasers are still not fully understood.

### 1.3 Existing Models for Semiconductor Lasers

The first step towards characterising or designing the properties of semiconductor lasers is to find a suitable physical model for the devices. Therefore, in this section, the existing theoretical models for semiconductor lasers, which are justified using the rate-equation approach, are surveyed. Obviously, any circuit model proposed for a device should be based on the physical model, that is, it should be physically-based, and to be free from unnecessary or arbitrary assumptions, and this is a prime objective in this work.

Although there are many different structures for semiconductor lasers, the physics of their basic working principles are rather similar. Generally, a semiconductor laser is a *p-i-n* semiconductor device in which electrons are injected from the *n*-type material and holes are injected from the *p*-type material into the active region of the *i*-type material. An electron and a hole might recombine with each other in the active region to generate

a photon. This photon circulates inside the laser cavity formed by two cleaved, etched or grating mirrors and provides an additional photon source to stimulate other electron-hole recombinations. A proportion of the photons circulate inside the laser cavity will leak through the mirror due to its finite reflectivity and produce the output laser light. The *p-i-n* structures in semiconductor lasers are constructed from heterostructure materials, such as  $\text{Al}_x\text{Ga}_{1-x}\text{As}/\text{GaAs}$ , in which the *i*-type materials have lower energy band-gap and higher optical refractivity than those of the *n*-type and *p*-type materials. Therefore, the *i*-type material, such as GaAs in a  $\text{Al}_x\text{Ga}_{1-x}\text{As}/\text{GaAs}$  laser, will not only provide a function of carrier confinement where the trapped electrons and holes can recombine and generate photons, but also present a function of photon confinement where the heterostructure becomes a waveguide.

Although the basic working principles of a semiconductor laser can roughly be explained by previous description, detailed physical models are certainly required to quantitatively understand its physical properties. The importance of the theoretical models for the development of any semiconductor device is definitely beyond doubt. In fact, theoretical models for semiconductor devices have been well developed; and several popular commercial packages, such as MEDICI, ATLAS and DESSIS, have been widely used by industrial and academic institutions [1]. Basically, any theoretical models for electronic devices should be able to describe the behaviour of electrons inside the devices. Theoretical models used for simulating the electronic devices can be categorised into three different methods based on the assumed nature of the carrier transport in the devices [15]. The comparisons of the complexity among three different numerical methods, the Monte Carlo analysis, partial differential equation

(PDE) or balance equation, and ordinary differential equation (ODE) or rate equation, are illustrated in Fig. 1.2. For each carrier, electron or hole, in a device, three parameters are needed to fully characterise its movement inside the device: time ( $t$ ), space ( $\mathbf{r}$ ) and momentum ( $\mathbf{k}$ ). The Boltzmann equation is used to describe the motions of all of the carriers inside the devices. Since it is almost impossible to analytically solve the Boltzmann equation even for a very simple and artificially defined case, a numerical method, such as the Monte Carlo method, is commonly implemented to solve the distribution of carriers in the  $(t, \mathbf{r}, \mathbf{k})$  domain. Although, this method includes all the details of device physics, its simulation is rather complicated and time-consuming. In most cases, it does not provide a transparent explanation for the physical properties of the device.

Alternatively, if the dynamics in the  $\mathbf{k}$ -coordinate can be calculated by first principles or represented by average quantities (such as density, momentum and energy relaxation times), then the Boltzmann equations can be established by partial differential equations or balance equations. These balance equations can describe the carrier distribution (for example, density and temperature) in the temporal ( $t$ ) and spatial ( $\mathbf{r}$ ) domains. Since the numerical methods for solving PDE equations are highly developed, simulating the devices' properties by solving such balance equations are certainly tractable. This is the reason why such PDE balance equations are implemented in all the major simulation packages for electronic devices.

However, since the measurable physical quantities such as current and voltage are only functions of time, this implies that all the spatial effects, such as carrier density and temperature distributions in the spatial

domain, that affect the output current or voltage can be further simplified if they can be represented by some average quantities. They can totally be neglected if such spatial effects are insignificant. Averaging or neglecting the physical quantities in the spatial domain can further simplify the original PDE balance equations into the ODE rate equations. This dramatically simplifies the theoretical models and numerical procedures for laser simulations. However, it should be noted that the approach is only applicable to semiconductor lasers with a uniform carrier distribution, which can really be treated as an average quantity.

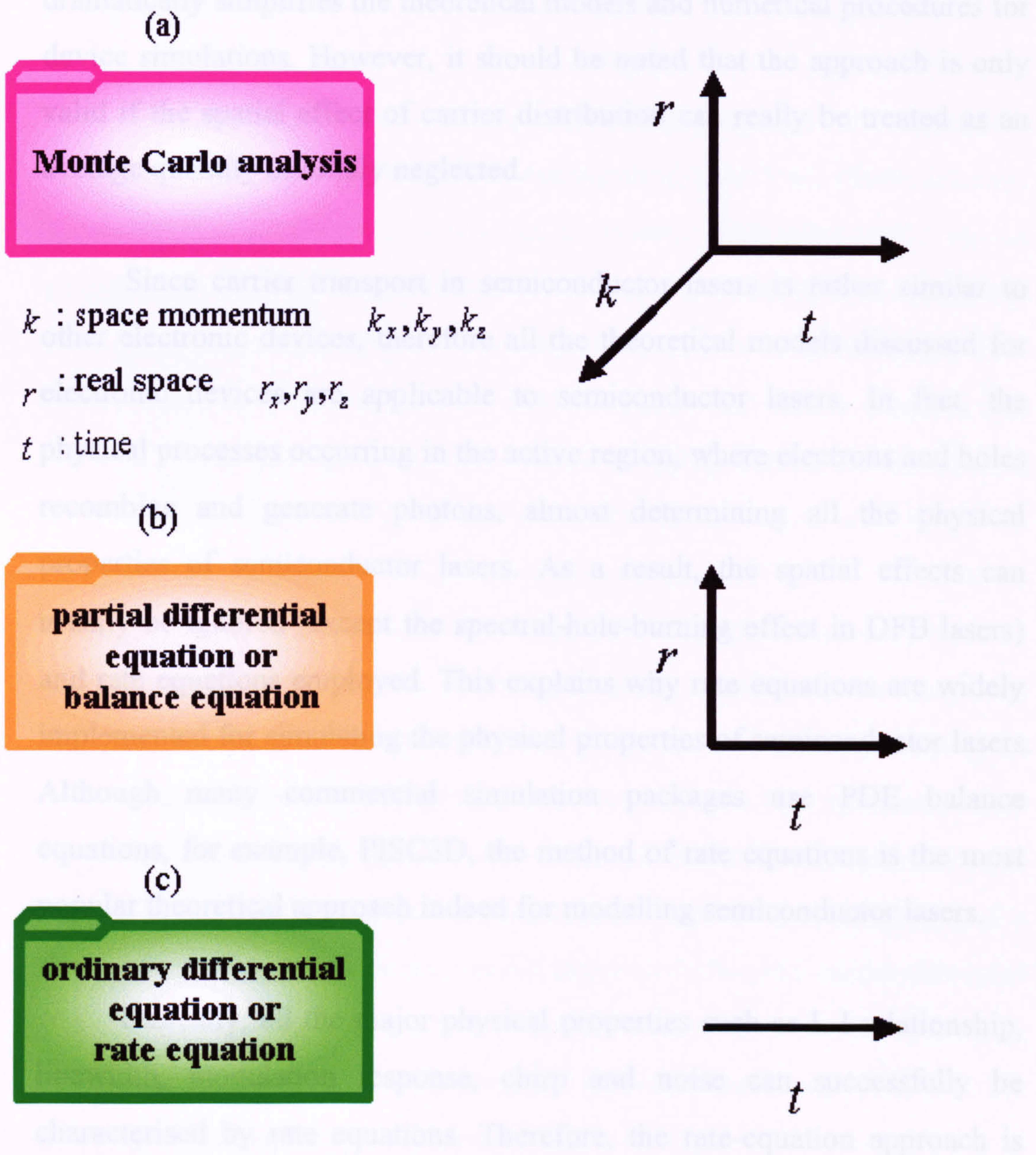


Fig. 1.2. Comparisons of the complexity among three numerical methods, the Monte Carlo analysis, partial differential equation or balance equation, and ordinary differential equation or rate equation.

domain, that affect the output current or voltage can be further simplified if they can be represented by some average quantities. They can totally be neglected if such spatial effects are insignificant. Averaging or neglecting the physical quantities in the spatial domain can further simplify the original PDE balance equations into the ODE rate equations. This dramatically simplifies the theoretical models and numerical procedures for device simulations. However, it should be noted that the approach is only valid if the spatial effect of carrier distribution can really be treated as an average quantity or totally neglected.

Since carrier transport in semiconductor lasers is rather similar to other electronic devices, therefore all the theoretical models discussed for electronic devices are applicable to semiconductor lasers. In fact, the physical processes occurring in the active region, where electrons and holes recombine and generate photons, almost determining all the physical properties of semiconductor lasers. As a result, the spatial effects can usually be ignored (except the spectral-hole-burning effect in DFB lasers) and rate equations employed. This explains why rate equations are widely implemented for simulating the physical properties of semiconductor lasers. Although many commercial simulation packages use PDE balance equations, for example, PISC3D, the method of rate equations is the most popular theoretical approach indeed for modelling semiconductor lasers.

Basically, all the major physical properties such as L-I relationship, linewidth, modulation response, chirp and noise can successfully be characterised by rate equations. Therefore, the rate-equation approach is used in this work. The details of the rate equations are discussed in Chapter

2. The SPICE circuit model proposed in this work is exactly achieved from the rate equations.

#### **1.4 Literature Review – SPICE Circuit Models for Semiconductor Lasers**

As discussed, it can be anticipated that developing SPICE models is invaluable for realising the EDA of optoelectronic devices, which are used in conjunction with electronic devices or systems. Following such a strong anticipation of future need, several SPICE models for semiconductor lasers have been proposed [16]-[27]. The circuit models for bulk semiconductor lasers, that is, heterostructure, derived from the carrier-photon rate equations were first proposed by Tucker [16][17]. Based on this model, Lu et al. developed a SPICE circuit model for quantum-well lasers by incorporating additional effects of carrier transport [18][19]. In contrast, instead of concentrating on the carrier transport effects which only became important in the high-speed modulation mode, the Xu group proposed SPICE circuit models for quantum well lasers particularly emphasising on the heating effects [20][21]. This is based on the fact that the nonlinearity in the L-I relationship of any semiconductor laser can satisfactorily be explained by considering the heating effect. Tsou et al. also proposed a SPICE circuit model for quantum-well lasers including the carrier-transport effect [22]. In addition, the effect of the coulomb enhancement on the gain coefficient and thus the properties of the high-speed modulation were investigated using their SPICE model [23].



t: A more evolved SPICE model including the carrier-transport effect was proposed by Rossi et al. [24]. They used their SPICE model to analyse and design 1.55  $\mu\text{m}$  quantum-well lasers for improving the high-speed performance. Madhan et al. proposed a SPICE circuit model for the multimode lasers and investigated the bistable behaviour of the devices [25]. Czotscher et al. produced an approach in which they combined their circuit model with the physical models of optical fibres and photodetectors to simulate the intensity modulation and chirp in a fibre optic communication system [26]. Recognising that heating has a paramount effect on the properties of vertical-cavity surface-emitting lasers (VCSELs), Mena et al. proposed a SPICE circuit model with heating effects for VCSELs [27]. Mena et al. used their model to fit experimental data and thereby extracted the related physical parameters of the device. However, it should be noted that heating effects in their model and in the model of the Xu group are only referred to the lattice heating. Carrier heating effects are neither included nor discussed in their models.

From the foregoing it is seen that the temperature-dependent performance characteristics of devices are well established in SPICE circuit models. Consequently, physical quantities such as resistance and capacitance are assigned to a function of temperature (*TEMP*) in the SPICE codes. Therefore, it is widely accepted that SPICE circuit models for semiconductor lasers should represent this temperature-dependent feature in order to further integrate their implementation into electronic circuits and increase their accuracy in predicting performance. In fact, the heating problem is well recognised as one of the most important factors influencing both the static and dynamic performance of semiconductor lasers [28]-[32]. However, all the published SPICE models, which include

heating effects in semiconductor lasers, solely refer to the lattice heating while the direct effect of the carrier heating has totally been neglected. It should be noted that the injection current supplies energy to carriers, which then release their energy to lattice via phonon emission. This is schematically illustrated in Fig. 1.3. Since the injection current supplies energy directly to electrons and holes, not directly to lattice in a semiconductor laser, any issue regarding the lattice heating in semiconductor lasers will inevitably involve the issue of the carrier heating. Consequently, theoretical models used for predicting the heating effects on the performance of semiconductor lasers are thus anticipated to be able to simultaneously accommodate the physical mechanisms of the carrier and lattice heating. This certainly implies that any attempt to establish the temperature-dependent feature for SPICE circuit models of semiconductor lasers should be able to incorporate the features of the carrier and lattice heating in the same model, not just the lattice heating alone.

## **1.5 Heating Models for Semiconductor Lasers**

Although many physical factors affect the properties and characteristics of semiconductor lasers, the heating problem which including both the carrier and lattice heating, is well known as one of the most important factors influencing the static and dynamic properties of semiconductor lasers. The details of such an influence have extensively been discussed in many textbooks and literature [1][8]-[14], and will not be restated here for simplicity. The most obvious example is that the threshold current will exponentially increase with the linearly increasing

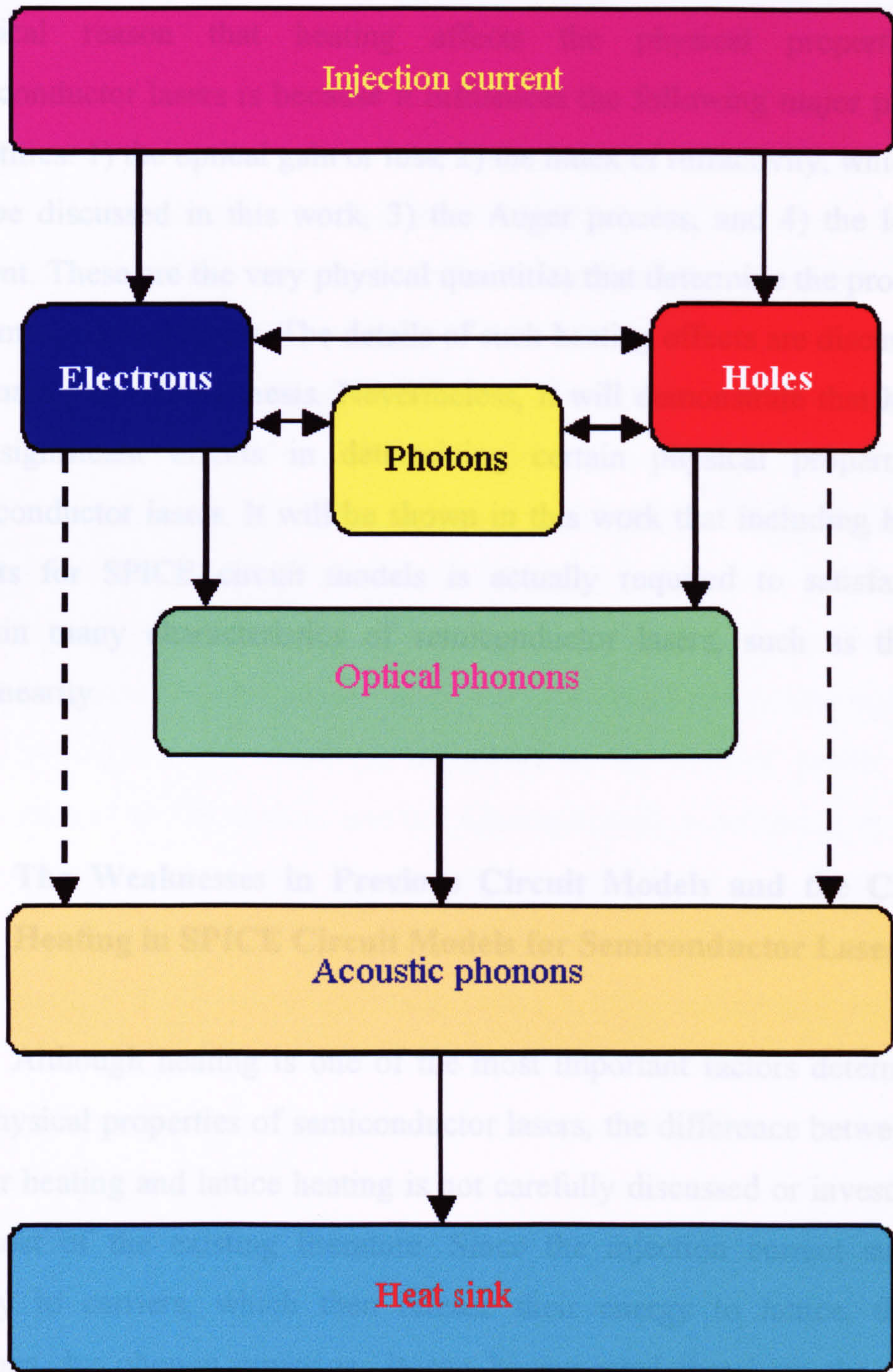


Fig. 1.3. Schematic diagram of energy transfer in semiconductor lasers.

heat-sink temperature. In addition, heating will cause the nonlinearity in the light-current relationship, that is, L-I curve, of a semiconductor laser. The physical reason that heating affects the physical properties of semiconductor lasers is because it influences the following major physical quantities: 1) the optical gain or loss, 2) the index of refractivity, which will not be discussed in this work, 3) the Auger process, and 4) the leakage current. These are the very physical quantities that determine the properties of semiconductor lasers. The details of such heating effects are discussed in the main part of this thesis. Nevertheless, it will demonstrate that heating has significant effects in determining certain physical properties of semiconductor lasers. It will be shown in this work that including heating effects for SPICE circuit models is actually required to satisfactorily explain many characteristics of semiconductor lasers, such as the L-I nonlinearity.

## **1.6 The Weaknesses in Previous Circuit Models and the Carrier Heating in SPICE Circuit Models for Semiconductor Lasers**

Although heating is one of the most important factors determining the physical properties of semiconductor lasers, the difference between the carrier heating and lattice heating is not carefully discussed or investigated by most of the existing literature. Since the injection current supplies energy to carriers, which then release their energy to lattice, that is, phonons, by phonon emission. It can be expected that both the carrier heating and lattice heating should be presented in semiconductor lasers although their effects in influencing the properties of semiconductor lasers may totally be different. As a result, any theoretical attempt to model the

heating in semiconductor lasers is expected to be able to simultaneously simulate the carrier and lattice heating effects separately.

The SPICE models proposed by the Xu group and Mena et al. have incorporated the lattice heating, but the carrier heating is totally neglected in their models. Such an approach has several shortcomings:

- 1) Since the carrier heating is neglected, the heating source of the lattice heating by the carrier energy relaxation, both intraband and interband phonons, cannot be included into their models. To circumvent such an obvious problem, a phenomenological lattice-heating source  $I \cdot V - P$  was heuristically defined to represent the total thermal power dissipated in the whole device, where  $I$  and  $V$  denote the external applied current and voltage onto the device and  $P$  denotes the output optical power. Intuitively, the total power injected from the current will either be dissipated as the thermal power or be emitted as the optical power. Although such a definition is rather straightforward, it should carefully be noted that  $I \cdot V - P$  represents the thermal power dissipated in the whole device. Consequently, using  $I \cdot V - P$  to represent the lattice-heating source and averaging  $I \cdot V - P$  to the volume of the device implies the whole device has a uniform distribution of the lattice temperature. This assumption is totally unacceptable for semiconductor lasers because all the major heating sources are concentrated on the active region where electrons and holes may recombine. As a result, using  $I \cdot V - P$  to model the lattice-heating source cannot represent the realistic heating distribution in the device and its validity is obviously questionable.
- 2) Neglecting the carrier heating in semiconductor lasers certainly implies that the magnitude of the carrier heating is negligible

compared to the magnitude of the lattice heating. However, such an assumption has not been verified for semiconductor lasers by experimental or theoretical methods. In practice, it is almost impossible to directly measure the carrier and lattice temperatures within the device. Since the carrier heating and lattice heating simultaneously exist within the device, it is almost impossible to distinguish their effects and contributions if their relative significance cannot be determined. Despite this, the SPICE models proposed by the Xu group and Mena et al. are claimed to be able to accurately fit the experimental L-I curves even though they ignore the possible contribution by the carrier heating. Unless it can be proved in the future that the carrier heating is indeed insignificant, attributing all the heating effects only to the lattice heating is questionable. In addition, if the models give acceptable results it is because they contain compensating errors.

- 3) In fact, some physical processes only affected by the carrier heating, for example, the leakage current and Auger process, while other physical processes only influenced by the lattice heating, for example, the thermal conduction. Attributing all heating effects only to the lattice heating certainly does not satisfy the realistic physical models. For example, the temperature-dependent threshold current level in a semiconductor laser is mostly determined by the Auger process and leakage current, which are closely determined by the carrier temperature. In other words, the carrier temperature mostly determines the threshold current level. Fitting threshold current by using a model only with lattice heating does not correspond to the realistic physical situations and could even cause conceptual confusion and misunderstanding.

As discussed, it is apparent that attributing all heating effects just to the lattice heating is not only physically unrealistic but also numerically questionable. Incorporating the carrier heating into the heating model, which appears necessary and indispensable if realistic physical models are to be established. It is emphasised that accurately fitting experimental data is not the most important criterion by which to judge the success of a SPICE model for semiconductor lasers. Usually, there are hundreds of undetermined parameters in SPICE circuit models. Therefore, it is not difficult to fit a set of experimental data by adjusting these parameters. It is not surprising that even a primitive SPICE circuit model can accurately fit a set of experimental data without too much difficulty. Judging the merit of a SPICE circuit model only by the ability of data fitting is certainly misleading. It is more appropriate to value the merit of a SPICE model by assessing its physical correctness.

## **1.7 Methodologies for Incorporating the Carrier Heating into the SPICE Circuit Model**

As discussed, it can be concluded that incorporating the carrier heating is certainly desirable if the heating problem in semiconductor lasers is to be investigated. To do this it is necessary to be able to simultaneously simulate the carrier and lattice temperatures in a device if the temperature-related properties of semiconductor lasers are to be understood. Otherwise, it is almost impossible to determine whether the carrier temperature or the lattice temperature causes the temperature-related properties. In addition to aid design and perform any quantitative numerical simulations to predict

the temperature-related characteristics of semiconductor lasers accurate models are required.

The first task for achieving this goal is to establish a realistic physical model with both the carrier and lattice heating. After the realistic physical model with carrier and lattice heating is established, then this physical model needs to be transformed into a circuit model without any further simplification. Once the circuit model has been transformed from the physical model, the SPICE codes can then be implemented in accordance with the circuit model. Following the development of the SPICE codes, predictions of performance can proceed. As mentioned, for a SPICE circuit model with ten or more adjustable parameters, it will be very easy to accurately fit a set of experimental data. However, such accuracy does not necessarily imply that the model is robust in other cases. Therefore, a more acceptable justification of success may be that a more physically realistic model needs to be incorporated in SPICE codes. Generally, it can be stated that a SPICE circuit model with more physical bases and more parameters has a greater ability to fit more data sets. Therefore, there is always a trade-off between the circuit complication and data-fitting ability. Nevertheless, it should be emphasised that incorporating the carrier heating is seen as a necessity rather than an option for modelling the heating effects presented in semiconductor lasers.



## 1.8 SPICE Circuit Models

The first task in transforming the rate equations of semiconductor lasers into the circuit models is to select an appropriate computing language for the circuits. Unlike simulation languages for digital circuits, which apparently lack any standard at present despite the existence of popular languages such as Verilog and VHDL, SPICE is well recognised as the standard simulation language for analogue electronics. Therefore, instead of developing a new simulation language, which will not be compatible with other electronic circuit models, it was decided to implement the circuit models for semiconductor lasers using the SPICE language.

SPICE is widely used in the academic and industrial worlds to simulate the operation of various electronic circuits and devices [33]. It was developed in the University of California and initially used on mainframe computers. The successor to the original version, SPICE2, is more powerful. Later versions are designed to operate on PCs, Macintoshes and minicomputers. One of them is the PSPICE from the *MicroSim* Corporation. PSPICE designed to mainly be used in PCs.

In order to simulate any circuit input file with PSPICE, standard PSPICE codes must first be written. This can be done using any suitable text editor. Using the built-in text editor, *Textedit.exe*, in PSPICE, can easily do this. The PSPICE codes created by using the *Textedit.exe* can be saved into a circuit file with the file extension *\*.cir*, for example, *laser.cir*. The compiler of the PSPICE language is in the *Pspicead.exe*, which can be called to compile the input circuit file *laser.cir*. The compiled result, whether containing errors or not, is stored in an output file called *laser.out*.

In PSPICE, a facility called *Probe* can be used to check the results of simulation by opening a graphic window. A simple *.PROBE* statement in the PSPICE codes can call the function of the *Probe*. Calling *.PROBE* in PSPICE in fact creates another output file with the file extension *\*.dat*, for example, *.PROBE* will create the *laser.dat* for the *laser.cir*.

The procedures for downloading, installing, creating, compiling, probing and plotting relating to the *MicroSim* PSPICE evaluation package is explained in APPENDIX A and schematically illustrated in Fig. 1.4. A summary of the syntaxes in the PSPICE language is listed in APPENDIX B. It should be noted that the evaluation package of *MicroSim* PSPICE has almost the same functions as the vendor one, except in the capacities for handling circuit elements in the schematic drawing and the library of circuit elements. Since the work in this thesis includes developing PSPICE codes, the PSPICE compiler provided in the evaluation package is adequate for this task.

## **1.9 The Aim and Objectives of the Thesis**

The aim of this thesis is to develop a SPICE circuit model for semiconductor lasers that incorporating the effects of the carrier and lattice heating. This SPICE circuit model is to be able to simulate the dc, ac and transient characteristics of semiconductor lasers.

The objectives are to:

- 1) Review and establish the physically-based rate-equations that can satisfactorily model the carrier and lattice heating in

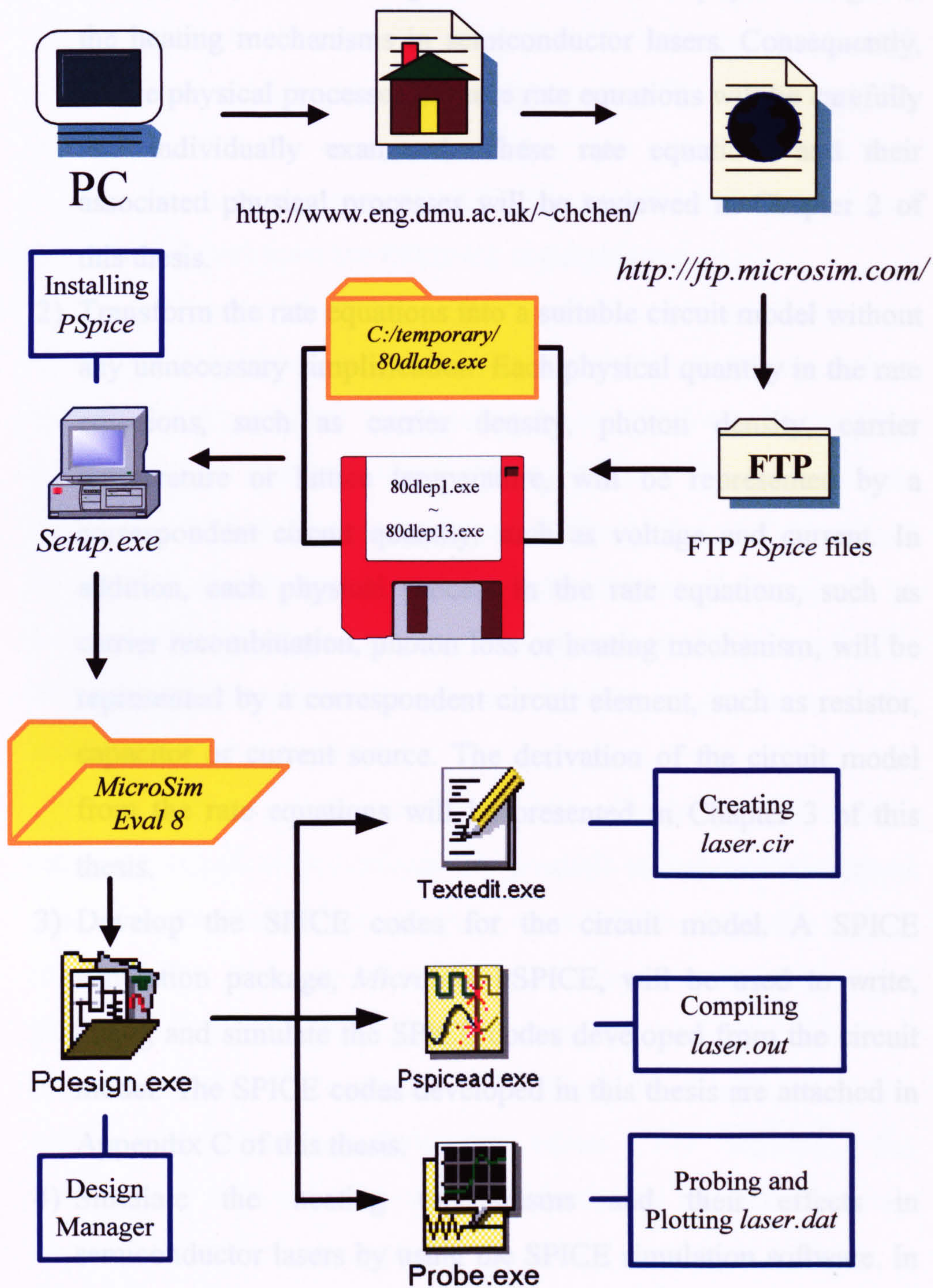


Fig. 1.4. Schematic diagram of downloading, installing, creating, compiling, probing and plotting relating to a PSPICE program.

semiconductor lasers. These rate equations should not have any heuristic or phenomenological definition on the physical origin of the heating mechanisms in semiconductor lasers. Consequently, all the physical processes in these rate equations will be carefully and individually examined. These rate equations and their associated physical processes will be reviewed in Chapter 2 of this thesis.

- 2) Transform the rate equations into a suitable circuit model without any unnecessary simplification. Each physical quantity in the rate equations, such as carrier density, photon density, carrier temperature or lattice temperature, will be represented by a correspondent circuit quantity, such as voltage and current. In addition, each physical process in the rate equations, such as carrier recombination, photon loss or heating mechanism, will be represented by a correspondent circuit element, such as resistor, capacitor or current source. The derivation of the circuit model from the rate equations will be presented in Chapter 3 of this thesis.
- 3) Develop the SPICE codes for the circuit model. A SPICE simulation package, *MicroSim* PSPICE, will be used to write, debug and simulate the SPICE codes developed from the circuit model. The SPICE codes developed in this thesis are attached in Appendix C of this thesis.
- 4) Simulate the heating mechanisms and their effects in semiconductor lasers by using the SPICE simulation software. In order to verify the ability of the new proposed circuit models when dealing with the carrier and lattice heating effects in semiconductor lasers, the effect of the lattice heating on the

nonlinearity of the light-current (L-I) relationship and the time variation of the carrier temperature in the transient response in semiconductor lasers will be simulated and demonstrated. Such simulations will be presented in Chapter 4 of this thesis.

In summary, a new proposed SPICE circuit model will be developed in this work, which will meet the following requirements:

- 1) The new proposed circuit model should be applicable for semiconductor lasers under different operating conditions, which include the dc, ac (that is, small-signal modulation) and transient (that is, large-signal modulation) responses. The conventional approach of developing separate and different dc, small-signal and large-signal circuit models for a single electron device is to be avoided. In short, this circuit model is to universally be applicable for predicting the physical properties of semiconductor lasers for all different operating conditions.
- 2) The new proposed circuit model should be achieved by a physically-based theoretical model without any heuristic and phenomenological arguments. In addition, the circuit model should be physically robust, free from any quantitative uncertain, unnecessary and phenomenological definitions. Consequently, all the physical processes relating to the circuit model should be directly calculable without assigning any arbitrary values. For example, the conventional approach of heuristically assigning the lattice-heating source is considered unacceptable.
- 3) The new proposed circuit model should be flexible enough to further accommodate expansions if more physical effects are incorporated. Of course, it is almost impossible to develop any circuit model that

can include all the physical processes and all the physical properties of semiconductor lasers. Although, the circuit model will emphasise the carrier and lattice heating effects in semiconductor lasers, this circuit model should be developed to consider further possible expansions and be able to accommodate other physical processes as well. In general, a circuit model cannot be viewed as a 'good' circuit model if it is only designed to account for certain effects.

- 4) The new proposed circuit model should be able to be used with circuit models representing other electronic devices and systems. Semiconductor lasers are usually used with other electronic devices in real working systems, such as transmitter modules in fibre optic communication systems. Since most of the electronic devices have equivalent SPICE circuit models developed for the purpose of simulation, it is certainly anticipated that the development of a SPICE circuit model for semiconductor lasers to be used in conjunction with these electronic devices is of practical value.

## CHAPTER 2

### RATE EQUATIONS FOR SEMICONDUCTOR LASERS

#### 2.1 Rate Equations

It has been well recognised that the conventional carrier-photon rate equations can successfully describe many static and dynamic properties of semiconductor lasers. Therefore, any theoretical model that is proposed for further refinement should be able to accommodate these rate equations. Theoretical models for semiconductor lasers based on such a rate-equation approach certainly implies that the spatial effects of physical quantities will be either averaged or neglected. For example, the optical confinement factor is an average quantity characterising the overlap of the optical field with the carriers in the active region. The injection efficiency is an average quantity describing the percentage of current goes into the active region. The behaviours of the carrier and lattice heating outside the active region were neglected. The validities of such assumptions can be found in a paper by Tsai et al. [15].

In order to incorporate the effects of the carrier and lattice heating, additional rate equations are needed to supplement the conventional carrier-photon rate equations. In this work, rate equations governing the carrier density  $n$ , photon density  $s$ , electron temperature  $T_e$ , hole temperature  $T_h$  and lattice temperature  $T_L$  will be used, that is, the five rate equations shown in Fig. 2.1 are used to describe the time variation of the carrier density  $n$ , photon density  $s$ , electron temperature  $T_e$ , hole temperature  $T_h$

and lattice temperature  $T_L$ . Each rate equation is schematically illustrated in Figs. 2.2, 2.3, 2.4, 2.5 and 2.6, respectively:

The conventional carrier-photon and photon density rate equations and photon density  $s$  are given by

$$\frac{dn}{dt} = \frac{qI}{qV} - \frac{1}{V} (R_{sp} + R_{sp} + R_{sp}) \quad (2.1)$$

$$\frac{ds}{dt} = \Gamma (R_{sp} - R_{sp}) + \Gamma R_{sp} \quad (2.2)$$

where  $n$  only denotes the carrier density of electrons,  $V$  is the volume of the laser,  $I$  is the injection current,  $R_{sp}$  represents the per-unit-volume injection current,  $R_{sp}$  represents the per-unit-volume recombination current,  $R_{sp}$  represents the per-unit-volume recombination current (i.e., loss of photons),  $\Gamma$  is the confinement factor,  $R_{sp}$  represents the per-unit-volume recombination current,  $R_{sp}$  represents the per-unit-volume recombination current.

The energy balance equations for the electron, hole, and lattice temperatures are given by

$$\frac{dT_e}{dt} = \frac{1}{C_e V} (qI - R_{sp} - R_{sp} - R_{sp}) \quad (2.3)$$

$$\frac{dT_h}{dt} = \frac{1}{C_h V} (qI - R_{sp} - R_{sp} - R_{sp}) \quad (2.4)$$

$$\frac{dT_L}{dt} = \frac{1}{C_L V} (qI - R_{sp} - R_{sp} - R_{sp}) \quad (2.5)$$

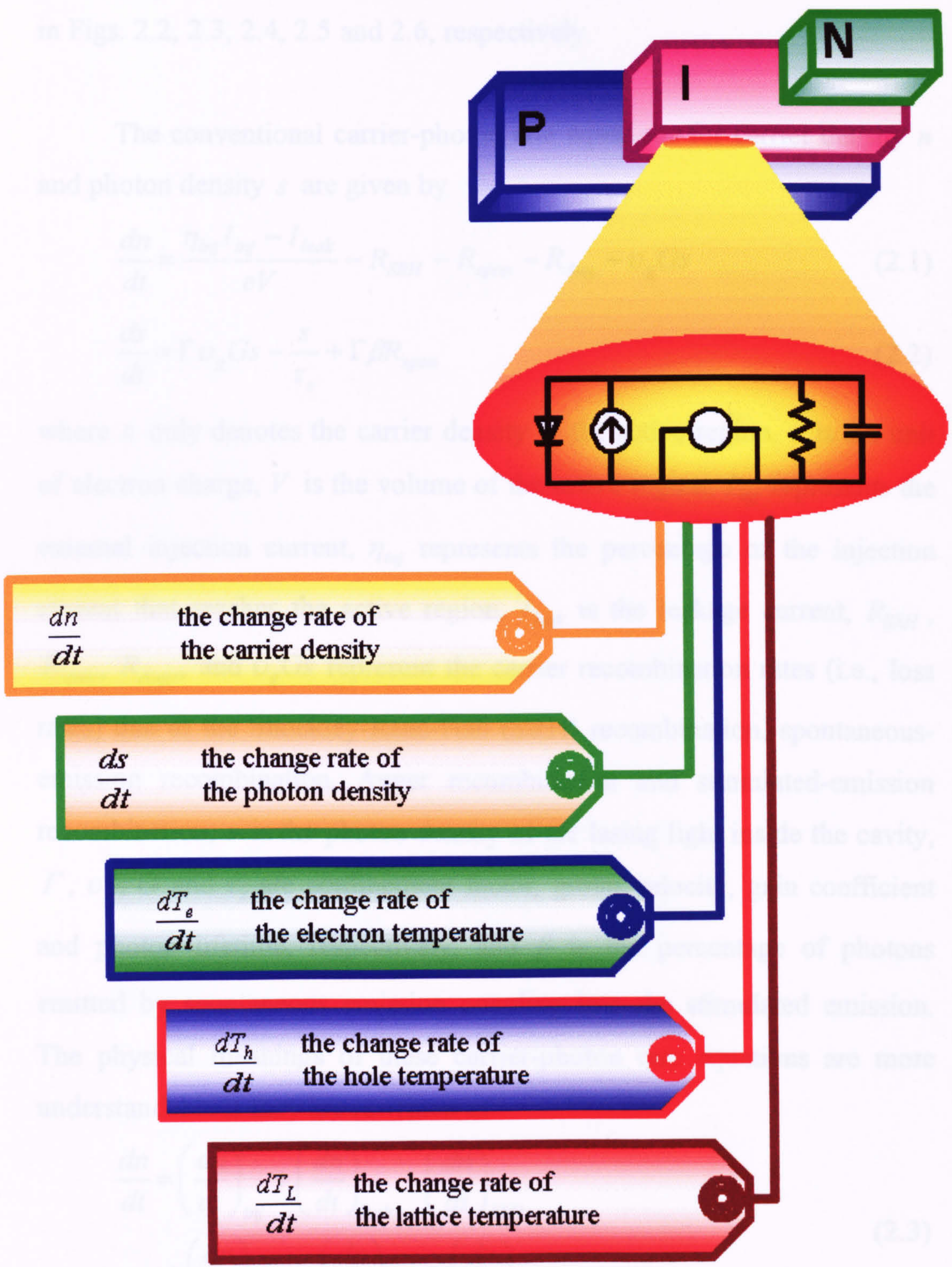


Fig. 2.1. Rate equations for semiconductor lasers.



and lattice temperature  $T_L$ . Each rate equation is schematically illustrated in Figs. 2.2, 2.3, 2.4, 2.5 and 2.6, respectively.

The conventional carrier-photon rate equations for carrier density  $n$  and photon density  $s$  are given by

$$\frac{dn}{dt} = \frac{\eta_{inj} I_{inj} - I_{leak}}{eV} - R_{SRH} - R_{spon} - R_{Aug} - \nu_g Gs \quad (2.1)$$

$$\frac{ds}{dt} = \Gamma \nu_g Gs - \frac{s}{\tau_s} + \Gamma \beta R_{spon} \quad (2.2)$$

where  $n$  only denotes the carrier density in the active region,  $e$  is the unit of electron charge,  $V$  is the volume of the active region,  $I_{inj}$  represents the external injection current,  $\eta_{inj}$  represents the percentage of the injection current that reaches the active region,  $I_{leak}$  is the leakage current,  $R_{SRH}$ ,  $R_{spon}$ ,  $R_{Auger}$  and  $\nu_g Gs$  represent the carrier recombination rates (i.e., loss rates) due to the Shockley-Read-Hall (SRH) recombination, spontaneous-emission recombination, Auger recombination and stimulated-emission recombination,  $s$  is the photon density of the lasing light inside the cavity,  $\Gamma$ ,  $\nu_g$ ,  $G$  and  $\tau_s$  are confinement factor, group velocity, gain coefficient and photon lifetime, respectively, and  $\beta$  is the percentage of photons emitted by spontaneous emission coupling into the stimulated emission. The physical meanings of these carrier-photon rate equations are more understandable if they are rewritten as

$$\begin{aligned} \frac{dn}{dt} = & \left( \frac{dn}{dt} \right)_{inj} + \left( \frac{dn}{dt} \right)_{leak} + \left( \frac{dn}{dt} \right)_{SRH} \\ & + \left( \frac{dn}{dt} \right)_{spon} + \left( \frac{dn}{dt} \right)_{Aug} + \left( \frac{dn}{dt} \right)_{stim} \end{aligned} \quad (2.3)$$

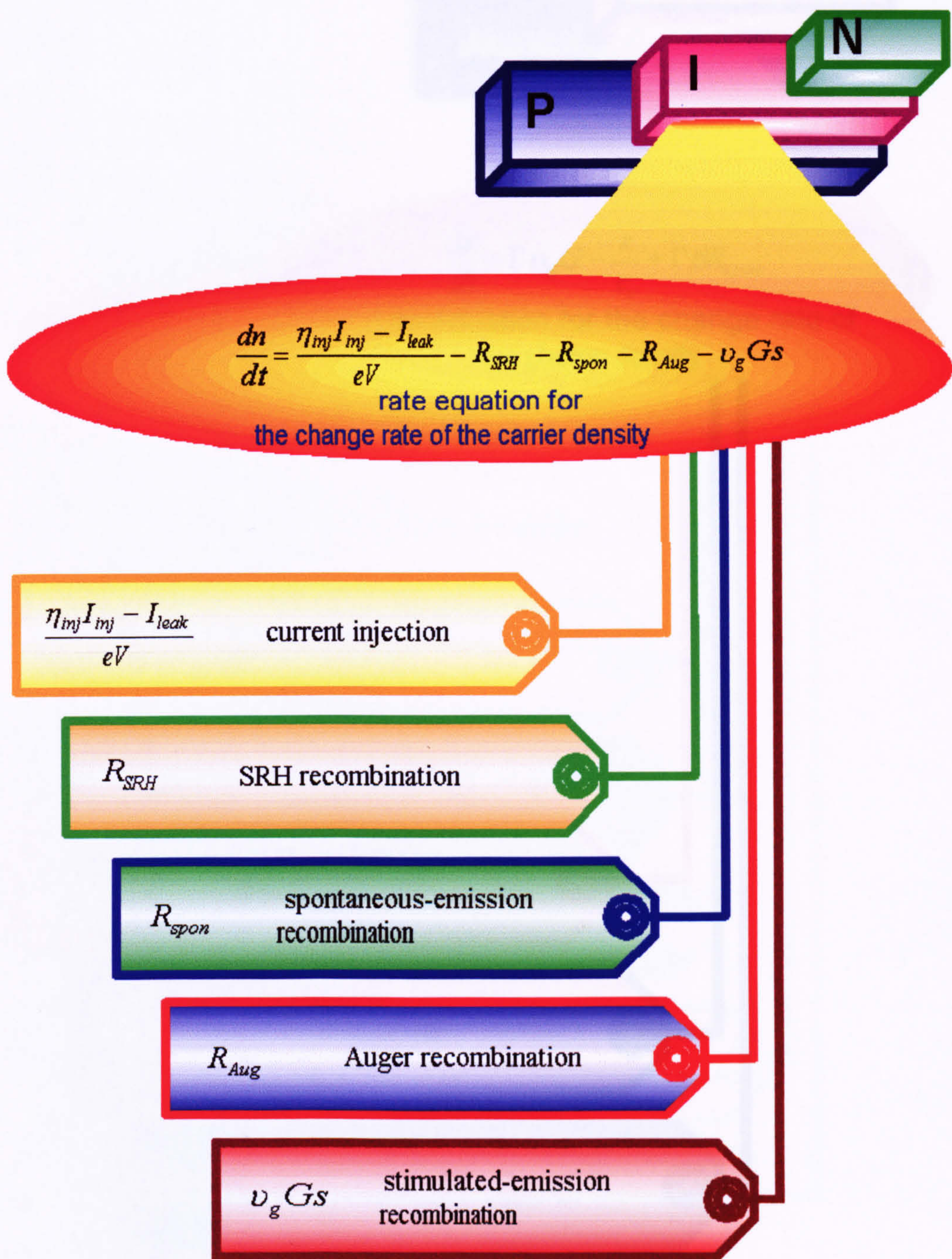


Fig. 2.2 Rate equation for the change rate of the carrier density.

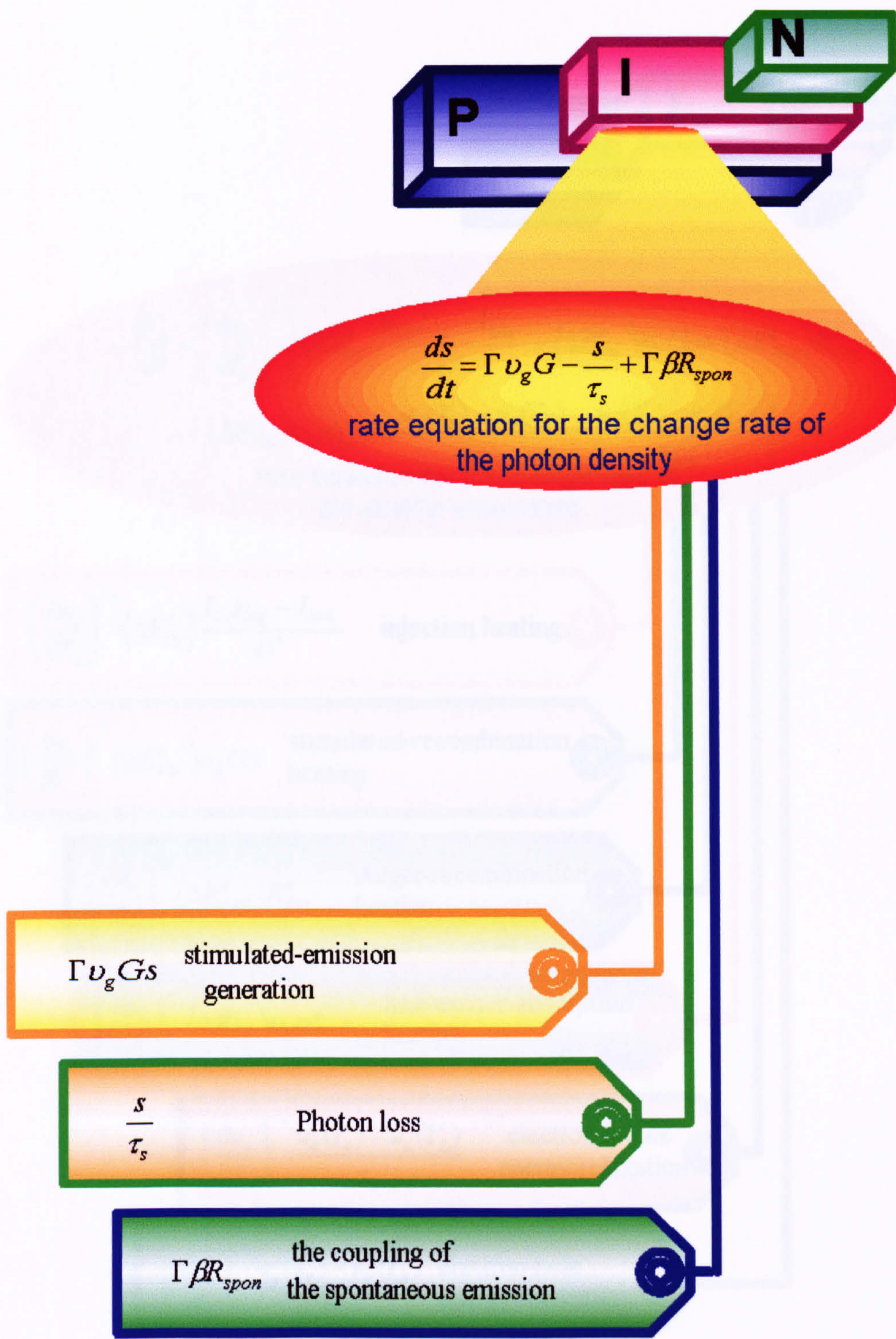


Fig. 2.3. Rate equation for the change rate of the photon density.

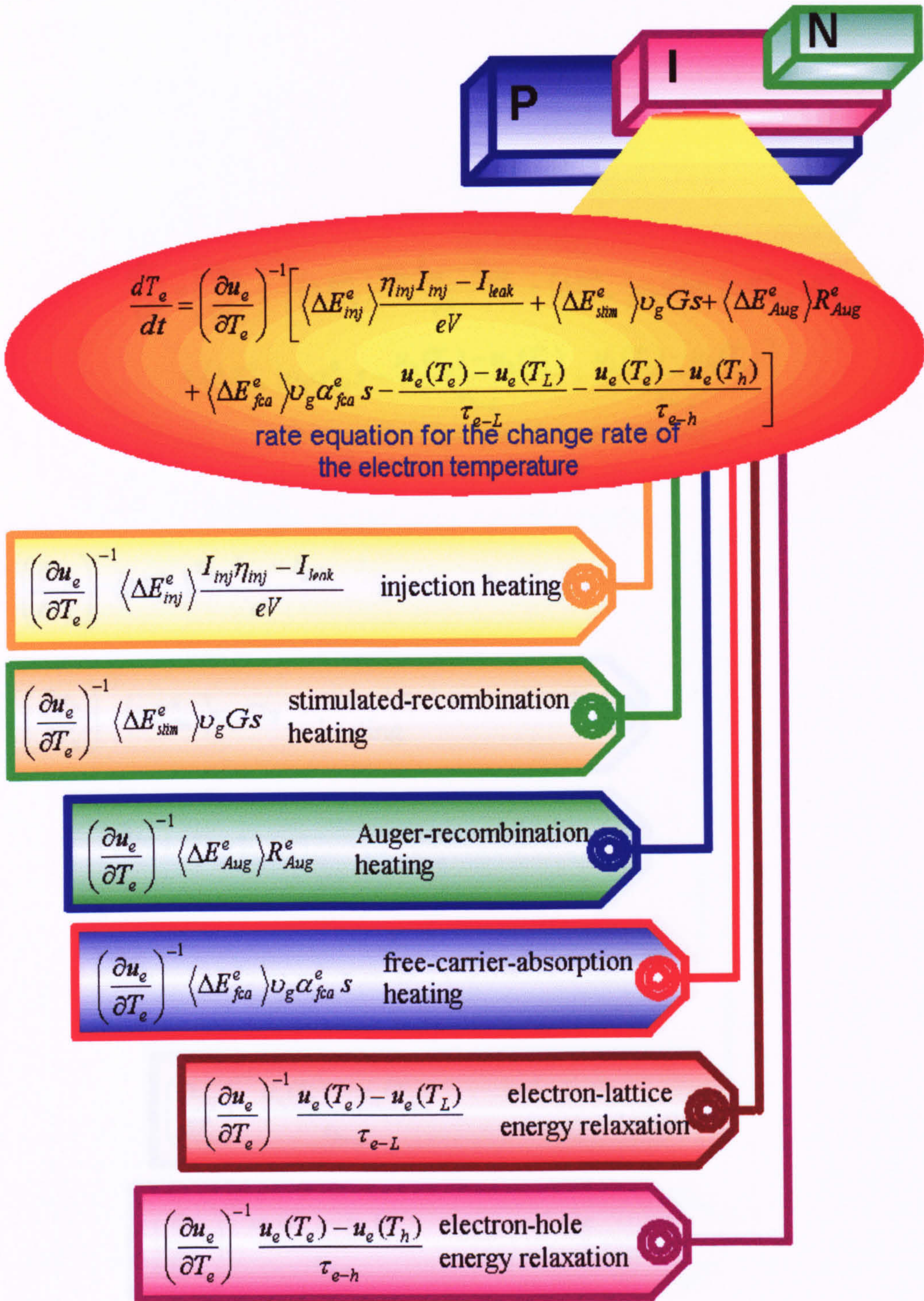
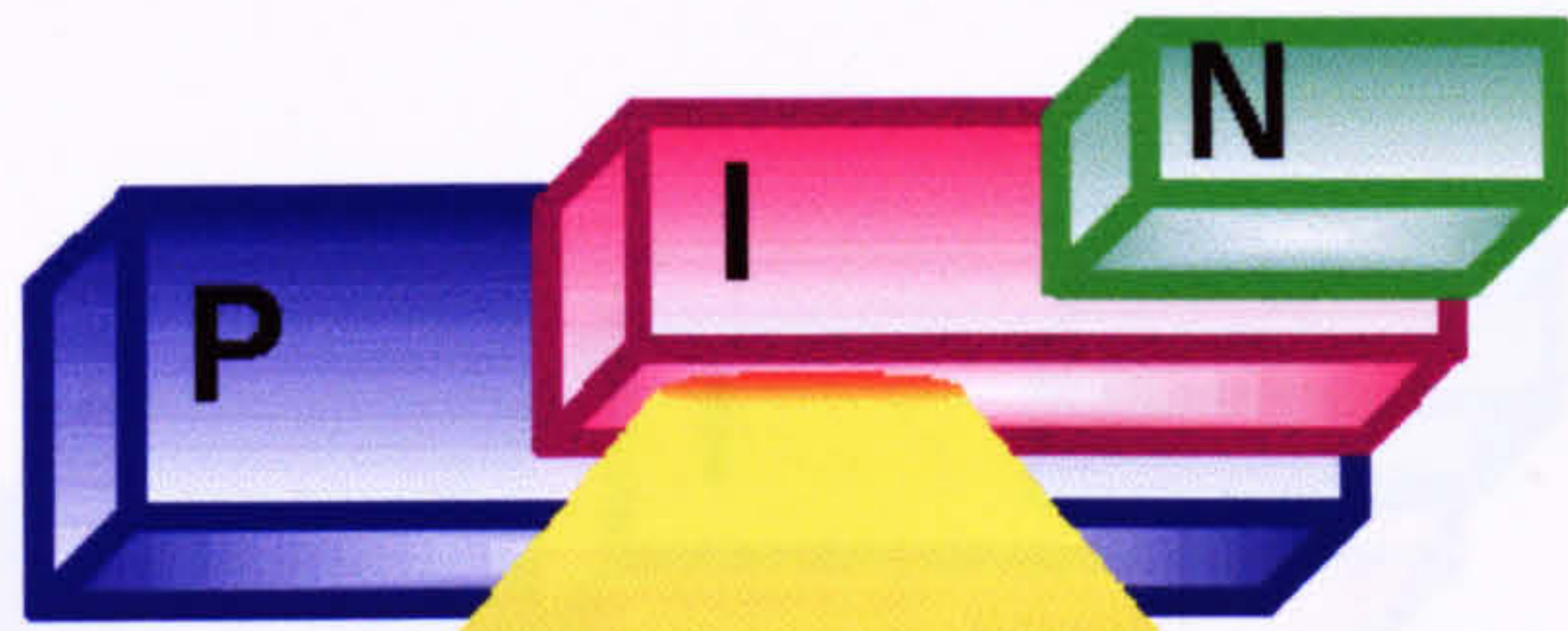


Fig. 2.4. Rate equation for the change rate of the electron temperature.



$$\frac{dT_h}{dt} = \left( \frac{\partial u_h}{\partial T_h} \right)^{-1} \left[ \langle \Delta E_{inj}^h \rangle \frac{\eta_{inj} I_{inj} - I_{leak}}{eV} + \langle \Delta E_{stim}^h \rangle \nu_g G S + \langle \Delta E_{Aug}^h \rangle R_{Aug}^h \right. \\ \left. + \langle \Delta E_{fca}^h \rangle \nu_g \alpha_{fca}^h S - \frac{u_h(T_h) - u_h(T_L)}{\tau_{h-L}} + \frac{u_h(T_h) - u_h(T_e)}{\tau_{h-e}} \right]$$

rate equation for the change rate of the hole temperature

$$\left( \frac{\partial u_h}{\partial T_h} \right)^{-1} \langle \Delta E_{inj}^h \rangle \frac{\eta_{inj} I_{inj} - I_{leak}}{eV} \quad \text{injection heating}$$

$$\left( \frac{\partial u_h}{\partial T_h} \right)^{-1} \langle \Delta E_{stim}^h \rangle \nu_g G S \quad \text{stimulated-recombination heating}$$

$$\left( \frac{\partial u_h}{\partial T_h} \right)^{-1} \langle \Delta E_{Aug}^h \rangle R_{Aug}^h \quad \text{Auger-recombination heating}$$

$$\left( \frac{\partial u_h}{\partial T_h} \right)^{-1} \langle \Delta E_{fca}^h \rangle \nu_g \alpha_{fca}^h S \quad \text{free-carrier-absorption heating}$$

$$\left( \frac{\partial u_h}{\partial T_h} \right)^{-1} \frac{u_h(T_h) - u_h(T_L)}{\tau_{h-L}} \quad \text{hole-lattice energy relaxation}$$

$$\left( \frac{\partial u_h}{\partial T_h} \right)^{-1} \frac{u_h(T_h) - u_h(T_e)}{\tau_{h-e}} \quad \text{electron-hole energy relaxation}$$

Fig. 2.5. Rate equation for the change rate of the hole temperature.

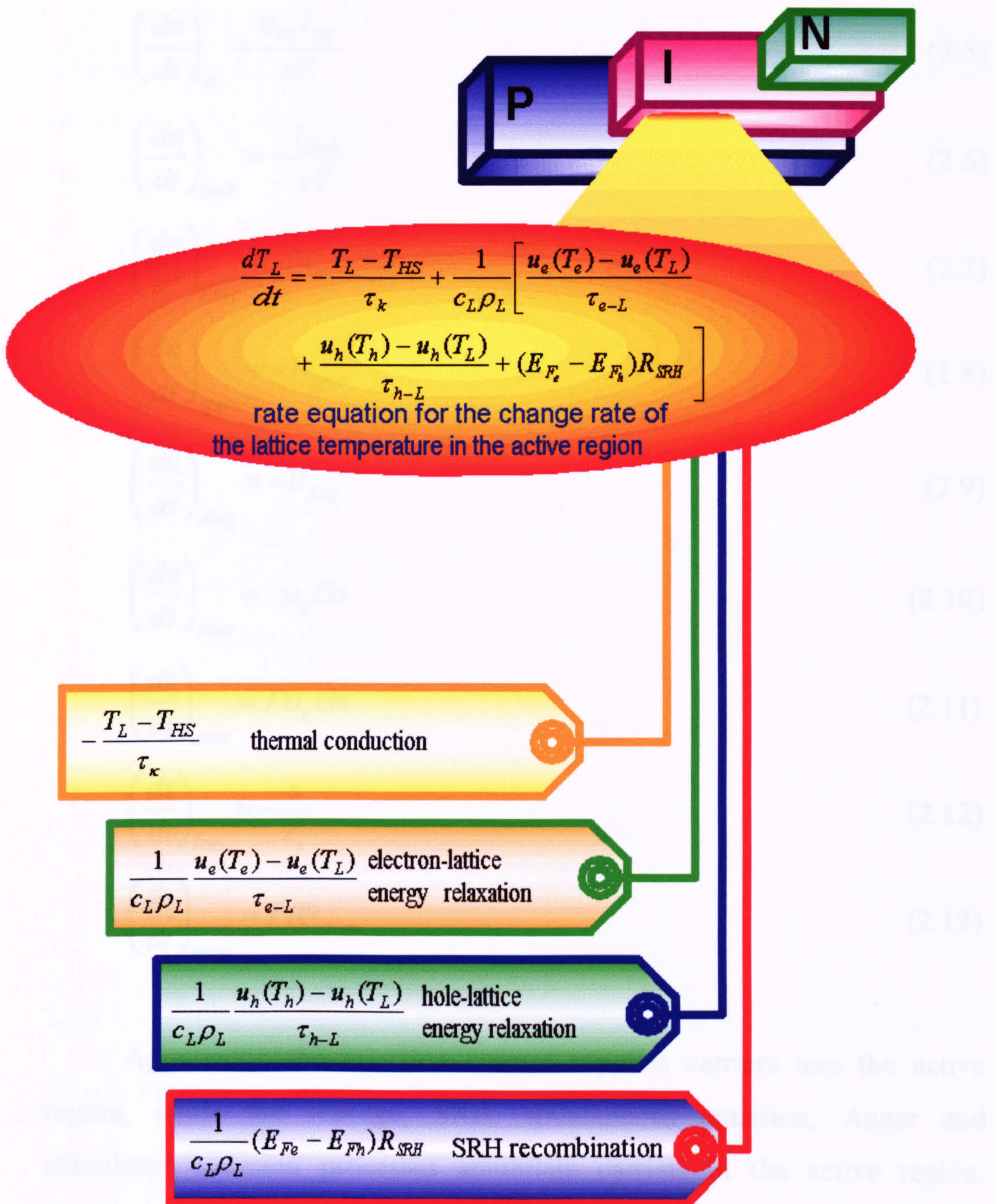


Fig. 2.6. Rate equation for the change rate of the lattice temperature in the active region.

$$\frac{ds}{dt} = \left(\frac{ds}{dt}\right)_{stim} + \left(\frac{ds}{dt}\right)_{loss} + \left(\frac{ds}{dt}\right)_{spon} \quad (2.4)$$

where

$$\left(\frac{dn}{dt}\right)_{inj} = \frac{\eta_{inj} I_{inj}}{eV} \quad (2.5)$$

$$\left(\frac{dn}{dt}\right)_{leak} = -\frac{I_{leak}}{eV} \quad (2.6)$$

$$\left(\frac{dn}{dt}\right)_{SRH} = -R_{SRH} \quad (2.7)$$

$$\left(\frac{dn}{dt}\right)_{spon} = -R_{spon} \quad (2.8)$$

$$\left(\frac{dn}{dt}\right)_{Aug} = -R_{Aug} \quad (2.9)$$

$$\left(\frac{dn}{dt}\right)_{stim} = -\nu_g Gs \quad (2.10)$$

$$\left(\frac{ds}{dt}\right)_{stim} = \Gamma \nu_g Gs \quad (2.11)$$

$$\left(\frac{ds}{dt}\right)_{loss} = -\frac{s}{\tau_s} \quad (2.12)$$

$$\left(\frac{ds}{dt}\right)_{spon} = \Gamma \beta R_{spon} \quad (2.13)$$

Apparently, the injection current supplies carriers into the active region, while the leakage, SRH, spontaneous emission, Auger and stimulated emission processes annihilate carriers in the active region. Similarly, the stimulated emission and the coupling of the spontaneous

emission supply the lasing photons, while the losses due to the internal loss and the mirror loss deplete the photons inside the cavity.

In order to characterise the time variation of the carrier and lattice temperatures in the active region, rate equations for the electron temperature  $T_e$ , hole temperature  $T_h$  and lattice temperature  $T_L$  are given by

$$\begin{aligned} \frac{dT_e}{dt} = & \left( \frac{\partial u_e}{\partial T_e} \right)^{-1} \left[ \langle \Delta E_{inj}^e \rangle \frac{\eta_{inj} I_{inj} - I_{leak}}{eV} + \langle \Delta E_{stim}^e \rangle \nu_g G_s \right. \\ & + \langle \Delta E_{Aug}^e \rangle R_{Aug}^e + \langle \Delta E_{fca}^e \rangle \nu_g \alpha_{fca}^e S \\ & \left. - \frac{u_e(T_e) - u_e(T_L)}{\tau_{e-L}} - \frac{u_e(T_e) - u_e(T_h)}{\tau_{e-h}} \right] \end{aligned} \quad (2.14)$$

$$\begin{aligned} \frac{dT_h}{dt} = & \left( \frac{\partial u_h}{\partial T_h} \right)^{-1} \left[ \langle \Delta E_{inj}^h \rangle \frac{\eta_{inj} I_{inj} - I_{leak}}{eV} + \langle \Delta E_{stim}^h \rangle \nu_g G_s \right. \\ & + \langle \Delta E_{Aug}^h \rangle R_{Aug}^h + \langle \Delta E_{fca}^h \rangle \nu_g \alpha_{fca}^h S \\ & \left. - \frac{u_h(T_h) - u_h(T_L)}{\tau_{h-L}} + \frac{u_h(T_h) - u_h(T_e)}{\tau_{e-h}} \right] \end{aligned} \quad (2.15)$$

$$\begin{aligned} \frac{dT_L}{dt} = & -\frac{T_L - T_{HS}}{\tau_k} + \frac{1}{c_L \rho_L} \left[ \frac{u_e(T_e) - u_e(T_L)}{\tau_{e-L}} \right. \\ & \left. + \frac{u_h(T_h) - u_h(T_L)}{\tau_{h-L}} + (E_{Fe} - E_{Fh}) R_{SRH} \right] \end{aligned} \quad (2.16)$$

where  $u_c(T)$ ,  $c = e$  or  $h$ , is the carrier energy density at temperature  $T$ ,  $\alpha_{fca}^c$  is the coefficient of the free-carrier absorption,  $\langle \Delta E_{process}^c \rangle$ ,  $process = inj, stim, Aug$  and  $fca$  is the average energy change per carrier due to the processes of the injection, stimulated-recombination, Auger recombination and free-carrier-absorption heating,  $T_{HS}$  is the temperature of the heat sink,



$c_L$  is the specific heat capacity of lattice, and  $\rho_L$  is the material density of lattice. In these rate equations, there are four time constants:  $\tau_\kappa$  is the thermal conduction time,  $\tau_{e-L}$  is the electron-lattice energy relaxation time,  $\tau_{h-L}$  is the hole-lattice energy relaxation time and  $\tau_{e-h}$  is the electron-hole energy relaxation time. These time constants govern the overall energy exchange rates between electrons, holes and lattice. Their physical meanings are discussed in the following sections.

Similarly, the three rate equations governing the time variation of the electron temperature  $T_e$ , hole temperature  $T_h$  and lattice temperature  $T_L$  are more understandable if they are rewritten in the following format:

$$\begin{aligned} \frac{dT_e}{dt} = & \left( \frac{dT_e}{dt} \right)_{inj} + \left( \frac{dT_e}{dt} \right)_{stim} + \left( \frac{dT_e}{dt} \right)_{Aug} \\ & + \left( \frac{dT_e}{dt} \right)_{fca} + \left( \frac{dT_e}{dt} \right)_{e-L} + \left( \frac{dT_e}{dt} \right)_{e-h} \end{aligned} \quad (2.17)$$

$$\begin{aligned} \frac{dT_h}{dt} = & \left( \frac{dT_h}{dt} \right)_{inj} + \left( \frac{dT_h}{dt} \right)_{stim} + \left( \frac{dT_h}{dt} \right)_{Aug} \\ & + \left( \frac{dT_h}{dt} \right)_{fca} + \left( \frac{dT_h}{dt} \right)_{h-L} + \left( \frac{dT_h}{dt} \right)_{e-h} \end{aligned} \quad (2.18)$$

$$\frac{dT_L}{dt} = \left( \frac{dT_L}{dt} \right)_{thermal\ conduction} + \left( \frac{dT_L}{dt} \right)_{e-L} + \left( \frac{dT_L}{dt} \right)_{h-L} + \left( \frac{dT_L}{dt} \right)_{SRH} \quad (2.19)$$

where

$$\left( \frac{dT_c}{dt} \right)_{inj} = \left( \frac{\partial u_c}{\partial T_c} \right)^{-1} \langle \Delta E_{inj}^c \rangle \frac{\eta_{inj} I_{inj} - I_{leak}}{eV} \quad (2.20)$$

$$\left( \frac{dT_c}{dt} \right)_{stim} = \left( \frac{\partial u_c}{\partial T_c} \right)^{-1} \langle \Delta E_{stim}^c \rangle \nu_g G_s \quad (2.21)$$

$$\left(\frac{dT_c}{dt}\right)_{Aug} = \left(\frac{\partial u_c}{\partial T_c}\right)^{-1} \langle \Delta E_{Aug}^c \rangle R_{Aug} \quad (2.22)$$

$$\left(\frac{dT_c}{dt}\right)_{fca} = \left(\frac{\partial u_c}{\partial T_c}\right)^{-1} \langle \Delta E_{fca}^c \rangle \nu_g \alpha_{fca}^c S \quad (2.23)$$

$$\left(\frac{dT_c}{dt}\right)_{c-L} = -\left(\frac{\partial u_c}{\partial T_c}\right)^{-1} \frac{u_c(T_c) - u_c(T_L)}{\tau_{c-L}} \quad (2.24)$$

$$\left(\frac{dT_e}{dt}\right)_{e-h} = -\left(\frac{dT_h}{dt}\right)_{e-h} = -\left(\frac{\partial u_c}{\partial T_c}\right)^{-1} \frac{u_e(T_e) - u_e(T_h)}{\tau_{e-h}} \quad (2.25)$$

$$\left(\frac{dT_L}{dt}\right)_{thermal\ conduction} = -\frac{T_L - T_{HS}}{\tau_\kappa} \quad (2.26)$$

$$\left(\frac{dT_L}{dt}\right)_{c-L} = \frac{1}{c_L \rho_L} \frac{u_c(T_c) - u_c(T_L)}{\tau_{c-L}} \quad (2.27)$$

$$\left(\frac{dT_L}{dt}\right)_{SRH} = \frac{1}{c_L \rho_L} (E_{F_e} - E_{F_h}) R_{SRH} \quad (2.28)$$

From these equations it can be seen that, the electron temperature will increase due to the injection heating (2.20), stimulated-recombination heating (2.21), Auger-recombination heating (2.22) and free-carrier-absorption heating (2.23); and it will decrease due to the electrons releasing their energy to lattice and holes as they relax. In the same manner the hole temperature will increase due to the same heating mechanisms and the receiving of electron energy. Similarly, it will decrease due to the holes releasing their energy to lattice. The lattice temperature will increase as it obtains energy from the electrons and holes via the intraband energy relaxation and the interband SRH process with multiple-phonon emission. This effect will be discussed in Section 2.2.

The detailed physical meaning of each effect described in the rate equations is discussed in the following sections. In this work, a typical  $\text{Al}_x\text{Ga}_{1-x}\text{As}/\text{GaAs}$  heterostructure laser is used as an example because many physical parameters presented are well characterised for the  $\text{Al}_x\text{Ga}_{1-x}\text{As}/\text{GaAs}$  material and are not so readily available for other material systems. An example to illustrate this point is the energy relaxation times.

In the following section, all the physical terms in the rate equations will be explained in details, and their related formulas for implementing in the new proposed SPICE circuit models will be given.

## 2.2 Parameters for Carrier Processes

The carrier density  $n_c$  is defined as the carrier numbers per unit volume. Higher carrier density means more carrier numbers within a unit volume. This can schematically be visualised shown in Fig. 2.7. In the following discussion, the sub-index  $c = e$  denotes electrons and  $c = h$  represents holes. From the principle of statistical physics, carrier density can be characterised by the Fermi-Dirac distribution, and the value of carrier density is determined by the quasi-Fermi energy  $\mu_{Fc}$  and carrier temperature  $T_c$ . If the carrier system is assumed to maintain the quasi-equilibrium condition,  $n_c$  can be calculated by

$$n_c = N_c F_{1/2} \left( \frac{\mu_{Fc} - E_c}{k_B T_c} \right) \quad (2.29)$$

where  $N_c$  is the effective density of states

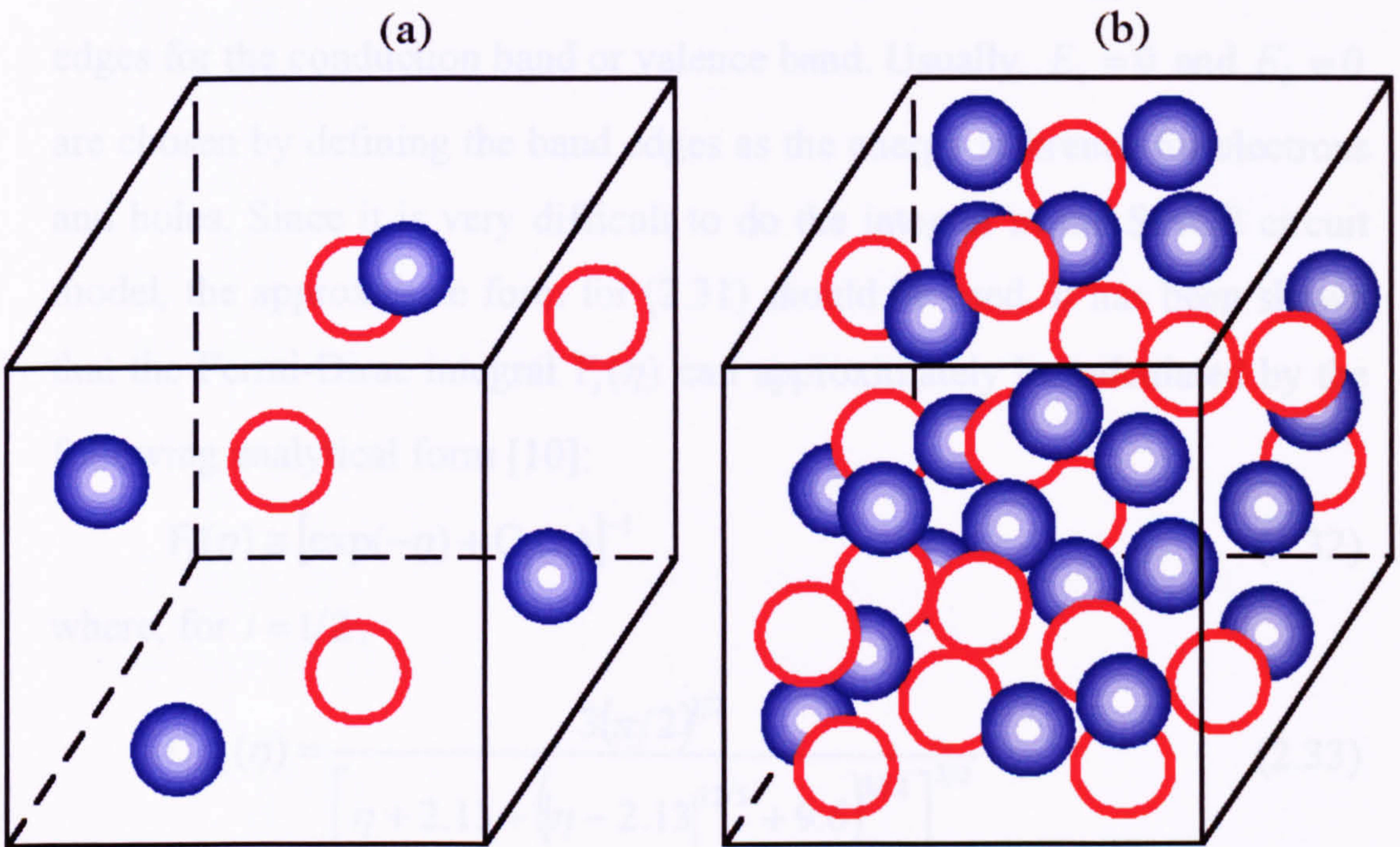
$$n_c = 2 \left( \frac{m_c^* k_B T_c}{2\pi\hbar^2} \right)^{3/2} F_1(\eta) \quad (2.30)$$

$m_c^*$  is the effective mass for the density of states in the conduction band or valence band,  $k_B$  is the Boltzmann constant and  $\hbar$  is the reduced Planck constant. In (2.29),  $F_1(\eta)$  is the Fermi-Dirac integral

$$F_1(\eta) = \frac{1}{\Gamma(1+1)} \int_0^\infty \frac{x^1}{1 + \exp(x - \eta)} dx \quad (2.31)$$

in which  $\Gamma(\nu+1)$  is the gamma function,  $E_c$  is the energy of the band edges for the conduction band or valence band. Usually,  $E_c$  and  $E_v$  are defined by defining the band edges as the energy levels where the carrier density is zero. Since the carrier density is zero at the band edges, the carrier density can be written in the form (10)

where  $\eta = (E - E_c)/k_B T_c$  for electrons and  $\eta = (E - E_v)/k_B T_c$  for holes.





-  : electron
-  : hole

Fig. 2.7. Schematic diagram of the carrier distributed at (a) low carrier density and (b) high carrier density.

$$N_c = 2 \left( \frac{m_c k_B T_c}{2\pi\hbar^2} \right)^{3/2} \quad (2.30)$$

$m_c$  is the effective mass for the density of states in the conduction band or valence band,  $k_B$  is the Boltzmann constant and  $\hbar$  is the reduced Plank constant. In (2.29),  $F_i(\eta)$  is the Fermi-Dirac integral

$$F_i(\eta) = \frac{1}{\Gamma(i+1)} \int_0^\infty \frac{x^i}{1 + \exp(x - \eta)} dx \quad (2.31)$$

in which  $\Gamma(i+1)$  is the gamma function.  $E_c$  is the energy of the band edges for the conduction band or valence band. Usually,  $E_e = 0$  and  $E_h = 0$  are chosen by defining the band edges as the energy reference for electrons and holes. Since it is very difficult to do the integral in the SPICE circuit model, the approximate form for (2.31) should be used. It has been shown that the Fermi-Dirac integral  $F_i(\eta)$  can approximately be calculated by the following analytical form [10]:

$$F_i(\eta) \cong [\exp(-\eta) + C_i(\eta)]^{-1} \quad (2.32)$$

where, for  $i = 1/2$ ,

$$C_{1/2}(\eta) = \frac{3(\pi/2)^{1/2}}{\left[ \eta + 2.13 + \left( |\eta - 2.13|^{12/5} + 9.6 \right)^{5/12} \right]^{3/2}} \quad (2.33)$$

As a result, the carrier density  $n_c$  can analytically be calculated by a given quasi-Fermi energy  $\mu_{Fc}$  and a carrier temperature  $T_c$ . In addition, the following analytical form can be used to approximately determine the quasi-Fermi energy if the carrier density  $n_c$  and carrier temperature  $T_c$  are given [10]:

$$\mu_{Fc} = E_c + k_B T_c \left[ \ln\left(\frac{n_c}{N_c}\right) + \sum_{i=1}^{\infty} C_i \left(\frac{n_c}{N_c}\right)^i \right] \quad (2.34)$$

where  $C_1 = 3.53553 \times 10^{-1}$ ,  $C_2 = -4.95009 \times 10^{-3}$ ,  $C_3 = 1.48386 \times 10^{-4}$  and  $C_4 = -4.42563 \times 10^{-6}$  for the approximation up to the fourth power of the approximate series. Note that the band-edge energies for electrons and holes,  $E_c$  and  $E_v$ , are set to zero because electrons and holes are treated as different energy systems. However, it should be noted that if the electron energy is chosen as the energy reference for holes, then the following conventional notations can be used  $n_e \rightarrow n$ ,  $n_h \rightarrow p$ ,  $\mu_{Fe} \rightarrow E_{Fe}$ ,  $\mu_{Fh} \rightarrow -E_{Fh}$ ,  $E_e \rightarrow E_c$  and  $E_h \rightarrow -E_v$ . Note that  $E_c - E_v = E_g$  when using such a notation. In the following discussion, both notation systems are used according to convenience in different situations.

The carrier energy density  $u_c$  is defined as the total energy of carriers per unit volume. It is a function of carrier density and carrier temperature as expressed in equation (2.35).

$$u_c = \frac{3}{2} n_c k_B T_c H_{1/2}^{3/2} \left( \frac{\mu_{Fc} - E_c}{k_B T_c} \right) + n_c E_c \quad (2.35)$$

In the equation  $H_j^l(\eta) \equiv F_l(\eta)/F_j(\eta)$ , note that, in the non-degenerate case, that is,  $(\mu_{Fc} - E_c) \ll k_B T_c$ ,  $u_c \cong 3n_c k_B T_c / 2$ , the result corresponds to the theorem of equi-partition of energy that states each particle has  $k_B T / 2$  energy for each degree of freedom. In the same way, an analytical approximation can be used to calculate  $F_{3/2}(\eta)$  by [10]

$$C_{3/2}(\eta) = \frac{15(\pi/2)^{1/2}}{\left[ \eta + 2.64 + \left( \left| \eta - 2.64 \right|^{9/4} + 14.9 \right)^{4/9} \right]^{5/2}} \quad (2.36)$$

The injection current is denoted by  $I_{inj}$ . As schematically shown in Fig. 2.8, the injection current on the p-type cladding region is established by a hole current, while the n-type cladding region by an electron current. It also shows that holes flowing from the p-type region will be trapped in the intrinsic (*i*) active region. The direction of holes is the same as that of the hole current. Electrons flow from the n-type region into the active region. The direction of electrons is opposite to that of the injection current since electrons have negative charge. Since not every electron transported across the n-type region or every hole transported through the p-type region will reach the active region where the stimulated emission proceeds. The coefficient of the injection efficiency  $\eta_{inj}$  is defined to characterise the percentage of carriers reaching the active region. In fact, the injection efficiency  $\eta_{inj}$  is determined by the lateral leakage current and the recombination of the majority carriers, that is, electrons in the n-type cladding region and holes in the p-type cladding region.

There are two types of leakage currents: the lateral type and transverse type, as schematically shown in Fig. 2.9. The lateral leakage current is attributed to the injection efficiency  $\eta_{inj}$  in this work. The transverse leakage current  $I_{leak}$  is defined as the electrons (holes) escaping from the recombination process in the active region and entering into p-type (n-type) cladding region, that is, which becoming as the minority carriers. Since the leakage current represents the carriers escaping from the

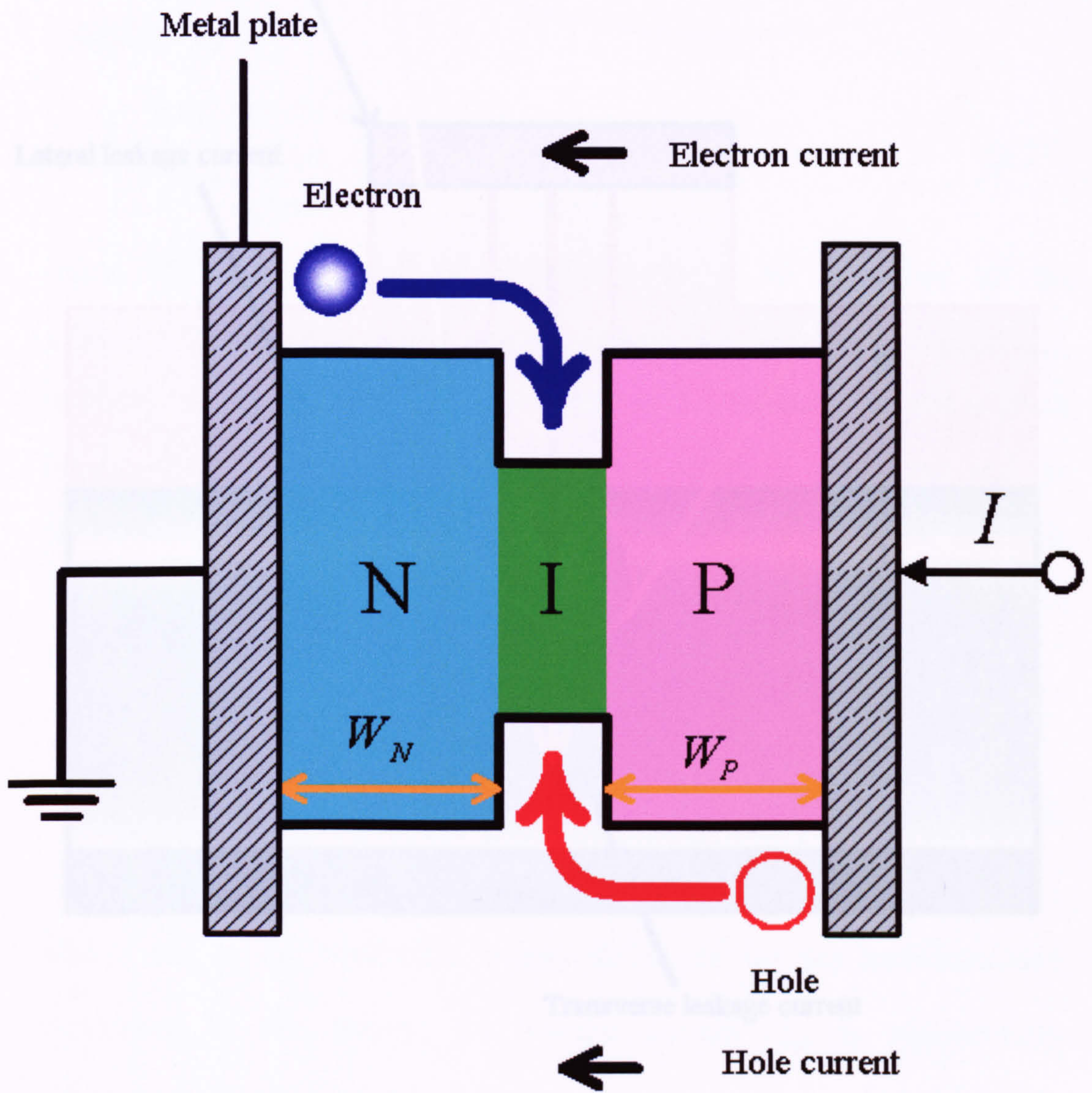


Fig. 2.8. Schematic diagram of the injection current.



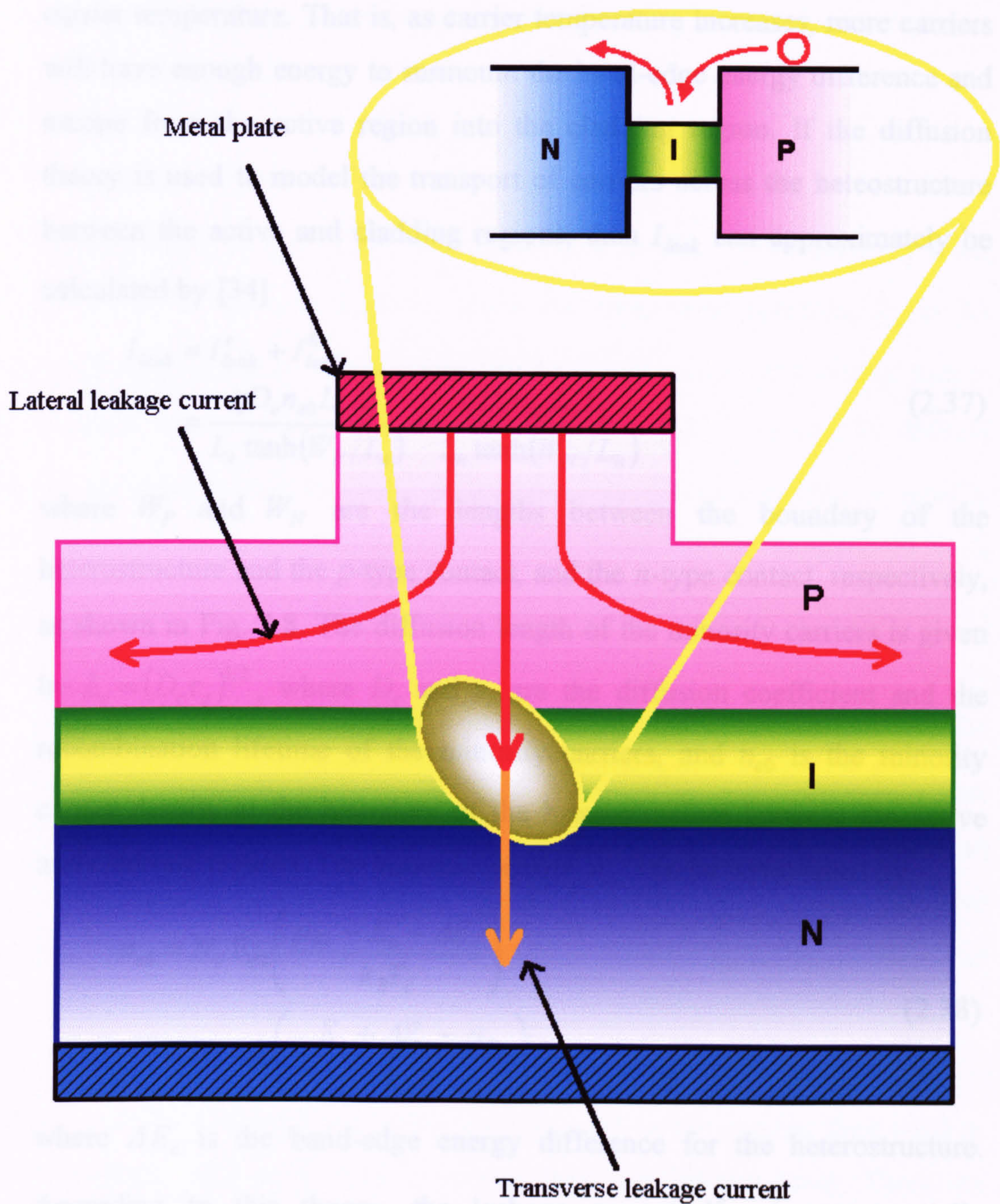


Fig. 2.9. Schematic diagram of the leakage currents (lateral and transverse directions).

lower band-edge energy of the active region into the higher band-edge energy of the cladding region. As a result, this process is very sensitive to carrier temperature. That is, as carrier temperature increases, more carriers will have enough energy to surmount the band-edge energy difference and escape from the active region into the cladding region. If the diffusion theory is used to model the transport of carriers across the heterostructure between the active and cladding regions, then  $I_{leak}$  can approximately be calculated by [34]

$$\begin{aligned}
 I_{leak} &= I_{leak}^e + I_{leak}^h \\
 &= \frac{qD_e n_{e0} L_y L_z}{L_e \tanh(W_p/L_e)} + \frac{qD_h n_{h0} L_y L_z}{L_h \tanh(W_n/L_h)}
 \end{aligned} \tag{2.37}$$

where  $W_p$  and  $W_n$  are the lengths between the boundary of the heterostructure and the  $p$ -type contact, and the  $n$ -type contact, respectively, as shown in Fig. 2.8. The diffusion length of the minority carriers is given by  $L_c = (D_c \tau_c)^{1/2}$ , where  $D_c$  and  $\tau_c$  are the diffusion coefficient and the recombination lifetime of the minority carriers, and  $n_{c0}$  is the minority carrier density at the boundary of the heterostructure between the active and cladding regions. The minority density  $n_{c0}$  can be determined by

$$\begin{aligned}
 n_{c0} &= N_c F_{1/2} \left( \frac{\mu_{Fc} - E_c - \Delta E_c}{k_B T_c} \right) \\
 &\cong N_c \exp \left( - \frac{E_c + \Delta E_c - \mu_{Fc}}{k_B T_c} \right)
 \end{aligned} \tag{2.38}$$

where  $\Delta E_c$  is the band-edge energy difference for the heterostructure. According to this theory, the leakage current  $I_{leak}^c$  is exponentially dependent on the carrier temperature,  $I_{leak}^c \propto n_{c0} \propto \exp(-1/T_c)$ . This suggests that the leakage current will exponentially increase when carrier

temperature increases. This corresponds to less current going into the active region when the carrier temperature increases. This behaviour has significant implications in determining the heating effect in semiconductor lasers.

The volume of the active region,  $V = L_x L_y L_z$ , is shown schematically in Fig. 2.10. As can be seen in Fig. 2.10 where  $L_x$  is the thickness of the active region along the transverse direction,  $L_y$  is the width of the active region along the lateral direction. For strong index-guiding lasers, such as buried-heterostructure types,  $L_y$  is exactly defined by the geometrical structure. In addition, for the gain-guided or weakly index-guided lasers, the definition of  $L_y$  becomes less obvious. In such cases, the effect of lateral current spread may become significant and the current density is not uniformly distributed along the y-direction. Under such circumstances,  $L_y$  can be treated as a parameter that characterises the width of the metal contact, normally, p-type upper metal contact, rather than the width of the active region. In addition, the effect of the lateral current spread, that is, lateral leakage current, and can be incorporated into the parameter of the injection efficient  $\eta_{inj}$ . Finally,  $L_z$  is the length of the cavity between two mirrors.

After electrons and holes enter into the active region, they need to recombine with each other to restore their equilibrium level. There are several carrier recombination mechanisms in the active region: the Shockley-Read-Hall (SRH) multi-phonon emission, spontaneous-emission of photons, Auger process and stimulated-emission of photons. The SRH

recombination describes that the electrons in the conduction band proceed the multi-photon emission to release the energy by emitting photons (or recombine) the holes in the valence band. The Auger recombination, which describes an energy transfer process between two electrons or two electrons and excite an impurity atom, is also a non-radiative process. The term 'spontaneous' emission is used to describe the process where an electron recombines with a hole and emits a photon in any direction, frequency and polarization. On the other hand, the stimulated emission could be in any direction and with any allowable frequency. This, of course, is the main difference between a laser and a light emitting diode (LED). In short, the injected electrons and holes in the active region can recombine with each other via the SRH, Auger, spontaneous emission and stimulated emission processes. Usually, the SRH and Auger are called the non-radiative recombination processes, while the spontaneous emission and stimulated emission are called the radiative recombination processes. It should be noted that the SRH process is differently related from the conventional definition [25]. In the conventional treatment, the SRH process includes the trap-assisted recombination process. However, it is preferred to include this process in the Auger process, while the definition of SRH is solely referred to the process of the trap-assisted interband multi-photon

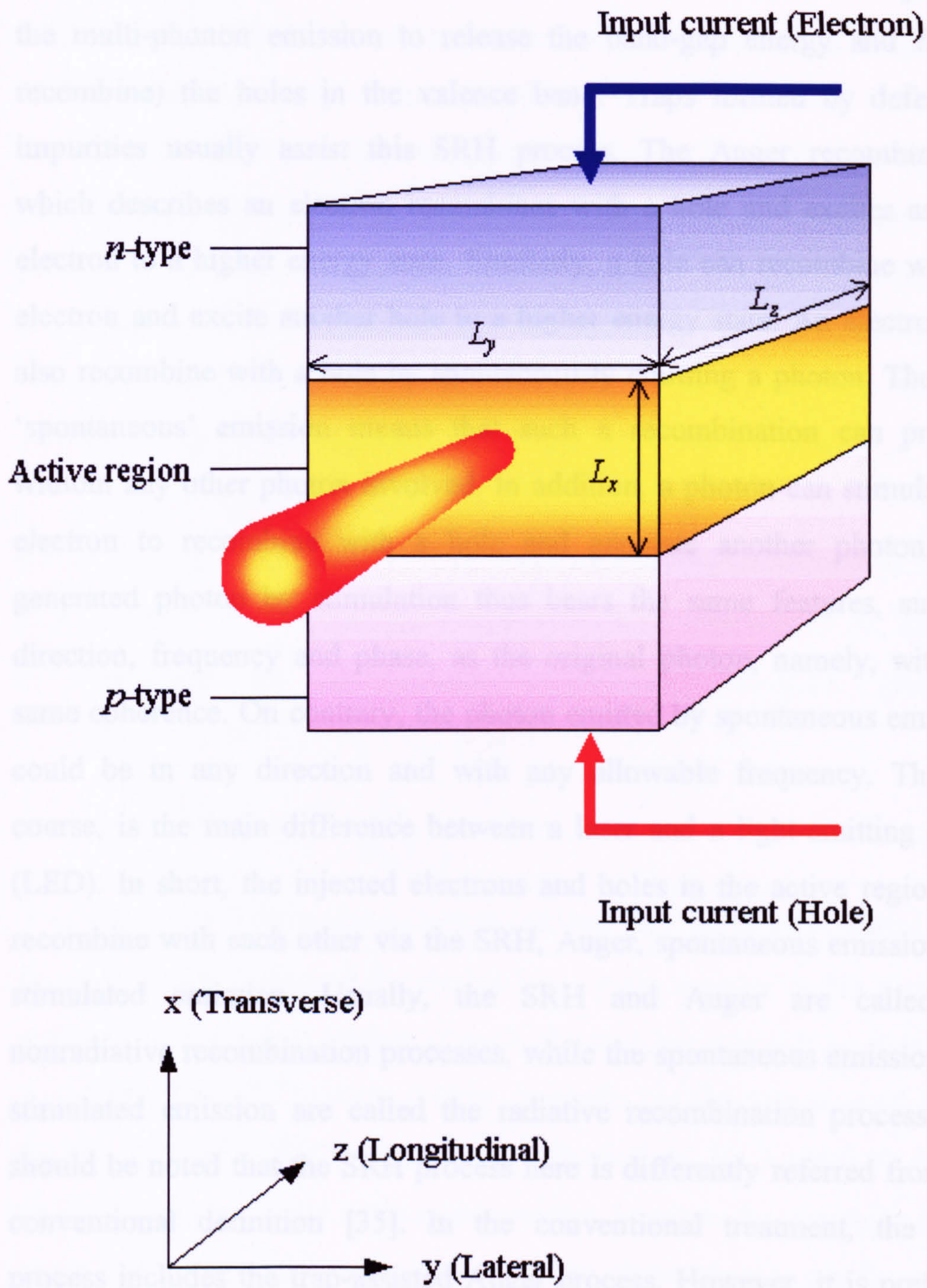


Fig. 2.10. Schematic diagram illustrating the volume of the active region.

recombination describes that the electrons in the conduction band proceed the multi-phonon emission to release the band-gap energy and fill (or recombine) the holes in the valence band. Traps formed by defects or impurities usually assist this SRH process. The Auger recombination, which describes an electron recombines with a hole and excites another electron to a higher energy state. Similarly, a hole can recombine with an electron and excite another hole to a higher energy state. An electron can also recombine with a hole by spontaneously emitting a photon. The term 'spontaneous' emission means that such a recombination can proceed without any other photon involved. In addition, a photon can stimulate an electron to recombine with a hole and generate another photon. The generated photon by stimulation thus bears the same features, such as direction, frequency and phase, as the original photon, namely, with the same coherence. On contrary, the photon emitted by spontaneous emission could be in any direction and with any allowable frequency. This, of course, is the main difference between a laser and a light-emitting diode (LED). In short, the injected electrons and holes in the active region can recombine with each other via the SRH, Auger, spontaneous emission and stimulated emission. Usually, the SRH and Auger are called the nonradiative recombination processes, while the spontaneous emission and stimulated emission are called the radiative recombination processes. It should be noted that the SRH process here is differently referred from the conventional definition [35]. In the conventional treatment, the SRH process includes the trap-assisted Auger process. However, it is preferred to include this process in the Auger process, while the definition of SRH is solely referred to the process of the trap-assisted interband multi-phonon emission [9].

The physical picture of the SRH process in the active region is illustrated in Fig. 11(a), in which an electron and a hole emit many phonons and recombine in a trap centre. The change rate of the carrier density via the SRH recombination is characterised by  $R_{SRH}$ . Calculating the  $R_{SRH}$  by first principles by considering the multi-phonon emission is an outstanding problem itself without a generally accepted answer. It is almost impractical to use any complicated formula for the SRH process in a circuit model. Nevertheless, the SRH recombination rate in semiconductor lasers is conventionally calculated by the following simplified formula [9]:

$$R_{SRH} \approx A_{SRH} (n - n_i) \quad (2.39)$$

where  $A_{SRH}$  is the coefficient of the SRH process,  $n_i$  is the intrinsic carrier density which characterises the electron and hole densities of the intrinsic semiconductors at the thermal equilibrium condition (that is,  $E_{Fe} = E_{Fh} \equiv E_i$  and  $T_e = T_h = T_L$ ) [35].

$$n_i = \sqrt{N_e N_h} \exp\left(-\frac{E_g}{2k_B T_L}\right) \quad (2.40)$$

Note that  $n = n_i$  before any current is injected into the semiconductor laser. Since the heating effect in the device is the main concern in this work, the temperature-dependent feature of each physical process will be discussed. In general, the SRH process mainly proceeds via the trap-assisted multi-phonon emission; therefore,  $A_{SRH}$  is supposed to be dependent on the carrier temperature and lattice temperature because the involvement of carriers and phonons. However, the SRH recombination is usually not the dominant recombination process in the active region, other recombination processes, such as spontaneous emission and Auger process are usually far more important than the SRH process in semiconductor lasers. Therefore,

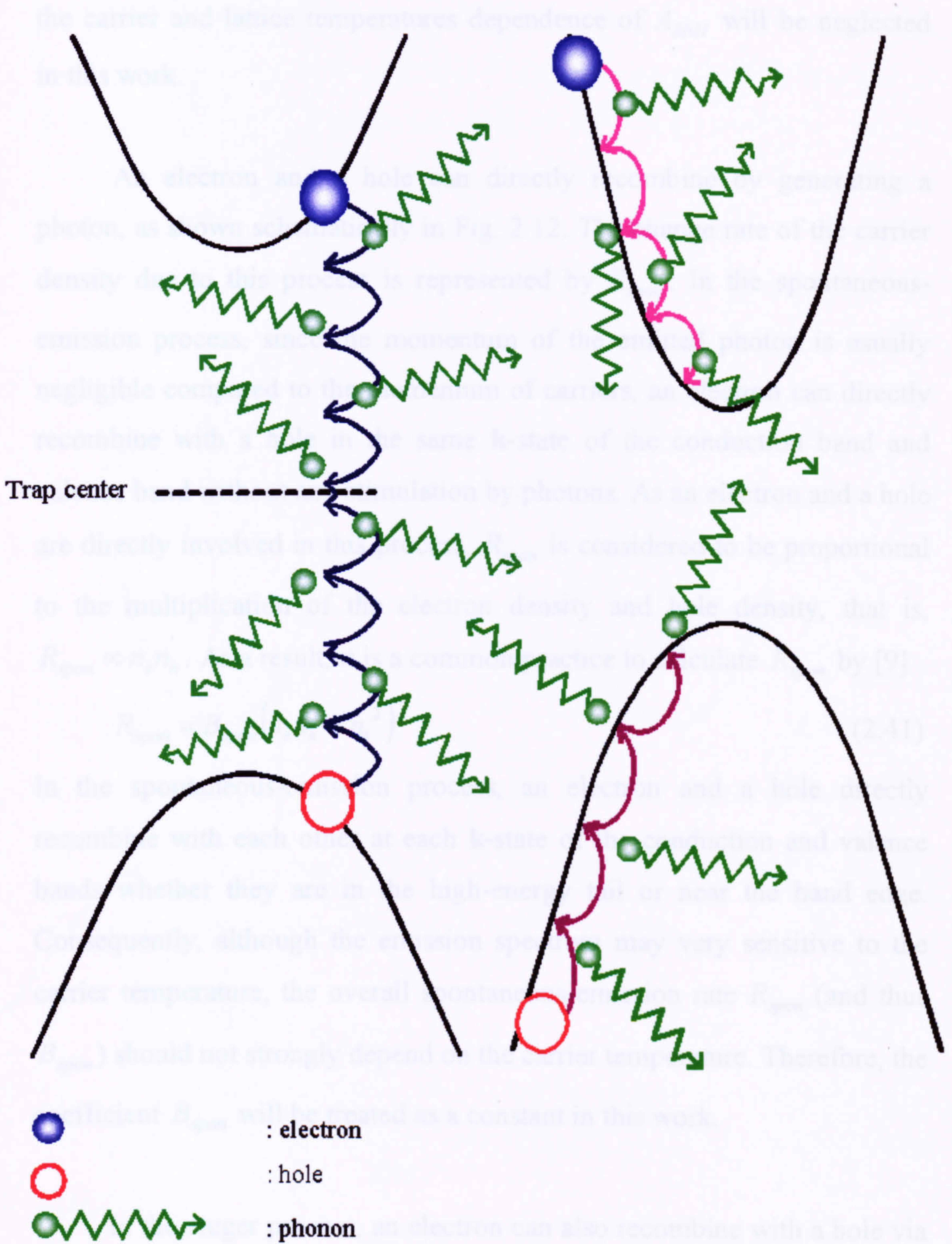


Fig. 2.11. (a) SRH (interband) (b) intraband carrier energy relaxation via emitting phonons.

the carrier and lattice temperatures dependence of  $A_{SRH}$  will be neglected in this work.

An electron and a hole can directly recombine by generating a photon, as shown schematically in Fig. 2.12. The change rate of the carrier density due to this process is represented by  $R_{spon}$ . In the spontaneous-emission process, since the momentum of the emitted photon is usually negligible compared to the momentum of carriers, an electron can directly recombine with a hole in the same  $\mathbf{k}$ -state of the conduction band and valence band without any stimulation by photons. As an electron and a hole are directly involved in this process,  $R_{spon}$  is considered to be proportional to the multiplication of the electron density and hole density, that is,  $R_{spon} \propto n_e n_h$ . As a result, it is a common practice to calculate  $R_{spon}$  by [9]

$$R_{spon} = B_{spon} (n_e n_h - n_i^2) \quad (2.41)$$

In the spontaneous-emission process, an electron and a hole directly recombine with each other at each  $\mathbf{k}$ -state of the conduction and valence bands whether they are in the high-energy tail or near the band edge. Consequently, although the emission spectrum may very sensitive to the carrier temperature, the overall spontaneous-emission rate  $R_{spon}$  (and thus  $B_{spon}$ ) should not strongly depend on the carrier temperature. Therefore, the coefficient  $B_{spon}$  will be treated as a constant in this work.

In the Auger process, an electron can also recombine with a hole via exciting another electron or hole to a higher energy state. The change rate of the carrier density due to this process is characterised by  $R_{Aug}$ .



Generally, the Auger process can be distinguished by direct or indirect (phonon-assisted or impurity-assisted) types. Each mechanism has several different routes by which electron-hole recombination proceeds, such as CCOH, CHHS and CHHL processes, as illustrated in Fig. 2.13. In addition, if the different valleys of the conduction band are further taken into account, the calculation of  $R_{Aug}$  becomes extremely involved. As a consequence, it is an almost numerically difficult problem to calculate  $R_{Aug}$  by first principles.

Since there are three carriers involving in the Auger process, the Auger recombination rate  $R_{Aug}$  is simply calculated by [9]

$$R_{Aug} = R_{Aug}^e + R_{Aug}^h \quad (2.42)$$

$$= C_{Aug}^e (n_1 n_2 - n_1^2 n_2^2) + C_{Aug}^h (n_1^2 n_2 - n_1^2 n_2^2) \quad (2.42)$$

where  $R_{Aug}^e$  represents the Auger process with two electrons and one hole (such as the CCOH process) and  $R_{Aug}^h$  represents the Auger process with two holes and an electron (such as the CHHS process).

It is commonly believed that  $R_{Aug}$  is very sensitive to the carrier temperature, especially for the material system with small band-gap energy.

The carrier-temperature dependent coefficient  $C_{Aug}$  can be characterized as suggested by Zory [30]

$$C_{Aug}(T_c) = C_{Aug}(300K) \exp \left[ \frac{E_g}{k_B} \left( \frac{1}{T_c} - \frac{1}{300} \right) \right] \quad (2.43)$$

where  $E_g = -0.0404 \text{ eV}$  and  $C_{Aug}(300K) = 4.22 \times 10^{-11} \text{ m}^3/\text{s}$  were

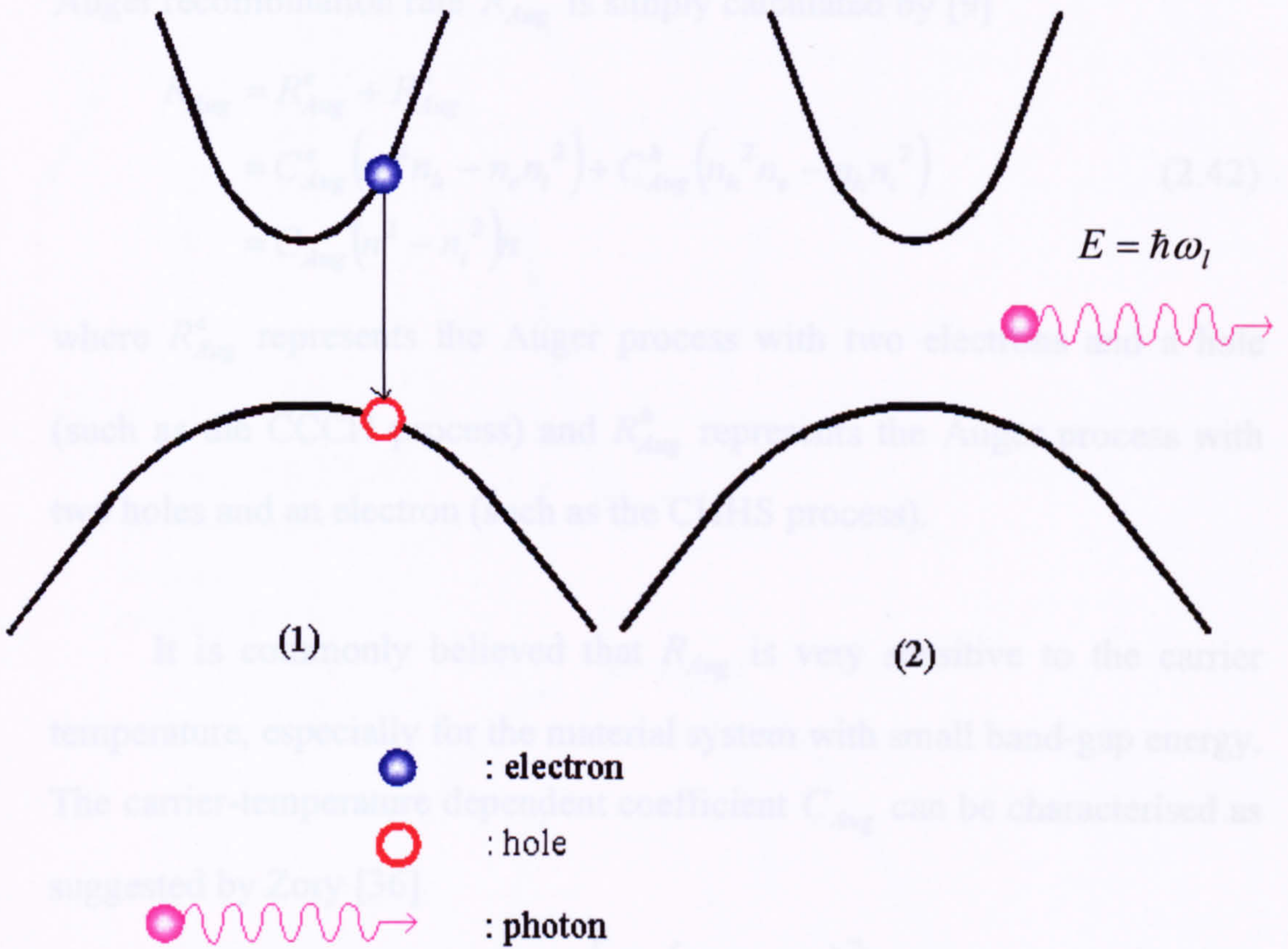


Fig. 2.12. Schematic diagram of spontaneous emission.

Generally, the Auger process can be distinguished by direct or indirect (phonon-assisted or impurity-assisted) types. Each mechanism has several different routes by which electron-hole recombination proceeds, such as CCCH, CHHS and CHHL processes, as illustrated in Fig. 2.13. In addition, if the different valleys of the conduction band are further taken into account, the calculation of  $R_{Aug}$  becomes extremely involved. As a consequence, it is an almost numerically difficult problem to calculate  $R_{Aug}$  by first principles.

Since there are three carriers involving in the Auger process, the Auger recombination rate  $R_{Aug}$  is simply calculated by [9]

$$\begin{aligned} R_{Aug} &= R_{Aug}^e + R_{Aug}^h \\ &= C_{Aug}^e (n_e^2 n_h - n_e n_i^2) + C_{Aug}^h (n_h^2 n_e - n_h n_i^2) \\ &= C_{Aug} (n^2 - n_i^2) n \end{aligned} \quad (2.42)$$

where  $R_{Aug}^e$  represents the Auger process with two electrons and a hole (such as the CCCH process) and  $R_{Aug}^h$  represents the Auger process with two holes and an electron (such as the CHHS process).

It is commonly believed that  $R_{Aug}$  is very sensitive to the carrier temperature, especially for the material system with small band-gap energy. The carrier-temperature dependent coefficient  $C_{Aug}$  can be characterised as suggested by Zory [36]

$$C_{Aug}^c(T_c) = C_{Aug}^c(300\text{K}) \exp\left[\frac{E_a}{k_B} \left(\frac{1}{T_c} - \frac{1}{300}\right)\right] \quad (2.43)$$

where  $E_a = -0.0404\text{ eV}$  and  $C_{Aug}^c(300\text{K}) = 4.22 \times 10^{-42}\text{ m}^6/\text{s}$  were

agreed. This formula will be implemented in the circuit model to discuss the effect of the carrier heating on the Auger process and thus the properties of semiconductor lasers.

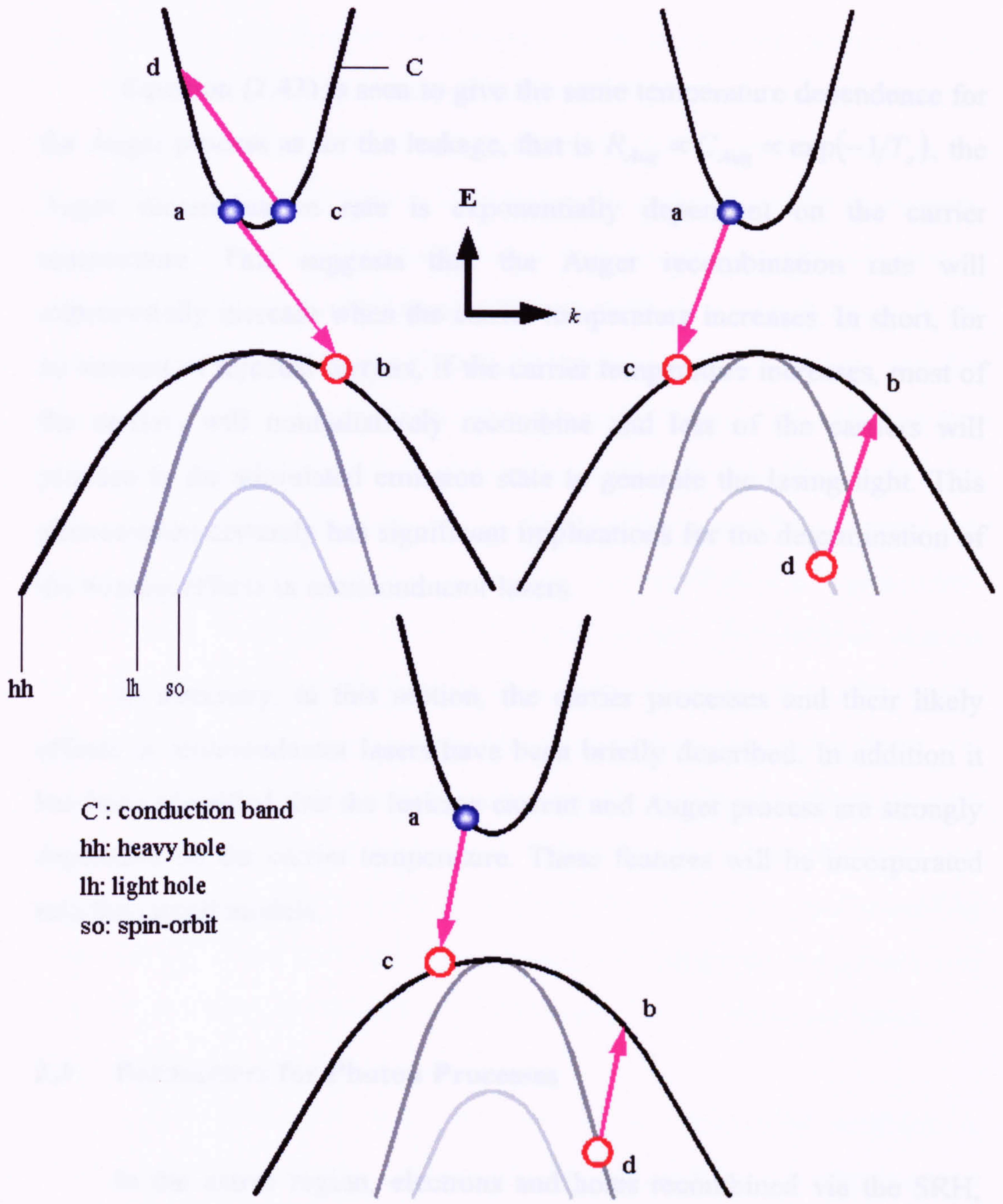


Fig. 2.13. Schematic diagram of Auger recombinations.

suggested. This formula will be implemented in the circuit model to discuss the effect of the carrier heating on the Auger process and thus the properties of semiconductor lasers.

Equation (2.43) is seen to give the same temperature dependence for the Auger process as for the leakage, that is  $R_{Aug} \propto C_{Aug} \propto \exp(-1/T_c)$ , the Auger recombination rate is exponentially dependent on the carrier temperature. This suggests that the Auger recombination rate will exponentially increase when the carrier temperature increases. In short, for an amount of injected carriers, if the carrier temperature increases, most of the carriers will nonradiatively recombine and less of the carriers will proceed to the stimulated emission state to generate the lasing light. This phenomenon certainly has significant implications for the determination of the heating effects in semiconductor lasers.

In summary, in this section, the carrier processes and their likely effects in semiconductor lasers have been briefly described. In addition it has been identified that the leakage current and Auger process are strongly dependent on the carrier temperature. These features will be incorporated into the circuit models.

### **2.3 Parameters for Photon Processes**

In the active region, electrons and holes recombined via the SRH, spontaneous emission and Auger process will not produce any 'lasing' light. However, in the stimulated-emission process, an electron can

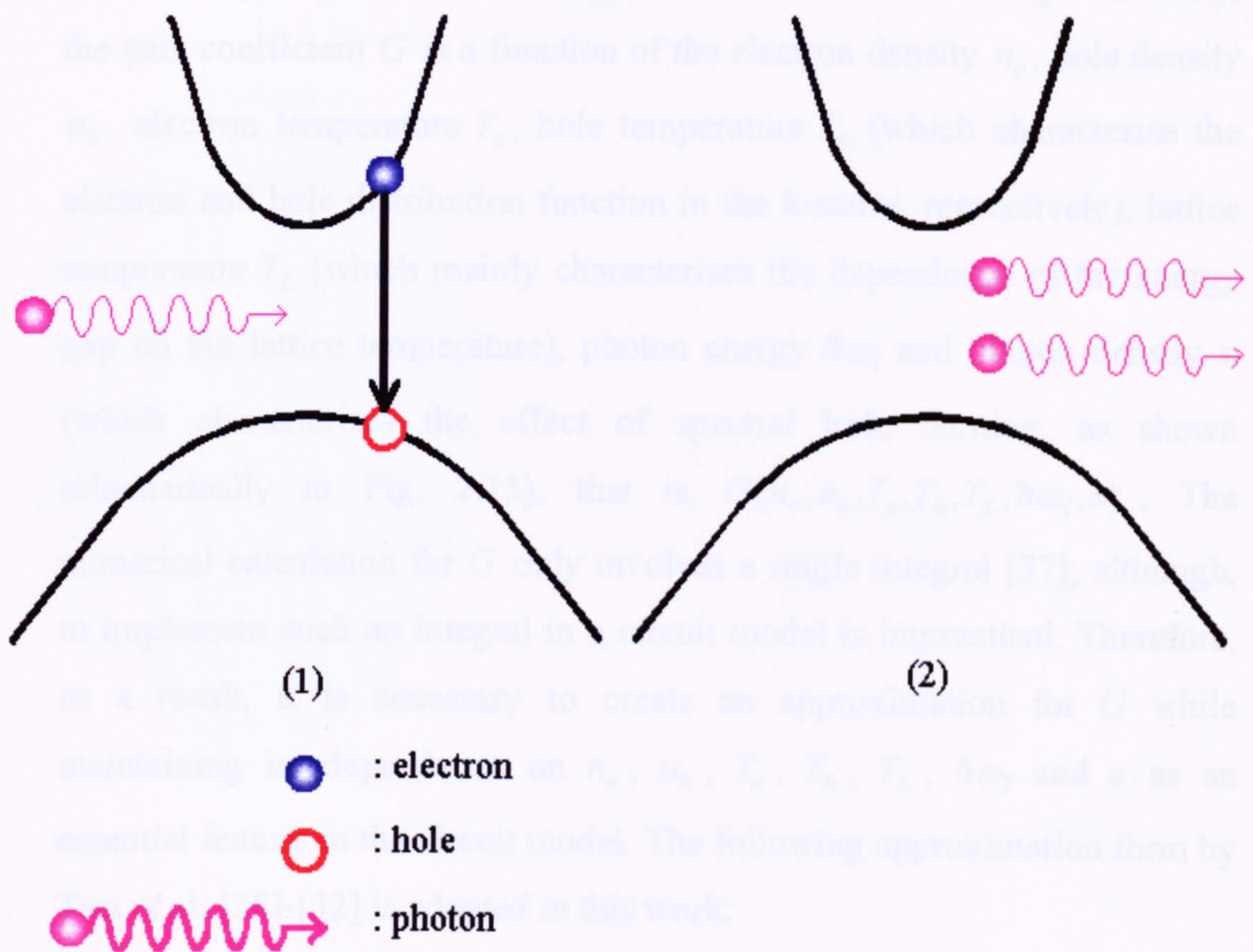
recombine with a hole in the presence of a photon and generate another photon, as shown diagrammatically in Fig. 2.14. The photon generated by the stimulated emission has the same characteristics as the original photon, and it can also stimulate an electron and a hole to generate another photon. In addition, an electron in the valence band can 'stimulatively' absorb a photon and transit into the conduction band, that is, leave a hole in the valence band at the same time. In other words, a photon can be absorbed to create a pair of an electron and a hole. Under the natural condition, that is, without any injection current, the photon absorption rate is much larger than the emission rate. As the current injects more electrons into the conduction band and more holes into the valence band, the emission rate will gradually increase and the absorption rate will decrease at the same time. When the current increases to a certain value where the emission rate equals to the absorption rate, the laser has reached the 'transparent' condition in which the photons propagate through the material without either loss or gain by stimulated process. However, at this stage, the photon will suffer from other loss mechanisms, such as free-carrier absorption. As the current increases further and reaches the 'threshold' condition, the gain provided by stimulated emission will overcome all the optical losses and the photons will start to amplify themselves. The device becomes an optical amplifier. However, in a laser, the feedback mechanism by the mirrors will force the amplifier to oscillate in a steady state, that is, lasing condition.

In semiconductor lasers, the term of the stimulated emission is actually referred as the net stimulated emission, that is, the emission rate minus the absorption rate. Apparently, the stimulated-emission process will

consume carriers and generate photons. The change rate of the carrier density by stimulated emission is usually described by the relationship

$$R_{\text{stim}} = u_g G \quad (2.44)$$

where  $u_g = c_0/n_g$  is the group velocity of photons,  $c_0$  is the speed of light in free space,  $n_g$  is the effective refractive index for the group velocity and  $G$  is the gain coefficient defined by the optical susceptibility that is induced by carrier injection. Calculating the gain coefficient by first principles by considering the details of the stimulated emission processes have been intensively investigated and can be referred to many textbooks [8]-[11], [23]-[35]. The results are summarized in the following: Generally,



$$G = \frac{e_1(n_1 - n_2) - e_2(\sigma_1 - \sigma_2) - e_3(\tau_1 - \tau_2) - e_4(\sigma_1 - \sigma_2)}{(1 + \epsilon_{\text{ph}})} \quad (2.45)$$

Fig. 2.14. Schematic diagram of stimulated emission.

consume carriers and generate photons. The change rate of the carrier density by stimulated emission is usually described by the relationship

$$R_{stim} = \nu_g G s \quad (2.44)$$

where  $\nu_g = c_0/n_g$  is the group velocity of photons,  $c_0$  is the speed of light in free space,  $n_g$  is the effective refractive index for the group velocity and  $G$  is the gain coefficient defined by the optical susceptibility that is induced by carrier injection. Calculating the gain coefficient by first principles by considering the details of the stimulated emission processes have been intensively investigated and can be referred to many textbooks [8]-[11][33]-[35]. The results are summarised in the following: Generally, the gain coefficient  $G$  is a function of the electron density  $n_e$ , hole density  $n_h$ , electron temperature  $T_e$ , hole temperature  $T_h$  (which characterise the electron and hole distribution function in the  $k$ -states, respectively), lattice temperature  $T_L$  (which mainly characterises the dependence of the energy gap on the lattice temperature), photon energy  $\hbar\omega_l$  and photon density  $s$  (which characterises the effect of spectral hole burning, as shown schematically in Fig. 2.15), that is,  $G(n_e, n_h, T_e, T_h, T_L, \hbar\omega_l, s)$ . The numerical calculation for  $G$  only involves a single integral [37]; although, to implement such an integral in a circuit model is impractical. Therefore, as a result, it is necessary to create an approximation for  $G$  while maintaining its dependence on  $n_e$ ,  $n_h$ ,  $T_e$ ,  $T_h$ ,  $T_L$ ,  $\hbar\omega_l$  and  $s$  as an essential feature in the circuit model. The following approximation form by Tsai et al. [28]-[32] is adapted in this work:

$$G = \frac{g_n(n - n_{tr}) - g_{T_e}(T_e - T_0) - g_{T_h}(T_h - T_0) - g_{T_L}(T_L - T_0)}{(1 + \varepsilon_{shb}s)} \quad (2.45)$$

Here  $n_{tr}$  is the carrier density in transparent condition when  $G = 0$ .  $\varepsilon_{shb}$  is

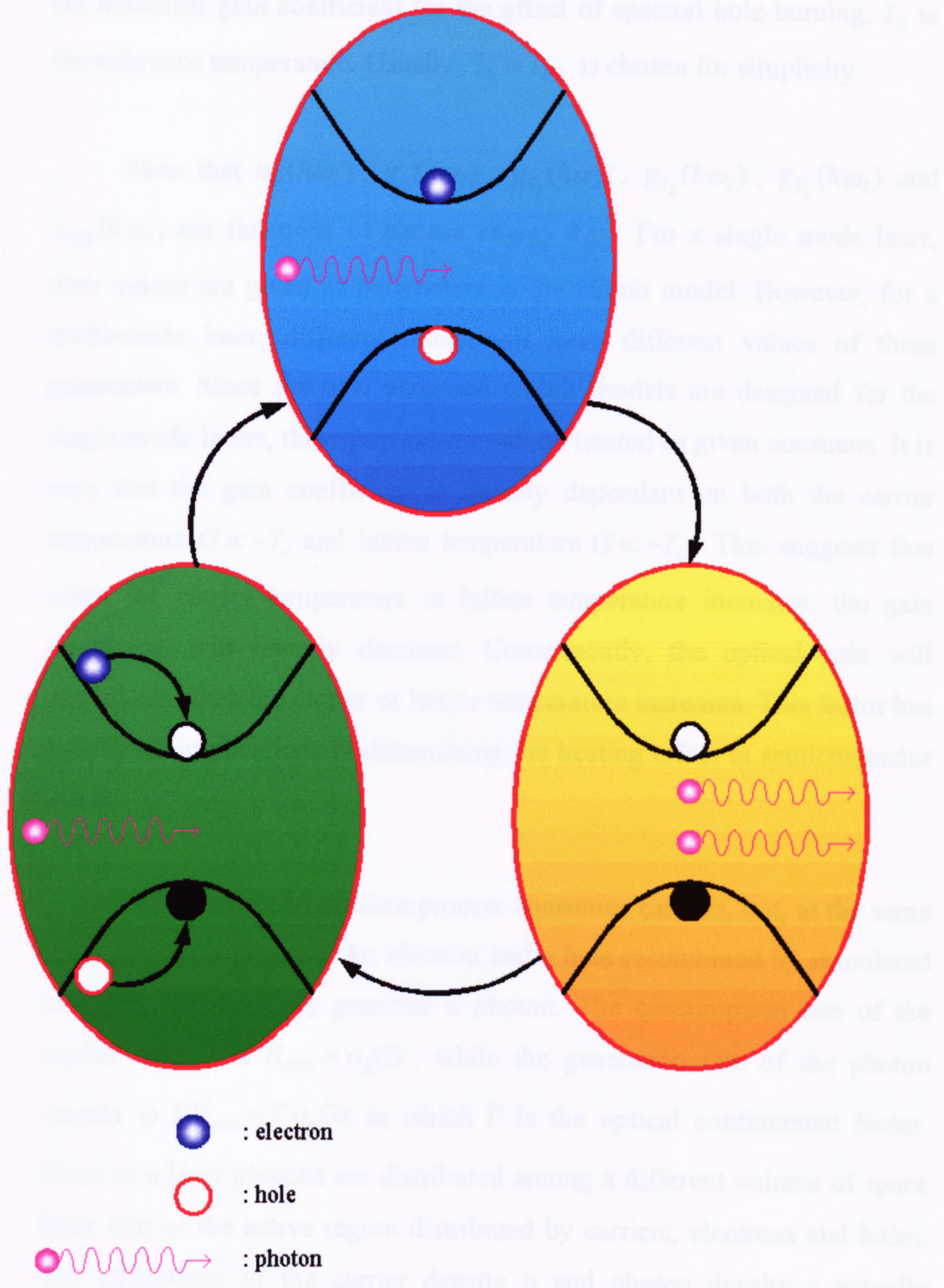


Fig. 2.15. Schematic diagram of spectral hole burning.



the nonlinear gain coefficient for the effect of spectral hole burning.  $T_0$  is the reference temperature. Usually,  $T_0 = T_{HS}$  is chosen for simplicity.

Note that  $n_{tr}(\hbar\omega_l)$ ,  $g_n(\hbar\omega_l)$ ,  $g_{T_c}(\hbar\omega_l)$ ,  $g_{T_h}(\hbar\omega_l)$ ,  $g_{T_L}(\hbar\omega_l)$  and  $\varepsilon_{shb}(\hbar\omega_l)$  are functions of photon energy  $\hbar\omega_l$ . For a single mode laser, their values are given as parameters in the circuit model. However, for a multi-mode laser, different mode will have different values of these parameters. Since the new proposed circuit models are designed for the single-mode lasers, these parameters will be treated as given constants. It is seen that the gain coefficient is linearly dependent on both the carrier temperature  $G \propto -T_c$  and lattice temperature  $G \propto -T_L$ . This suggests that when the carrier temperature or lattice temperature increases, the gain coefficient will linearly decrease. Consequently, the optical gain will deteriorate when the carrier or lattice temperature increases. This factor has significant implications in determining the heating effect in semiconductor lasers.

The stimulated-emission process consumes carriers, but, at the same time, generates photons. An electron and a hole recombined by stimulated emission will certainly generate a photon. The consumption rate of the carrier density is  $R_{stim} = \nu_g G s$ , while the generation rate of the photon density is  $\Gamma R_{stim} = \Gamma \nu_g G s$  in which  $\Gamma$  is the optical confinement factor. Since in a laser photons are distributed among a different volume of space from that of the active region distributed by carriers, electrons and holes. The definitions of the carrier density  $n$  and photon density  $s$  actually referred to different volumes. That is, even the recombination rate of the carrier number equals the generation rate of the photon number, their

'density' change rates will be different when they are referred to different distributed volumes. This is the reason for introducing the optical confinement factor  $\Gamma$  for photons, and  $R_{stim}$  is determined by carriers. Therefore, the optical confinement factor is defined as  $\Gamma$  characterising the overlap between the carrier density in the active region and optical field in the device, as shown schematically in Fig. 2.16.

For carriers, the injection current supplies carriers and the recombinations deplete carriers. Similarly for photons, the stimulated emission generates photons and the optical loss depletes photons in the cavity. Photons are generated by stimulated emission will go through the mirrors and become useful output, or be absorbed inside the cavity, or be randomly scattered outside the cavity. The loss rate of the photon density due to these processes is characterised by the photon lifetime  $\tau_s$ . Generally, the photon lifetime in the cavity is calculated by

$$\frac{1}{\tau_s} = v_g (\alpha_{int} + \alpha_{mirr}) \quad (2.46)$$

where  $\alpha_{int}$  and  $\alpha_{mirr}$  are the absorption coefficients due to internal losses and mirror losses, respectively. The mirror losses describe the photons going through the two mirrors and becoming a useful output. If the reflectivities of these two mirrors are  $R_1$  and  $R_2$ , respectively, and the distance between them is  $L_z$ , then the mirror losses  $\alpha_{mirr}$  can be calculated by [9]

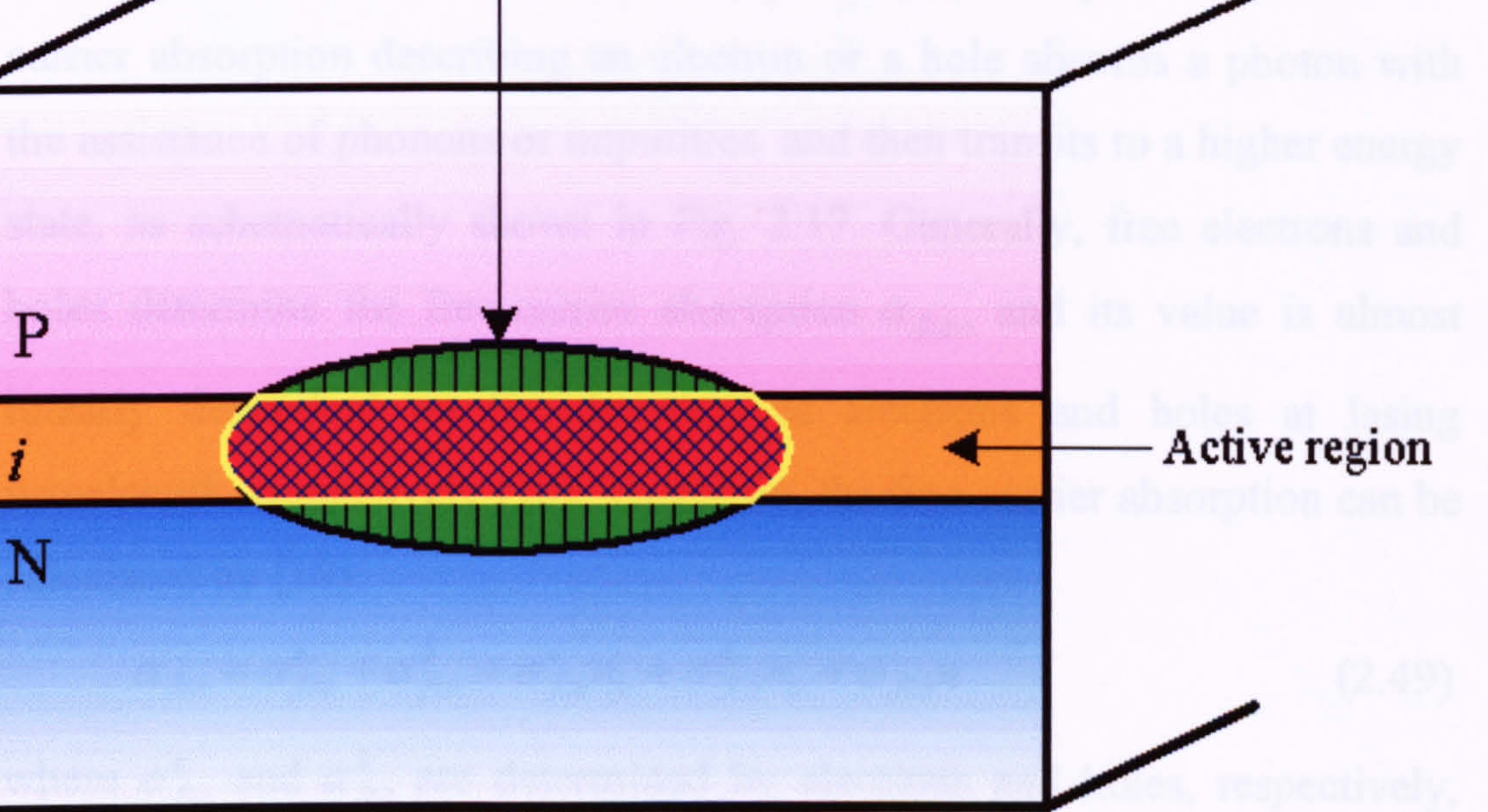
$$\alpha_{mirr} = \frac{1}{2L_z} \ln \left( \frac{1}{R_1 R_2} \right) \quad (2.47)$$

There are several physical processes that contribute to the internal losses where the photons are absorbed or scattered. Generally, it was believed that

the major contributions of the internal losses due to the free-carrier absorption, scattering and coupling, and its value can be calculated by [9]

$$\alpha_{int} = \Gamma \alpha_{p,act} + (1 - \Gamma) \alpha_{p,pass} + \alpha_s + \alpha_c \quad (2.48)$$

where  $\Gamma \alpha_{p,act}$  and  $(1 - \Gamma) \alpha_{p,pass}$  are the free-carrier absorption in the active region and passive region, respectively.  $\alpha_s$  is the scattering loss due to the scattering of photons by material interfaces, junctions, impurities, defects and strains.  $\alpha_c$  is the coupling loss due to the optical field spreading beyond the confinement layers because the wave nature of photons. However, it has been shown that free-carrier absorption is the dominant optical loss in semiconductor lasers [9]. The physical process of the free-carrier absorption depends on the absorption of a hole electron or a photon with the assistance of phonon participation, and then transitions to a higher energy state, which is accompanied by the emission of a photon, free electrons and holes, respectively. Its value is almost independent of the laser wavelength and layer thickness. Free-carrier absorption can be calculated by [10]



Optical confinement factor =  $\frac{\text{area} \text{ (red cross-hatched oval)}}{\text{area} \text{ (green oval)}}$  experimentally

$$\alpha_{p,act} (\text{m}^{-1}) = 3 \times 10^{-20} n_2 (\text{m}^{-3}) + 7 \times 10^{-20} N_2 (\text{m}^{-3}) \quad (2.50)$$

This relationship will be implemented in the new proposed circuit models.

Fig. 2.16. Schematic diagram of the optical confinement factor.

the major contributions of the internal losses due to the free-carrier absorption, scattering and coupling, and its value can be calculated by [9]

$$\alpha_{int} = \Gamma\alpha_{fca,a} + (1 - \Gamma)\alpha_{fca,p} + \alpha_s + \alpha_c \quad (2.48)$$

where  $\Gamma\alpha_{fca,a}$  and  $(1 - \Gamma)\alpha_{fca,p}$  are the free-carrier absorption in the active region and passive region, respectively.  $\alpha_s$  is the scattering loss due to the scattering of photons by material interfaces, junctions, impurities, defects and strains.  $\alpha_c$  is the coupling loss due to the optical field spreading beyond the confinement layers because the wave nature of photons. However, it has been shown that free-carrier absorption is the dominant optical loss in semiconductor lasers [9]. The physical process of the free-carrier absorption describing an electron or a hole absorbs a photon with the assistance of phonons or impurities, and then transits to a higher energy state, as schematically shown in Fig. 2.17. Generally, free electrons and holes determine the free-carrier absorption  $\alpha_{fca}$ , and its value is almost linearly dependent on the densities of electrons and holes at lasing wavelength, respectively [10]. Therefore, the free-carrier absorption can be calculated by [10]:

$$\alpha_{fca} = \alpha_{fca}^e + \alpha_{fca}^h = \sigma_{fca}^e n_e + \sigma_{fca}^h n_h = \sigma_{fca} n \quad (2.49)$$

where  $\alpha_{fca}^e$  and  $\alpha_{fca}^h$  are determined by electrons and holes, respectively, and  $\sigma_{fca}^e$  and  $\sigma_{fca}^h$  are their associated coefficients. Although  $\alpha_{fca}$  can be calculated by first principles, for GaAs, which magnitude is experimentally determined by [34]

$$\alpha_{fca} (\text{m}^{-1}) \approx 3 \times 10^{-22} n_e (\text{m}^{-3}) + 7 \times 10^{-22} n_h (\text{m}^{-3}) \quad (2.50)$$

This relationship will be implemented in the new proposed circuit models.

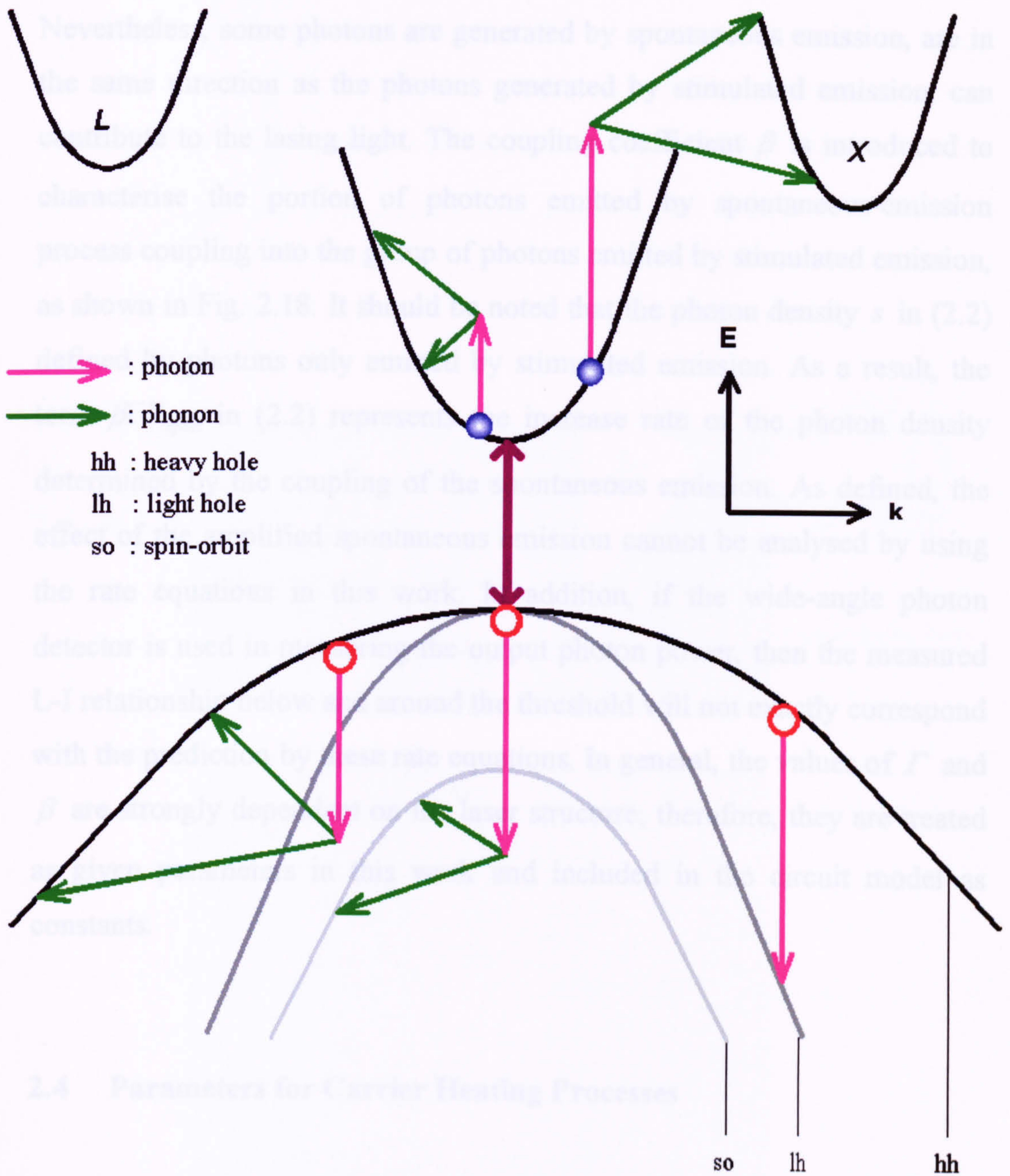


Fig. 2.17. Schematic diagram of free-carrier absorption.

Photons are created not only by stimulated emission but also by spontaneous emission; therefore, the spontaneous emission should also contribute to the photon generation. However, for semiconductor lasers, the photons generated by stimulated emission are the main interest. Nevertheless, some photons are generated by spontaneous emission, are in the same direction as the photons generated by stimulated emission, can contribute to the lasing light. The coupling coefficient  $\beta$  is introduced to characterise the portion of photons emitted by spontaneous-emission process coupling into the group of photons emitted by stimulated emission, as shown in Fig. 2.18. It should be noted that the photon density  $s$  in (2.2) defined by photons only emitted by stimulated emission. As a result, the term  $\beta\Gamma R_{spont}$  in (2.2) represents the increase rate of the photon density determined by the coupling of the spontaneous emission. As defined, the effect of the amplified spontaneous emission cannot be analysed by using the rate equations in this work. In addition, if the wide-angle photon detector is used in measuring the output photon power, then the measured L-I relationship below and around the threshold will not exactly correspond with the prediction by these rate equations. In general, the values of  $\Gamma$  and  $\beta$  are strongly dependent on the laser structure; therefore, they are treated as given parameters in this work and included in the circuit model as constants.

## 2.4 Parameters for Carrier Heating Processes

In a semiconductor laser, the injection current supplies energy to carriers; these carriers then release their energy to lattice by carrier-lattice

collisions, that is, carrier-phonon interactions. Therefore, it is expected that the carrier heating and lattice heating will both be presented in semiconductor lasers; however, the carrier temperature and lattice temperature will be different from the condition where there is no injection current. In the active region of semiconductor lasers, the major heating mechanisms for carriers are due to the injection current, stimulated recombination, free-carrier absorption, and carrier-phonon interactions.

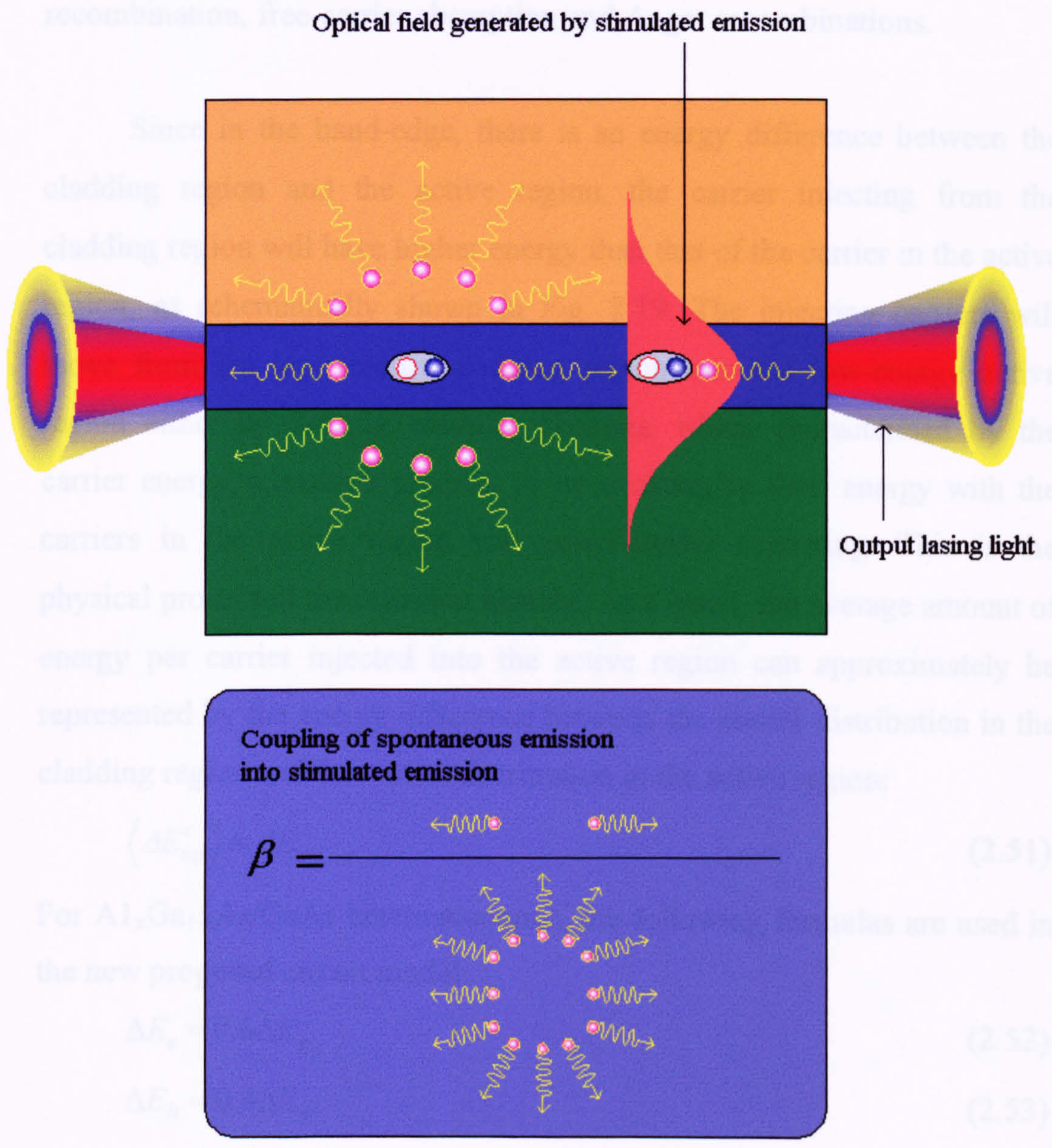


Fig. 2.18. Schematic diagram of the coupling coefficient for spontaneous emission.

collisions, that is, carrier-phonon interactions. Therefore, it is expected that the carrier heating and lattice heating will both be presented in semiconductor lasers; however, the carrier temperature and lattice temperature will be different from the condition where there is no injection current. In the active region of semiconductor lasers, the major heating mechanisms for carriers are due to the injection current, stimulated recombination, free-carrier absorption and Auger recombinations.

Since in the band-edge, there is an energy difference between the cladding region and the active region, the carrier injecting from the cladding region will have higher energy than that of the carrier in the active region, as schematically shown in Fig. 2.19. The injecting carriers will move from the high-energy cladding region into the low-energy active region either by directly emitting phonons, which characterised by the carrier energy relaxation process, or by exchanging their energy with the carriers in the active region via carrier-carrier scattering. This is the physical process of the injection heating. As a result, the average amount of energy per carrier injected into the active region can approximately be represented by the energy difference between the carrier distribution in the cladding region and the carrier distribution in the active region:

$$\langle \Delta E_{inj}^c \rangle = \Delta E_c \quad (2.51)$$

For  $\text{Al}_x\text{Ga}_{1-x}\text{As}/\text{GaAs}$  heterostructures, the following formulas are used in the new proposed circuit model:

$$\Delta E_e = 0.6\Delta E_g \quad (2.52)$$

$$\Delta E_h = 0.4\Delta E_g \quad (2.53)$$

$$\Delta E_g = E_g(\text{Al}_x\text{Ga}_{1-x}\text{As}) - E_g(\text{GaAs}) \quad (2.54)$$



Since the actual current goes into the active region is  $\eta_{inj}I_{inj} - I_{loss}$ , the power density generated by the injection heating is

$$\left(\frac{dW_c}{dt}\right)_{inj} = (\Delta E_{inj}) \frac{\eta_{inj}I_{inj} - I_{loss}}{eV} \quad (2.55)$$

The change rate of the carrier temperature due to the injection heating will be

$$\left(\frac{dT_c}{dt}\right)_{inj} = \left(\frac{\partial W_c}{\partial T}\right)^{-1} (\Delta E_{inj}) \frac{\eta_{inj}I_{inj} - I_{loss}}{eV} \quad (2.56)$$

Spontaneous emission deprives a pair of an electron and a hole, and thus removes a certain amount of energy from carriers. It should be noted that the simulated recombination process removes not only the carrier energy but also the carriers themselves. The carrier temperature defined under the quasi-equilibrium condition maintained by the carrier-carrier scattering, which can statistically be viewed as the average energy of the whole carrier system, will certainly change according to the change of the average energy of the whole carrier system. This will be more clearly illustrated by the following derivations. The loss rate of the carrier energy density due to the simulated emission can be expressed by:

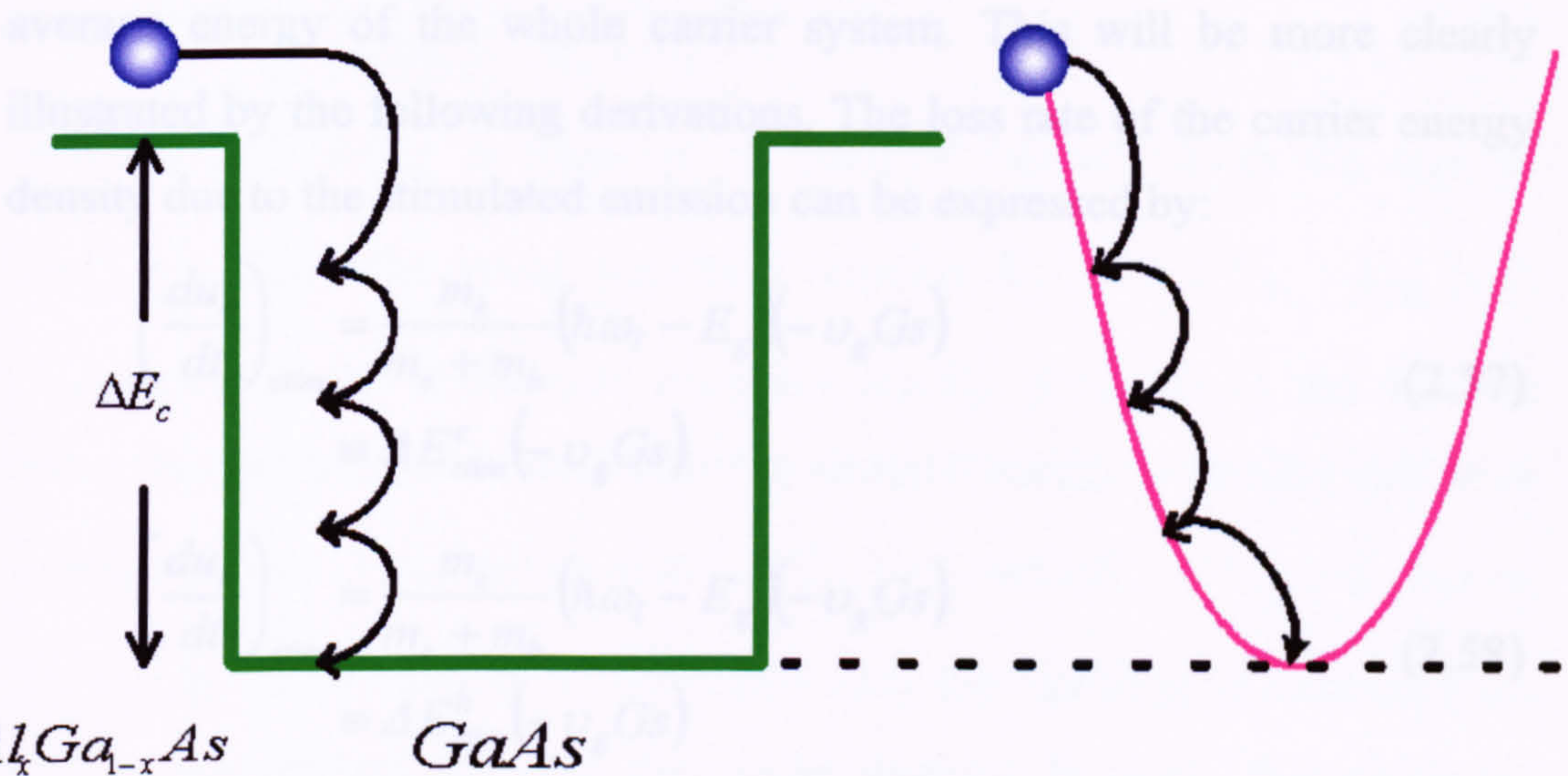


Fig. 2.19. Schematic diagram of carrier energy relaxation in the injection heating process.

Since the actual current goes into the active region is  $\eta_{inj}I_{inj} - I_{leak}$ , the power density generated by the injection heating is

$$\left(\frac{du_c}{dt}\right)_{inj} = \langle \Delta E_{inj}^c \rangle \frac{\eta_{inj}I_{inj} - I_{leak}}{eV} \quad (2.55)$$

The change rate of the carrier temperature due to the injection heating will be

$$\left(\frac{dT_c}{dt}\right)_{inj} \cong \left(\frac{\partial u_c}{\partial T}\right)^{-1} \langle \Delta E_{inj}^c \rangle \frac{\eta_{inj}I_{inj} - I_{leak}}{eV} \quad (2.56)$$

Simulated emission deprives a pair of an electron and a hole, and thus removes a certain amount of energy from carriers. It should be noted that the stimulated recombination process removes not only the carrier energy but also the carriers themselves. The carrier temperature defined under the quasi-equilibrium condition maintained by the carrier-carrier scattering, which can statistically be viewed as the average energy of the whole carrier system, will certainly change according to the change of the average energy of the whole carrier system. This will be more clearly illustrated by the following derivations. The loss rate of the carrier energy density due to the stimulated emission can be expressed by:

$$\begin{aligned} \left(\frac{du_e}{dt}\right)_{stim} &= \frac{m_h}{m_e + m_h} (\hbar\omega_l - E_g) (-\nu_g Gs) \\ &\equiv \Delta E_{stim}^e (-\nu_g Gs) \end{aligned} \quad (2.57)$$

$$\begin{aligned} \left(\frac{du_h}{dt}\right)_{stim} &= \frac{m_e}{m_e + m_h} (\hbar\omega_l - E_g) (-\nu_g Gs) \\ &\equiv \Delta E_{stim}^h (-\nu_g Gs) \end{aligned} \quad (2.58)$$

Since the carrier energy density  $u_c$  is a function of the carrier density  $n_c$  and the carrier temperature  $T_c$ , by the chain rule of partial differentiation,

$$\left(\frac{du_c}{dt}\right)_{stim} = \left(\frac{\partial u_c}{\partial n_c}\right)\left(\frac{dn_c}{dt}\right)_{stim} + \left(\frac{\partial u_c}{\partial T_c}\right)\left(\frac{dT_c}{dt}\right)_{stim} \quad (2.59)$$

In order to manifest the change of the carrier temperature  $(dT_c/dt)_{stim}$ , the above equation can be rearranged as the following:

$$\begin{aligned} \left(\frac{dT_c}{dt}\right)_{stim} &= \left(\frac{\partial u_c}{\partial T_c}\right)^{-1} \left[ \left(\frac{du_c}{dt}\right)_{stim} - \left(\frac{\partial u_c}{\partial n_c}\right)\left(\frac{dn_c}{dt}\right)_{stim} \right] \\ &= \left(\frac{\partial u_c}{\partial T_c}\right)^{-1} \left[ \left(\frac{\partial u_c}{\partial n_c}\right) - \Delta E_{stim}^c \right] \nu_g Gs \\ &\equiv \left(\frac{\partial u_c}{\partial T_c}\right)^{-1} \langle \Delta E_{stim}^c \rangle \nu_g Gs \end{aligned} \quad (2.60)$$

Note that  $(dn_c/dt)_{stim} = -\nu_g Gs$  and  $(\partial u_c/\partial n_c)$  represent the average energy per carrier. From the definition, the average energy change per carrier due to the stimulated recombination becomes

$$\langle \Delta E_{stim}^e \rangle = \left(\frac{\partial u_e}{\partial n_e}\right) - \frac{m_h}{m_e + m_h} (\hbar\omega_l - E_g) \quad (2.61)$$

$$\langle \Delta E_{stim}^h \rangle = \left(\frac{\partial u_h}{\partial n_h}\right) - \frac{m_e}{m_e + m_h} (\hbar\omega_l - E_g) \quad (2.62)$$

Whether  $(dT_c/dt)_{stim}$  is negative or positive depends upon the sign of  $\langle \Delta E_{stim}^c \rangle$ . Since the lasing condition requires  $E_g \leq \hbar\omega_l \leq E_{Fe} - E_{Fh}$  [10]. Consequently, the stimulated emission usually proceeds in the  $\mathbf{k}$ -states between electrons and holes where the carriers' energy is smaller than their average energy. This implies that  $\langle \Delta E_{stim}^c \rangle > 0$  and  $(dT_c/dt)_{stim} > 0$ , that is, the carrier recombination by stimulated emission resulting in increasing the carrier temperature and thus the carrier heating. In short, the stimulated recombination removes the carriers from the lower-energy states; therefore the average energy of the whole carrier system will increase and thus the

carrier temperature increases. It should be noted that although the stimulated emission reduces the total carrier energy but it increases the *average* carrier energy and thus the carrier temperature, because the carrier temperature is proportional to the average carrier energy rather than the whole carrier energy.

The Auger recombination heating describes an electron and a hole recombine with each other by exciting another electron or hole to a higher energy state. For example, in the case of the Auger process that involves recombining an electron and a hole and exciting another electron into a higher energy state, that is, CCCH process [9], the electron system will approximately gain the amount of the band-gap energy. Alternatively, if a hole recombines with an electron via exciting another hole into a higher energy state, such as CHHS process, the hole system will approximately gain the amount of the band-gap energy. Therefore, in this work, it is assumed that the average energy variation for each Auger process is just the band-gap energy; that is,

$$\langle \Delta E_{Aug}^c \rangle \approx E_g \quad (2.63)$$

As a result, the power density generated by the Auger recombination is

$$\left( \frac{du_c}{dt} \right)_{Aug} = \langle \Delta E_{Aug}^c \rangle R_{Aug} \quad (2.64)$$

The change rate of the carrier temperature due to the Auger recombination heating is

$$\left( \frac{dT_c}{dt} \right)_{Aug} \cong \left( \frac{\partial u_c}{\partial T_c} \right)^{-1} \langle \Delta E_{inj}^c \rangle R_{Aug}^c \quad (2.65)$$

It should be noted that, by the original definition of the recombination heating, the SRH and spontaneous-emission recombination processes might

also induce a certain amount of the carrier heating. However, generally their magnitudes should be much smaller than that of the Auger recombination heating and will be neglected in this work.

In the process of free-carrier absorption, a carrier will absorb a photon and transit into a higher energy state. In this process, a carrier will gain an exact amount of one-photon energy. Therefore,

$$\langle \Delta E_{fca}^c \rangle = \hbar \omega_l \quad (2.66)$$

The power density generated by the free-carrier absorption is

$$\left( \frac{du_c}{dt} \right)_{fca} = \langle \Delta E_{fca}^c \rangle \nu_g \alpha_{fca}^c S \quad (2.67)$$

The change rate of the carrier temperature due to the free-carrier-absorption heating is

$$\left( \frac{dT_c}{dt} \right)_{fca} = \left( \frac{\partial u_c}{\partial T_c} \right)^{-1} \langle \Delta E_{fca}^c \rangle \nu_g \alpha_{fca}^c S \quad (2.68)$$

Since the free-carrier-absorption process does not consume any electron-hole pairs, that is,  $(dn_c/dt)_{fca} = 0$ , therefore,  $\langle \Delta E_{fca}^c \rangle$  in (2.68) does not have the term  $(\partial u_c / \partial n_c)$  as in the case of the stimulated-emission heating.

In the active region, carriers can increase their temperature via the injection heating, stimulated recombination heating, Auger recombination heating and free-carrier-absorption heating. Therefore, they need some cooling processes to reduce their temperature to keep the balance of the energy flow. In order to cool their temperature and thereby reach mutual thermal equilibrium with the ambient environment, carriers must exchange their energy either with the phonon bath via phonon emission or with the

photon bath via thermal photon emission (i.e., black-body radiation). For solid-state devices, carrier energy relaxation via the phonon emission is usually much more efficient than via the photon emission. In semiconductor lasers, photons are generated by stimulated emission do not help carriers to cool down their temperature but increase the carrier temperature. As a result, it can be assumed that carriers relax their energy by emitting phonons in semiconductor lasers. If the carrier system is assumed to maintain its quasi-equilibrium with temperature  $T_c$  and the phonon system is assumed to maintain its thermal equilibrium with temperature  $T_L$ , then the carrier energy relaxation rate, that is, the loss rate of the power density, within the conduction band or valence band can be expressed by

$$\left(\frac{du_c}{dt}\right)_{c-L} = -\frac{u_c(T_c) - u_c(T_L)}{\tau_{c-L}} \quad (2.69)$$

where  $\tau_{c-L}$  is defined by the carrier energy relaxation time characterising the time scale for  $T_c$  to equalise with  $T_L$ . The value of the carrier energy relaxation time  $\tau_{c-L}$  is typically within a range of several picosecond [37].

It should be noted that electrons and holes not only exchange their energy with lattice via electron-phonon and hole-phonon scattering but also exchange energy with each other by electron-hole scattering and phonon-bath sharing. Since the effective mass of electron is much smaller than the effective mass of hole, the electron heating is supposed to be more severe than the hole heating when electrons and holes are under the same condition of energy injection. As a result, the electron temperature is naturally higher than the hole temperature, and inevitably electrons will transfer parts of their energy to holes to equalise their temperatures. The

electron energy relaxation rate due to the electron-hole energy transfer can be expressed by

$$\left(\frac{du_e}{dt}\right)_{e-h} = -\frac{u_e(T_e) - u_e(T_h)}{\tau_{e-h}} = -\left(\frac{du_h}{dt}\right)_{h-e} \quad (2.70)$$

where  $\tau_{e-h}$  is the electron-hole energy exchange time characterising the time scale for  $T_e$  to equalise with  $T_h$ . It should be emphasised again that although the electron-hole scattering provides a direct route for such energy exchange, electrons might also indirectly transfer their energy to holes via phonon bath sharing in which phonons emitted by electrons are absorbed by holes. Note that the negative sign before  $(du_h/dt)_{h-e}$  indicates that the energy released by electrons is obtained by holes.

Apparently, carriers release their energy by emitting phonons, and the released energy will be obtained by the phonon system. Therefore, the lattice will increase their temperature by the carrier energy relaxation processes. Similarly, the lattice needs some cooling mechanisms to reduce its temperature in order to keep the balance of energy flow. In fact, the lattice is cooled via the thermal-conduction process. This will be discussed in the next section.

## 2.5 Parameters for Lattice Heating Processes

Thermal-conduction processes of phonons can be described according to Carslaw and Jaeger [38] by the equation of thermal conduction:

$$c_L \rho_L \frac{\partial T_L}{\partial t} = \nabla \cdot (\kappa_L \nabla T_L) + g_{th} \quad (2.71)$$

where  $c_L$  is the specific heat capacity of lattice,  $\rho_L$  is the material density of lattice,  $\kappa_L$  is the coefficient of thermal conductivity and  $g_{th}$  is the thermal source in the unit of power density. The meaning of the thermal-conduction equation becomes more transparent if (2.71) is expressed by the following form:

$$\begin{aligned} \frac{\partial T_L}{\partial t} &= \frac{1}{c_L \rho_L} \nabla \cdot (\kappa_L \nabla T_L) + \frac{g_{th}}{c_L \rho_L} \\ &\equiv \left( \frac{\partial T_L}{\partial t} \right)_{lc} + \left( \frac{\partial T_L}{\partial t} \right)_{source} \end{aligned} \quad (2.72)$$

In equation (2.72) it can be seen that the change rate of the lattice temperature at a specific position  $\partial T_L / \partial t$  is determined by the loss rate from the thermal conduction  $(\partial T_L / \partial t)_{lc}$  and the generation rate from the heat source  $(\partial T_L / \partial t)_{source}$ . Since only the lattice temperature in the active region will be considered in this work,  $T_L$  will be denoted as the lattice temperature in the active region in the following discussion. In semiconductor lasers or any semiconductor device, the intraband carrier energy relaxation and the interband SRH process with multiple-phonon emission determine the heat source of the lattice heating. Therefore, increase rate of the lattice temperature can be expressed by



$$\left(\frac{\partial T_L}{\partial t}\right)_{source} = \frac{1}{c_L \rho_L} \left[ \frac{u_e(T_e) - u_e(T_L)}{\tau_{e-L}} + \frac{u_h(T_h) - u_h(T_L)}{\tau_{h-L}} + (E_{Fe} - E_{Fh})R_{SRH} \right] \quad (2.73)$$

It is assumed that the lattice temperature in the active region  $T_L$  takes  $\tau_\kappa$  second to cool down to the heat-sink temperature  $T_{HS}$ , then the reduce rate of the lattice temperature can be calculated by

$$\left(\frac{\partial T_L}{\partial t}\right)_{tc} = -\frac{T_L - T_{HS}}{\tau_\kappa} \quad (2.74)$$

Apparently, the thermal conduction process determines the thermal conduction time  $\tau_\kappa$  in the devices [30]. However, the thermal conduction time will be treated as a constant in the new proposed circuit model.

In summary, the rate equations for modelling semiconductor lasers with the effects of the carrier and lattice heating have been introduced in this chapter. Every physical process in the rate equations has been carefully explained in order to ensure that the theoretical approach used in this work is based on realistic physical models. The method of transforming the rate equations into the new proposed SPICE circuit models is discussed in the next chapter.

# CHAPTER 3

## TRANSFORMING THE RATE EQUATIONS INTO THE SPICE CIRCUIT MODELS

### 3.1 The Derivations of Circuit Models from Rate Equations

In order to implement the rate equations into the circuit models as schematically shown in Fig. 3.1, the physical quantities described by the equations require to be transformed into circuit quantities which model each physical process, for example, currents, voltages and passive elements. Perhaps the most challenging aspect in such a transformation is to adequately represent the carrier density by a circuit quantity or element. For example, the Xu group [20][21], Rossi et al. [24] and Mena et al. [27], represented the carrier density by voltage, while in other groups it has been represented by current [16]-[19] [22][23][25][26]. Consequently, the philosophical arguments are undecided and a careful discussion on this aspect is first considered.

The rate equation for carrier density (2.1) can be rewritten in a 'current form' as:

$$eV \frac{dn}{dt} = \eta_{inj} I_{inj} - I_{leak} - eVR_{SRH} - eVR_{spon} - eVR_{Aug} - eV \nu_g Gs \quad (3.1)$$

$$\equiv \eta_{inj} I_{inj} - I_{leak} - I_{SRH} - I_{spon} - I_{Aug} - I_{stim}$$

where

$$I_{SRH} = eVR_{SRH} \quad (3.2)$$

$$I_{spon} = eVR_{spon} \quad (3.3)$$

$$I_{sp} = eV_{sp}n \quad (3.4)$$

$$I_{sp} = eV_{sp}p \quad (3.5)$$

represent the recombination currents due to the SRH, spontaneous emission, Auger and stimulated emission, respectively. The task in transforming this rate equation is to choose a proper circuit element to represent the term  $eV_{sp}(dn/dt)$ . The most obvious one is by using a capacitor as

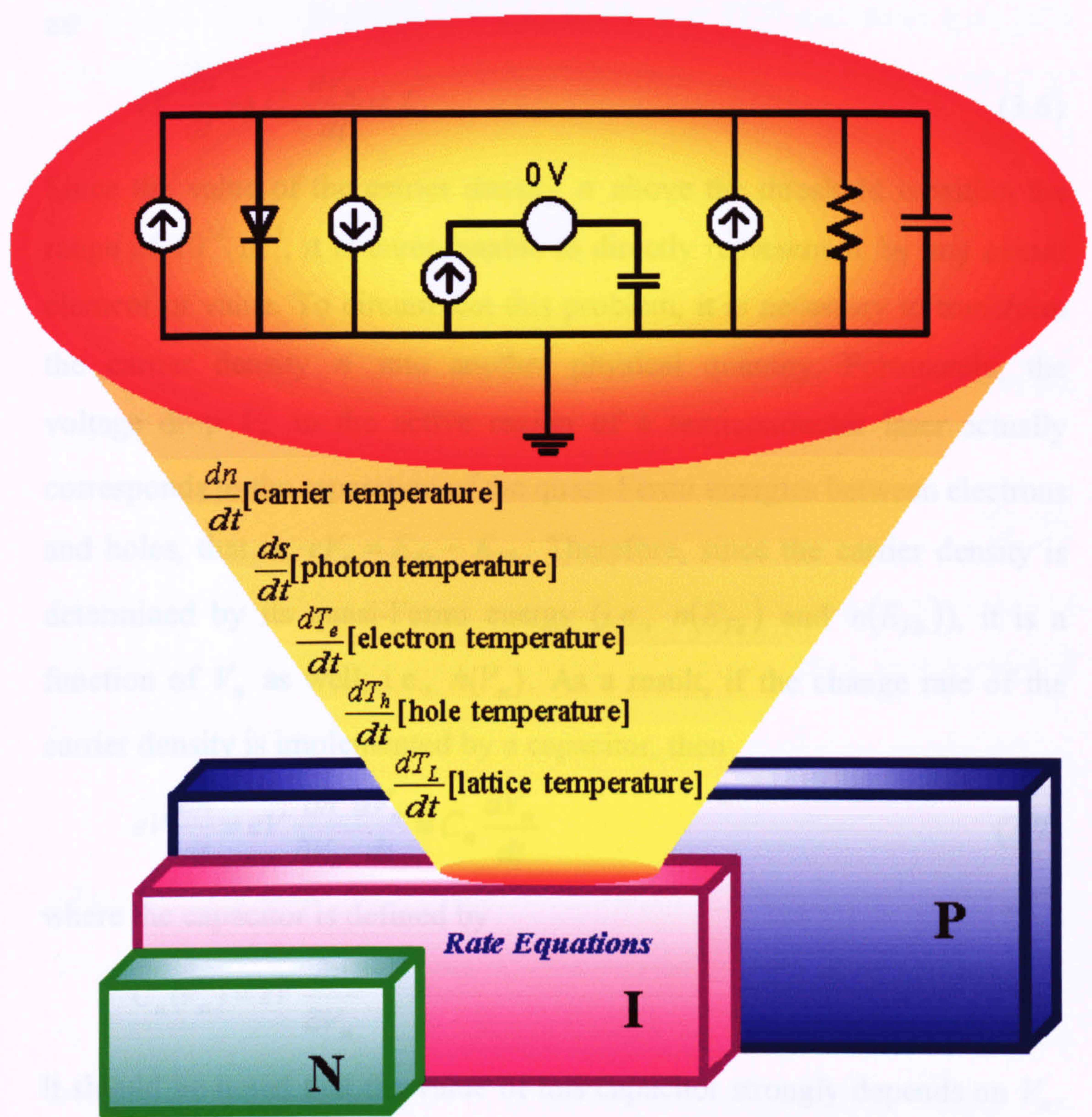


Fig. 3.1. Schematic diagram of transformation from rate equations to circuit models.

$$I_{Aug} = eVR_{Aug} \quad (3.4)$$

$$I_{stim} = eVv_gGs \quad (3.5)$$

represent the recombination currents due to the SRH, spontaneous emission, Auger and stimulated emission, respectively. The task in transforming this rate equation is to choose a proper circuit element to represent the term  $eV(dn/dt)$ . The most obvious one is by using a capacitor as:

$$eV \frac{dn}{dt} \rightarrow C_n \frac{dV_n}{dt} \propto I \quad (3.6)$$

Since the value of the carrier density  $n$  above the threshold is within the range of  $10^{24} \text{ m}^{-3}$ , it is unreasonable to directly represent  $n$  by any circuit element or value. To circumvent this problem, it is necessary to transform the carrier density  $n$  into another physical quantity. Fortunately, the voltage drop  $V_n$  in the active region of a semiconductor laser actually corresponds to the separation of the quasi-Fermi energies between electrons and holes, that is,  $eV_n = E_{Fe} - E_{Fh}$ . Therefore, since the carrier density is determined by its quasi-Fermi energy (i.e.,  $n(E_{Fe})$  and  $n(E_{Fh})$ ), it is a function of  $V_n$  as well; i.e.,  $n(V_n)$ . As a result, if the change rate of the carrier density is implemented by a capacitor, then

$$eV \frac{dn}{dt} = eV \frac{\partial n}{\partial V_n} \frac{dV_n}{dt} \equiv C_n \frac{dV_n}{dt} \quad (3.7)$$

where the capacitor is defined by

$$C_n(V_n) = eV \frac{\partial n}{\partial V_n} \quad (3.8)$$

It should be noted that the value of this capacitor strongly depends on  $V_n$ . In fact, it resembles the exponential relationship. In the SPICE syntax, the

nonlinear element of a capacitor can only be represented by a second-order polynomial form as given in [4]. That is:

$$C(V) = C_0(1 + a_1V + a_2V^2) \quad (3.9)$$

Since the carrier density is exponentially dependent on the Fermi energy, it is almost impossible to represent  $C_n(V_n)$  by such a second-order polynomial form with reasonable accuracy. However, such an approach has been used by the Xu group [20][21], Rossi et al. [24] and Mena et al. [27]. Unfortunately, no justification is given for representing the rate equation by  $C_n(V_n)$  in their work, nor is the method by which the relationship is implemented the  $C_n(V_n)$  in SPICE codes given. As a consequence of this discussion, it was decided not to use this approach in this work.

An alternative approach is to transform the change rate of the carrier density as:

$$eV \frac{dn}{dt} \rightarrow \tau_n \frac{dI_n}{dt} \propto I \quad (3.10)$$

Such a transformation links the value of the carrier density to the value of the current. This can be achieved if the carrier density  $n$  is transformed into a current  $I_n$  by the definition

$$I_n \equiv \frac{eV}{\tau_n} n \quad (3.11)$$

where  $\tau_n$  is arbitrary time constant. The reason for the choice is that since the value of  $n$  is a function of  $V_n$ ; the current  $I_n$  should be a function of  $V_n$ . As a result, a circuit element must be found to represent the relationship between  $I_n$  and  $V_n$ . Since the value of the carrier density  $n$  is exponentially dependent on the value of the quasi-Fermi energy  $E_{F_c}$ , and

thus  $V_n$ , it can be expected that  $I_n$  will also be exponentially dependent on  $V_n$ . Coincidentally, the current in a diode exponentially depends on the voltage; therefore,  $I_n(V_n)$  can be well represented by a diode. In SPICE, the  $I$ - $V$  relationship of a diode is described by

$$I_n(V_n) \approx I_s \left[ \exp\left(\frac{V_n - I_n R_s}{\eta_d V_T}\right) - 1 \right] \quad (3.12)$$

where  $V_T = k_B T / q$ ,  $I_s$  is the saturation current,  $R_s$  is the series resistor of the diode, and  $\eta_d$  is the parameter to distinguish the different contribution between the diffusion current ( $\eta_d \approx 1$ ) and the recombination generation current ( $\eta_d \approx 2$ ). The parameters  $I_s$ ,  $R_s$  and  $\eta_d$  are chosen to represent the real  $I_n(V_n)$  as close as possible. In this model,

$$\eta_d = 2 \quad (3.13)$$

is chosen to characterise the recombination feature in the active region. Note that at  $V_n = 0$  and  $I_n = I_s$ , the carrier density is the intrinsic carrier density for the intrinsic active region, i.e.,  $n = n_i$ . Therefore,

$$I_s = \frac{eV}{\tau_n} n_i \quad (3.14)$$

The intrinsic carrier density is calculated by

$$n_i = \sqrt{N_e N_h} \exp\left(-\frac{E_g}{2k_B T}\right) \quad (3.15)$$

where  $N_e$  and  $N_h$  are given in (3.15),  $E_g$  is the energy bandgap and  $T$  is the ambient temperature.

The only parameter left to fit the relationship  $I_n = eVn(V_n)/\tau_n$  is  $R_s$ . The percentage error introduced by using different values for  $R_s$  to

represent the  $I_n$ - $V_n$  relationship is shown in Fig. 3.2. As suggested by this result, different values of  $R_s$  will always cause some errors in such a fitting, especially for an applied voltage smaller than 0.2 V or larger than 1.2 V. To account for the typical value of the serial resistance associated with a real laser diode [8][16],

$$R_s = 10 \Omega \quad (3.16)$$

is assumed and used in this work. However,  $R_s$  can always be treated as a fitting parameter for the circuit model presented in this work.

Representing  $I_n = eVn(V_n)/\tau_n$  by a diode, (3.1) can be rewritten as

$$\eta_{inj}I_{inj} = I_{leak} + I_{SRH} + I_{spont} + I_{Aug} + I_{stim} + \tau_n \frac{dI_n}{dt} \quad (3.17)$$

Following this transformation, the physical meaning of the original rate equation is more transparent. For the dc case, that is,  $\tau_n \cdot dI_n/dt = 0$  in (3.17), the injection current is channelled into the leakage current, SRH recombination, spontaneous-emission recombination, Auger recombination or stimulated-emission recombination. Of course, the leakage, SRH and Auger process do not produce any light, so they are nonradiative recombinations. In contrast, the spontaneous-emission and stimulated-emission recombinations are radiative processes because they generate light: incoherent light by spontaneous emission and coherent light by stimulated emission. It should be noted that if

$$I_n = I_{leak} + I_{SRH} + I_{spont} + I_{Aug} \quad (3.18)$$

is used in (3.17), then

$$\eta_{inj}I_{inj} = I_n + I_{stim} + \tau_n \frac{dI_n}{dt} \quad (3.19)$$

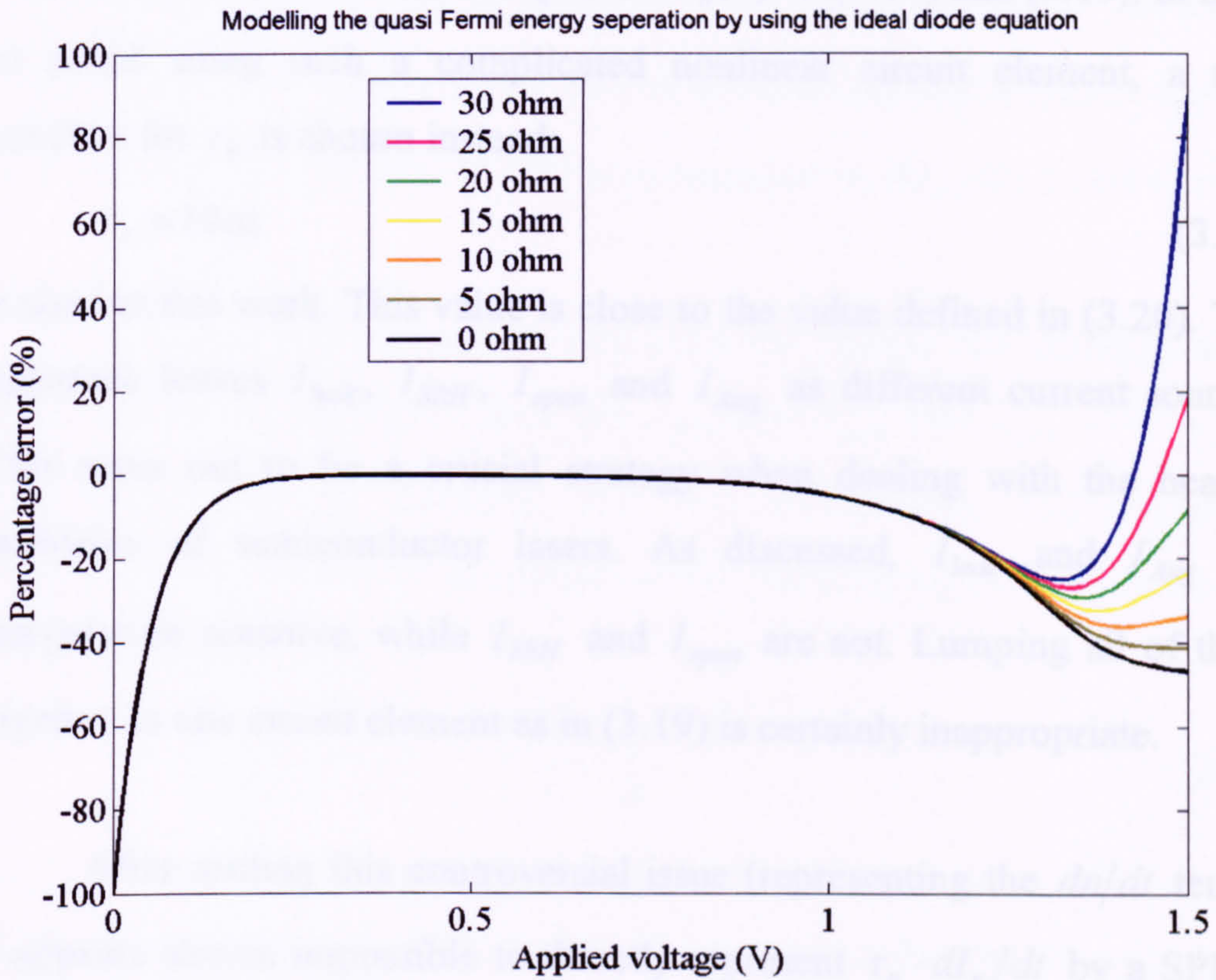


Fig. 3.2. The percentage error as a function of the separation of the quasi-Fermi energies between electrons and holes modelled by a  $p$ - $n$  diode.



which represents the basic circuit model for a semiconductor laser used in many previous publications [16]-[19][22][23][25][26]. However, using the relationships (3.11) and (3.18) imply that the arbitrary time constant is decided by

$$\frac{1}{\tau_n} = \frac{1}{n} \left( \frac{I_{leak}}{eV} + R_{SRH} + R_{spont} + R_{Aug} \right) \quad (3.20)$$

This turns out to be a very crude approximation. As discussed in Chapter 2,  $R_{SRH} \propto n$ ,  $R_{spont} \propto n^2$  and  $R_{Aug} \propto n^3$ ; therefore,  $\tau_n(n)$  should be dependent on the carrier density. Therefore, if  $\tau_n(n)$  is determined by (3.20) instead of using a constant, the circuit element for  $\tau_n(n)$  will be dependent on  $I_n$  because of  $n$  is determined by  $I_n$  by the definition in (3.11). This requires a nonlinear circuit element to represent  $\tau_n(n)$  in (3.17) and (3.19). In order to avoid using such a complicated nonlinear circuit element, a time constant for  $\tau_n$  is chosen instead:

$$\tau_n = 10\text{ns} \quad (3.21)$$

is used in this work. This value is close to the value defined in (3.20). This approach leaves  $I_{leak}$ ,  $I_{SRH}$ ,  $I_{spont}$  and  $I_{Aug}$  as different current sources. This turns out to be a crucial strategy when dealing with the heating problems of semiconductor lasers. As discussed,  $I_{leak}$  and  $I_{Aug}$  are temperature sensitive, while  $I_{SRH}$  and  $I_{spont}$  are not. Lumping all of them together in one circuit element as in (3.19) is certainly inappropriate.

After settling this controversial issue (representing the  $dn/dt$  term), it appears almost impossible to directly represent  $\tau_n \cdot dI_n/dt$  by a SPICE circuit. To circumvent this problem, a ‘derivative circuit’ with an *artificial* capacitor and a current-controlled voltage source  $C_n(dV_{I_n}/dt)$  can be used

to represent  $\tau_n(dI_n/dt)$  utilising the following transformations:  $\tau_n \rightarrow C_n$  and  $I_n \rightarrow V_{I_n}$ . Note that in the discussion, the arrow symbol is used to indicate the transformation of variables, although such a transformation may not preserve the physical unit of the original variables. For example, in this case, if  $\tau_n = 10$  ns is assumed, then its correspondent capacitance will be  $C_n = 10$  nF. This part of circuit should be detached from the main circuits for carrier density. If it is connected to the main circuits for carrier density, then there will be a conflict between the voltage on the diode  $V_n$  and the 'dummy' voltage  $V_{I_n}$ . However, because  $V_n$  represents a real physical quantity, the quasi-Fermi energy separation in the active region, the diode is kept in the main circuit for carrier density and the circuit representing  $C_n(dV_{I_n}/dt)$  is detached from the main circuit for carrier density. For this reason,  $C_n(dV_{I_n}/dt)$  is termed a derivative circuit, because the main function of  $C_n(dV_{I_n}/dt)$  is to represent  $\tau_n(dI_n/dt)$  in the circuits.

The next step taken is to transform the photon rate equation into a circuit equation bearing in mind that  $I_{spont} = eVR_{spont}$  and  $I_{stim} = eV\nu_g Gs$  in the device are to represent the real spontaneous and stimulated recombination currents in the circuit model. Multiplying (2.2) on both sides by  $eV/\Gamma$ , this gives

$$I_{stim} + \beta I_{spont} = \frac{eV}{\Gamma} \cdot \frac{s}{\tau_s} + \frac{eV}{\Gamma} \cdot \frac{ds}{dt} \quad (3.22)$$

Since the unit on the right-hand side of (3.22) is current, and only the circuit element of a capacitor has the characteristics that the time derivative of its voltage equals its current, that is,  $C_s(dV_s/dt) = I_s$ ; there is no choice but to relate the photon density to the voltage, that is,  $s \propto V_s$ . In addition, if

the photon density is chosen to be related to the current,  $s \propto I_s$ , then  $(eV/\Gamma) \cdot (ds/dt)$  will be in the form of  $\tau_s (dI_s/dt)$ . The drawback of this latter choice is that another additional “derivative circuit” becomes involved, which is more complicated than incorporating a simple capacitor. Therefore, a voltage in this work will represent the photon density.

However, it can be proved to be very impractical if the photon density  $s$  is directly transformed into voltage, since usually  $s \approx 10^{20} \sim 10^{22} \text{ m}^{-3}$  when the device is biased above the threshold. In addition, the SPICE compiler will not accept such a range of voltage values. Fortunately, the optical power  $P$ , which directly relates to the photon density  $s$ , emitted by a laser diode is usually within the mW range. This suggests that the emitted optical power turns out to be a suitable variable for transforming photon density  $s$  into the voltage unit having a mV range. It is well known that the total output power from *two mirror facets* is related to the photon density  $s$  by [8]:

$$P = \frac{\hbar\omega_l \nu_g \alpha_{\text{mirr}} V}{\Gamma} s \quad (3.23)$$

Defining the ‘optical voltage’ by

$$P[\text{W}] \rightarrow V_s[\text{V}] \quad (3.24)$$

and substituting (3.23) and (3.24) into (3.22), the final circuit equation for the photon rate equation becomes:

$$I_{\text{stim}} + \beta I_{\text{spont}} = \frac{V_s}{R_s} + C_s \frac{dV_s}{dt} \quad (3.25)$$

where the resistor  $R_s$  and the capacitor  $C_s$  are defined by

$$\frac{\hbar\omega_l \tau_s}{e\tau_m} \rightarrow R_s \quad (3.26)$$

$$\frac{e\tau_m}{\hbar\omega_l} \rightarrow C_s \quad (3.27)$$

respectively, and the mirror lifetime of a photon  $\tau_m \equiv 1/\nu_g \alpha_{mirr}$  is used in the equations. It should be noted that the real physical units are not directly represented by circuit elements under such transformations. For example, the unit for  $\hbar\omega_l\tau_s/e\tau_m$  is Volts, not Ohms, because the optical power (Watts) has been assigned to a voltage value. However, it must be emphasised that the voltage value of  $V_s$  in fact represents the power value of  $P$ .

Transforming the rate equation for the electron temperature into a circuit model follows a similar pattern. First, equation (2.14) is multiplied through by  $\tau_{e-L}$  giving:

$$\begin{aligned} & \frac{\tau_{e-L}}{eV} \left( \frac{\partial u_e}{\partial T_e} \right)^{-1} \langle \Delta E_{inj}^e \rangle (\eta_{inj} I_{inj} - I_{leak}) + \frac{\tau_{e-L}}{eV} \left( \frac{\partial u_e}{\partial T_e} \right)^{-1} \langle \Delta E_{stim}^e \rangle eV \nu_g G_s \\ & + \frac{\tau_{e-L}}{eV} \left( \frac{\partial u_e}{\partial T_e} \right)^{-1} \langle \Delta E_{Aug}^e \rangle eV R_{Aug}^e + \frac{\tau_{e-L}}{eV} \left( \frac{\partial u_e}{\partial T_e} \right)^{-1} \langle \Delta E_{fca}^e \rangle eV \nu_g \alpha_{fca}^e S \\ & = \left( \frac{\partial u_e}{\partial T_e} \right)^{-1} [u_e(T_e) - u_e(T_L)] + \left( \frac{\partial u_e}{\partial T_e} \right)^{-1} \frac{\tau_{e-L}}{\tau_{e-h}} [u_e(T_e) - u_e(T_h)] + \tau_{e-L} \cdot \frac{dT_e}{dt} \end{aligned} \quad (3.28)$$

For simplicity, some coefficients are defined the following:

$$\gamma_{inj}^e \equiv \frac{\tau_{e-L}}{eV} \left( \frac{\partial u_e}{\partial T_e} \right)^{-1} \langle \Delta E_{inj}^e \rangle \quad (3.29)$$

$$\gamma_{stim}^e \equiv \frac{\tau_{e-L}}{eV} \left( \frac{\partial u_e}{\partial T_e} \right)^{-1} \langle \Delta E_{stim}^e \rangle \quad (3.30)$$

$$\gamma_{Aug}^e \equiv \frac{\tau_{e-L}}{eV} \left( \frac{\partial u_e}{\partial T_e} \right)^{-1} \langle \Delta E_{Aug}^e \rangle \quad (3.31)$$

$$\gamma_{fca}^e \equiv \frac{\tau_{e-L}}{eV} \left( \frac{\partial u_e}{\partial T_e} \right)^{-1} \langle \Delta E_{fca}^e \rangle \quad (3.32)$$

and the free-carrier-absorption current by

$$I_{fca}^e \equiv eV \nu_g \alpha_{fca}^e S \quad (3.33)$$

Note that

$$u(T_e) \cong \frac{\partial u_e}{\partial T_e} T_e \quad (3.34)$$

can be used on the right-hand side of (3.28) and also it can be assumed that

$$\frac{\partial u_e}{\partial T_e} \approx \frac{\partial u_h}{\partial T_h} \quad (3.35)$$

Since  $u_e \approx 3n_e k_B T_e / 2$ ,  $u_h \approx 3n_h k_B T_h / 2$  and  $n_e = n_h$  are also assumed in this work, this assumption implies that  $T_e \approx T_h$ . As long as the electron temperature is not significantly different from the hole temperature, this assumption seems to be reasonable. Implementing the assumption, (3.28) becomes

$$\begin{aligned} & \gamma_{inj}^e (\eta_{inj} I_{inj} - I_{leak}) + \gamma_{stim}^e I_{stim} + \gamma_{Aug}^e I_{Aug}^e + \gamma_{fca}^e I_{fca}^e \\ & = (T_e - T_L) + \frac{\tau_{e-L}}{\tau_{e-h}} (T_e - T_h) + \tau_{e-L} \frac{dT_e}{dt} \end{aligned} \quad (3.36)$$

Since the physical quantities on the left-hand side of (3.36) are currents, the same unit on the right-hand side of (3.36) should be kept as well. Therefore, either  $C_e(dV_e/dt)$  or  $\tau_e(dI_e/dt)$  can be used to represent the  $\tau_{e-L}(dT_e/dt)$  term on the right-hand side of (3.36) to match the unit of current. However, since  $C_e(dV_e/dt)$  only involves a single capacitor, while  $\tau_e(dI_e/dt)$  needs an additional 'derivative circuit'.  $C_e(dV_e/dt)$  is chosen rather than  $\tau_e(dI_e/dt)$  to represent  $\tau_{e-L}(dT_e/dt)$ . Now since the

temperatures  $T_e$ ,  $T_h$  and  $T_L$  in the device are usually of the order of 300 K, it is sensible directly to represent them by voltages:

$$T_e[\text{K}] \rightarrow V_e[\text{V}] \quad (3.37)$$

$$T_h[\text{K}] \rightarrow V_h[\text{V}] \quad (3.38)$$

$$T_L[\text{K}] \rightarrow V_L[\text{V}] \quad (3.39)$$

and the capacitor by

$$\tau_{e-L}[\text{s}] \rightarrow C_e[\text{F}] \quad (3.40)$$

It should be noted that the values of voltage, resistance and capacitance defined in this part of the circuits do not really represent the physical units of volts, ohms and farads. They represent the values of the original variables instead. For example, the voltage  $V_L$  in volt actually represents the lattice temperature  $T_L$  in Kelvin. The original physical unit of  $\gamma$  is K/A while it is dimensionless in (3.36).

The choice of representing the electron temperature  $T_e$  by a voltage  $V_e$  certainly causes difficulties for the first and second terms on the right-hand side of (3.36) because of the disagreement among their units with others. To circumvent this problem, two 'dummy' resistors are used

$$1\Omega \rightarrow R_{eL} \quad (3.41)$$

and

$$\frac{\tau_{e-h}[\ ]}{\tau_{e-L}} \rightarrow R_{eh}[\Omega] \quad (3.42)$$

adding to the first and second terms in (3.36), respectively. As a result, the units of all the terms in (3.36) are currents. Finally, the rate equation of the electron temperature becomes

$$\begin{aligned} & \gamma_{inj}^e (\eta_{inj} I_{inj} - I_{leak}) + \gamma_{stim}^e I_{stim} + \gamma_{Aug}^e I_{Aug}^e + \gamma_{fca}^e I_{fca}^e \\ &= \frac{V_e - V_L}{R_{eL}} + \frac{V_e - V_h}{R_{eh}} + C_e \frac{dV_e}{dt} \end{aligned} \quad (3.43)$$

which can be implemented into SPICE codes.

By a similar derivation, transforming the rate equation for the hole temperature into a circuit model can be achieved by setting the hole temperature  $T_h$  to a voltage  $V_h$ . For simplicity, only the final result is given:

$$\begin{aligned} & \gamma_{inj}^h (\eta_{inj} I_{inj} - I_{leak}) + \gamma_{stim}^h I_{stim} + \gamma_{Aug}^h I_{Aug}^h + \gamma_{fca}^h I_{fca}^h \\ &= \frac{V_h - V_L}{R_{hL}} - \frac{V_h - V_e}{R_{he}} + C_h \frac{dV_h}{dt} \end{aligned} \quad (3.44)$$

with the following definitions:

$$\gamma_{inj}^h \equiv \frac{\tau_{h-L}}{eV} \left( \frac{\partial u_h}{\partial T_h} \right)^{-1} \langle \Delta E_{inj}^h \rangle \quad (3.45)$$

$$\gamma_{stim}^h \equiv \frac{\tau_{h-L}}{eV} \left( \frac{\partial u_h}{\partial T_h} \right)^{-1} \langle \Delta E_{stim}^h \rangle \quad (3.46)$$

$$\gamma_{Aug}^h \equiv \frac{\tau_{h-L}}{eV} \left( \frac{\partial u_h}{\partial T_h} \right)^{-1} \langle \Delta E_{Aug}^h \rangle \quad (3.47)$$

$$\gamma_{fca}^h \equiv \frac{\tau_{h-L}}{eV} \left( \frac{\partial u_h}{\partial T_h} \right)^{-1} \langle \Delta E_{fca}^h \rangle \quad (3.48)$$

$$I_{fca}^h \equiv eV v_g \alpha_{fca}^h s \quad (3.49)$$

$$\tau_{h-L} [s] \rightarrow C_h [F] \quad (3.50)$$

$$1\Omega \rightarrow R_{hL} \quad (3.51)$$

$$\frac{\tau_{h-e}}{\tau_{h-L}} [ ] \rightarrow R_{he} [\Omega] \quad (3.52)$$

Transforming the rate equation for the lattice temperature (2.16) has its own ambiguity. The last term on the right-hand side of (2.16) has two natural circuit quantities:  $E_{Fe} - E_{Fh} = eV_n$  and  $eVR_{SRH} = I_{SRH}$ . Choosing any one of them should be workable. Nevertheless, carrier density, photon density, electron temperature and hole temperature in (2.1), (2.2), (2.14) and (2.15) are represented by current units in the previously derived circuit equations, therefore, to maintain consistency the same unit will be kept. Therefore, the original physical quantity of the SRH recombination current is retained.

In the same way when transforming the rate equations for the electron and hole temperature, on both sides of (2.16) are multiplied by  $\tau_\kappa$ . This gives

$$\begin{aligned} & \frac{\tau_\kappa}{c_L \rho_L} \frac{u_e(T_e) - u_e(T_L)}{\tau_{e-L}} + \frac{\tau_\kappa}{c_L \rho_L} \frac{u_h(T_h) - u_h(T_L)}{\tau_{h-L}} + \frac{\tau_\kappa V_n}{c_L \rho_L V} I_{SRH} \\ & = (T_L - T_{HS}) + \tau_\kappa \frac{dT_L}{dt} \end{aligned} \quad (3.53)$$

The expression  $C_L(dV_L/dt)$  is used to represent  $\tau_\kappa(dT_L/dt)$  so that the unit of current is kept to represent the SRH recombination current  $I_{SRH}$ . As the value of  $T_L$  is about 300 K at room temperature, it is convenient directly to represent  $T_L$  by a voltage as in (3.53) and  $\tau_\kappa$  by a capacitor.

$$\tau_\kappa [\text{s}] \rightarrow C_L [\text{F}] \quad (3.54)$$

Since the thermal conduction time is usually in the range of nanosecond, the correspondent capacitance should be acceptable within



SPICE simulations. Similarly, the temperature of the heat sink  $T_{HS}$  at room temperature, a voltage can directly represent it.

$$T_{HS}[\text{K}] \rightarrow V_{HS}[\text{V}] \quad (3.55)$$

Since the choice has been made to keep the equation in the current unit, the following ‘artificial’ current sources must be defined

$$I_{e-L} = \frac{\tau_{\kappa}}{C_L \rho_L} \frac{u_e(T_e) - u_e(T_L)}{\tau_{e-L}} \quad (3.56)$$

$$I_{h-L} = \frac{\tau_{\kappa}}{C_L \rho_L} \frac{u_h(T_h) - u_h(T_L)}{\tau_{h-L}} \quad (3.57)$$

to match the current unit in both sides of (3.53). In addition, a dimensionless coefficient

$$\gamma_{SRH} = \frac{\tau_{\kappa} V_n}{V C_L \rho_L} \quad (3.58)$$

needs to be defined and a ‘dummy’ resistor will be used as

$$1\Omega \rightarrow R_L \quad (3.59)$$

Finally, the circuit model for representing the rate equation of the lattice temperature effect, as it is required, this is:

$$I_{e-L} + I_{h-L} + \gamma_{SRH} I_{SRH} = \frac{V_L - V_{HS}}{R_L} + C_L \frac{dV_L}{dt} \quad (3.60)$$

In summary, (3.17), (3.25), (3.43), (3.44) and (3.60) represent the circuit models for the carrier density, photon density, electron temperature, hole temperature and lattice temperature effects, respectively. Having achieved the circuit models from the rate equations, the next step is implementing these circuit models in SPICE code form. This step is considered in the next section.

### 3.2 The Representations of Circuit Models by SPICE Codes

Implementing circuit models (3.17), (3.25), (3.43), (3.44) and (3.60) by SPICE codes is not as straightforward as it appears. Here an explanation is given on the procedures adopted for developing SPICE codes for circuit models. The circuit diagram of these SPICE codes is shown in Fig. 3.3 and the correspondent SPICE codes are attached as APPENDIX C.4. The procedures to implement circuit models by SPICE codes are:

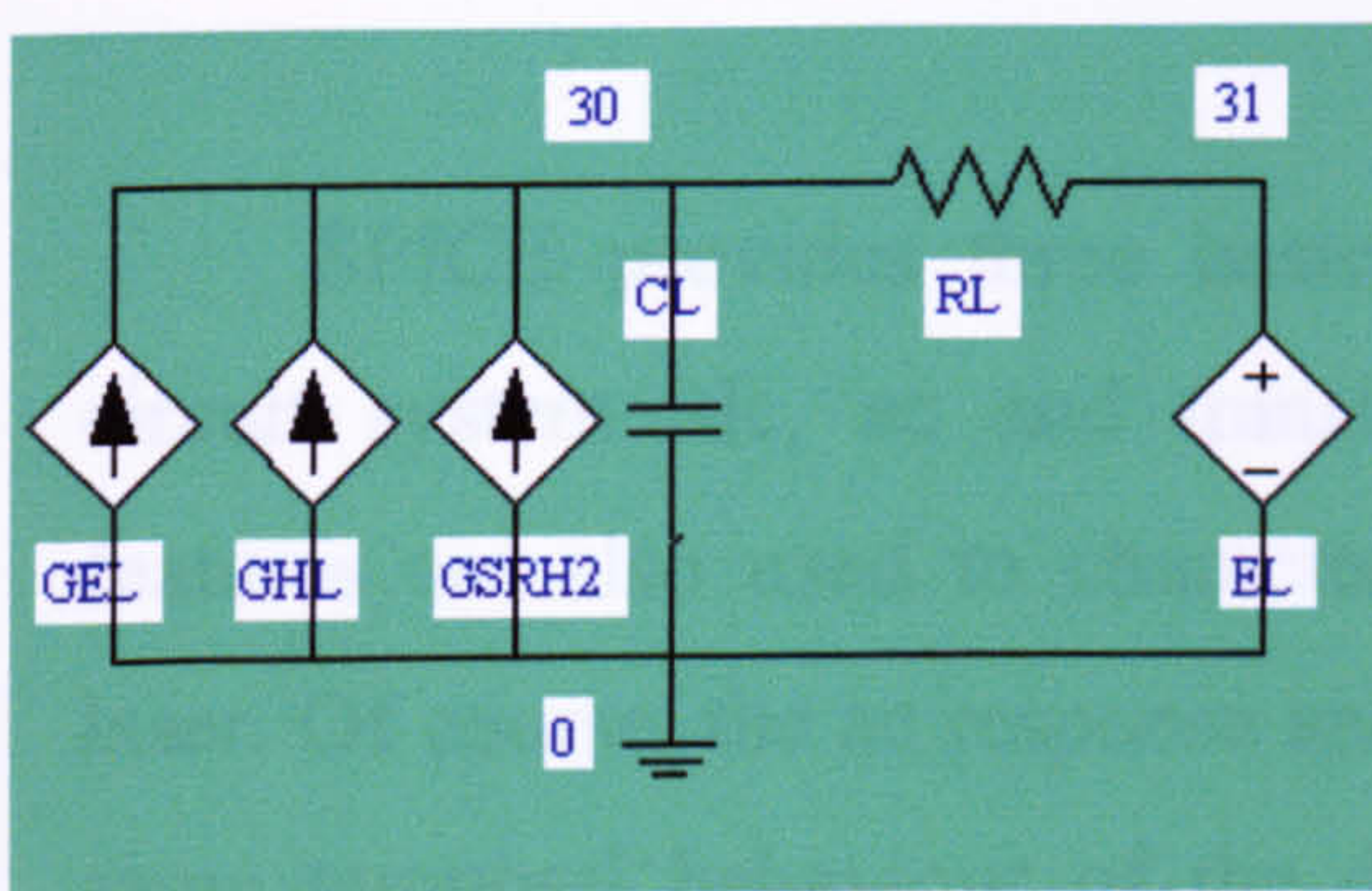
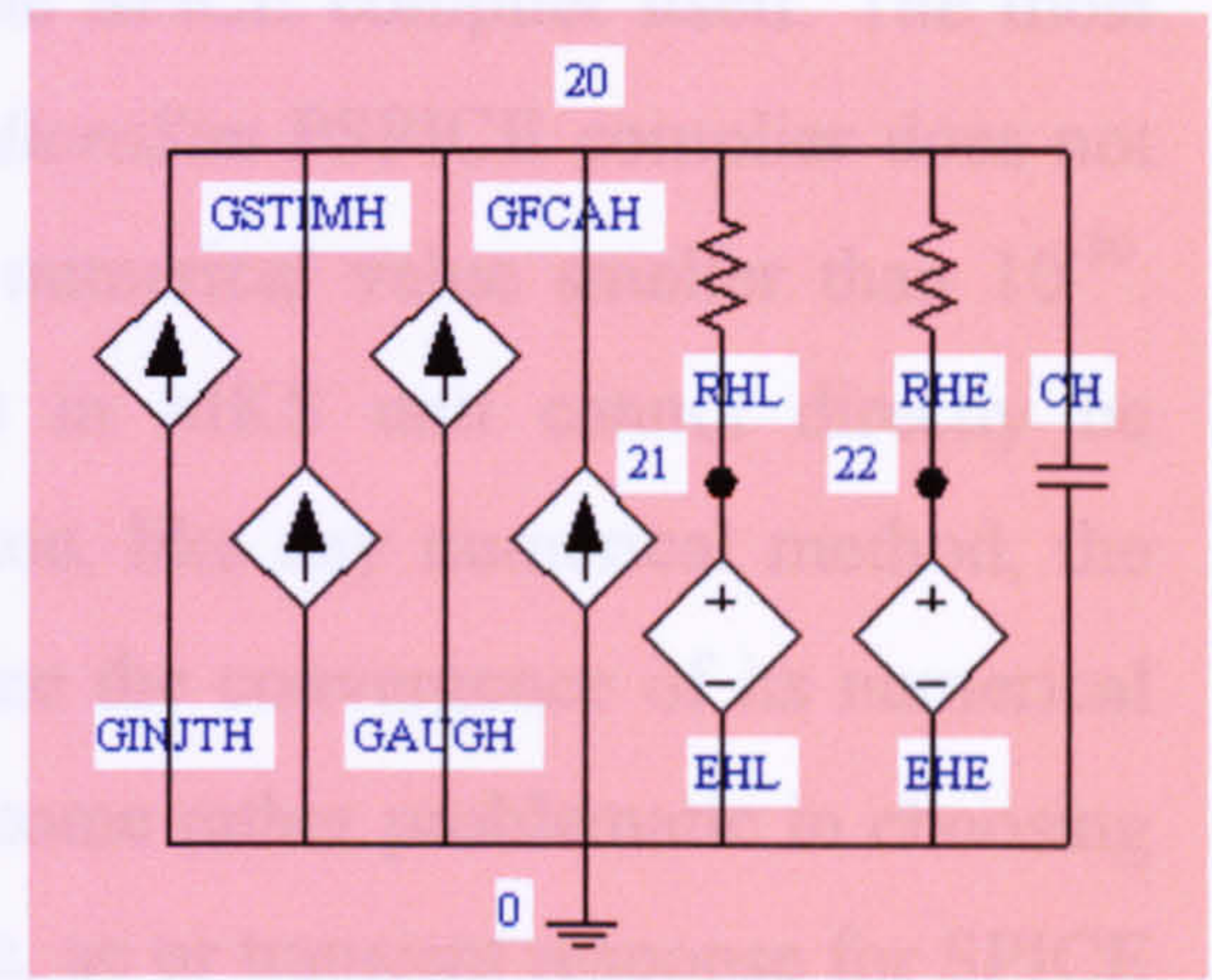
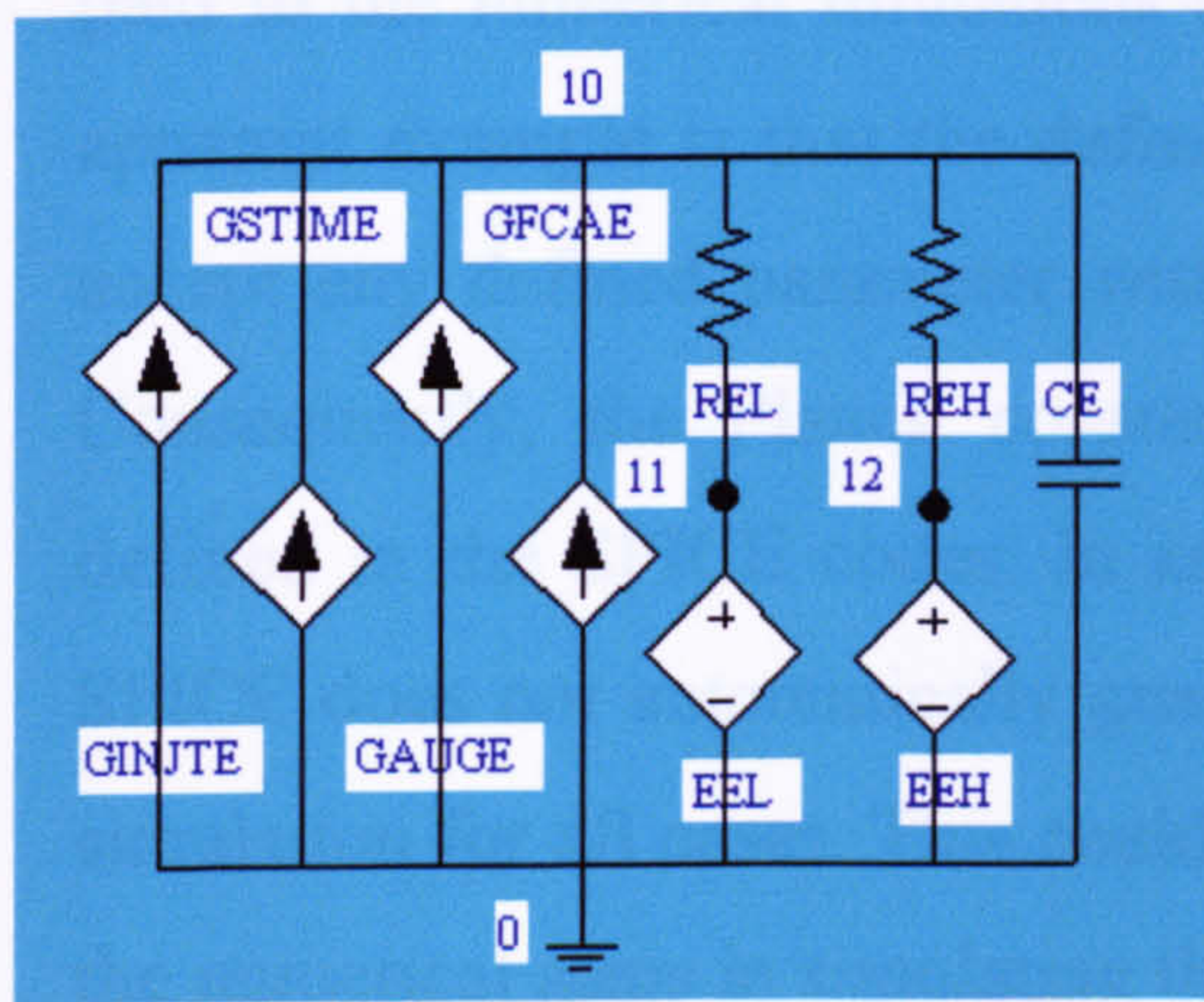
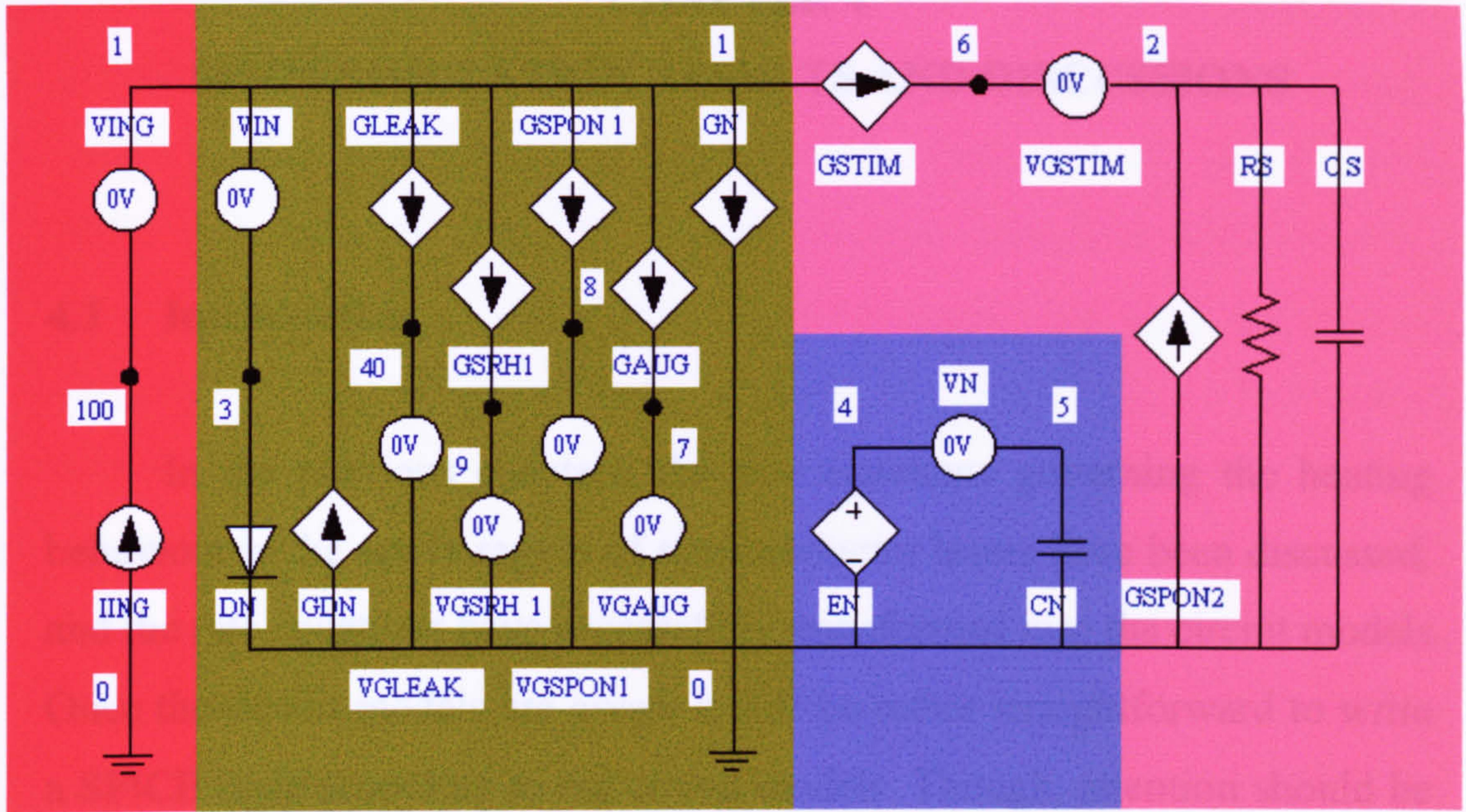
- 1) Defining parameters. The parameters categorised comprise: fundamental constants, material parameters, structure parameters, photon parameters, lattice parameters, parameters of physical processes, gain parameters and other dependent parameters. Categorising the parameters is very important for the purposes of debugging and fitting data. Naming these parameters in the SPICE codes follows the symbols in the rate equations as close as possible.
- 2) Writing functions for calculating  $n_e$ ,  $n_h$ ,  $\mu_{Fe}$ ,  $\mu_{Fh}$ ,  $u_e$  and  $u_h$ . Their relationships are given in (2.29)-(2.36). It must be noted that the PSPICE compiler used will not accept any numerical value smaller than  $10^{-30}$ . As a result, any equation which contains the electron mass  $m_0$  and the Plank constant  $\hbar$  should be calculated before transforming to the SPICE models and precautions taken to check whether any numerical value is smaller than  $10^{-30}$ .
- 3) When calculating  $\partial u_c / \partial n_c$ ,  $\partial u_c / \partial T_c$  and their associated coefficients  $\gamma$ , a simple central finite-difference procedure is used to calculate the derivatives.
- 4) Calculating the leakage current  $I_{leak}$  according to (2.37). The leakage current components,  $I_{SRH} = eVA_{SRH}n$ ,  $I_{spon} = eVB_{spon}n^2$ ,

$I_{stim} = eV\nu_g Gs$  and  $I_{Aug}$  calculated by (2.42) and (2.43) are directly written in their associated circuits. Note that the carrier density  $n$  is calculated by  $n = I_n \tau_n / eV$  once the value of  $I_n$  is known. The value of  $I_n$  can be retrieved from the current in the diode which may be obtained by an ‘artificial’ ammeter. This artificial ammeter is a 0V voltage source that has no effect on the circuit. SPICE provides a very unique feature to read the current passing through the voltage source by declaring  $I(V_{source})$ , where  $V_{source}$  is the name of the voltage source.

- 5) The photon density  $s$  is simply calculated by the relationship  $s = V_s \Gamma \tau_m / \hbar \omega_l V$ .
- 6) A ‘dummy’ voltage-controlled current source  $G_{DN}$  is used to counteract the current in the diode. This is because it is desirable to keep the individuality of the different recombination currents, as discussed in Section 3.1.
- 7) Using a ‘derivative circuit’ to represent  $\tau_n (dI_n / dt)$ . Since this circuit is detached from the main circuits for carrier density, its contribution is represented by a voltage-controlled current source in the main circuits for carrier density.
- 8) It is seen that the circuits for the carrier density and photon density are connected together by the stimulated-emission current  $I_{stim}$ . In addition, the circuits for the electron temperature, hole temperature and lattice temperature are detached from each other. The unique feature of the voltage-controlled current source in SPICE provides for their mutual effects. Since most of the physical quantities are determined by  $n$ ,  $s$ ,  $T_e$ ,  $T_h$  and  $T_L$  in the rate equations, that is,  $V_n$ ,

$V_s$ ,  $V_e$ ,  $V_h$  and  $V_L$  in the circuits. Using voltage-controlled current sources is a satisfactory way for implementing the current sources, such as  $I_{inj}$ ,  $I_{leak}$ ,  $I_{SRH}$ ,  $I_{spon}$ ,  $I_{Aug}$  and  $I_{stim}$  in the circuit models.

Once the SPICE codes have been developed, they can be used to simulate the performance of the device. The next chapter presents results that describe the performance characteristics of laser diodes incorporating the various physical effects discussed. The basic model, which completely ignores the heating effects, is used as the benchmark for assessing performance.



- DC input
- circuit for carrier density
- derivative circuit for  $dn/dt$
- circuit for photon density
- circuit for electron heating
- circuit for hole heating
- circuit for lattice heating

Fig. 3.3. SPICE circuit model with carrier and lattice heating.

## CHAPTER 4

### SPICE SIMULATION RESULTS AND DISCUSSIONS

#### 4.1 Introduction

In the previous chapters, the rate equations governing the heating behaviour in the active region of semiconductor lasers have been discussed, and the rate equations have successfully transformed into the circuit models. Once the circuit models are given, it will be rather straightforward to write a SPICE code according to the circuit models. Though, attention should be paid to the numerical limitations of the SPICE compiler itself. The most apparent example is that the default *MicroSim* PSPICE compiler does not accept any defined parameter with a numerical value smaller than  $10^{-30}$ . Consequently, the Planck constant  $\hbar$  in MKS unit cannot directly be defined in the SPICE codes. In addition, like any numerical method, the SPICE does not automatically guarantee the convergence of its numerical simulation for all cases. This could become rather problematic in choosing the numerical steps in simulating the dc, ac or transient response for SPICE circuits.

SPICE provides three basic features to probe and characterise a circuit system: dc, ac and transient responses. Generally, these three features are also used to characterise the properties of a semiconductor laser. Of course, the ac response and the transient response characterise the same temporal behaviour of the device. The ac response represents the system properties in the frequency domain while the transient response directly characterises the system behaviour in the time domain. For

semiconductor lasers, the ac response is generally used to characterise the bandwidth of the devices. In addition, the transient response is usually employed to describe the turn-on behaviour of the devices. These built-in features in simulating the dc, ac and transient responses unquestionably give SPICE circuit models an unambiguous merit over their counterpart, the rate equations. For example, in order to simulate the ac response, a small-signal analysis on the rate equations must be provided. Such an analysis can be rather involved (sometimes unnecessarily complicated) especially in the case when dealing with the issues of the carrier and lattice heating [32]. In addition, different numerical procedures must be implemented separately for the ac and transient responses when using the rate-equation approach. This certainly adds more numerical complexity onto the theoretical models themselves, even to the models representing the same device. Apparently, the simplicity and consistency in simulating the dc, ac and transient responses by using the SPICE circuit model provides a definite merit to allow the extraction of the physical parameters from the measurement data of the device.

The most involved parts for constructing any SPICE circuit model for a given device are in finding the physical model for the device and transforming this model into the correspondent circuit elements. Writing the SPICE codes for a given circuit is not a straightforward task. However, compared with the commercial simulation packages for formal programming language such as C++, the debugging function provided by the SPICE compiler is rather sophisticated. Therefore, for a complicated model, debugging can become a rather involved task. The commercial vendor should improve such a shortcoming in the debugging capability of the SPICE in the near future.

The parameters used in the SPICE circuit model are listed in APPENDIX D. Except for the physical constants, these parameters can be roughly categorised as the following:

- 1) Structure parameters:  $L_x$ ,  $L_y$  and  $L_z$ .
- 2) Material parameters: mole fraction  $x$  for  $\text{Al}_x\text{Ga}_{1-x}\text{As}$ .
- 3) Physical-process parameters:  $A_{SRH}$ ,  $B_{spon}$ ,  $C_{Aug}$ ,  $\tau_{e-L}$ ,  $\tau_{h-L}$ ,  $\tau_{e-h}$  and  $\tau_{\kappa}$ .
- 4) Optical-process parameters:  $G$ ,  $\alpha_{int}$ ,  $\tau_s$  and  $\beta$ .
- 5) Defined parameters:  $\varepsilon_{shb}$ ,  $g_n$ ,  $g_{Te}$ ,  $g_{T_h}$  and  $g_{T_l}$ .

Ideally, each parameter should be capable of being individually adjusted to verify its unique role in determining the properties of semiconductor lasers. However, the value of each parameter is usually within its typical range. For example, the cavity thickness of a laser  $L_x$  is typical within 100 ~ 500  $\mu\text{m}$ . In addition, although some of the parameters, such as  $\tau_{e-L}$ ,  $\tau_{h-L}$  and  $\tau_{e-h}$ , can be evaluated by first-principle's calculations, their precise values are still unresolved [31].

It should be kept in mind that, the purpose of the simulations presented in this work is not to exhaustively evaluate the effect of each parameter on the performance of the device, or to extract the values of these parameters by fitting the simulation results with the measurement data. The simulation presented in the following is for the purpose of demonstrating the capabilities especially with respect to the influences or performance of the heating effects and versatilities of the SPICE circuit models for semiconductor lasers. In order more clearly to discuss the effect



of different parameters, SPICE circuit models without carrier and lattice heating will initially be discussed. These results are to provide the baseline performance data. Subsequently, the lattice heating will be added to the models to quantify the effect and performance. Finally, SPICE circuit models incorporating both the carrier and lattice heating are simulated and the results discussed.

## 4.2 SPICE Circuit Model without Carrier and Lattice Heating

If the effects of the carrier and lattice heating are neglected, then (2.1) and (2.2) will become the conventional carrier-photon rate equations presented in almost every textbook of semiconductor lasers. These equations can provide a basic and fundamental understanding of the static (i.e., dc) and dynamic (i.e., ac and transient responses) properties of semiconductor lasers. The SPICE circuits associated with the carrier-photon rate equations are shown in Fig. 4.1. The SPICE codes are given in APPENDIX C.1.

In most cases, when the carrier-photon rate equations are used, the SRH, spontaneous emission and Auger recombination processes are normally lumped into a single expression and represented by the carrier lifetime  $\tau_n$  as in the following equation:

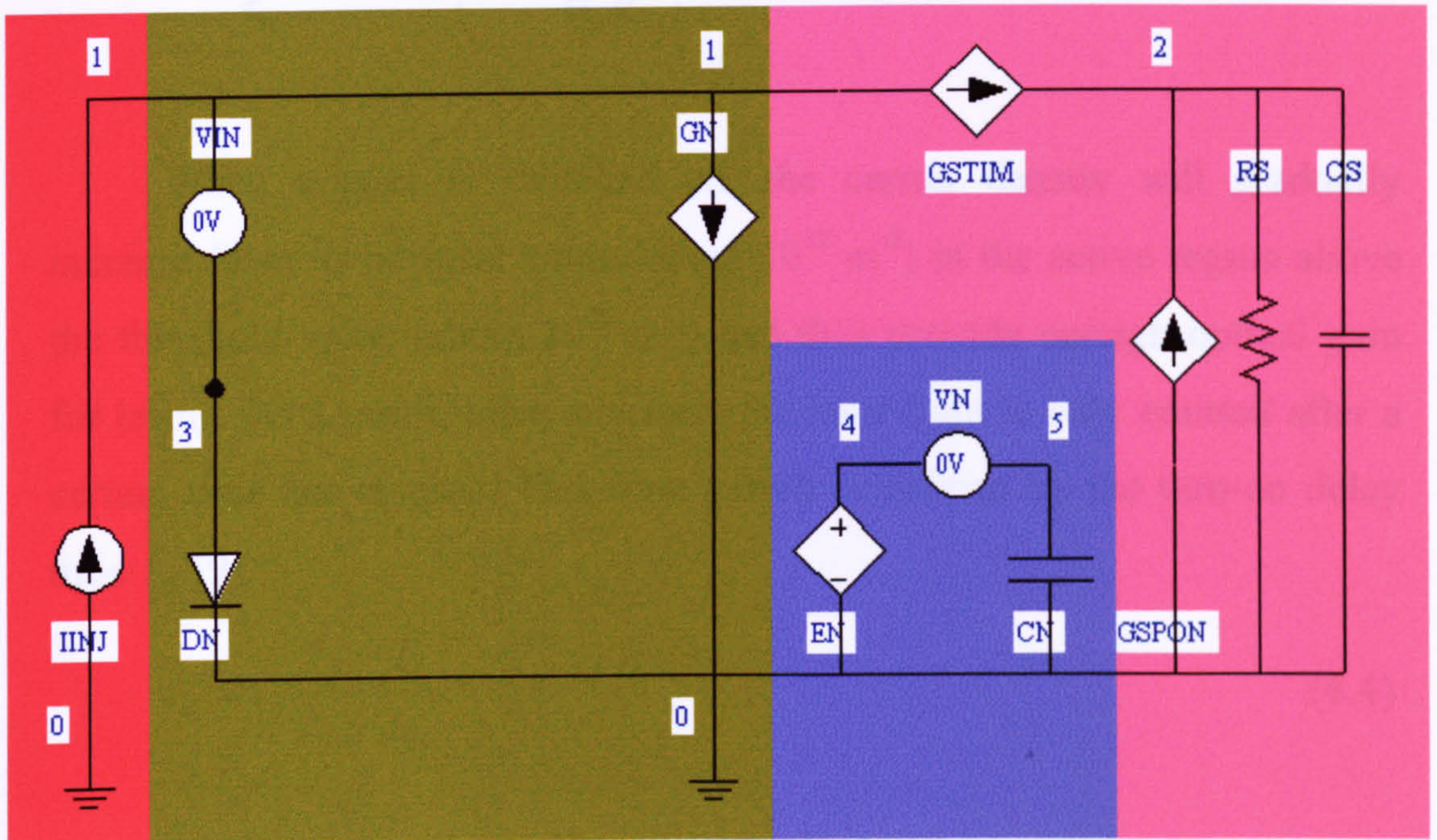
$$R_{SRH} + R_{spon} + R_{Aug} = \frac{n - n_i}{\tau_n} \cong \frac{n}{\tau_n} \quad (4.1)$$

In this definition,  $\tau_n$  represents the carrier lifetime. Coincidentally, the recombination current  $I_n \equiv neV/\tau_n$  defined by the carrier lifetime  $\tau_n$

becomes a convenient method to characterize the value of the applied voltage in the active region. From the small-signal analysis on the carrier-photon rate equations, it can be shown that the ac response can be characterized by two parameters: the resonant frequency  $f_r$  and damping rate  $\gamma$  [9].

$$f_r = \frac{1}{2\pi} \sqrt{\frac{V_{ph} B - I_0}{\tau_c}} \quad (4.2)$$

$$\gamma = \frac{1}{2} + 4\pi^2 f_r^2 \left( \tau_c + \frac{2\tau_c}{B} \right) \quad (4.3)$$



Apparently, the resonant frequency  $f_r$  and damping rate  $\gamma$  are much easier to characterize in the ac response. The circuit model is more related with the transient response. In our mind, the transient response of a series resonant circuit with lifetimes  $\tau_c$  are shown in Fig. 4.2. It shows that the resonant frequency  $f_r$  is proportional to the carrier lifetime  $\tau_c$ .

- DC input
- circuit for carrier density
- derivative circuit for  $dn/dt$
- circuit for photon density

Fig. 4.1. SPICE circuit model without carrier and lattice heating.

becomes a convenient method to characterise the value of the applied voltage in the active region. From the small-signal analysis on the carrier-photon rate equations, it can be shown that the ac response can be characterised by two parameters: the resonant frequency  $f_r$  and damping rate  $\gamma$  [9].

$$f_r \cong \frac{1}{2\pi} \sqrt{\frac{v_g g_n s_0}{\tau_s}} \quad (4.2)$$

$$\gamma = \frac{1}{\tau_n} + 4\pi^2 f_r^2 \left( \tau_s + \frac{\epsilon_{shb}}{v_g g_n} \right) \quad (4.3)$$

When a laser is switched on, the carrier density will gradually increase from its intrinsic value (about  $10^{12} \text{ m}^{-3}$ ) in the active region above the threshold value (about  $10^{24} \text{ m}^{-3}$ ) and thus provide enough optical gain for lasing. As a result, after injecting, the laser light is only emitted after a certain time has elapsed. This time period is defined by the turn-on delay time  $t_d$  [9].

$$t_d \approx \tau_n \frac{I_f - I_i}{I_f - I_{th}} \quad (4.4)$$

Apparently, the resonant frequency  $f_r$  and damping rate  $\gamma$  are much easier to characterise in the ac response while the turn-on delay time  $t_d$  is more related with the transient response. Bearing such relationships in mind, the transient response of a semiconductor laser with different carrier lifetimes  $\tau_n$  are shown in Fig. 4.2. It clearly verifies the turn-on delay time  $t_d$  is proportional to the carrier lifetime  $\tau_n$ .

As indicated in (4.2) and (4.3), increasing the differential gain  $g_d$  will increase the resonant frequency but respectively has no significant effect on the damping rate. This is clearly verified by the simulation results shown in Fig. 4.3. Similarly, as indicated in (4.2) and (4.3), increasing the photon lifetime  $\tau_p$  will decrease the resonant frequency and has no significant effect on the damping rate. This is clearly demonstrated in the simulation results shown in Fig. 4.4 where increasing the cavity length  $L_c$  represents the increase of the photon lifetime  $\tau_p$ . It is clearly seen in equations (4.2) and (4.3), that the value of the spontaneous gain coefficient  $g_{sp}$  only affects the damping rate and does not significantly affect the value of the resonant frequency. This is also clearly verified by the simulation results shown in Fig. 4.5. Figures 4.2 to 4.5 clearly demonstrate

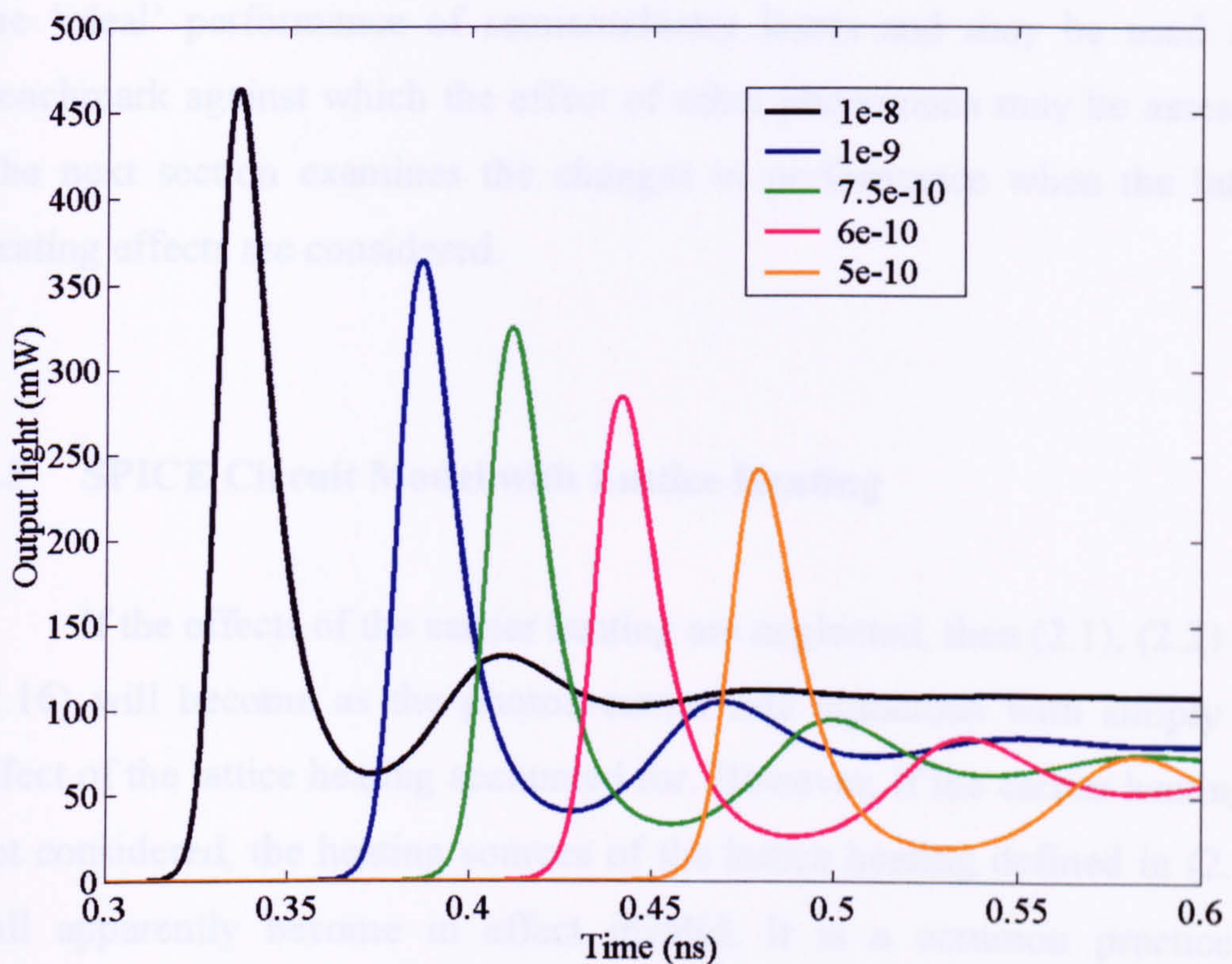


Fig. 4.2. Transient response of a semiconductor laser with different carrier lifetimes  $\tau_n$  (in the unit of second).

As indicated in (4.2) and (4.3), increasing the differential gain  $g_n$  will increase the resonant frequency but respectively has no significant effect on the damping rate. This is clearly verified by the simulation results shown in Fig. 4.3. Similarly, as indicated in (4.2) and (4.3), increasing the photon lifetime  $\tau_s$  will decrease the resonant frequency and has no significant effect on the damping rate. This is clearly demonstrated in the simulation results shown in Fig. 4.4 where increasing the cavity length  $L_z$  represents the increase of the photon lifetime  $\tau_s$ . It is clearly seen in equations (4.2) and (4.3), that the value of the nonlinear gain coefficient  $\epsilon_{shb}$  only affects the damping rate and does not significantly affect the value of the resonant frequency. This is also clearly verified by the simulation results shown in Fig. 4.5. Figures 4.2 to 4.5 clearly characterise the ‘ideal’ performance of semiconductor lasers and may be used as a benchmark against which the effect of other phenomena may be assessed. The next section examines the changes in performance when the lattice heating effects are considered.

### 4.3 SPICE Circuit Model with Lattice Heating

If the effects of the carrier heating are neglected, then (2.1), (2.2) and (2.16) will become as the photon-carrier rate equations with simply the effect of the lattice heating accounted for. However, if the carrier heating is not considered, the heating sources of the lattice heating defined in (2.16) will apparently become in effect invalid. It is a common practice to circumvent this problem by defining the heating sources contributing to the lattice heating heuristically. Intuitively, the total power injected by the

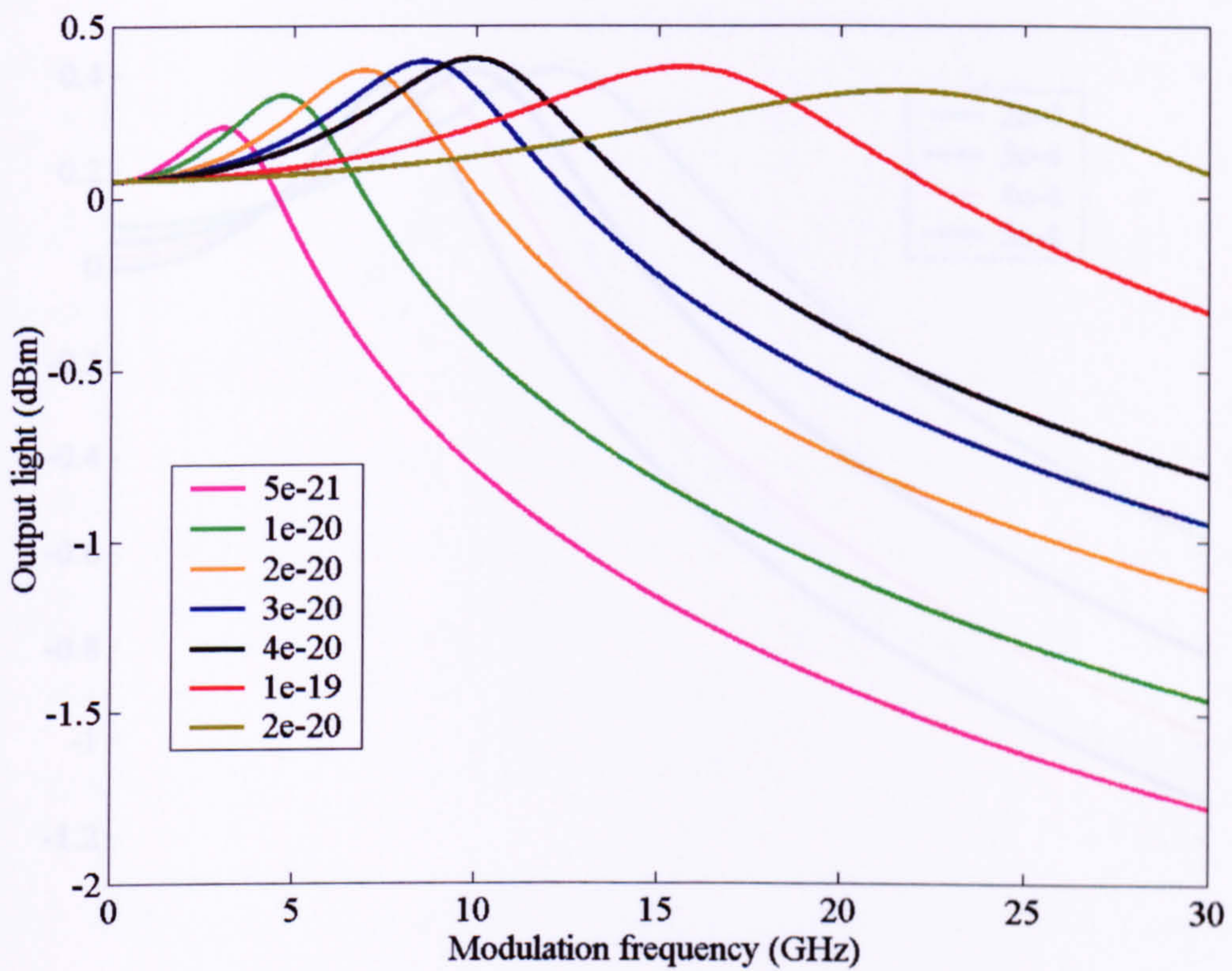


Fig. 4.3. AC response of a semiconductor laser with different differential gains  $g_n$  (in the unit of  $\text{m}^2$ ).

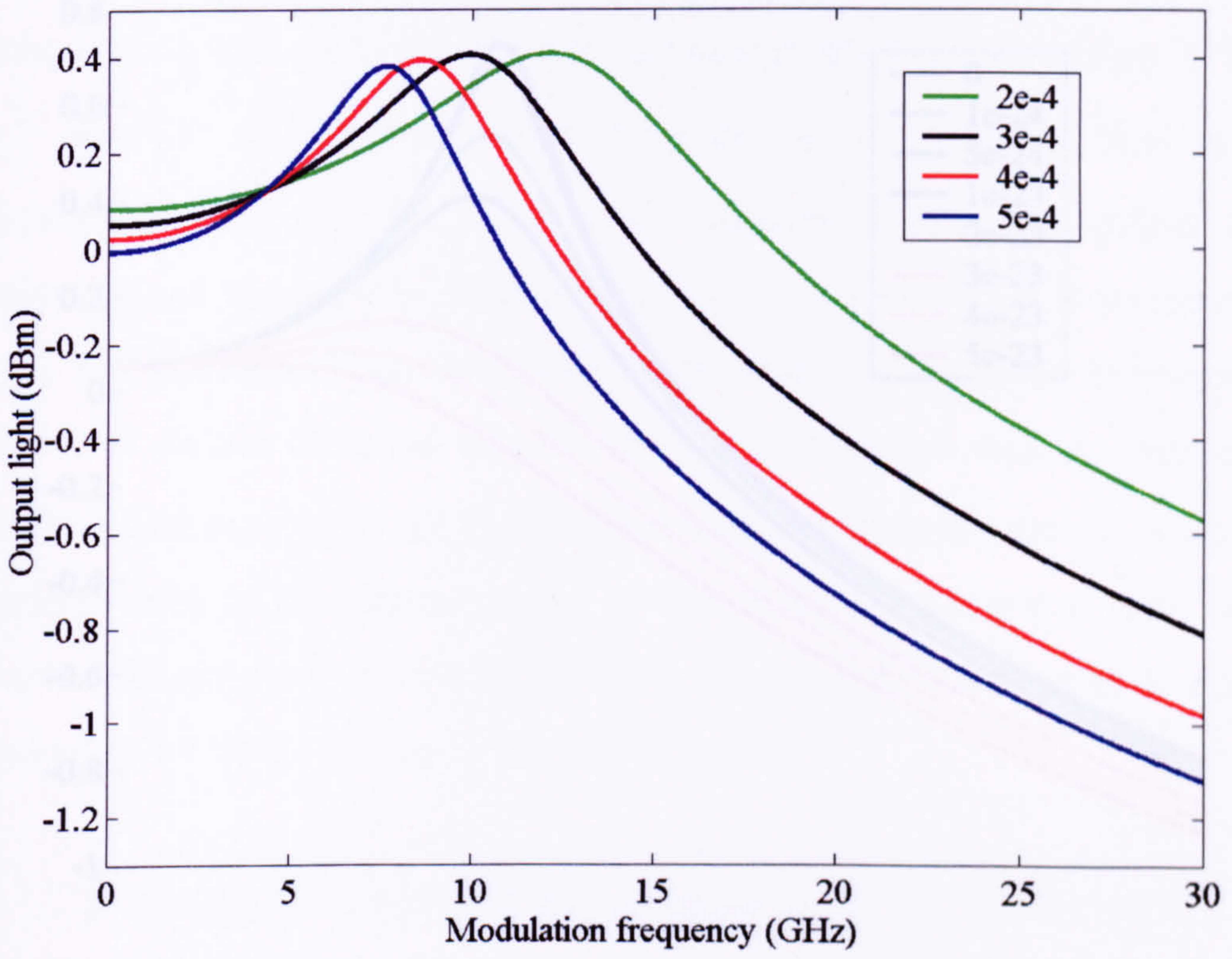


Fig. 4.4. AC response of a semiconductor laser with different cavity lengths  $L_z$  (in the unit of m).

current will either be dissipated as thermal power or be emitted as optical power. Therefore, if  $I$  and  $V$  represent the external applied current and voltage onto the device and  $P$  represents the output optical power, then  $I \cdot V - P$  will represent the total thermal power dissipated in the whole device. If the ohmic resistance is neglected, that is, all the voltage drop is assumed to be in the active region then  $V$  can approximately be made to correspond to the quasi-Fermi energy separation within the active region. Moreover, if the percentage of the injection current that reaches the active region is represented by  $\eta_{inj} I_{inj}$ , and then  $\eta_{inj} I_{inj} V - P$  corresponds to the lattice heating sources in the active region, and the validity of this approach is discussed in the next section. The correspondent SPICE circuit is given in Fig. 4.6 and the SPICE codes for the circuit model is given in APPENDIX C.2. The simulation of the L-I relationship and the lattice temperature with different thermal and thermal conduction coefficients are shown in Figs. 4.7 and 4.8. As expected, the value of  $\epsilon_{shb}$  has a significant impact on the output light intensity and is greater than the other bias current because the temperature is determined by the thermal conductivity within the device. Since the experimental or theoretical value of this thermal conduction coefficient for a semiconductor laser cannot be found in the published literature, it will be treated as a fitting variable in the circuit model.

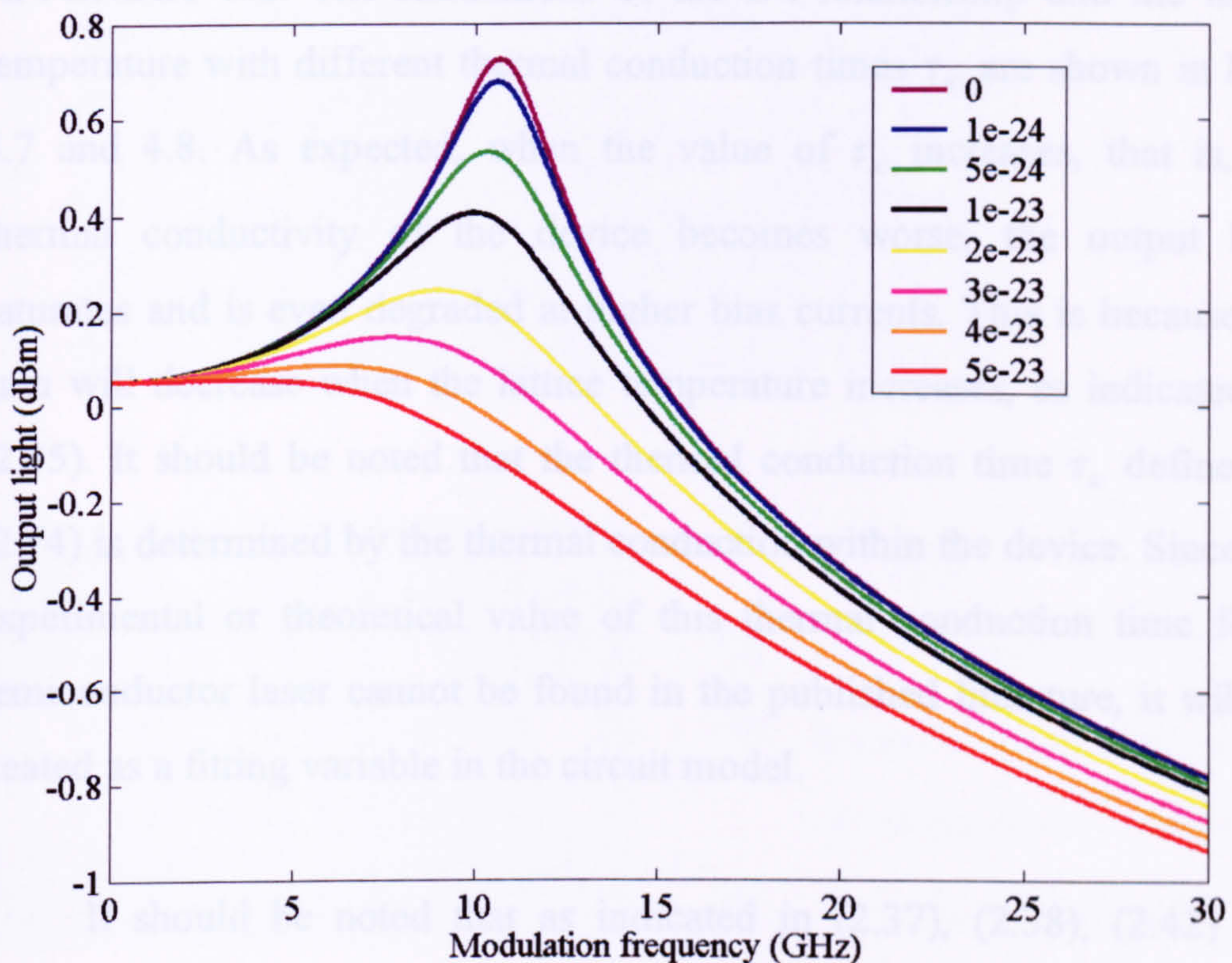
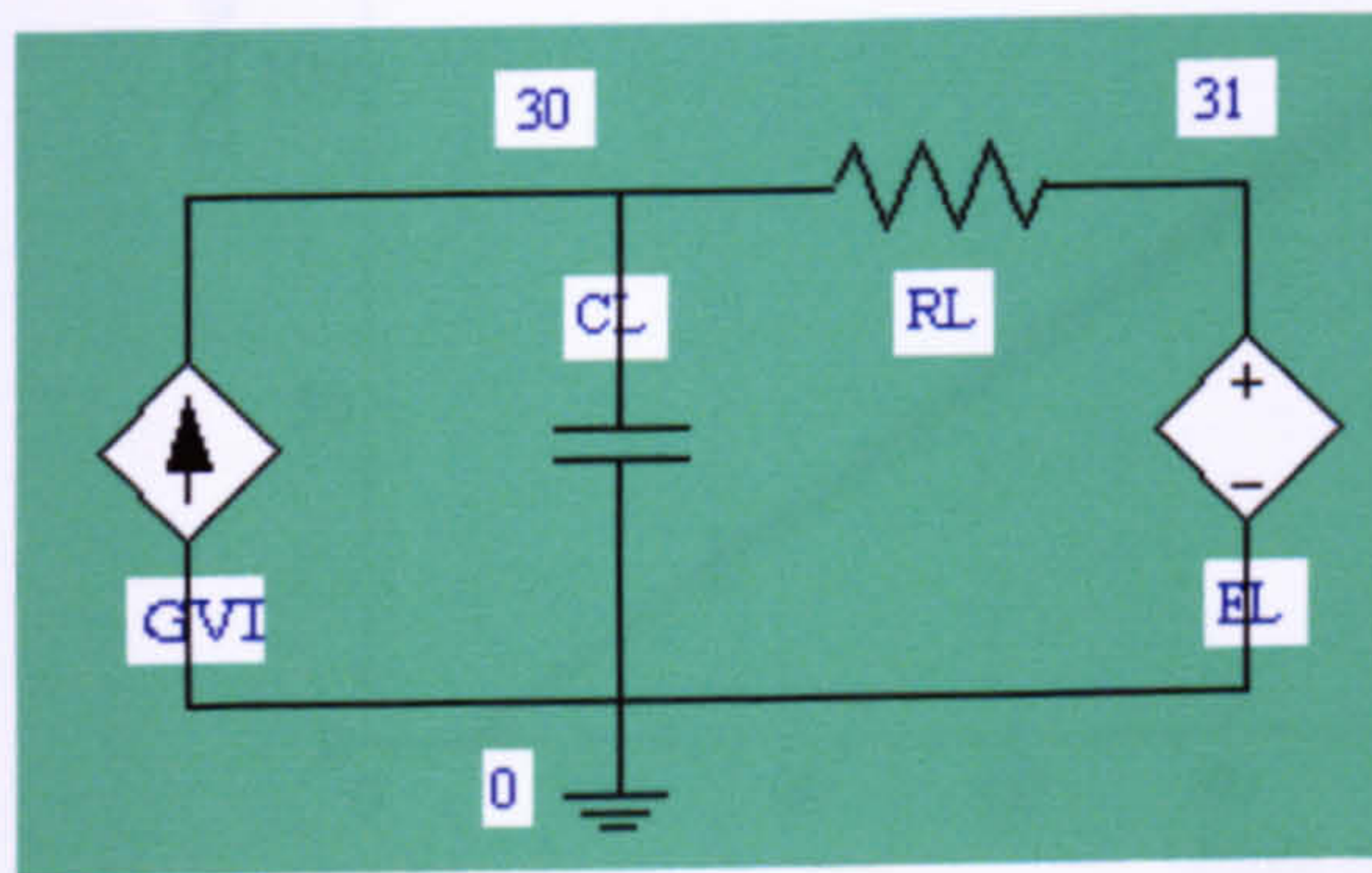
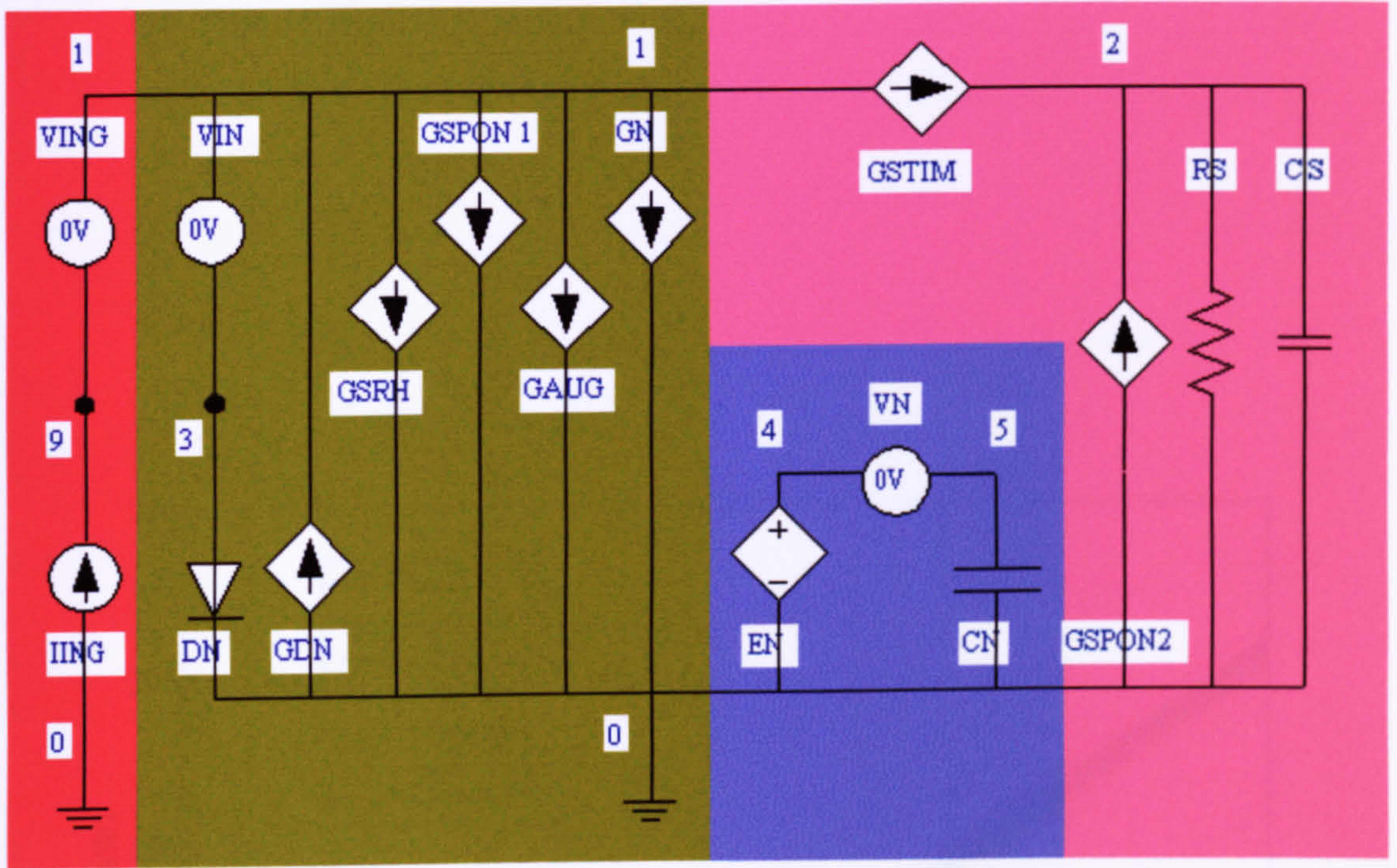


Fig. 4.5. AC response of a semiconductor laser with different nonlinear gain coefficients  $\epsilon_{shb}$  (in the unit of  $\text{m}^3$ ).



current will either be dissipated as thermal power or be emitted as optical power. Therefore, if  $I$  and  $V$  represent the external applied current and voltage onto the device and  $P$  represents the output optical power, then  $I \cdot V - P$  will represent the total thermal power dissipated in the whole device. If the ohmic resistance is neglected, that is, all the voltage drop is assumed to be in the active region then  $V$  can approximately be made to correspond to the quasi-Fermi energy separation within the active region. Moreover, if the percentage of the injection current that reaches the active region is represented by  $\eta_{inj} I_{inj}$ , and then  $\eta_{inj} I_{inj} \cdot V - P$  corresponds to the lattice heating sources in the active region, and the validity of this approach is discussed in the next section. The correspondent SPICE circuit is given in Fig. 4.6 and the SPICE codes for the circuit model is given in APPENDIX C.2. The simulations of the L-I relationship and the lattice temperature with different thermal conduction times  $\tau_\kappa$  are shown in Figs. 4.7 and 4.8. As expected, when the value of  $\tau_\kappa$  increases, that is, the thermal conductivity of the device becomes worse, the output light saturates and is even degraded at higher bias currents. This is because the gain will decrease when the lattice temperature increases, as indicated by (2.45). It should be noted that the thermal conduction time  $\tau_\kappa$  defined in (2.74) is determined by the thermal conduction within the device. Since the experimental or theoretical value of this thermal conduction time for a semiconductor laser cannot be found in the published literature, it will be treated as a fitting variable in the circuit model.

It should be noted that as indicated in (2.37), (2.38), (2.42) and (2.43), the coefficient of the leakage current  $I_{leak}$  and the Auger process  $C_{Aug}$  are dependent on the carrier temperature, but not the lattice



- DC input
- circuit for carrier density
- derivative circuit for  $dn/dt$
- circuit for photon density
- circuit for lattice heating

Fig. 4.6. SPICE circuit model with lattice heating.

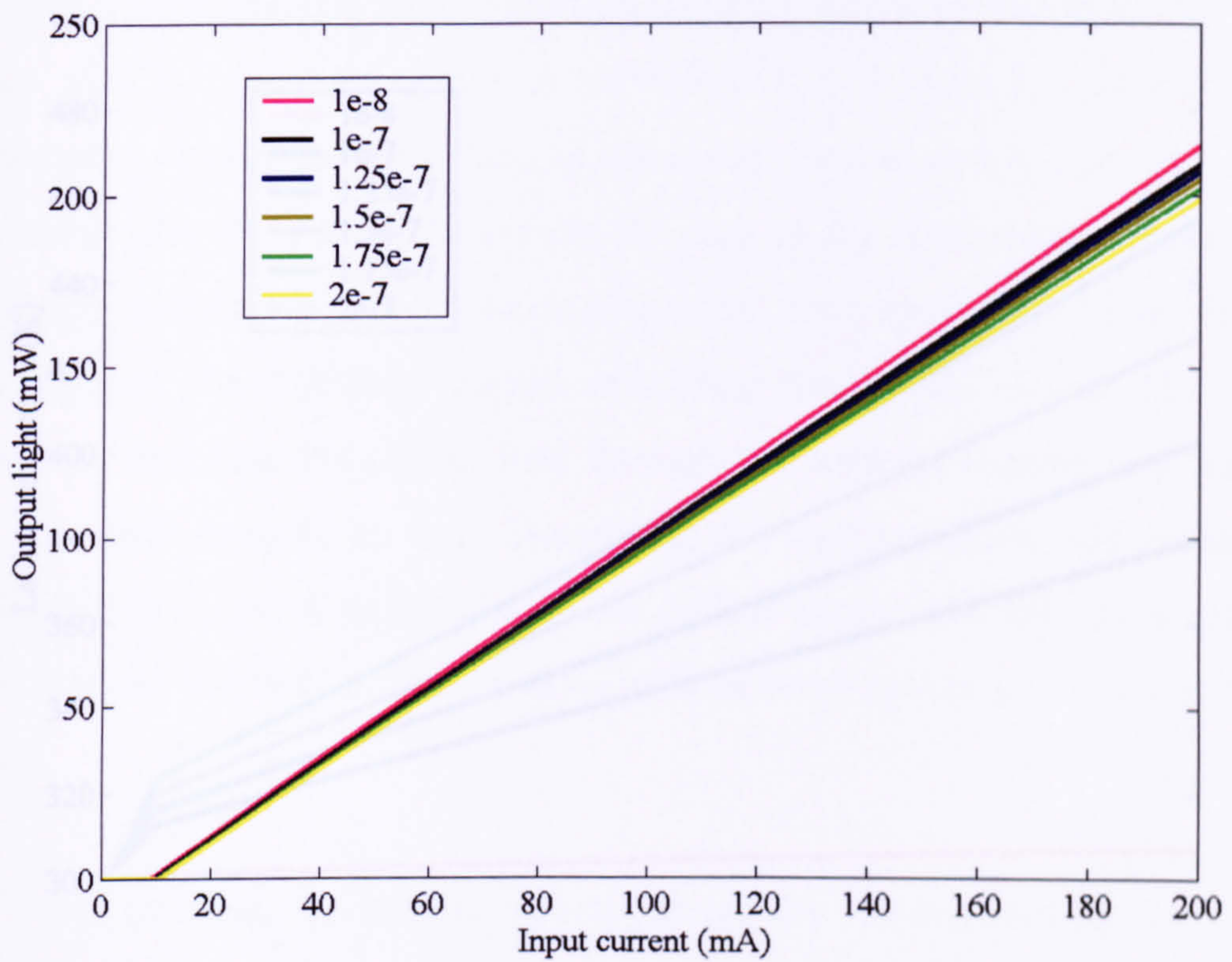


Fig. 4.7. L-I relationship of a semiconductor laser simulated with the effect of the lattice heating but without carrier heating for different thermal conduction times  $\tau_{\kappa}$  (in the unit of second).

temperature. Since the effect of the carrier heating is assumed to be negligible (zero) in this model, then the temperature-dependence feature is ignored in the circuit model shown in Fig. 4.6. However,  $C_{\text{diff}}$  and  $I_{\text{diff}}$  can be assumed to depend on the lattice temperature in the way as the carrier temperature in order to manifest the overall effect of the lattice heating. Even though, the Lattice temperature does not directly influence the leakage current and Auger process. In fact, such a theoretical approach is based on the assumption that the magnitude of the carrier heating is totally negligible and the lattice temperature equals the carrier temperature, that is,  $T_L = T_c$ .

If the temperature-dependent features for the leakage current and Auger recombinations are incorporated into the circuit as shown in Fig. 4.9,

The SPICE codes are given in APPENDIX C.3. The L-I relationship studied clearly indicates that, in the same thermal conductivity time, the thermal rollover is more severe for the case of the temperature-dependent leakage current and Auger recombinations. This result can certainly be explained. As injection current increases, the lattice temperature will increase and thus the carrier loss through the leakage current and Auger process will increase as well. Decreasing the carrier density will reduce the optical gain and thus the laser will stop lasing. As a result, the thermal rollover will be more severe as shown in Fig. 4.10.

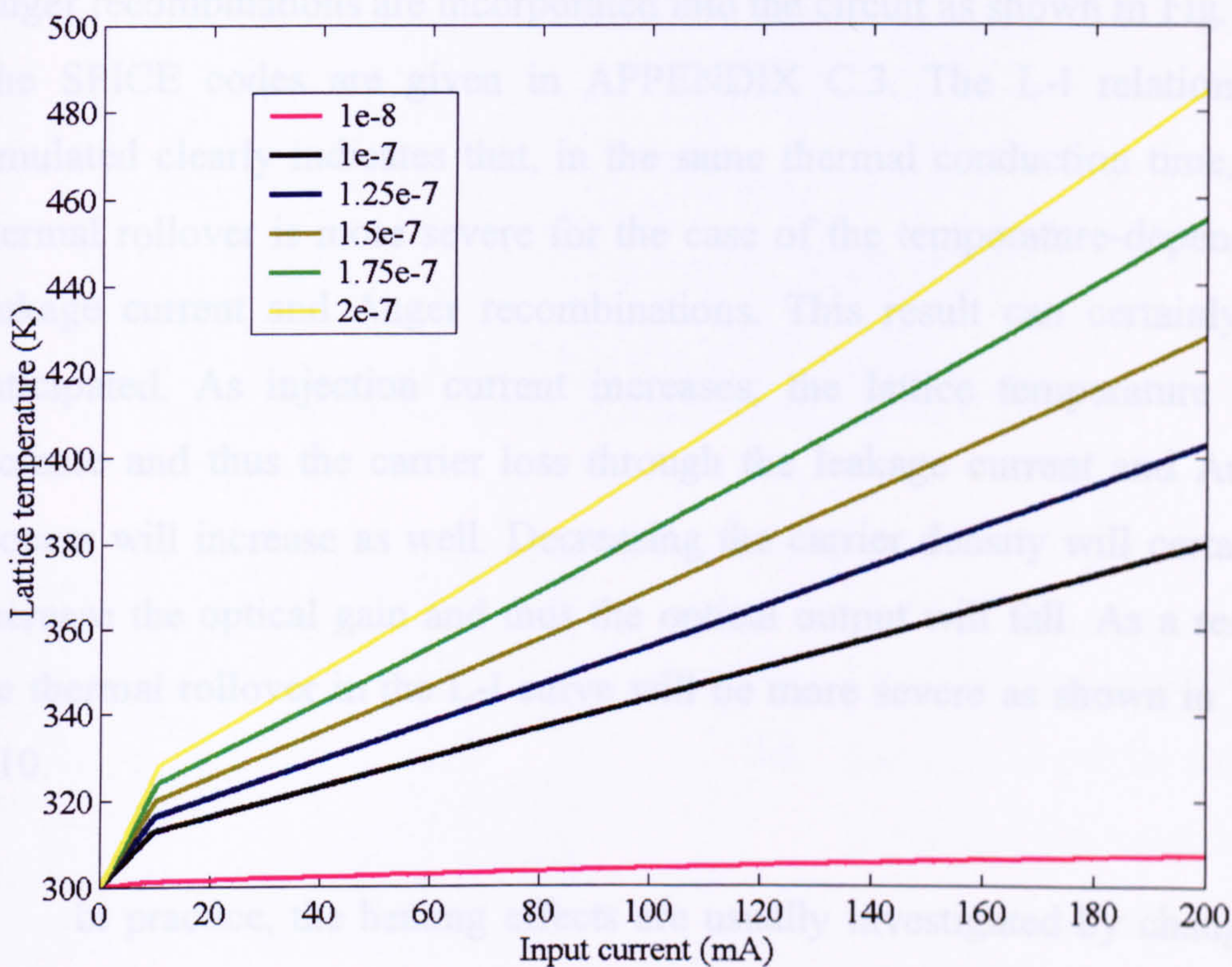
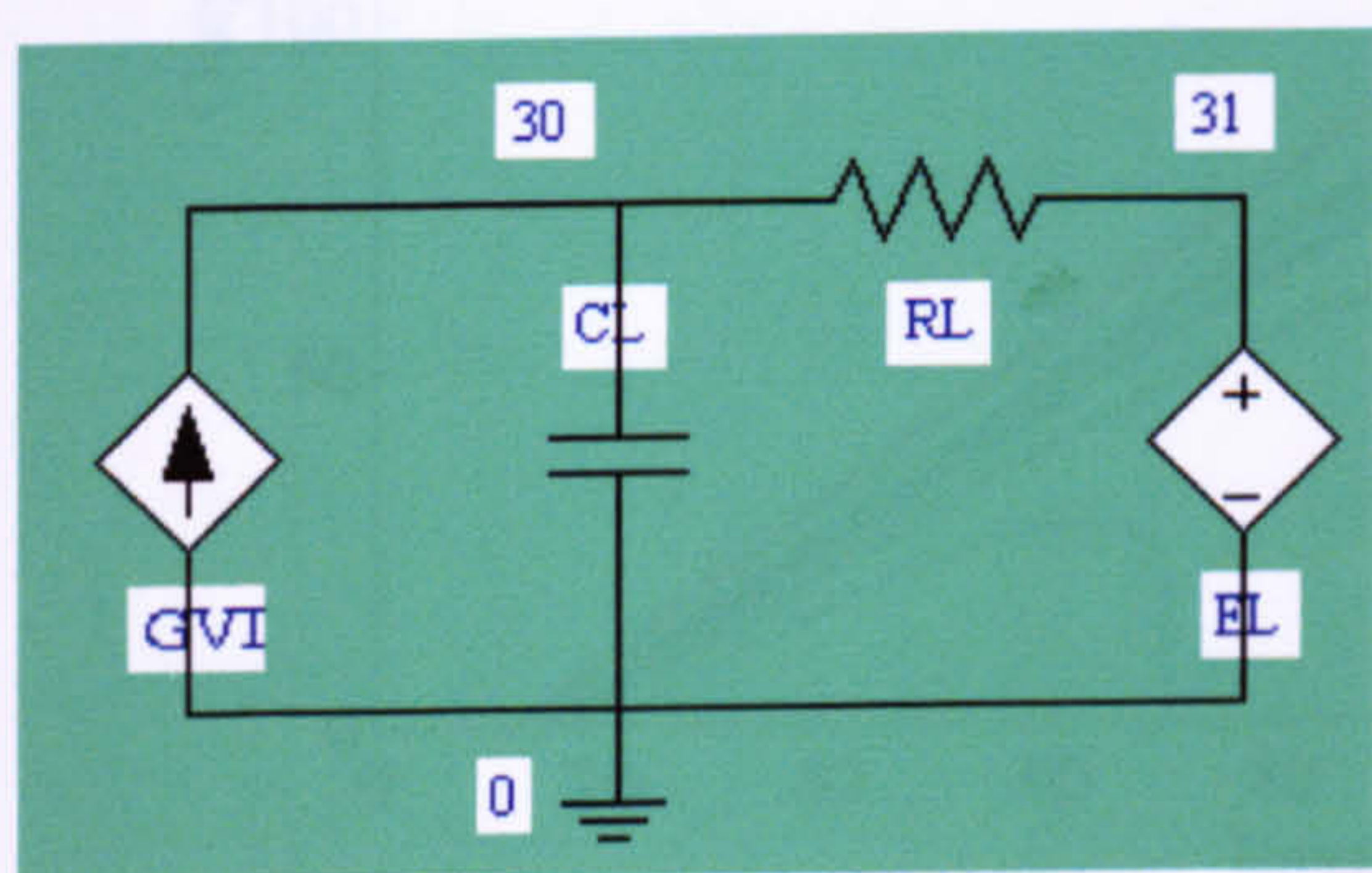
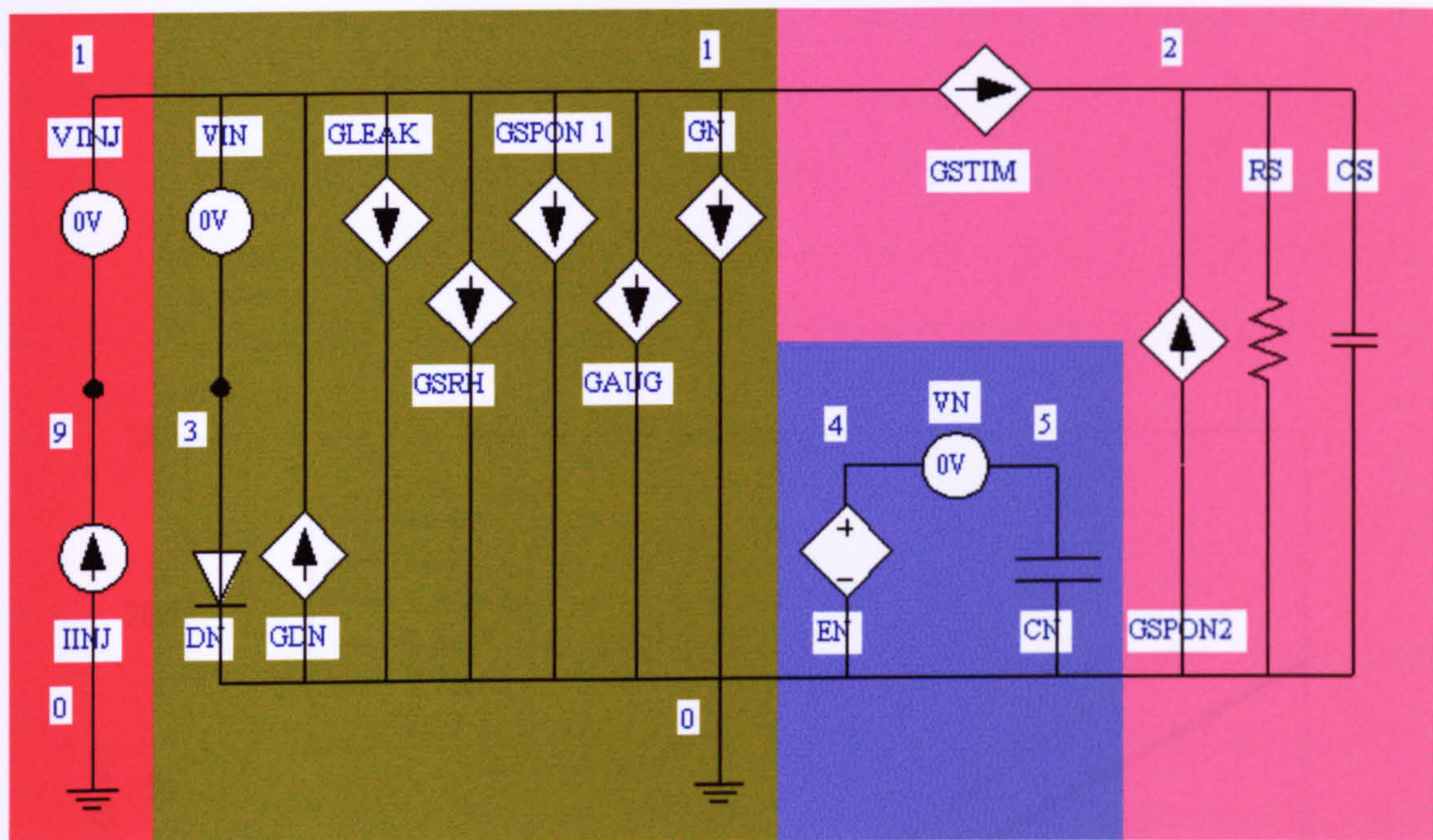


Fig. 4.8. Lattice temperature as a function of the input current for different thermal conduction times  $\tau_k$  (in the unit of second).

temperature. Since the effect of the carrier heating is assumed to be negligible (zero) in this model, then the temperature-dependence feature is ignored in the circuit model shown in Fig. 4.6. However,  $C_{Aug}$  and  $I_{leak}$  can be assumed to depend on the lattice temperature in the way as the carrier temperature in order to manifest the overall effect of the lattice heating. Even though, the lattice temperature does not directly influence the leakage current and Auger process. In fact, such a theoretical approach is based on the assumption that the magnitude of the carrier heating is totally negligible and the lattice temperature equals the carrier temperature, that is,  $T_L = T_c$ .

If the temperature-dependent features for the leakage current and Auger recombinations are incorporated into the circuit as shown in Fig. 4.9. The SPICE codes are given in APPENDIX C.3. The L-I relationship simulated clearly indicates that, in the same thermal conduction time, the thermal rollover is more severe for the case of the temperature-dependent leakage current and Auger recombinations. This result can certainly be anticipated. As injection current increases, the lattice temperature will increase and thus the carrier loss through the leakage current and Auger process will increase as well. Decreasing the carrier density will certainly decrease the optical gain and thus the optical output will fall. As a result, the thermal rollover in the L-I curve will be more severe as shown in Fig. 4.10.

In practice, the heating effects are usually investigated by changing the heat-sink temperature. This is because the changes of the carrier or lattice temperature within the device due to the injection current is almost



- DC input
- circuit for carrier density
- derivative circuit for  $dn/dt$
- circuit for photon density
- circuit for lattice heating

Fig. 4.9. SPICE circuit model with lattice heating including the temperature-sensitive leakage current and Auger process.

Auger process for different thermal conductivities times  $\tau_a$  (in the unit of second).

impossible to directly measure by experimental means, and can only be estimated by theoretical tests. Of course, this work is useful in predicting the carrier and lattice temperatures in the active region of the devices but is carried out following device fabrication. However, the circuit models developed can be used to simulate realistic experimental situations by changing the heat-sink temperatures  $T_{HS}$  in the SPICE codes. The simulation results of the L-I relationship for different heat-sink temperatures  $T_{HS}$  are shown in Fig. 4.11. Apparently, increasing the heat-sink temperature increases the threshold current and L-I nonlinearity. In this simulation, if the heat-sink temperature changes from 200K to 400K, the threshold current will change from 10 mA to 80 mA. This certainly validates that the threshold current is almost exponentially dependent on the heat-sink temperature [9].

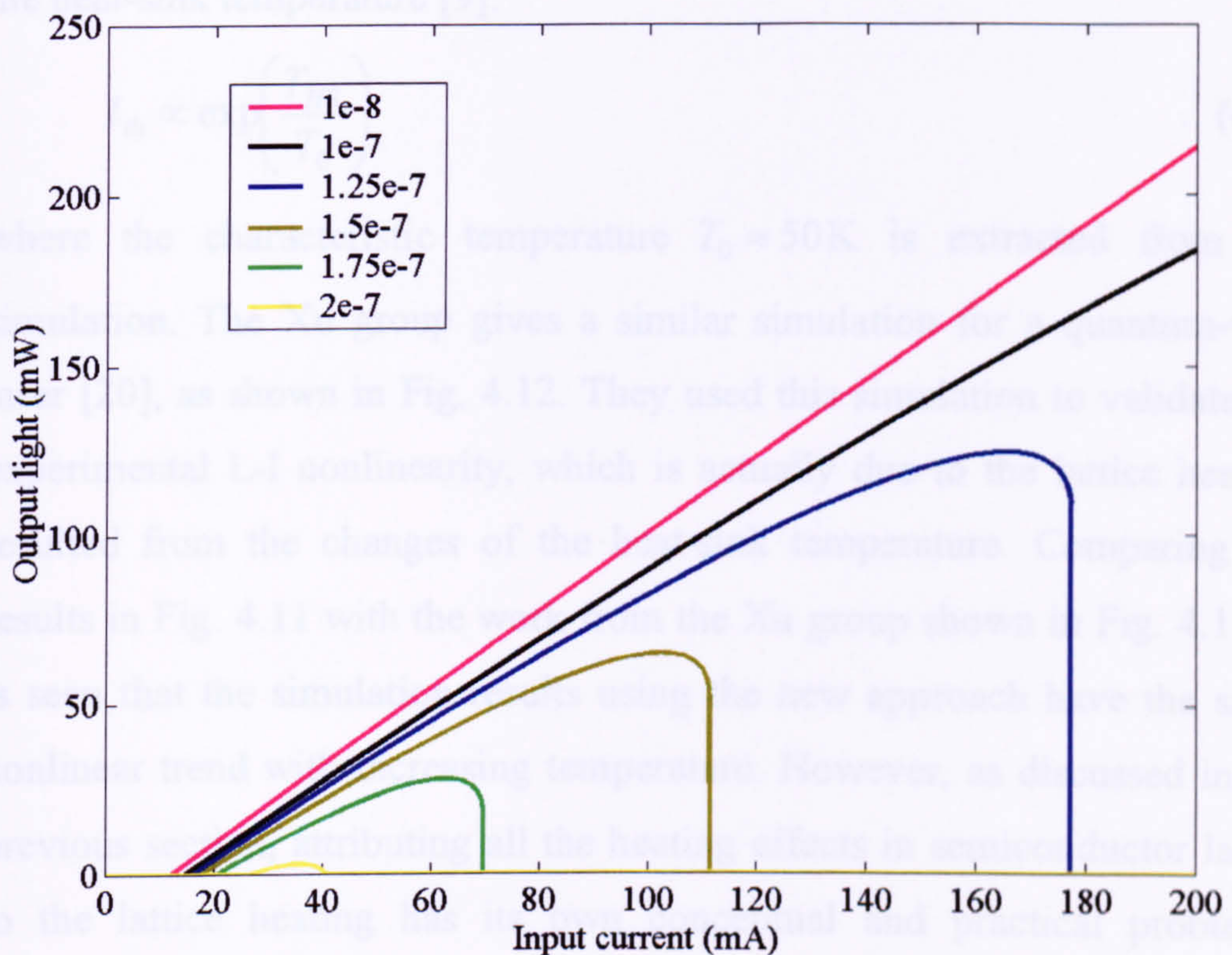


Fig. 4.10. L-I relationship of a semiconductor laser simulated with the temperature-dependent feature of the leakage current and Auger process for different thermal conduction times  $\tau_\kappa$  (in the unit of second).

impossible to directly measure by experimental means, and can only be estimated by theoretical tests. Of course, this work is useful in assessing the carrier and lattice temperatures in the active region of the devices but is carried out following device fabrication. However the circuit models developed can be used to simulate realistic experimental situations by changing the heat-sink temperatures  $T_{HS}$  in the SPICE codes. The simulation results of the L-I relationship for different heat-sink temperatures  $T_{HS}$  are shown in Fig. 4.11. Apparently, increasing the heat-sink temperature increases the threshold current and L-I nonlinearity. In this simulation, if the heat-sink temperature changes from 300K to 400K, the threshold current will change from 10 mA to 80 mA. This certainly validates that the threshold current is almost exponentially dependent on the heat-sink temperature [9]:

$$I_{th} \propto \exp\left(\frac{T_{HS}}{T_0}\right) \quad (4.5)$$

where the characteristic temperature  $T_0 \approx 50\text{K}$  is extracted from the simulation. The Xu group gives a similar simulation for a quantum-well laser [20], as shown in Fig. 4.12. They used this simulation to validate the experimental L-I nonlinearity, which is actually due to the lattice heating resulted from the changes of the heat-sink temperature. Comparing the results in Fig. 4.11 with the work from the Xu group shown in Fig. 4.12. It is seen that the simulation results using the new approach have the same nonlinear trend with increasing temperature. However, as discussed in the previous section, attributing all the heating effects in semiconductor lasers to the lattice heating has its own conceptual and practical problems. Therefore, in the following the carrier and lattice heating in the devices are simultaneously considered.



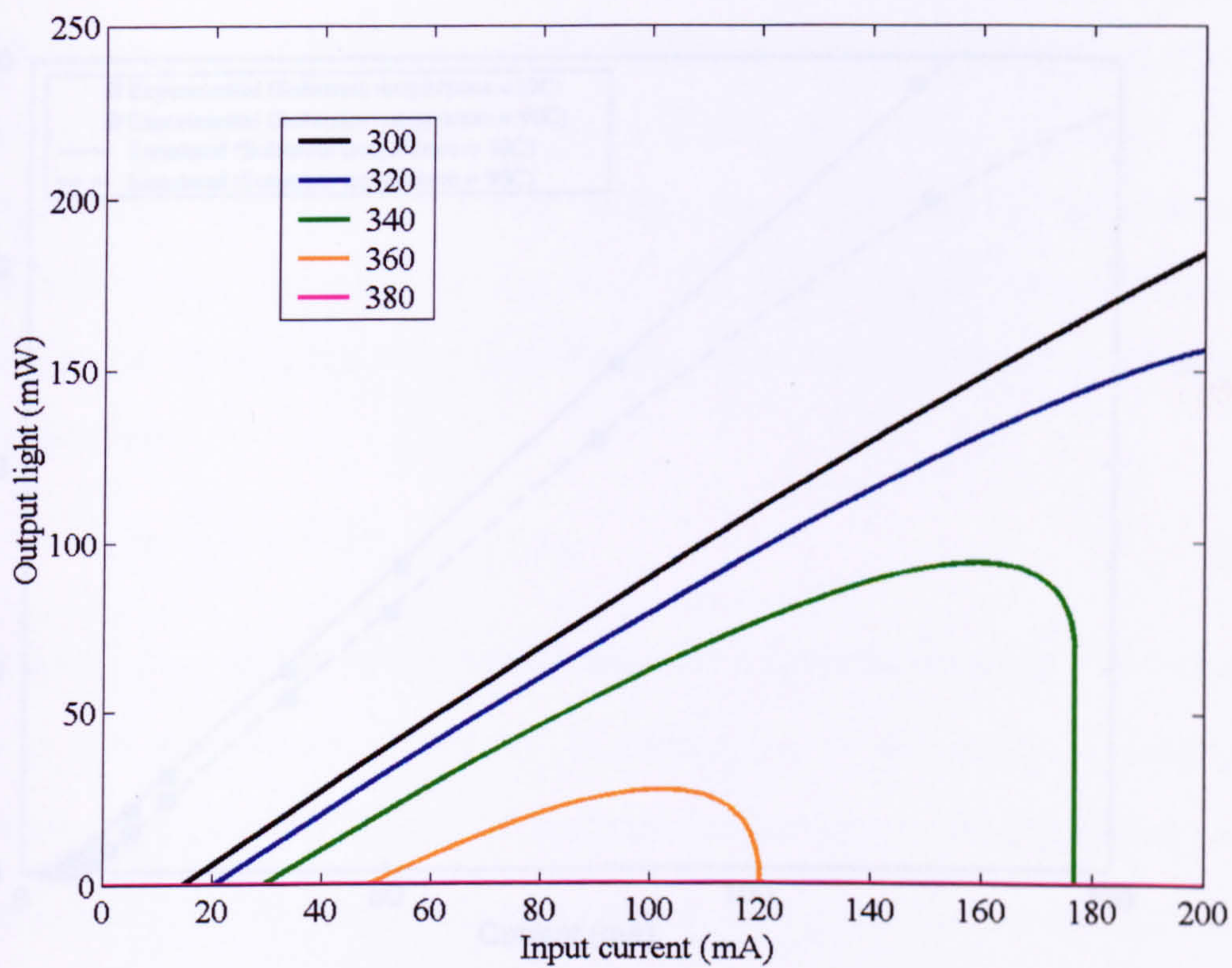


Fig. 4.11 L-I relationship of a semiconductor laser simulated with the temperature-dependent feature of the leakage current and Auger process for different heat-sink temperatures  $T_{HS}$  (in the unit of Kelvin).

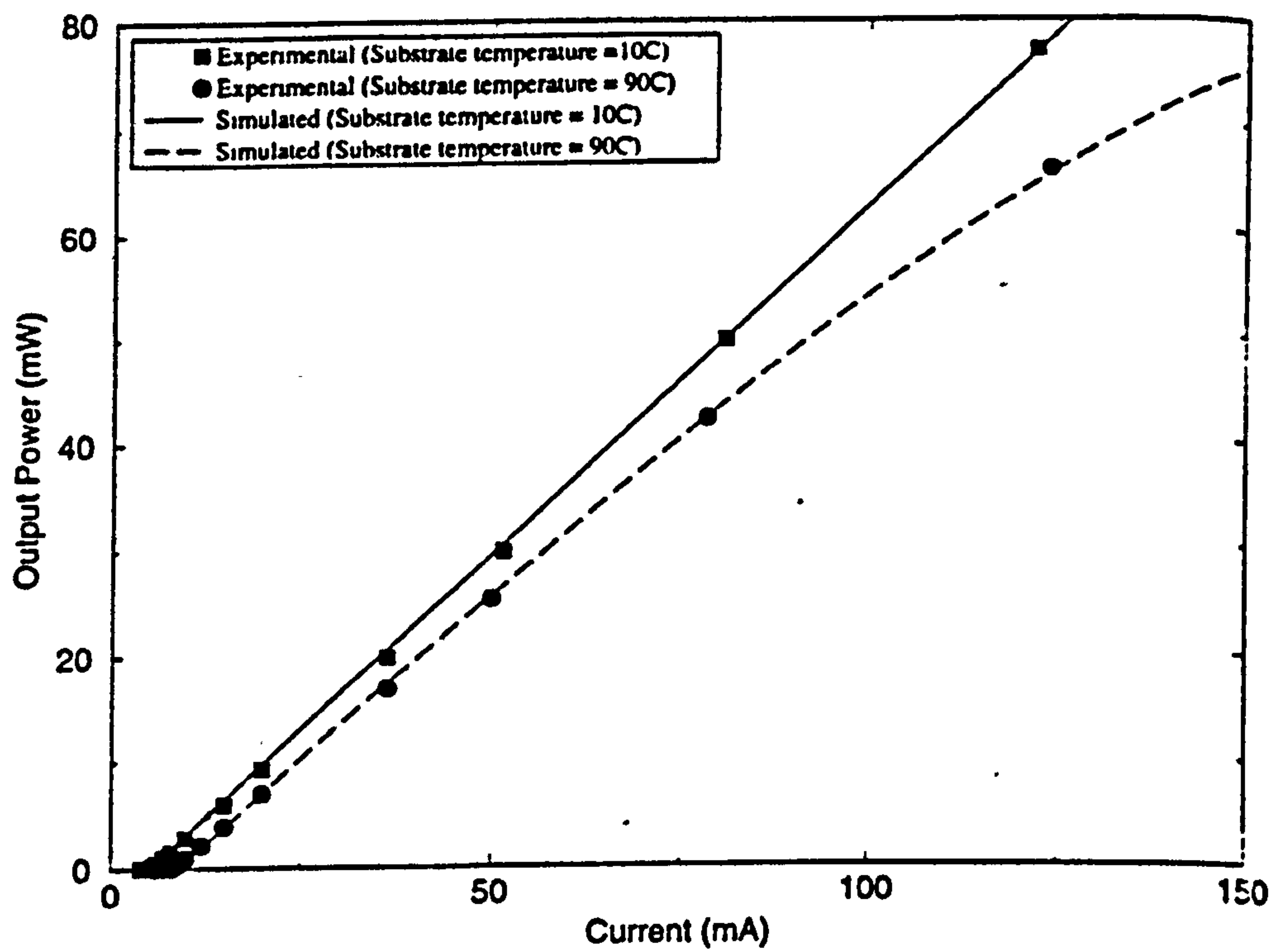


Fig. 4.12 Comparison of the experimental and simulated L-I relationship for different heat-sink temperatures in a quantum-well laser. (Xu group)

#### 4.4 SPICE Circuit Model with Carrier and Lattice Heating

As indicated by the previous results, the lattice heating has a dramatic effect on the dc properties of a semiconductor laser. Accounting for the lattice heating effect alone, the thermal rollover of the P-I relationship commonly seen in any semiconductor laser can satisfactorily be explained. However, dedicating all the heating effects in semiconductor lasers to the lattice heating has its own conceptual and practical problems. First of all, the heuristic definition of the lattice-heating source  $I \cdot V - P$  is not in itself physically transparent; sometimes, it may become misleading. For example, if  $I$  and  $V$  represent the external applied current and voltage, respectively, then  $I \cdot V - P$  will represent the total power dissipated in the whole device, not just the active region. Using this crude lumped approach, it becomes impossible to represent the heating source (more precisely, the power density) at different locations within the device, by the  $I \cdot V - P$  expression. This argument can further be amplified by the following discussion and illustrated as Fig. 4.13. The lattice temperature distribution within the device can normally be described by the equation of thermal conduction

$$c_L \rho_L \frac{\partial T_L}{\partial t} = \nabla \cdot (\kappa_L \nabla T_L) + g_{th} \quad (4.6)$$

where  $T_L(\mathbf{r}, t)$  is the lattice temperature at a specific location  $\mathbf{r}$  and time  $t$ ,  $c_L$  is the specific heat capacity of lattice,  $\rho_L$  is the material density of lattice,  $\kappa_L$  is the coefficient of thermal conduction governing the speed of the distribution of the lattice temperature, and  $g_{th}$  is the generation rate of the energy density at a specific location  $\mathbf{r}$  and a specific time  $t$ . By the definition of  $g_{th}$ , the  $I \cdot V - P$  expression cannot apparently be used in

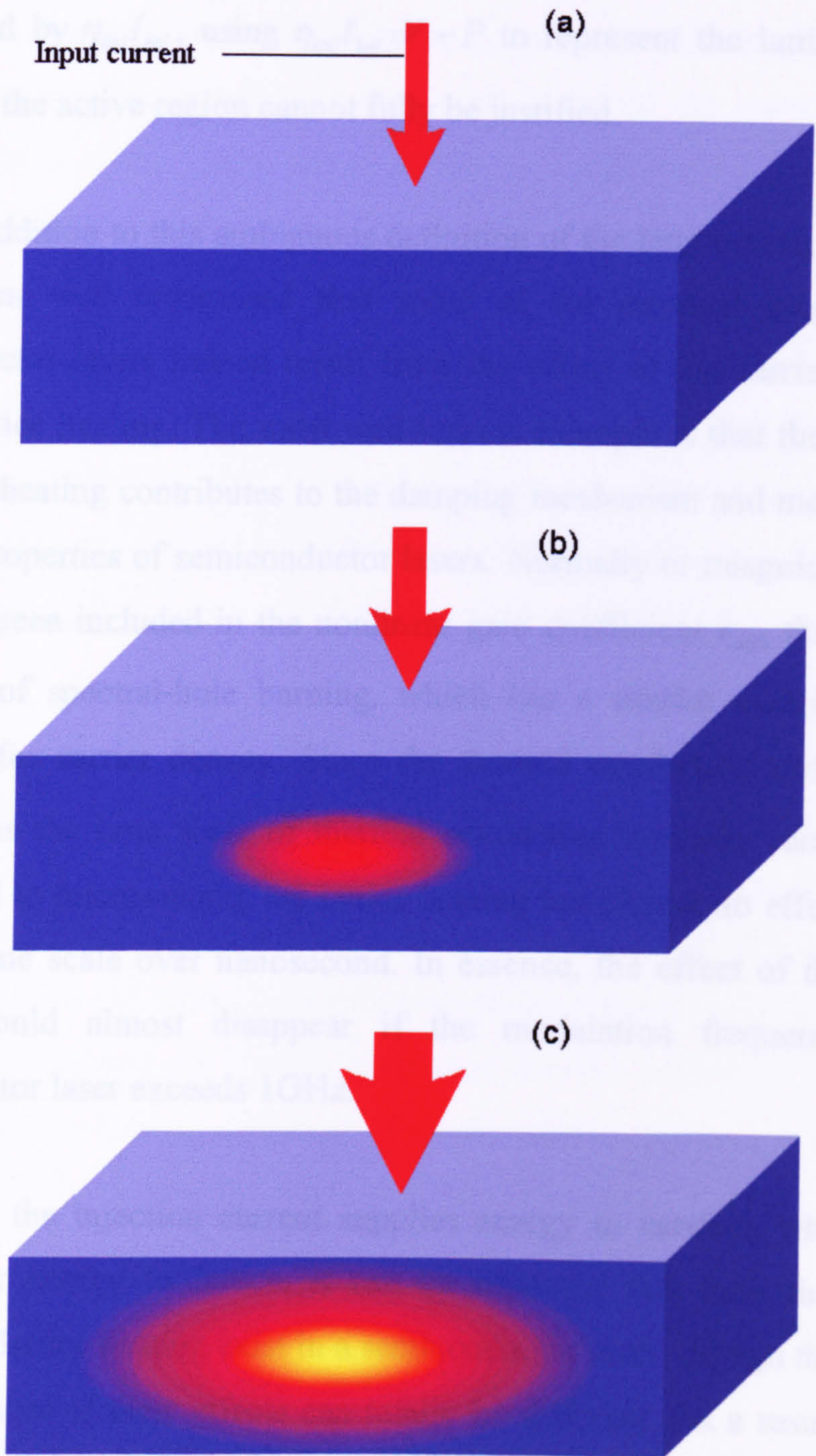


Fig. 4.13. Schematic diagrams of lattice heating under different conditions: (a) no current injection; (b) low current injection; and (c) high current injection.

conjunction with the equation of thermal conduction. Even when  $V$  is assigned to represent the quasi-Fermi energy separation within the active region, and the percentage of injection reaches the active region is represented by  $\eta_{inj}I_{inj}$ , using  $\eta_{inj}I_{inj} \cdot V - P$  to represent the lattice heating sources in the active region cannot fully be justified.

In addition to this ambiguous definition of the lattice-heating source, it has been well recognised that some of the physical properties of semiconductor lasers indeed result from the effect of the carrier heating, not the lattice heating. The most well known example is that the effect of the carrier heating contributes to the damping mechanism and modifies the dynamic properties of semiconductor lasers. Normally or misguidedly, this effect has been included in the nonlinear gain coefficient  $\varepsilon_{shb}$  that models the effect of spectral-hole burning, which has a similar contribution is accounted for carrier density. Since the thermal conduction time  $\tau_{\kappa}$  that characterises the time scale of thermal conduction typically ranges from nanosecond to microsecond, the lattice heating has almost no effect on the dynamic time scale over nanosecond. In essence, the effect of the lattice heating should almost disappear if the modulation frequency of a semiconductor laser exceeds 1GHz.

Since the injection current supplies energy to carriers, which then release their energy to lattice, it can be expected that both the carrier heating and lattice heating exist in a semiconductor laser, though the ranges and magnitudes of their effects can totally be different. As a result, it has almost become a common practice to disaggregate the effects of the carrier heating and lattice heating to different domains: the lattice heating only

affects the static (dc) properties of semiconductor lasers while the carrier heating only affects their dynamic (ac and transient) properties through the nonlinear gain coefficient  $\varepsilon_{shb}$ . This approach is embedded in the circuit model discussed in Sec. 4.3. Despite its simplicity, such an approach still has deficiencies. For example, it is entirely based on the assumption that the magnitude of the static carrier heating is negligible compared to the magnitude of the static lattice heating. Such an optimistic assumption cannot fully be validated for all different cases. Furthermore, chirping in semiconductor lasers, one of the obvious cases cannot satisfactorily be explained by such an approach [12]. In fact, further confusion in the definitions of adiabatic and transient chirping has unnecessarily resulted from attempting to explain performance in this way. It has also been shown that even the nonlinear gain coefficient itself is not well defined [14].

Following the discussion, artificially differentiating the effects between the carrier heating and lattice heating cannot adequately resolve the critical heating issues associated with semiconductor lasers. Attributing the lattice heating only to the static properties and ascribing the carrier heating solely to the dynamic properties not only cannot fully be justified but also misrepresents the physical origins of the laser properties. Therefore, to understand the heating problems of semiconductor lasers, it is necessary to simultaneously include the carrier and lattice heating.

Based on the previous theoretical equations that were proposed to model the processes of the carrier heating and lattice heating in semiconductor lasers, the rate equations for the electron temperature  $T_e$ , hole temperature  $T_h$  and lattice temperature  $T_L$  are given in (2.14), (2.15)

and (2.16). These equations have three important parameters determining the magnitude of the carrier heating: the electron-lattice energy relaxation time  $\tau_{e-L}$ , hole-lattice energy relaxation time  $\tau_{h-L}$  and electron-hole energy relaxation time  $\tau_{e-h}$ . The electron-lattice energy relaxation time  $\tau_{e-L}$  determines the time scale for the electron temperature to equalise the lattice temperature,  $\tau_{h-L}$  determines the time scale for the hole temperature to equalise the lattice temperature, and  $\tau_{e-h}$  determines the time scale for the electron temperature to equalise the hole temperature. Apparently, if the value of  $\tau_{e-L}$  is larger, the electron heating will be more severe. Similarly, if the value of  $\tau_{h-L}$  is larger which means that electrons will transfer less energy to holes, the electron heating will be more severe while the hole heating will be reduced.

It should be noted that the physical processes of energy transfer among electrons, holes and lattice are extremely complicated. For example, carriers and phonons interact with each other via different types of physical mechanisms, such as the polar-optical-phonon, deformation-potential-optical-phonon, deformation-potential-acoustic-phonon, piezoelectric-acoustic-phonon and intervalley-phonon interactions. Optical phonons do not participate in the thermal-conduction processes because of their negligible group velocity. In other words, the thermal conduction is almost entirely determined by the acoustic phonons. The optical phonons emitted by carriers will decay into the acoustic phonons. To exactly model all these processes in semiconductor lasers is certainly beyond the scope of this thesis. In fact, some of the physical processes are still not well defined or properly discussed. For instance, the interactions among phonons themselves are still the subject of many debates. Theories for the

multiple-phonon emission in the SRH process are still not fully developed. It is thus not feasible to incorporate these phonon processes into the SPICE models proposed. Nevertheless, the foregoing certainly implies that the physical processes of energy transfer among electrons, holes and lattice are characterised by the electron-lattice energy relaxation time  $\tau_{e-L}$ , hole-lattice energy relaxation time  $\tau_{h-L}$  and electron-hole energy relaxation time  $\tau_{e-h}$ . As demonstrated that these energy relaxation times can be calculated by first principles, but they are treated as adjustable parameters in this work.

The completed effects of the electron-lattice energy relaxation time  $\tau_{e-L}$  on the dc L-I relationship, electron temperature, hole temperature and lattice temperature are shown in Figs. 4.14, 4.15, 4.16 and 4.17, respectively. As expected an increase in the value of the electron-lattice energy relaxation time  $\tau_{e-L}$  increases the magnitude of the electron heating. As a result, the electron temperature, lattice temperature and hole temperature will increase due to the higher electron temperature, and thus the thermal rollover will become more severe. It is evident from the dc response characteristic that the lattice heating is far more dominant than the carrier heating for the case of  $\tau_{\kappa} = 4 \times 10^{-7}$  sec. The effects of changing the value of the hole-lattice energy relaxation time  $\tau_{h-L}$  are rather similar to that of the  $\tau_{e-L}$  characteristic and therefore their simulation results are not presented here.

Similarly, the transient responses simulated by SPICE for the output power, electron temperature and hole temperature with different electron-lattice energy relaxation time  $\tau_{e-L}$  are shown in Fig. 4.18, 4.19 and 4.20,



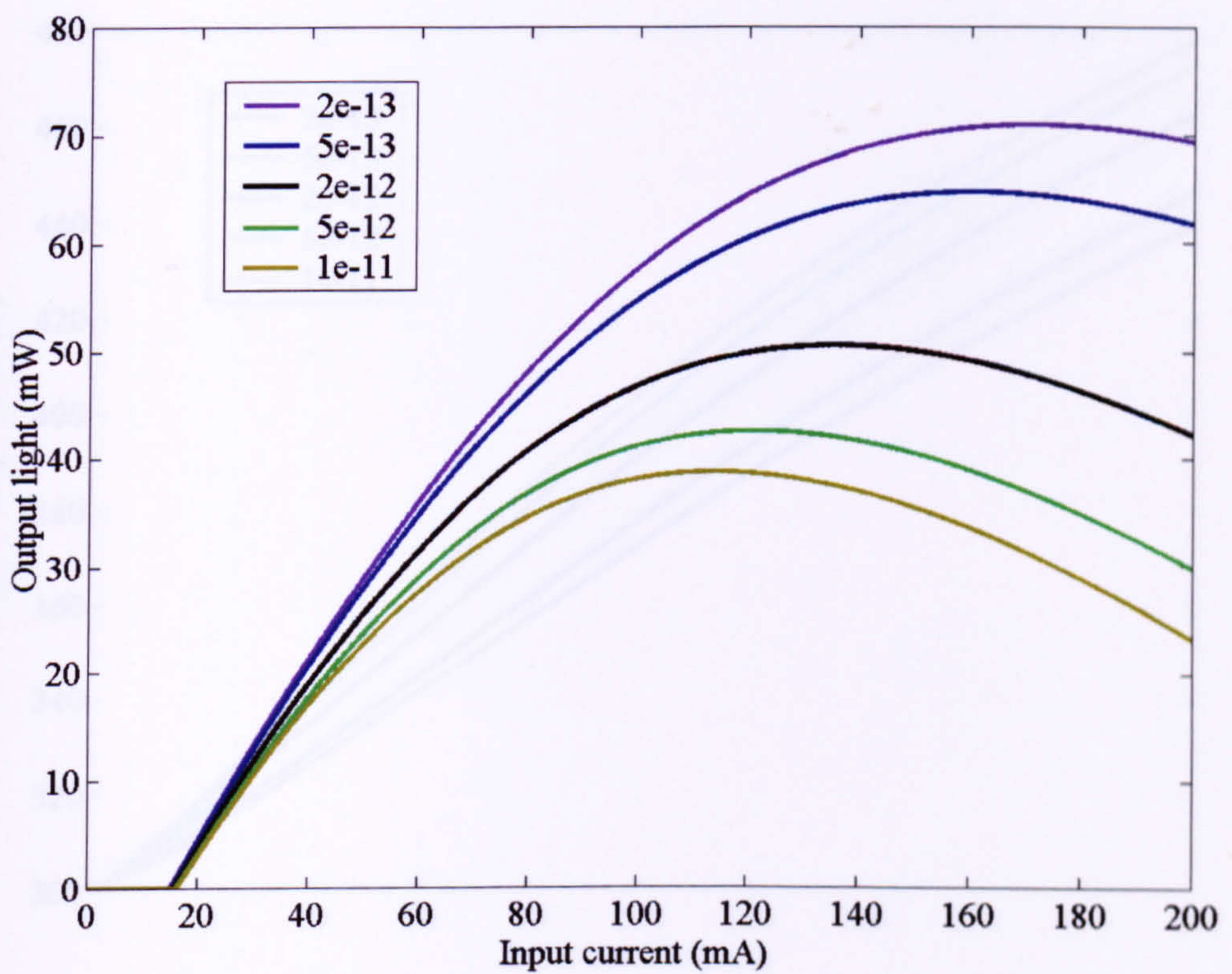


Fig. 4.14. L-I relationship for different electron-lattice energy relaxation times  $\tau_{e-L}$  (in the unit of second).

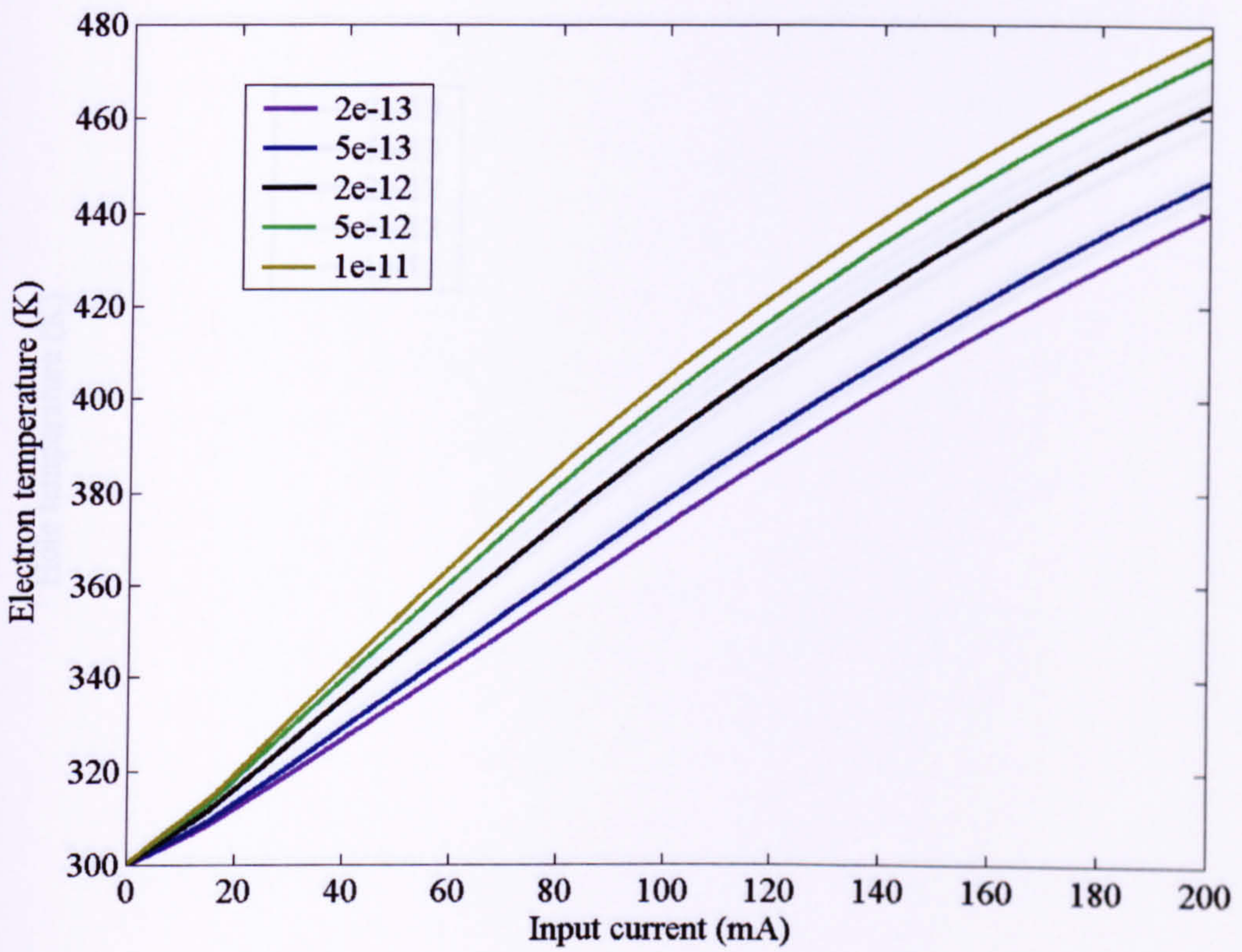


Fig. 4.15. Electron temperature as a function of the input current for different electron-lattice energy relaxation times  $\tau_{e-L}$  (in the unit of second).

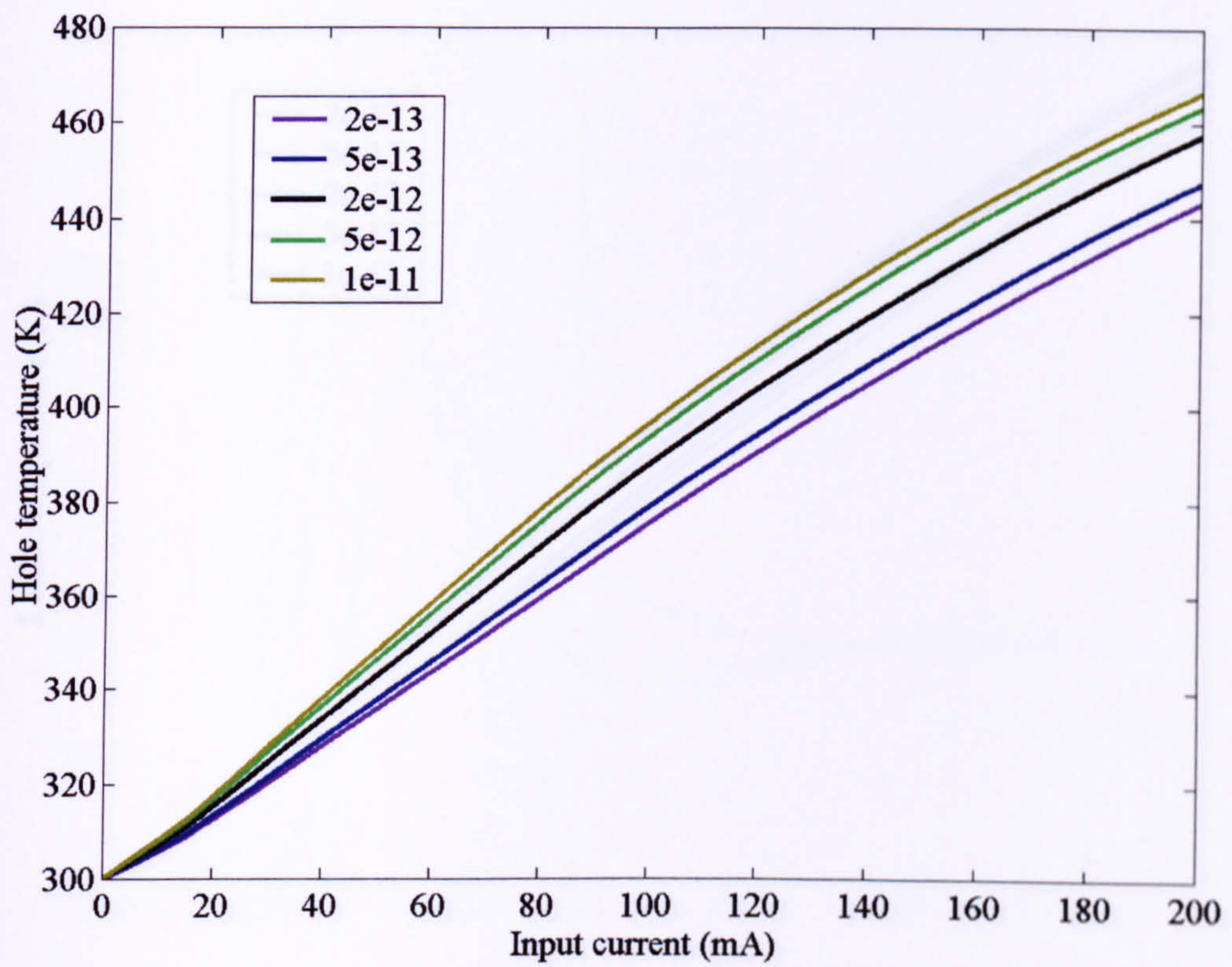


Fig. 4.16. Hole temperature as a function of the input current for different electron-lattice energy relaxation times  $\tau_{e-L}$  (in the unit of second).

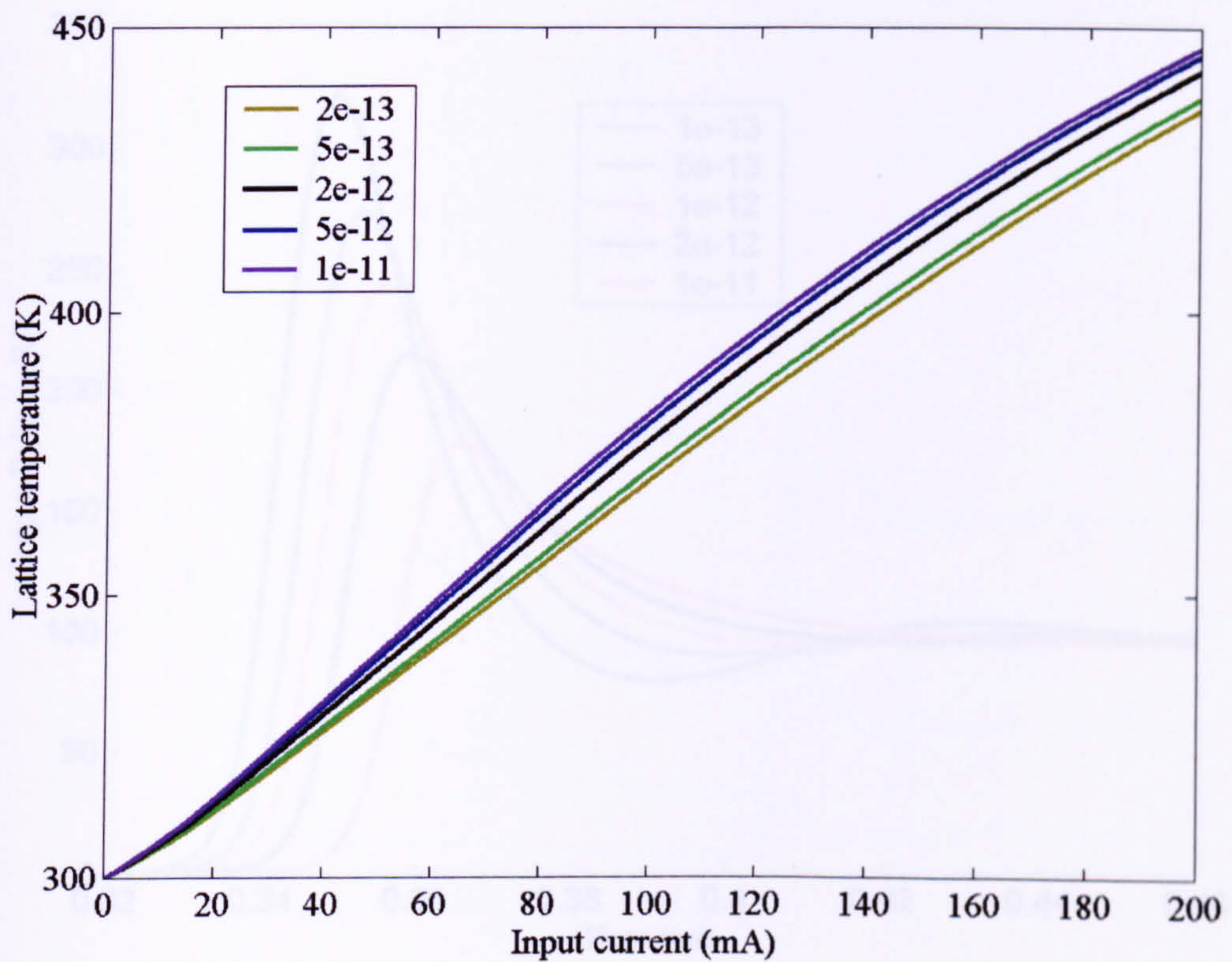


Fig. 4.17. Lattice temperature as a function of the input current for different electron-lattice energy relaxation times  $\tau_{e-L}$  (in the unit of second).

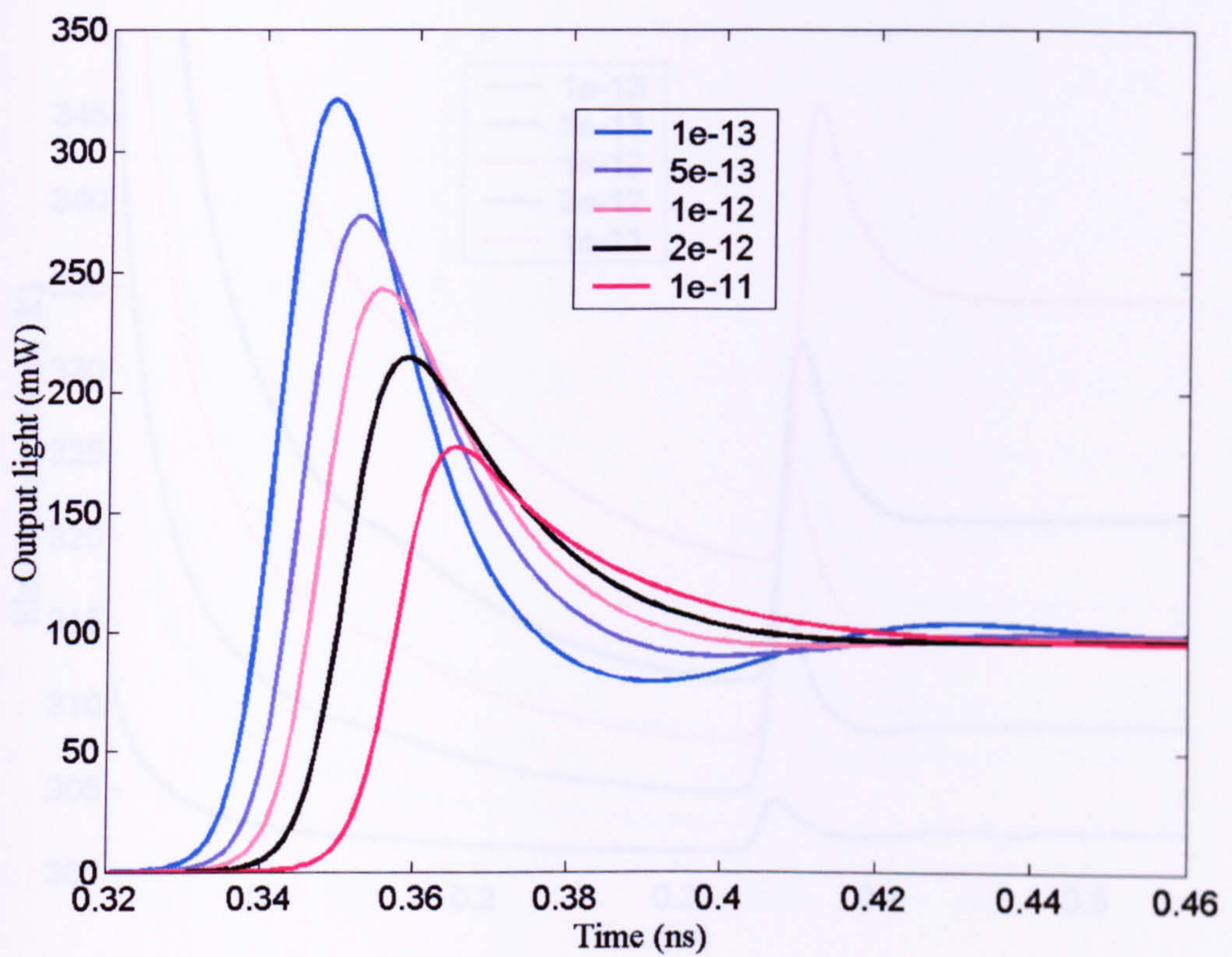


Fig. 4.18. Transient response of the output light for different electron-lattice energy relaxation times  $\tau_{e-L}$  (in the unit of second).

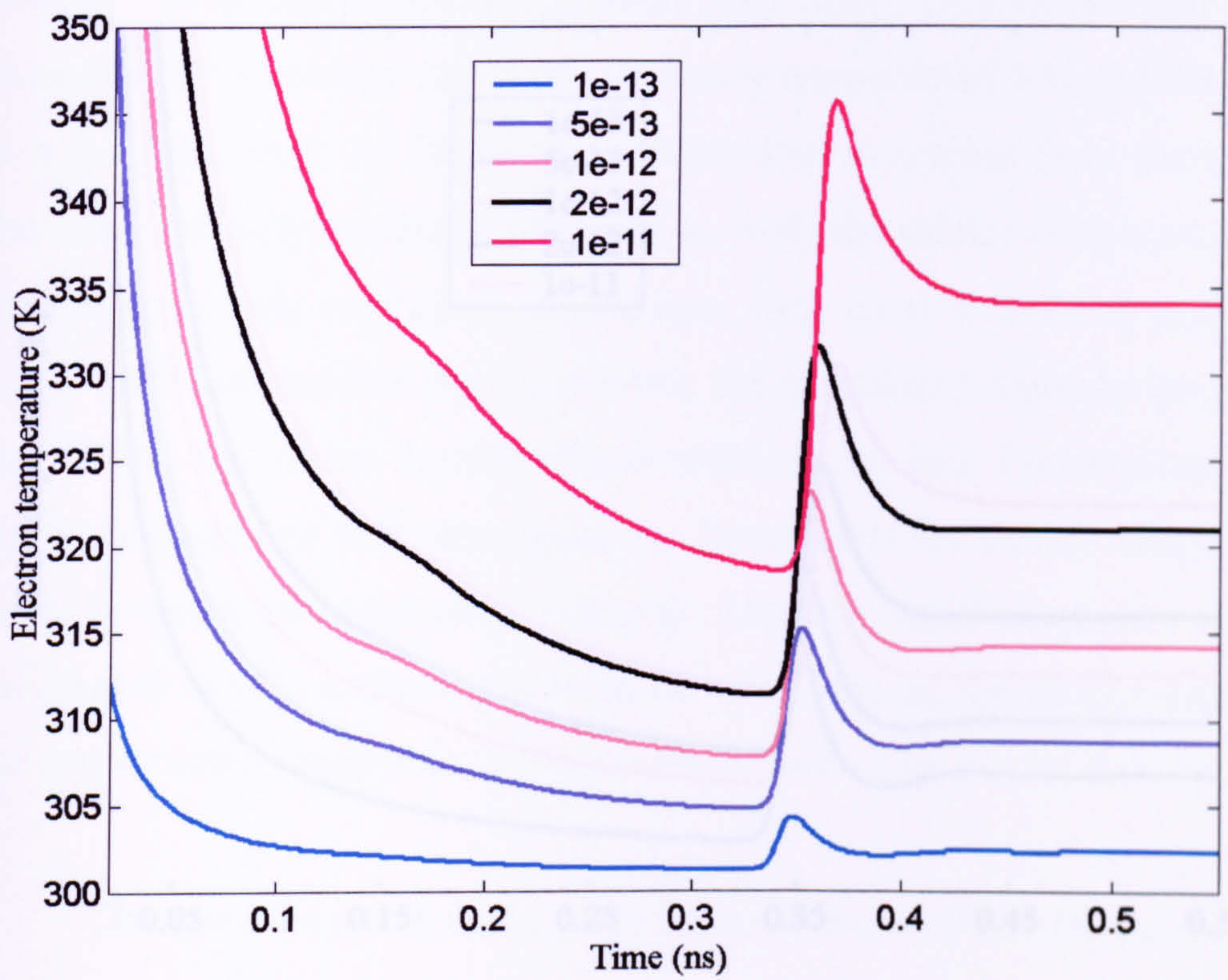


Fig. 4.19. Transient response of the electron temperature for different electron-lattice energy relaxation times  $\tau_{e-L}$  (in the unit of second).

respectively. Unambiguously, the results in Fig. 4.18 show that increasing  $\tau_{e-L}$  will increase the damping rate  $\gamma$  in the transient response case. That is, the carrier heating will result in a damping in the dynamic properties of a semiconductor laser. The damping caused by the carrier heating coincidentally has similar features to the damping due to the spectral-hole burning. As a result, the effects of the carrier heating are conventionally included into the nonlinear gain coefficient  $\epsilon_{NL}$  as the effect of spectral-hole burning.

The electron and hole temperatures will rapidly increase as the injection current switches on at  $t = 0$  sec. Initially, only a small number of carriers exist in the active region, and the sudden supply of the injection heating will be distributed among them. As a result, each carrier will gain a

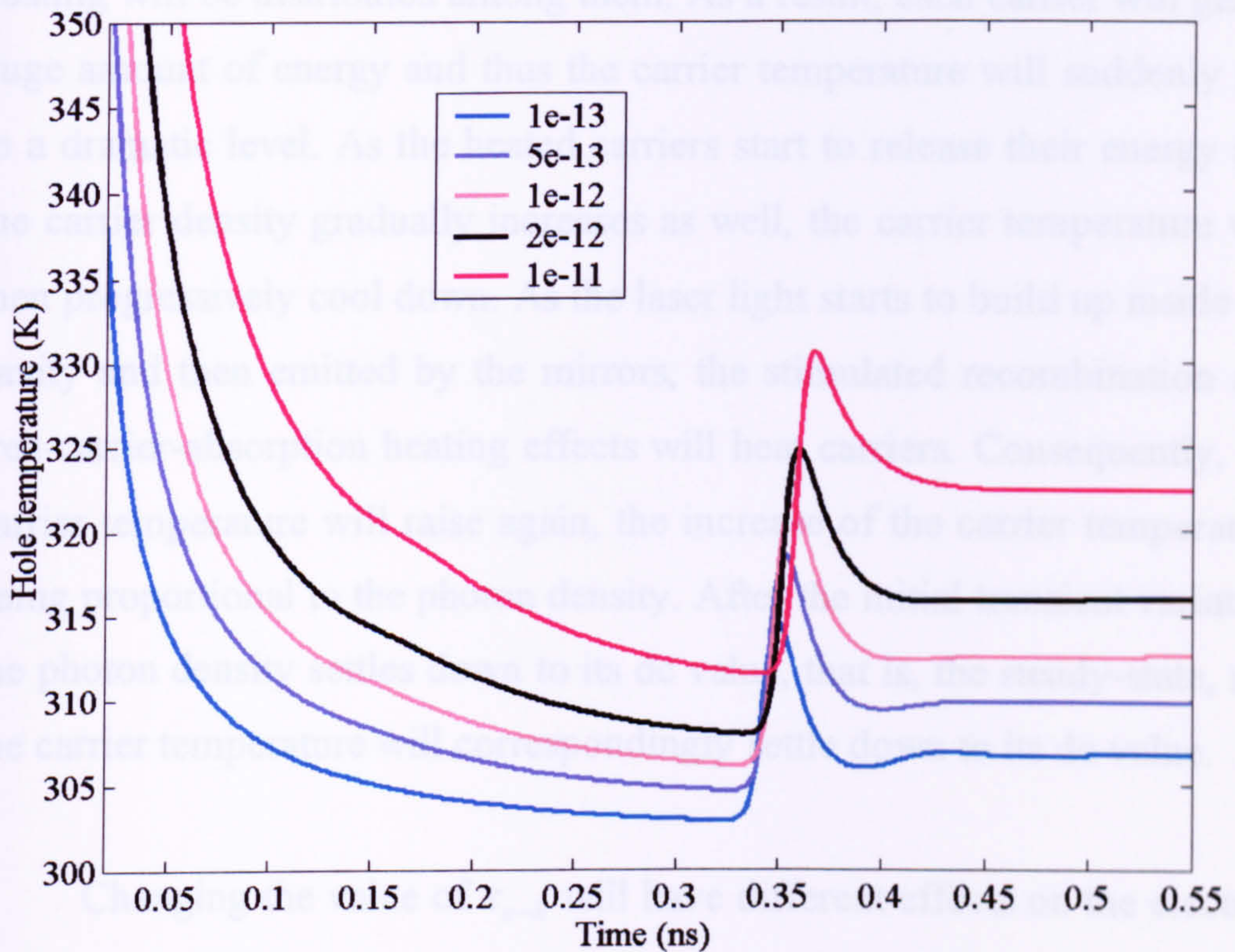


Fig. 4.20. Transient response of the hole temperature for different electron-lattice energy relaxation times  $\tau_{e-L}$  (in the unit of second).

respectively. Unambiguously, the results in Fig. 4.18 show that increasing  $\tau_{e-L}$  will increase the damping rate  $\gamma$  in the transient response case. That is, the carrier heating will result in a damping in the dynamic properties of a semiconductor laser. The damping caused by the carrier heating coincidentally has similar features to the damping due to the spectral-hole burning. As a result, the effects of the carrier heating are conventionally included into the nonlinear gain coefficient  $\varepsilon_{shb}$  as the effect of spectral-hole burning.

The electron and hole temperatures will rapidly increase as the injection current switches on at  $t = 0$  sec. Initially, only a small number of carriers exist in the active region, and the sudden supply of the injection heating will be distributed among them. As a result, each carrier will gain a huge amount of energy and thus the carrier temperature will suddenly rise to a dramatic level. As the heated carriers start to release their energy and the carrier density gradually increases as well, the carrier temperature will then progressively cool down. As the laser light starts to build up inside the cavity and then emitted by the mirrors, the stimulated recombination and free-carrier-absorption heating effects will heat carriers. Consequently, the carrier temperature will raise again, the increase of the carrier temperature being proportional to the photon density. After the initial transient variation the photon density settles down to its dc value, that is, the steady-state, and the carrier temperature will correspondingly settle down to its dc value.

Changing the value of  $\tau_{e-h}$  will have different effects on the electron temperature and hole temperature. It can be expected that increasing  $\tau_{e-h}$  will decrease the amount of the electron energy releasing to holes. As a



result, increasing the value of the electron-hole energy relaxation time  $\tau_{e-h}$  will result an increase in the electron temperature and a decrease in the hole temperature. This is clearly demonstrated by the SPICE simulations shown in Figs. 4.21 and 4.22.

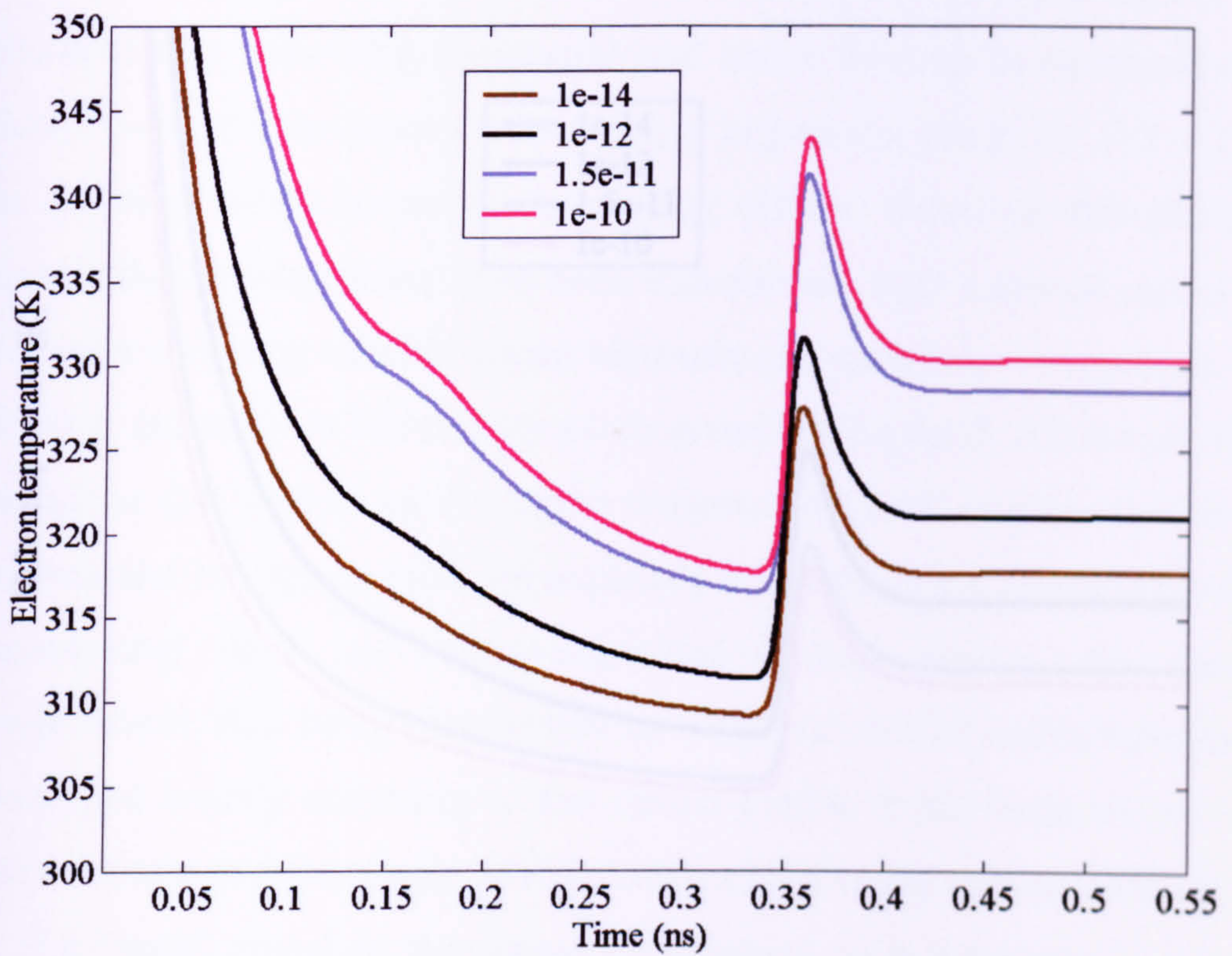


Fig. 4.21. Transient response of the electron temperature for different electron-hole energy relaxation times  $\tau_{e-h}$  (in the unit of second).

### 5.1 Summary of Previous Work and this Thesis

In this thesis, a new proposed SPICE circuit model for semiconductor lasers incorporating the effects of the carrier and lattice heating, which has been developed, implemented and realized. The model is achieved from the rate equations that govern the dynamics of carrier density, photon density, electron temperature, hole temperature and lattice temperature in the active region of semiconductor lasers. The set of the rate equations used provide a solid, sound and physically-based theoretical

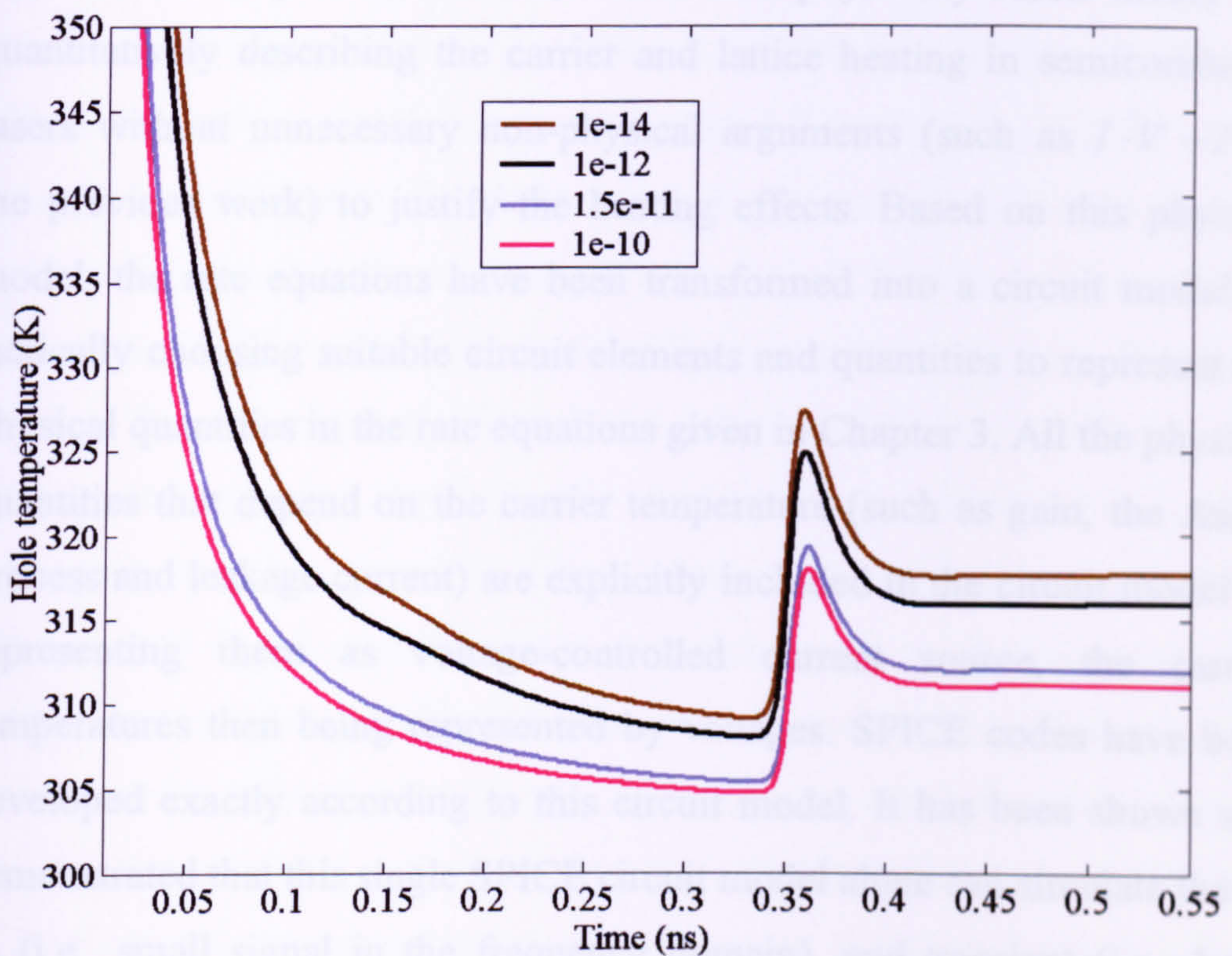


Fig. 4.22. Transient response of the hole temperature for different electron-hole energy relaxation times  $\tau_{e-h}$  (in the unit of second).

## CHAPTER 5

### CONCLUSION AND SUGGESTIONS FOR FUTURE WORK

#### 5.1 Summary of Previous Work and this Thesis

In this thesis, a new proposed SPICE circuit model for semiconductor lasers incorporating the effects of the carrier and lattice heating, which has been developed, implemented and realised. The circuit is achieved from the rate equations that govern the dynamics of carrier density, photon density, electron temperature, hole temperature and lattice temperature in the active region of semiconductor lasers. The set of the rate equations used provide a solid, sound and physically-based theory for quantitatively describing the carrier and lattice heating in semiconductor lasers without unnecessary non-physical arguments (such as  $I \cdot V - P$  in the previous work) to justify the heating effects. Based on this physical model, the rate equations have been transformed into a circuit model by tactically choosing suitable circuit elements and quantities to represent the physical quantities in the rate equations given in Chapter 3. All the physical quantities that depend on the carrier temperature (such as gain, the Auger process and leakage current) are explicitly included in the circuit model by representing them as voltage-controlled current source, the carrier temperatures then being represented by voltages. SPICE codes have been developed exactly according to this circuit model. It has been shown and demonstrated that this single SPICE circuit model alone can simulate the dc, ac (i.e., small signal in the frequency domain), and transient (i.e., large signal in the time domain) responses of the carrier density, photon density, electron temperature, hole temperature and lattice temperature (Chapter 4).

The new proposed SPICE circuit thus fully meets the initial objectives set, i.e. it is universal, physically-based, flexible and expandable.

Of course, it can be argued that, due to the complexity of the physical processes in any semiconductor laser, it is almost impossible to develop a SPICE circuit model to account for all the physical properties inside the device. Therefore, developing any circuit model will consider some effects while inevitably neglecting others. Consequently, all the circuit models proposed for semiconductor lasers so far have emphasised certain effects and neglected others. This illustrates that there is unlikely to be any “super” model for semiconductor lasers that is capable of including every physical process and explaining every physical property of the devices. Nevertheless, from the results of this work, it is clearly shown that the L-I nonlinearity cannot be explained without considering the heating effects. Therefore, the circuit models proposed by Tucker [16][17] cannot be used to realistically discuss the dc L-I relationship. Although this L-I nonlinearity can fully be explained by the circuit models proposed by the Xu group [20][21] and Mena et al. [27] by incorporating only the lattice heating, the non-physically-based and intuitive definition of the lattice-heating source using the  $I \cdot V - P$  argument makes their circuit model quantitatively questionable. To obtain correspondence between experimental and theoretical results they simply adjust other parameters to fit the experimental data. Nevertheless, it is emphasised that fitting a set of data is not the only criterion by which to judge the merit of a circuit model. For any circuit model with more than ten adjustable parameters, it is easy to fit a set of data by tweaking these parameters. In general, circuit models with more adjustable parameters can fit more sets of data with good accuracy. However, it should be noted that if the effect of the carrier

heating is totally neglected (that is, the carrier temperature equals to the lattice temperature in any case), any effect caused by the carrier heating or influenced by the carrier temperature cannot be explained by current models.

In addition, their models cannot simulate the transient carrier temperature variation with time, which is a feature of the new SPICE circuit model presented. Subsequently, the transient photon damping caused by this transient carrier heating and consequently other models cannot explain the transient response of semiconductor lasers. Indeed, the simulation result from the Xu group has shown that the effect of the lattice heating alone almost has no influence on the transient response; Mena et al. did not discuss the usability of their model for the transient response. The circuit models proposed by Lu et al., Tsou et al. and Madhan et al. have emphasised the effect of carrier transport for quantum-well lasers but the heating effects have totally been neglected. Apparently, their interest was in the high-speed behaviour of quantum-well lasers while the L-I nonlinearity was not the main concern.

Although different models have their own merits and shortcomings, it is confident that the new SPICE circuit model presented in this work is the most advanced one for dealing with the heating issues of semiconductor lasers. In addition, the aim for circuit models which deal with all the physical effects and cover a wide operating range of the device under study, with well understood parameters, is itself a major contribution for theoretical, design and application studies.

## 5.2 The Achievements of the Thesis

Transforming the rate equations of the carrier heating into a correspondent circuit model, the mathematical derivations and the assembly of the relevant SPICE-codes is a complex task. Indeed, the complexity of the new proposed SPICE circuit model should not be underestimated. For example, the Ebers-Moll circuit model (as shown schematically in Fig. 5.1.), the very famous circuit model for p-n-p or n-p-n junction transistors, has only 4 circuit components. A more advanced circuit model for junction transistors, the Gummel-Poon circuit model (as shown schematically in Fig. 5.2.), has only 14 circuit components. The new circuit model derived has 38 circuit components in total, where 18 circuit components are dedicated to the electron and hole heating effects. It should be noted that all of the circuit components are achieved from the physically-based rate equations, similar to the approach taken to produce the Ebers-Moll and Gummel-Poon circuit models.

As previously mentioned, it is almost impossible to realise a “super” model that can incorporate all the physical processes and explain all the physical properties of semiconductor lasers. Nevertheless, to a modest extent, the new proposed SPICE circuit model has shown the following:

- 1) The carrier heating can be incorporated into a SPICE circuit model for semiconductor lasers. As far as is known, this is the first circuit model explicitly including the carrier heating so far.
- 2) The carrier heating can simultaneously be modelled with the lattice heating. This clearly solves the ambiguous problem associated with the lattice-heating source  $I \cdot V - P$  in previous work.

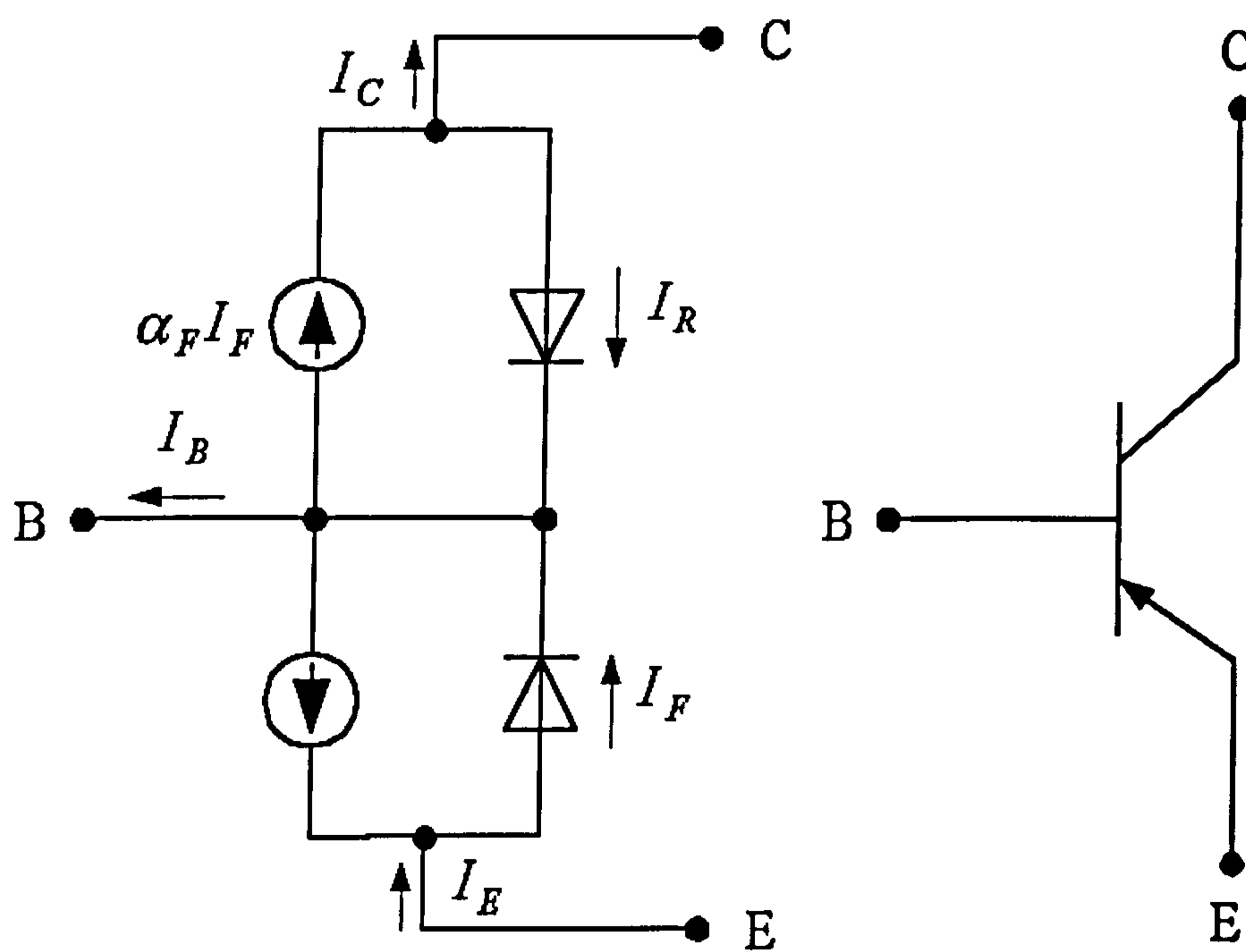


Fig. 5.1. Schematic diagram of the Ebers-Moll circuit model.



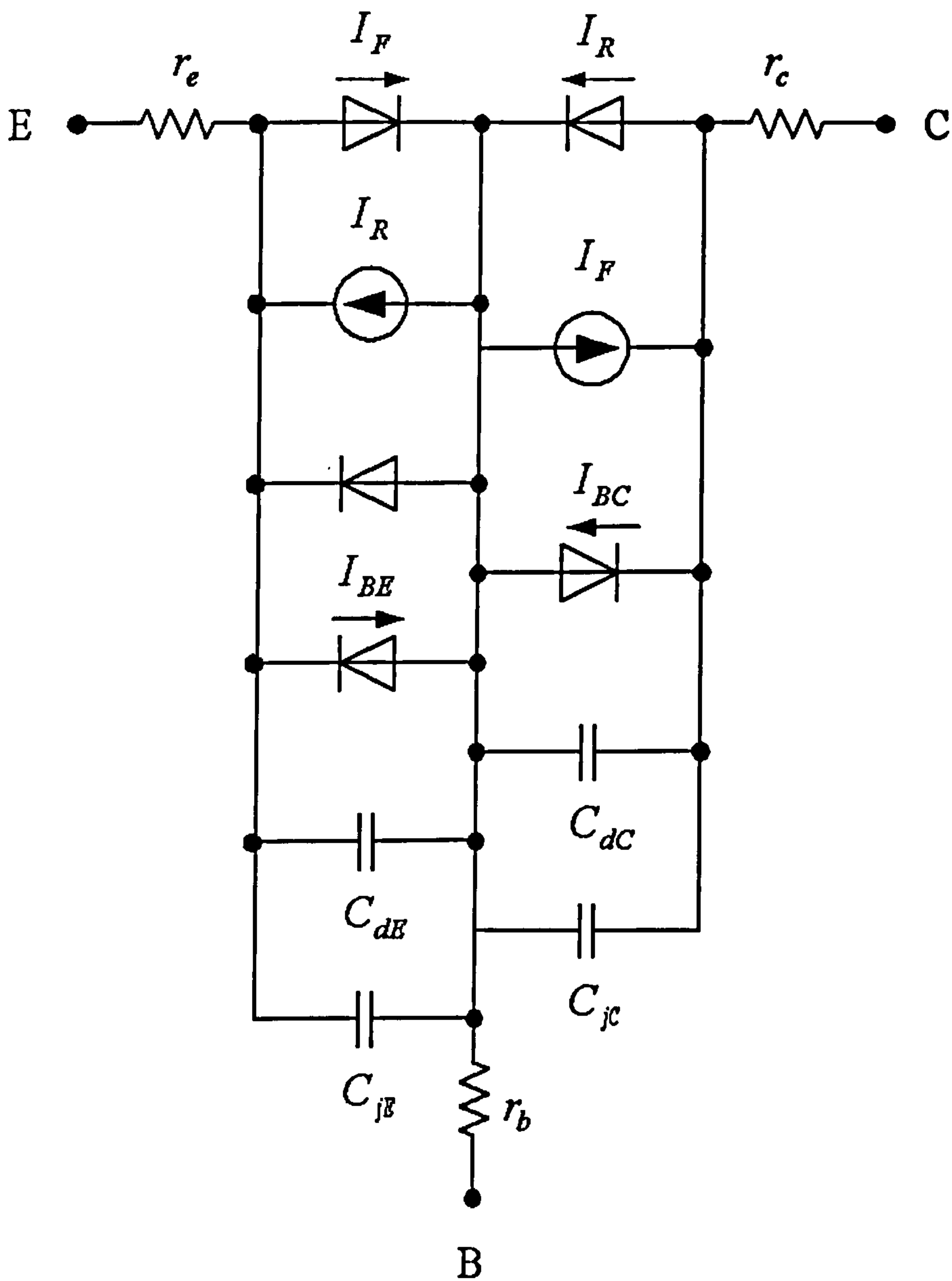


Fig. 5.2. Schematic diagram of the Gummel-Poon circuit model.

- 3) A single circuit model alone can simulate the dc, ac and transient responses of the carrier density, photon density, electron temperature, hole temperature and lattice temperature. Compared with other electronic devices where separate circuit models are usually developed for predicting the dc, ac or transient response, this ability certainly provides an additional advantage for the new proposed SPICE circuit model especially for using in an Electronic Design Automation (EDA) environment.
- 4) The new proposed SPICE circuit model can simulate the time variation of the carrier temperature, as shown in Figs. 4.19, 4.20, 4.21 and 4.22. As far as is known, the simulation of the carrier temperature varying with time (that is, in the time domain) has never been performed for semiconductor lasers. Although the ac response (that is, small-signal response in the frequency domain) of the carrier temperature has recently been investigated [32].

### **5.3 Suggestions for Future Work**

In this work, a new SPICE circuit model with the carrier and lattice effects has been presented for semiconductor lasers. The numerical simulation of the dc, ac and transient responses of this circuit model is implemented by the *MicroSim* PSPICE simulation package that can freely be downloaded from the Internet. This suggests the circuit model can be employed for other uses, if the source codes of this work are provided, to verify their experimental results and extracted the useful physical parameters, such as the differential gain and thermal conduction time. Such

parameters are extremely crucial for the characteristics of semiconductor lasers and almost impossible to directly measure by experiments.

Without doubt, the role of Electronic Design Automation (EDA) in the modern electronic industries cannot be over emphasised. SPICE circuit simulation is almost indispensable in designing analogue electronic circuits. The needs of the SPICE circuit models for semiconductor lasers used in conjunction with other electronic circuits and systems (for example, the transmitter modules of fibre optic communication systems) are thus foreseeable. One of the major merits of using SPICE circuit models for devices is its flexibility in modifying the developed SPICE codes to accommodate more physical properties associated with devices. In other words, any physical properties that can be transformed into the models of resistances, capacitances, inductance, voltage and current sources can be incorporated into the original circuits without too many elaborate efforts. This suggests that further work can be under taken in order to improve the new SPICE circuit models presented in this work, for example:

- 1) In this work, the new SPICE circuit model only simulated the physical processes in the active region. In other words, the physical processes outside the active region were either neglected (for example, the heating mechanism outside the active region) or averaged (such as the injection efficiency). It should be noted that, in vertical-cavity surface-emitting lasers (VCSELs), the heating processes in the distributed Bragg reflection (DBR) mirrors could be as significant as in the active region. Under such a circumstance, additional circuits are needed to correctly model the overall heating behaviour within the devices. To incorporate these physical processes into the circuit model is certainly

feasible; but attentions should be paid to the numerical complexity or numerical stability for SPICE codes with too many circuit elements.

- 2) In this work, only the intrinsic physical properties were considered for semiconductor lasers. In other words, their extrinsic properties, such as parasitic resistances and capacitances associated with the devices themselves or the external wire bonding, were not considered. In practice, the parasitic properties might be an important factor affecting the properties of semiconductor lasers, especially in their high-speed performance. Including parasitic resistances and capacitances into the SPICE circuit model will be reasonably straightforward. However, their values usually cannot directly be assessed by either experimental measurements or theoretical calculations. But, if the parasitic resistances and capacitances are included into the circuit model presented in this work, their values can be estimated by measured ac data. This feature demonstrates another merit of using an extensive SPICE circuit model in characterising the properties of semiconductor lasers.
- 3) Only bulk semiconductor lasers are used as the numerical examples in this work, while quantum-well (QW) lasers are not particularly discussed. However, the physical models presented in this work are general and can be applied to QW lasers if the correspondent parameters are given. The carrier and lattice heating processes in QW lasers should be rather similar to those in bulk lasers. It has been shown that the carrier energy relaxation time for QW lasers calculated by first principles do not present any considerable difference from those for bulk lasers. The

differential gain of QW lasers is substantially higher than that of bulk lasers. In addition, it should be noted that, other physical processes, such as the carrier transport, capture and escape, are not presented in bulk lasers but unique to QW lasers. In some cases, for example, if the separate confinement heterostructure (SCH) is very large, their effects may become crucial. Under such a circumstance, additional rate equations are needed to characterise their effects. Accordingly, extra circuits should be incorporated to describe the carrier transport, capture and escape processes.

- 4) The SPICE circuit model provides an indisputable advantage for designing semiconductor lasers used in conjunction with other electronic circuits or systems, especially in designing the transmitter modules for fibre optic communication systems. The transmitter modules, receiver modules and the optical fibres are the three major components in a fibre optic communication system. It is thus perceivable that, if SPICE circuit models can be further implemented for the receiver modules and optical fibres, they can be used to simulate a whole fibre optic communication system. This surely defines one of the ultimate goals for using SPICE circuit models in simulating the optoelectronic devices and systems.

In conclusion, the SPICE circuit models presented in this work demonstrate the capability and versatility of SPICE in simulating the complicated carrier and lattice heating processes in semiconductor lasers and represent a state of the art modelling tool using leading edge understanding of physical processes. Further enhancement to this work can

provide a step towards simulating the optoelectronic devices and systems for fibre optic communication systems.

## REFERENCES

- [1] G. F. Carey, W. B. Richardson, C. S. Reed, B. J. Mulvaney, *Circuit, Device, and Process Simulation: Mathematical and Numerical Aspects*, New York: John Wiley & Sons, 1996.
- [2] B. Al-Hashimi, *The Art of Simulation Using PSpice: Analog and Digital*, Florida: CRC Press, 1995.
- [3] M. H. Rashid, *SPICE for Circuits and Electronics Using PSpice*, New Jersey: Prentice Hall, 1995.
- [4] P. W. Tuinenga, *SPICE: A Guide to Circuit Simulation & Analysis Using PSpice*, 3rd ed., New Jersey: Prentice-Hall, 1995.
- [5] J. Keown, *MicroSim PSpice and Circuit Analysis*, 3rd ed., New Jersey: Prentice Hall, 1998.
- [6] E. Brumgnach, *PSpice for Windows*, New York: Delmar Publishers, 1995.
- [7] R. W. Dutton and Z. Yu, *Technology CAD: Computer Simulation of IC Processes and Devices*, Boston: Kluwer Academic Publishers, 1993.
- [8] G. P. Agrawal and N. K. Dutta, *Semiconductor Lasers*, 2nd ed., New York: Van Nostrand Reinhold, 1993.
- [9] L. A. Coldren and S. W. Corzine, *Diode Lasers and Photonic Integrated Circuits*, New York: John Wiley & Sons, 1995.
- [10] S. L. Chuang, *Physics of Optoelectronic Devices*, New York: John Wiley & Sons, 1995.
- [11] K. Petermann, *Laser Diode Modulation and Noise*, The Netherlands: Kluwer Academic Publishers.

- [12] C. Y. Tsai, C. H. Chen, T. L. Sung, C. Y. Tsai, and J. M. Rorison, "Theoretical modeling of carrier and lattice heating effects for frequency chirping in semiconductor lasers," *Appl. Phys. Lett.*, vol. 74, pp. 917-919, 1999.
- [13] C. Y. Tsai, C. Y. Tsai, Y. H. Lo, and R. M. Spencer, "Effects of spectral hole burning, carrier heating, and carrier transport on the small-signal modulation response of quantum well lasers," *Appl. Phys. Lett.*, vol. 67, pp. 3084-3086, 1995.
- [14] C. Y. Tsai, F. P. Shih, C. H. Cheng, T. Y. Wu, T. L. Sung, and C. Y. Tsai, "Effects of electron-hole energy transfer on the nonlinear gain coefficients in the small-signal modulation response of semiconductor lasers," *Appl. Phys. Lett.*, vol. 71, pp. 1747-1749, 1997.
- [15] C. Y. Tsai, F. P. Shih, C. H. Chen, T. L. Sung, T. Y. Wu, and C. Y. Tsai, "Thermal modeling in semiconductor lasers by incorporating the effects of carrier heating, nonequilibrium optical phonons, and thermal conduction of acoustic phonons," *Optoelectronic Materials and Devices, Proc. SPIE*, vol. 3419, pp. 399-421, 1998.
- [16] R. S. Tucker, "Circuit model of double-heterojunction laser below threshold," *IEE Proc. -Optoelectron.*, vol. 128, pp. 101-106, 1981.
- [17] R. S. Tucker, "Large-signal circuit model for simulation of injection-laser modulation dynamics," *IEE Proc. -Optoelectron.*, vol. 128, pp. 180-184, 1981.
- [18] M. F. Lu, C. Juang, M. J. Jou, B. J. Lee, "Study of carrier transport effects on quantum well lasers using a SPICE simulator," *IEE Proc. -Optoelectron.*, vol. 142, pp. 237-240, 1995.



- [19] M. F. Lu, J. S. Deng, C. Juang, M. J. Jou, and B. J. Lee, "Equivalent circuit model of quantum-well lasers," *IEEE J. Quantum Electron.*, vol. 31, pp. 1418-1422, 1995.
- [20] N. Bewra, D. A. Suda, G. L. Tan, F. Chatenoud, and J. M. Xu, "Modeling of quantum-well lasers with electro-opto-thermal interaction," *IEEE J. Quantum Electron.*, vol. 1, pp. 331-340, 1995.
- [21] D. S. Ellis and J. M. Xu, "Electro-opto-thermal modeling of threshold current dependence on temperature," *IEEE J. Quantum Electron.*, vol. 3, pp. 640-648, 1997.
- [22] Benjamin P. C. Tsou and David L. Pulfrey, "A versatile SPICE model for quantum-well lasers," *IEEE J. Quantum Electron.*, vol. 33, pp. 246-254, 1997.
- [23] Benjamin P. C. Tsou and David L. Pulfrey, "The influence of coulomb enhancement on modulation properties of quantum-well lasers," *IEEE J. Quantum Electron.*, vol. 34, pp. 318-324, 1998.
- [24] Giammarco Rossi, Roberto Paoletti and Marina Meliga, "SPICE stimulation for analysis and design of fast 1.55  $\mu\text{m}$  MQW laser diodes," *IEEE J. Lightwave Technol.*, vol. 16, pp. 1509-1516, 1998.
- [25] M. Ganesh Madhan, P. R. Vaya, and N. Gunasekaran, "Circuit Modeling of multimode bistable laser diodes," *IEEE Photon. Technol. Lett.*, vol. 11, pp. 27-29, 1999.
- [26] K. Czotscher, S. Weisser, A. Leven and J. Rosenzweig, "Intensity modulation and chirp of 1.55- $\mu\text{m}$  multiple-quantum-well laser diodes: modeling and experimental verification," *IEEE J. Quantum Electron.*, vol. 5, pp. 606-612, 1999.
- [27] P. V. Mena, J. J. Morikuni, S. M. Kang, A. V. Harton, and K. W. Wyatt, "A simple rate-equation-based thermal VCSEL model," *IEEE J. Lightwave Technol.*, vol. 17, pp. 865-872, 1999.

- [28] C. Y. Tsai, C. H. Chen, T. L. Sung, C. Y. Tsai, and J. M. Rorison, "Theoretical modeling of the frequency response of the carrier and lattice temperatures with nonequilibrium optical phonons in semiconductor lasers," *Electron. Lett.* vol. 34, pp. 2337-2339, 1998.
- [29] C. Y. Tsai, C. H. Chen, T. L. Sung, C. Y. Tsai, and J. M. Rorison, "Theoretical modeling of the frequency response of the carrier and lattice temperatures with nonequilibrium optical phonons in semiconductor lasers," *Electron. Lett.* vol. 34, pp. 2337-2339, 1998.
- [30] C. Y. Tsai, F. P. Shih, T. L. Sung, C. H. Chen, T. Y. Wu, and C. Y. Tsai, "Effects of carrier heating, nonequilibrium LO phonons, and lattice heating on the small-signal modulation response of semiconductor lasers," *IEE Proc.-Optoelectronics*, vol. 145, pp. 13-20, 1998.
- [31] C. Y. Tsai, F. P. Shih, C. H. Chen, T. L. Sung, T. Y. Wu, and C. Y. Tsai, "Thermal modeling in semiconductor lasers by incorporating the effects of carrier heating, nonequilibrium optical phonons, and thermal conduction of acoustic phonons," *Optoelectronic Materials and Devices, Proc. SPIE*, vol. 3419, pp. 399-421, 1998.
- [32] C. Y. Tsai, C. H. Chen, T. L. Sung, C. Y. Tsai, and J. M. Rorison, "Theoretical modeling of the small-signal modulation response of carrier and lattice temperatures with the dynamics of nonequilibrium optical phonons in semiconductor lasers," *IEEE J. Select. Topics Quantum Electron.*, vol. 5, pp. 596-605, 1999.
- [33] Britt Brooks, "Standardising Compact Models for IC Simulation," *IEEE Circuit and Devices*, vol. 15, pp. 10-13, 1999.
- [34] H. C. Casey, Jr., and M. B. Panish, *Heterostructure Lasers*, Parts A and B, Academic, Orlando, FL, 1978.

- [35] S. M. Sze, *Physics of Semiconductor Theory and Device. Physics*, Prentice Hall, Englewood Cliffs, NJ, 1989.
- [36] P. S. Zory, Jr., Ed., *Quantum Well Lasers*, Academic, San Diego, 1993.
- [37] C. Y. Tsai, C. Y. Tsai, R. M. Spencer, Y. H. Lo, and L. F. Eastman, "Nonlinear gain coefficients in semiconductor lasers: Effects of carrier heating," *IEEE J. Quantum Electron.*, vol. 32, pp. 201-212, 1996.
- [38] H. S. Carslaw and J. C. Jaeger, *Conduction of Heat in Solids*, 2nd ed., Oxford, U.K.: Clarendon Press, 1959.

## APPENDIX A: GETTING STARTED WITH PSPICE

A very brief outline for downloading, installing and running the PSPICE program are given in this appendix. The evaluation (educational) version of the *MicroSim* PSPICE software can be downloaded from the website <http://ftp.microsim.com/>.

### A.1 Downloading the PSPICE:

1. Type '<http://ftp.microsim.com/>' on the web browser.
2. Click the '*Eval\_Versions.*' Then click the '*80dlabe.exe*' to download the *MicroSim* PSPICE Evaluation Version 8.0 to a *temporary* directory in the PC.
3. Either way, click '*eval\_pieces*' to download PSPICE from *80dlepl.exe* to *80dlepl3.exe* into 13 floppy disks. Save all these 13 *80dlepl\*.exe* files into the *temporary* directory of the PC.

### A.2 Installing the PSPICE:

1. Double click the *80dlabe.exe* (or all the *80dlepl\*.exe* files) file in the *temporary* directory. It will generate several executable files in the *temporary* directory.
2. Double click the *setup.exe* file in the *temporary* directory. It will automatically install the PSPICE program in the PC.
3. During the installation, it will ask whether to install '*Design Center*' or '*PSPICE A\_D.*' Please choose '*PSPICE A\_D.*'

4. After the installation, it will create a '*MicroSim Eval 8*' folder in the start program. Then it is ready to run PSPICE simulation program on the PC.

### **A.3 Running a PSPICE program:**

1. Go to '*MicroSim Eval 8*' folder in the start program. In the '*Design Manager*,' click '*Run TextEdit*' the bottom icon of the left toolbar to activate the *MicroSim* Text Editor to write the PSPICE program.
2. Type any of PSPICE programs and use 'Save' to save a file with a extension name '*.cir*,' for example, *jenkins.cir*, in the '*project*' folder.
3. Click '*Run PSPICE A/D*' in the second icon of the left toolbar in the Design Manager to activate the *MicroSim PSPICE A/D*. Then open the saved *jenkins.cir* file. It will start to compile and run the *jenkins.cir* program.
4. If it runs successfully, click the '*File*' in the PSPICE window and activate '*Run Probe*' command to run the probe. The graphic '*MicroSim Probe*' screen will appear. Click the '*Trace*' '*Add*', then it gives a list of all the currents in each circuit element and all the voltages in each node, and the voltage drop in each element.
5. Click the currents or voltages to plot on the '*Probe*' screen. More that one current or voltage can be selected for the same plot.

## APPENDIX B: SUMMARY OF THE PSPICE SYNTAXES

Although the SPICE is a simple but powerful simulation language for electronic circuits, it is still rather complicated to memorise all the details of its formats and syntaxes. In this appendix, the syntaxes of the PSPICE will be listed for possible future work. Although this list is not complete, it does provide all the major syntaxes that are relevant to this work and its possible further expansion.

### □ Components

#### ❖ Passive components

##### Δ Linear

###### ◆ Resistor

*R*<name> <+ node> <- node> <value>

###### ◆ Capacitor

*C*<name> <+ node> <- node> <value>

###### ◆ Inductor

*L*<name> <+ node> <- node> <value>

##### Δ Nonlinear

###### ◆ Resistor

*R*<name> <+ node> <- node> <model name> <value>

*.MODEL* <model name> *RES* [model parameters]

where [model parameters] is (R = ? TC1 = ? TC2 = ? TCE = ?)

###### ◆ Capacitor

*C*<name> <+ node> <- node> <model name> <value>

*.MODEL* <model name> *CAP* [model parameters]

where [model parameters] is (C = ? TC1 = ? TC2 = ? VC1 = ? VC2 = ?)

### ◆ Inductor

*L*<name> <+ node> <- node> <model name> <value>

.MODEL <model name> IND [model parameters]

where [model parameters] is (C = ? TC1 = ? TC2 = ? IL1 = ? IL2 = ?)

## Δ Semiconductor components

### ◆ Diode

*D*<name> <A node> <K node> <model name>

.MODEL <model name> D [model parameters]

### ◆ Bipolar transistor

*Q*<name> <C node> <B node> <E node> <model name>

.MODEL <model name> <type> [model parameters]

where <type> is either NPN or PNP

## □ Sources

### ❖ Independent sources

#### Δ Independent current source

*I*<name> N+ N- [DC<value>]

+ I[(transient value)]

+ [PULSE][SW][EXP][PWL][SFFM][Source arguments]]

#### Δ Independent voltage source

*V*<name> N+ N- [DC<value>]

+ V[(transient value)]

+ [PULSE][SW][EXP][PWL][SFFM][Source arguments]]

#### Δ DC

*V*<name> <+ node> <- node> DC <value>

.DC <source name> <start value> <end value> <step value>

#### Δ AC

*V*<name> <+ node> <- node> AC <magnitude> <phase>

.AC <sweep type> <N points> <start frequency> <stop frequency>

where <sweep type> is LIN, OCT, or DEC.

#### Δ Transient

.TRAN <time step> <stop time> [<time start> <maximum time step>] [UIC]

## Δ Exponential

*V<name>* <+ node> <-node> *EXP* (*V1 V2 TD1 TAU1 TD2 TAU2*)

## Δ Pulse

*V<name>* <+ node> <-node> *PULSE* (*V1 V2 TD TR TF TW PER*)

## Δ Sinusoidal

*V<name>* <+ node> <-node> *SIN* (*VO VA FREQ TD DF PHASE*)

## Δ Single-frequency frequency-modulated

*V<name>* <+ node> <-node> *SFFM* (*VO VA FC MDI FS*)

## Δ Piece-wise linear

*V<name>* <+ node> <-node> *PWL* (*(T1, V1) (T2, V2) ....(TN, VN)*)

## ❖ Dependent sources

Spice name	Description
E	Voltage-controlled voltage source (VCVS)
G	Voltage-controlled current source (VCCS)
F	Current-controlled current source (CCCS)
H	Current-controlled voltage source (CCVS)

## □ Sources

### ❖ Linear sources

#### Δ VCVS

*E<name>* <+ node> <-node> <+ controlling node> <-controlling node> <gain value>

#### Δ VCCS

*G<name>* <+ node> <-node> <+ controlling node> <-controlling node> <transconductance value>

#### Δ CCCS

*F<name>* <+ node> <-node> <Vxxx> <gain value>

#### Δ CCVS

*H<name>* <+ node> <- node> <Vxxx> <transresistance value>



## ❖ Nonlinear (polynomial)

### Δ One-dimensional

$E\langle name \rangle \langle + node \rangle \langle - node \rangle POLY(1) (\langle + controlling node \rangle \langle - controlling node \rangle) (\langle polynomial coefficient values \rangle)$

### Δ Two-dimensional

$E\langle name \rangle \langle + node \rangle \langle - node \rangle POLY(2) (\langle + controlling node 1 \rangle \langle - controlling node 1 \rangle) (\langle + controlling node 2 \rangle \langle - controlling node 2 \rangle) (\langle polynomial coefficient values \rangle)$

## □ Analogue behavioural modelling

### ❖ VALUE

#### Δ Voltage-controlled voltage source (VCVS)

$E\langle name \rangle \langle + node \rangle \langle - node \rangle VALUE = \{ \langle expression \rangle \}$

#### Δ Voltage-controlled current source (VCCS)

$G\langle name \rangle \langle + node \rangle \langle - node \rangle VALUE = \{ \langle expression \rangle \}$

where  $\langle expression \rangle$  is the output voltage value for E and current value for G

### ❖ TABLE

$E\langle name \rangle \langle + node \rangle \langle - node \rangle TABLE \{ \langle expression \rangle \} = \langle (i1, o1) (i2, o2) \dots (in, on) \rangle$

$G\langle name \rangle \langle + node \rangle \langle - node \rangle TABLE \{ \langle expression \rangle \} = \langle (i1, o1) (i2, o2) \dots (in, on) \rangle$

where  $\langle expression \rangle$  is the input controlled values

### ❖ FREQ

$E\langle name \rangle \langle + node \rangle \langle - node \rangle FREQ \{ \langle expression \rangle \} = \langle (f1, db1, p1) (f2, db2, p2) \dots (fn, dbn, pn) \rangle$

$G\langle name \rangle \langle + node \rangle \langle - node \rangle FREQ \{ \langle expression \rangle \} = \langle (f1, db1, P1) (f2, db2, 2) \dots (fn, dbn, pn) \rangle$

### ❖ LAPLACE

$E\langle name \rangle \langle + node \rangle \langle - node \rangle LAPLACE \{ \langle expression \rangle \} = \{ \langle transform \rangle \}$

$G\langle name \rangle \langle + node \rangle \langle - node \rangle LAPLACE \{ \langle expression \rangle \} = \{ \langle transform \rangle \}$

### ❖ CHEBYSHEV

$E\langle name \rangle \langle + node \rangle \langle - node \rangle CHEBYSHEV \{ \langle expression \rangle \} = \langle type \rangle \langle cutoff frequency \rangle \langle attenuations \rangle$

$G\langle name \rangle \langle + node \rangle \langle - node \rangle CHEBYSHEV \{ \langle expression \rangle \} = \langle type \rangle \langle cutoff frequency \rangle \langle attenuations \rangle$

where  $\langle type \rangle$  is LP (low pass), HP (high pass), BP (band pass), or BR (band reject)

## □ Advanced commands

### ❖ Function

*.FUNC* <name> (arguments) {<expression of arguments>}

### ❖ Parameters

*.PARAM* <name> = <value> or {<expression>}

### ❖ Subcircuit

*.SUBCKT* <name> <nodes> [PARAMS: <name> = <value>, ...]

*.ENDS* [<subcircuit name>]

*X*<name> [nodes] <subcircuit name> [PARAMS: <name> = <value>, ...]

## □ Output options of simulation results

### ❖ Text mode

#### Δ Tabulated outputs

*.PRINT* <type> <output variables>

#### Δ Plotted outputs

*.PLOT* <type> <output variables>

#### Δ Direct outputs

*.OP*

*.TF*

*.FOUR*

*.SENS*

### ❖ Graphic mode

*.PROBE* [output variables]

## APPENDIX C: SPICE CODES OF THIS THESIS

### C.1 SPICE Circuit Model without Carrier and Lattice Heating

\*COPYRIGHT BY MR. JENKINS CHIH-HSIUNG CHEN AND DR. CHIN-YI TSAI

```

.FUNC          LIM(X)          LIMIT(X,0,800E-3)

.PARAM        Q0              = 1.6022E-19
.PARAM        ELIGHT          = {1.45*Q0}
.PARAM        LX              = 1E-7
.PARAM        LY              = 2E-6
.PARAM        LZ              = 3E-4
.PARAM        TAUN            = 1E-8
.PARAM        VG              = 6.67E7
.PARAM        TAUCONF        = 0.35
.PARAM        ALPHAINIT      = 1E3
.PARAM        RMIRR          = 0.32
.PARAM        BETA            = 5E-5
.PARAM        TAUSPON        = 1E-8
.PARAM        DG              = 4E-20
.PARAM        NTR             = 2.5E24
.PARAM        ESHB           = 1E-23
.PARAM        NI0            = 2.045E12
.PARAM        VOL             = {LX*LY*LZ}
.PARAM        ALPHAMIRR      = {1/LZ*LOG(1/RMIRR)}
.PARAM        TAUM           = {1/(VG*ALPHAMIRR)}
.PARAM        TAUS           = {1/(VG*(ALPHAINIT+ALPHAMIRR))}
.PARAM        R_S            = {ELIGHT/Q0*TAUS/TAUM}
.PARAM        C_S            = {Q0/ELIGHT*TAUM}
.PARAM        DGP            = {DG*TAUCONF*VG*TAUN*TAUM/ELIGHT/VOL}
.PARAM        ESHBP         = {ESHB*TAUCONF*TAUM/ELIGHT/VOL}
.PARAM        ITR            = {Q0*VOL*NTR/TAUN}
.PARAM        ISN            = {Q0*VOL*NI0/TAUN}

VIN           1      3      DC      0V
DN            3      0      DNEQ
.MODEL       DNEQ    D      (IS={ISN} N=2 RS=10)
GN           1      0      VALUE = {I(VN)}
EN           4      0      VALUE = {I(VIN)}
VN           4      5      DC      0V
CN           5      0      {TAUN}
GSTIM        1      2      VALUE = {DGP*(I(VIN)-ITR)*LIM(V(2))/(1+ESHBP*LIM(V(2)))}
GSPON        0      2      VALUE = {BETA*I(VIN)*TAUN/TAUSPON}

```

```

RS      2      0      {R_S}
CS      2      0      {C_S}

IINJ    0      1      DC      1MA
.DC     IINJ    0.1MA  100MA  0.1MA

*IINJ   0      1      PULSE (0MA 100MA 0 0 0 2NS 4NS)
*.TRAN  0.1FS  0.6NS  0.2NS  0.1PS

*IINJDC 0      1      DC      50MA
*IINJAC 0      1      AC      1MA
*.AC    DEC    1000  1K     30G

.PROBE
.END

```

## C.2 SPICE Circuit Model with Lattice Heating but without Carrier Heating

\*THIS CIRCUIT IS THE SAME AS C.3 BUT THE CIRCUIT IN THE  
\*LATTICE HEATING REPRESENTED BY A RESISTOR.

\*COPYRIGHT BY MR. JENKINS CHIH-HSIUNG CHEN AND DR. CHIN-YI TSAI

\*FUNDAMENTAL CONSTANTS

```
.PARAM      M0          = 9.1095E-31
.PARAM      Q0          = 1.60219E-19
.PARAM      KB          = 1.38066E-23
.PARAM      HDASH       = 1.05458E-34
.PARAM      PI          = 3.14159265358979
```

\*MATERIAL PARAMETERS

```
.PARAM      ME          {0.067*M0}
.PARAM      MH          {0.45*M0}
.PARAM      EG          {1.4225*Q0}
.PARAM      NI0         = 2.045E12

*.FUNC      EG(TL,NE,NH)  {(1.519-5.405E-4*TL^2/(TL+204)-1.6e-10*PWR(NE,1/3)-1.6E-
+
10*PWR(NH,1/3))*Q0}
*.FUNC      NI0(TL)      QRT(2*PWR((ME*KB*TL/PI/HDASH/HDASH),1.5)*2*PWR((MH*KB
+
/PI/HDASH/HDASH),1.5))*EXP(-EG(TL,0,0)/2/KB/TL));
```

\*STRUCTURE PARAMETERS

```
.PARAM      LX          = 1E-7
.PARAM      LY          = 2E-6
.PARAM      LZ          = 3E-4
.PARAM      WN          = 10E-6
.PARAM      WP          = 2E-6
.PARAM      XC          = 0.3
.PARAM      DE          {0.6*1.247*XC*Q0}
.PARAM      DH          {0.4*1.247*XC*Q0}
```

\*PHOTON PARAMETERS

```
.PARAM      ELIGHT      = {1.45*Q0}
.PARAM      VG          = 6.67E7
.PARAM      TAUCONF     = 0.35
.PARAM      ALPHANT     = 1E3
```

.PARAM RMIRR = 0.32  
 .PARAM BETA = 5E-5

\*LATTICE PARAMETERS

.PARAM DENSITY = 5.36E3  
 .PARAM KL = 50  
 .PARAM CL0 = 0.35E3  
 .PARAM THS = 300

\*PARAMETERS OF PHYSICAL PROCESSES

.PARAM ASRH = 1E7  
 .PARAM BSPON = 1E-16  
 .PARAM CAUG = 4.22E-42  
 .PARAM TAUN = 1E-8  
 .PARAM TAUEL = 2E-12  
 .PARAM TAUHL = 1E-12  
 .PARAM TAUEH = 1E-12  
 .PARAM TAUKE = 4E-7  
 .PARAM DIFFE = 200E-4; {(KB\*300/Q0)\*0.85}  
 .PARAM DIFFH = 10E-4; (KB\*300/Q0)\*0.04

\*GAIN PARAMETERS

.PARAM DG = 4E-20  
 .PARAM NTR = 2.5E24  
 .PARAM ESHB = 1E-23  
 .PARAM DGDTE = 2.167E2  
 .PARAM DGDTH = 2.482E2  
 .PARAM DGDTL = 3.484E2

\*OTHER DEPENDENT PARAMETERS

.PARAM VOL = {LX\*LY\*LZ}  
 .PARAM ALPHAMIRR = {1/LZ\*LOG(1/RMIRR)}  
 .PARAM TAUM = {1/(VG\*ALPHAMIRR)}  
 .PARAM TAUS = {1/(VG\*(ALPHAINT+ALPHAMIRR))}  
 .PARAM R\_S = {ELIGHT/Q0\*TAUS/TAUM}  
 .PARAM C\_S = {Q0/ELIGHT\*TAUM}  
 .PARAM ISN = {Q0\*VOL\*NI0/TAUN}

\*COEFFICIENTS FOR THE APPROXIMATION OF THE FERMI ENERGY

.PARAM CF1 = 3.53553E-1  
 .PARAM CF2 = -4.95009E-3  
 .PARAM CF3 = 1.48386E-4  
 .PARAM CF4 = -4.42563E-6

\*DEFINED FUNCTIONS

.FUNC LIM(X) {LIMIT(X,0,10)}

\*FUNCTIONS FOR THE APPROXIMATIONS OF THE FERMI-DIRAC INTEGRALS

.FUNC C12(X) {3\*SQRT(PI/2)/PWR(X+2.13+PWR(PWR(ABS(X-2.13),12/5)+9.6,5/12),1.5)}  
 .FUNC C32(X) {15\*SQRT(PI/2)/PWR(X+2.64+PWR(PWR(ABS(X-2.64),9/4)+14.9,4/9),2.5)}  
 .FUNC FD12(X) {1/(EXP(-X)+C12(X))}  
 .FUNC FD32(X) {1/(EXP(-X)+C32(X))}

\*FUNCTIONS FOR THE CARRIER DENSITY AND ITS FERMI ENERGY

\*.FUNC NC(TE) {2\*PWR(ME\*KB\*TE/2/PI/HDASH/HDASH,1.5)}  
 \*.FUNC NV(TH) {2\*PWR(MH\*KB\*TH/2/PI/HDASH/HDASH,1.5)}  
 .FUNC NC(TE) {2\*(ME\*TE\*1.7999E14)\*\*1.5}  
 .FUNC NV(TH) {2\*(MH\*TH\*1.7999E14)\*\*1.5}  
 .FUNC NE(MUE,TE) {NC(TE)\*FD12(MUE/KB/TE)}  
 .FUNC NH(MUH,TH) {NV(TH)\*FD12(MUH/KB/TH)}  
 .FUNC MUE(NE,TE) {KB\*TE\*(LOG(NE/NC)+CF1\*(NE/NC)+CF2\*PWR(NE/NC,2)  
 +CF3\*PWR(NE/NC,3)+CF4\*PWR(NE/NC,3))}  
 +  
 .FUNC MUH(NH,TH) {KB\*TH\*(LOG(NH/NV)+CF1\*(NH/NV)+CF2\*PWR(NH/NV,2)  
 +CF3\*PWR(NH/NV,3)+CF4\*PWR(NH/NV,3))}  
 +

\*FUNCTIONS FOR THE CARRIER ENERGY DENSITY

.FUNC UE(NE,TE) {1.5\*NE\*KB\*TE\*FD32(MUE(NE,TE)/KB/TE)  
 + /FD12(MUE(NE,TE)/KB/TE)}  
 .FUNC UH(NH,TH) {1.5\*NH\*KB\*TH\*FD32(MUH(NH,TH)/KB/TH)  
 + /FD12(MUH(NH,TH)/KB/TH)}  
 .FUNC PUEPNE(NE,TE) (UE(NE+NE/1E6,TE)-UE(NE-NE/1E6,TE))/(2\*NE/1E6)}  
 .FUNC PUHPNH(NH,TH) (UH(NH+NH/1E6,TH)-UH(NH-NH/1E6,TH))/(2\*NH/1E6)}  
 .FUNC PUEPTE(NE,TE) {(UE(NE,TE+TE/1E6)-UE(NE,TE-TE/1E6))/(2\*TE/1E6)}  
 .FUNC PUHPTH(NH,TH) (UH(NH,TH+TH/1E6)-UH(NH,TH-TH/1E6))/(2\*TH/1E6)}

\*FUNCTION FOR CONVERSION

.FUNC NOFI(IN) {IN\*TAUN/Q0/VOL}  
 .FUNC SOFP(P) {P\*TAUCONF\*TAUM/VOL/ELIGHT}

\*CIRCUIT FOR CARRIER DENSITY

VIN 1 3 DC 0V  
 DN 3 0 DNEQ  
 .MODEL DNEQ D (IS={ISN} N=2 RS=10)  
 GDN 0 1 VALUE = {I(VIN)}  
 GSRH 1 0 VALUE = {Q0\*VOL\*ASRH\*NOFI(I(VIN))}  
 GSPON1 1 0 VALUE = {Q0\*VOL\*BSPON\*PWR(NOFI(I(VIN)),2)}  
 GAUG 1 0 VALUE = {Q0\*VOL\*CAUG\*PWR(NOFI(I(VIN)),3)}  
 GN 1 0 VALUE = {I(VN)}

\*DERIVATIVE CIRCUIT FOR DN/DT

EN	4	0	VALUE = {I(VIN)}
VN	4	5	DC 0V
CN	5	0	{TAUN}

\*CIRCUIT FOR PHOTON DENSITY

GSTIM	1	2	VALUE = {Q0*VOL*VG*(DG*(NOFI(I(VIN))-NTR)-DGDTL*(V(30)-THS))*SOFP(LIM(V(2)))/(1+ESHB*SOFP(LIM(V(2))))}
GSPON2	0	2	ALUE = {BETA*Q0*VOL*BSPON*PWR(NOFI(I(VIN)),2)}
RS	2	0	{R_S}
CS	2	0	{C_S}

\*CIRCUIT FOR LATTICE HEATING

GVI	0	30	VALUE = {(V(1,0)*I(VINJ)-V(2,0))/VOL/CL0/DENSITY}
RL	30	31	{TAUK}
EL	31	0	VALUE = {THS}
CL	30	0	1F

\*INPUT AND OUTPUT

VINJ	9	1	DC	0V
IINJ	0	9	DC	1MA
.DC	IINJ	0.1MA	200MA	0.1MA
*IINJ	0	1	PULSE (0MA 100MA 0 0 0 2NS 4NS)	
*.TRAN	0.1FS	0.6NS	0.2NS	0.1PS
*INJDC 0	1	DC	50MA	
*INJAC 0	1	AC	1MA	
*.AC	DEC	1000	1K	30G

.PROBE  
.END



### C.3 SPICE Circuit Model with Lattice Heating but without Carrier Heating but with the addition of the Temperature-Sensitive Leakage Current and Auger Process

\*THIS CIRCUIT IS THE SAME AS C.2 IN ADDITION WITH  
 \*LEAKAGE CURRENT AND TEMPERATURE-SENSITIVE AUGER.

\*COPYRIGHT BY MR. JENKINS CHIH-HSIUNG CHEN AND DR. CHIN-YI TSAI

#### \*FUNDAMENTAL CONSTANTS

```
*.PARAM      M0          = 9.1095E-31
.PARAM      Q0          = 1.60219E-19
.PARAM      KB          = 1.38066E-23
*.PARAM      HDASH      = 1.05458E-34
.PARAM      PI          = 3.14159265358979
```

#### \*MATERIAL PARAMETERS

```
.PARAM      ME          = 0.067
.PARAM      MH          = 0.45
.PARAM      EG          = {1.4225*Q0}
.PARAM      NI0         = 2.045E12

*.FUNC      EG(TL,NE,NH)  {(1.519-5.405E-4*TL^2/(TL+204)-1.6E-10*PWR(NE,1/3)-1.6E-
+                          10*PWR(NH,1/3))*Q0}
*.FUNC      NI0(TL)      {SQRT(2*PWR((ME*KB*TL/2/PI/HDASH/HDASH),1.5))*2*PWR((MH*KB
+                          *TL/2/PI/HDASH/HDASH),1.5))*EXP(-EG(TL,0,0)/2/KB/TL)}
```

#### \*STRUCTURE PARAMETERS

```
.PARAM      LX          = 1E-7
.PARAM      LY          = 2E-6
.PARAM      LZ          = 3E-4
.PARAM      WN          = 10E-6
.PARAM      WP          = 2E-6
.PARAM      XC          = 0.3
.PARAM      DE          = {0.6*1.247*XC*Q0}
.PARAM      DH          = {0.4*1.247*XC*Q0}
```

#### \*PHOTON PARAMETERS

```
.PARAM      ELIGHT      = {1.45*Q0}
.PARAM      VG          = 6.67E7
```

.PARAM	TAUCONF	= 0.35
.PARAM	ALPHAINT	= 1E3
.PARAM	RMIRR	= 0.32
.PARAM	BETA	= 5E-5

\*LATTICE PARAMETERS

.PARAM	DENSITY	= 5.36E3
.PARAM	KL	= 50
.PARAM	CL0	= 0.35E3
.PARAM	THS	= 300

\*PARAMETERS OF PHYSICAL PROCESSES

.PARAM	ASRH	= 1E7
.PARAM	BSPON	= 1E-16
.PARAM	CAUG	= 4.22E-42
.PARAM	TAUN	= 1E-8
.PARAM	TAUEL	= 2E-12
.PARAM	TAUHL	= 1E-12
.PARAM	TAUEH	= 1E-12
.PARAM	TAUK	= 1E-7
.PARAM	DIFFE	= 200E-4; {(KB*300/Q0)*0.85}
.PARAM	DIFFH	= 10E-4; (KB*300/Q0)*0.04

\*GAIN PARAMETERS

.PARAM	DG	= 4E-20
.PARAM	NTR	= 2.5E24
.PARAM	ESHB	= 1E-23
.PARAM	DGDTE	= 2.167E2
.PARAM	DGDTH	= 2.482E2
.PARAM	DGDTL	= 3.484E2

\*OTHER DEPENDENT PARAMETERS

.PARAM	VOL	= {LX*LY*LZ}
.PARAM	ALPHAMIRR	= {1/LZ*LOG(1/RMIRR)}
.PARAM	TAUM	= {1/(VG*ALPHAMIRR)}
.PARAM	TAUS	= {1/(VG*(ALPHAINT+ALPHAMIRR))}
.PARAM	R_S	= {ELIGHT/Q0*TAUS/TAUM}
.PARAM	C_S	= {Q0/ELIGHT*TAUM}
.PARAM	ISN	= {Q0*VOL*NI0/TAUN}

\*COEFFICIENTS FOR THE APPROXIMATION OF THE FERMI ENERGY

.PARAM	CF1	= 3.53553E-1
.PARAM	CF2	= -4.95009E-3
.PARAM	CF3	= 1.48386E-4

.PARAM CF4 = -4.42563E-6

\*MAXIMUM ALLOWABLE PHOTON DENSITY AND TEMPERATURE

.PARAM SMAX = 10

\*DEFINED FUNCTIONS

.FUNC LIM(X) {LIMIT(X,0,SMAX)}

\*FUNCTIONS FOR THE APPROXIMATIONS OF THE FERMI-DIRAC INTEGRALS

.FUNC C12(X) {3\*SQRT(PI/2)/(X+2.13+(ABS(X-2.13)\*\*(12/5)+9.6)\*\*(5/12))\*\*(1.5)}

.FUNC C32(X) {15\*SQRT(PI/2)/(X+2.64+(ABS(X-2.64)\*\*(9/4)+14.9)\*\*(4/9))\*\*(2.5)}

.FUNC FD12(X) {1/(EXP(-X)+C12(X))}

.FUNC FD32(X) {1/(EXP(-X)+C32(X))}

\*FUNCTIONS FOR THE CARRIER DENSITY AND ITS FERMI ENERGY

\*.FUNC NC(TE) {2\*PWR(ME\*KB\*TE/2/PI/HDASH/HDASH,1.5)}

\*.FUNC NV(TH) {2\*PWR(MH\*KB\*TH/2/PI/HDASH/HDASH,1.5)}

.FUNC NC(TE) {2\*(ME\*TE\*1.7999E14)\*\*1.5}

.FUNC NV(TH) {2\*(MH\*TH\*1.7999E14)\*\*1.5}

.FUNC NE(MUE,TE) {NC(TE)\*FD12(MUE/KB/TE)}

.FUNC NH(MUH,TH) {NV(TH)\*FD12(MUH/KB/TH)}

.FUNC MUE(NE,TE) {KB\*TE\*(LOG(NE/NC(TE))+CF1\*(NE/NC(TE))+CF2\*(NE/NC(TE))\*\*2+CF3\*(NE/NC(TE))\*\*3+CF4\*(NE/NC(TE))\*\*4)}

.FUNC MUH(NH,TH) {KB\*TH\*(LOG(NH/NV(TH))+CF1\*(NH/NV(TH))+CF2\*(NH/NV(TH))\*\*2+CF3\*(NH/NV(TH))\*\*3+CF4\*(NH/NV(TH))\*\*4)}

\*FUNCTIONS FOR THE CARRIER ENERGY DENSITY

.FUNC UE(NE,TE) {1.5\*NE\*KB\*TE\*FD32(MUE(NE,TE)/KB/TE)/FD12(MUE(NE,TE)/KB/TE)}

.FUNC UH(NH,TH) {1.5\*NH\*KB\*TH\*FD32(MUH(NH,TH)/KB/TH)/FD12(MUH(NH,TH)/KB/TH)}

.FUNC PUEPNE(NE,TE) {(UE(NE+NE/1E6,TE)-UE(NE-NE/1E6,TE))/(2\*NE/1E6)}

.FUNC PUHPNH(NH,TH) {(UH(NH+NH/1E6,TH)-UH(NH-NH/1E6,TH))/(2\*NH/1E6)}

.FUNC PUEPTE(NE,TE) {(UE(NE,TE+TE/1E6)-UE(NE,TE-TE/1E6))/(2\*TE/1E6)}

.FUNC PUHPTH(NH,TH) {(UH(NH,TH+TH/1E6)-UH(NH,TH-TH/1E6))/(2\*TH/1E6)}

\*FUNCTION FOR CONVERSION

.FUNC NOFI(IN) {IN\*TAUN/Q0/VOL}

.FUNC SOFP(P) {P\*TAUCONF\*TAUM/VOL/ELIGHT}

\*NORMALISED AVERAGE ENERGY LOSS PER CARRIER

.FUNC RINJEP(NE,TE) {TAUEL\*DE/PUEPTE(NE,TE)/Q0/VOL}

.FUNC	RINJHP(NH,TH)	{TAUHL*DH/PUHPH(NH,TH)/Q0/VOL}
.FUNC	RSTIMEP(NE,TE)	{TAUEL*(PUEPNE(NE,TE)-(ELIGHT-
+		EG)*MH/(ME+MH)/PUEPTE(NE,TE)/Q0/VOL}
.FUNC	RSTMHP(NH,TH)	{TAUHL*(PUHPNH(NH,TH)-(ELIGHT-
+		EG)*ME/(ME+MH)/PUHPH(NH,TH)/Q0/VOL}
.FUNC	RAUGEP(NE,TE)	{TAUEL*EG/PUEPTE(NE,TE)/Q0/VOL}
.FUNC	RAUGH(NH,TH)	{TAUHL*EG/PUHPH(NH,TH)/Q0/VOL}
.FUNC	RFCAEP(NE,TE)	{TAUEL*ELIGHT/PUEPTE(NE,TE)/Q0/VOL}
.FUNC	RFCAHP(NH,TH)	{TAUHL*ELIGHT/PUHPH(NH,TH)/Q0/VOL}

\*PARAMETERS AND FUNCTIONS FOR LEAKAGE CURRENT

.PARAM	TAUE	= 1E-9
.PARAM	TAUH	= 1E-9
.PARAM	LE	= {(DIFFE*TAUE)**0.5}
.PARAM	LH	= {(DIFFH*TAUH)**0.5}
.FUNC	NE0(NE,TE)	{NC(TE)*EXP(-(DE-MUE(NE,TE))/KB/TE)}
.FUNC	NH0(NH,TH)	{NV(TH)*EXP(-(DH-MUH(NH,TH))/KB/TH)}
.FUNC	ILEAKE(NE,TE)	{Q0*DIFFE*NE0(NE,TE)*LY*LZ/LE/TANH(WN/LE)}
.FUNC	ILEAKH(NH,TH)	{Q0*DIFFH*NH0(NH,TH)*LY*LZ/LH/TANH(WP/LH)}

\*PARAMETER FOR AUGER RECOMBINATION

.PARAM	EA	= {Q0*-0.0404}
--------	----	----------------

\*CIRCUIT FOR CARRIER DENSITY

VIN	1	3	DC	0V
DN	3	0	DNEQ	
.MODEL	DNEQ	D	(IS={ISN} N=2 RS=10)	
GDN	0	1	VALUE = {I(VIN)}	
GLEAK	1	0	VALUE = {ILEAKE(NOFI(I(VIN)),V(10))+ILEAKH(NOFI(I(VIN)),V(20))}	
GSRH	1	0	VALUE = {Q0*VOL*ASRH*NOFI(I(VIN))}	
GSPON1	1	0	VALUE = {Q0*VOL*BSPON*PWR(NOFI(I(VIN)),2)}	
GAUG	1	0	VALUE = {Q0*VOL*CAUG*PWR(NOFI(I(VIN)),3)	
+			{(EXP(-EA*(1/KB/V(30)-1/KB/300)))}	
GN	1	0	VALUE = {I(VN)}	

\*DERIVATIVE CIRCUIT FOR DN/DT

EN	4	0	VALUE = {I(VIN)}	
VN	4	5	DC	0V
CN	5	0	{TAUN}	

\*CIRCUIT FOR PHOTON DENSITY

GSTM	1	2	VALUE = {Q0*VOL*VG*(DG*(NOFI(I(VIN))-NTR)-DGDTL*(V(30)-
+			THS))*SOFP(LIM(V(2)))/(1+ESIB*SOFP(LIM(V(2))))}
GSPON2	0	2	VALUE = {BETA*Q0*VOL*BSPON*PWR(NOFI(I(VIN)),2)}

```
RS      2      0      {R_S}
CS      2      0      {C_S}
```

\*CIRCUIT FOR LATTICE HEATING

```
GVI      0      30      VALUE = {(V(1)*I(VINJ)-V(2))/VOL/CL0/DENSITY*TAUK}
RL      30      31      1
EL      31      0      VALUE = {THS}
CL      30      0      {TAUK}
```

\*INPUT AND OUTPUT

```
VINJ     9      1      DC      0V
IINJ     0      9      DC      1MA
.DC      IINJ    0.01MA 200MA 0.01MA
```

```
*IINJ     0      1      PULSE (0MA 100MA 0 0 0 2NS 4NS)
*.TRAN    0.1FS  0.6NS  0.2NS  0.1PS
```

```
*IINJDC   0      1      DC      50MA
*IINJAC   0      1      AC      1MA
*.AC      DEC    1000   1K      30G
```

```
.PROBE
.END
```

## C.4 SPICE Circuit Model with Carrier and Lattice Heating

\*COPYRIGHT BY MR. JENKINS CHIH-HSIUNG CHEN AND DR. CHIN-YI TSAI

### \*FUNDAMENTAL CONSTANTS

```
*.PARAM      M0          = 9.1095E-31
.PARAM      Q0          = 1.60219E-19
.PARAM      KB          = 1.38066E-23
*.PARAM      HDASH      = 1.05458E-34
.PARAM      PI          = 3.14159265358979
```

### \*MATERIAL PARAMETERS

```
.PARAM      ME          = 0.067
.PARAM      MH          = 0.45
.PARAM      EG          {1.4225*Q0}
.PARAM      NI0         = 2.045E12

*.FUNC      EG(TL,NE,NH)  {(1.519-5.405E-4*TL^2/(TL+204)-1.6e-10*PWR(NE,1/3)-1.6E-
+                          10*PWR(NH,1/3))*Q0}
*.FUNC      NI0(TL)      {SQRT(2*PWR((ME*KB*TL/2/PI/HDASH/HDASH),1.5)*2*PWR((MH*KB
+                          *TL/2/PI/HDASH/HDASH),1.5))*EXP(-EG(TL,0,0)/2/KB/TL)};
```

### \*STRUCTURE PARAMETERS

```
.PARAM      LX          = 1E-7
.PARAM      LY          = 2E-6
.PARAM      LZ          = 3E-4
.PARAM      WN          = 10E-6
.PARAM      WP          = 2E-6
.PARAM      XC          = 0.3
.PARAM      DE          {0.6*1.247*XC*Q0}
.PARAM      DH          {0.4*1.247*XC*Q0}
```

### \*PHOTON PARAMETERS

```
.PARAM      ELIGHT      = {1.45*Q0}
.PARAM      VG          = 6.67E7
.PARAM      TAUCONF     = 0.35
.PARAM      ALPHANT     = 1E3
.PARAM      SIGMAFCAE   = 3E-22
.PARAM      SIGMAFCAH   = 7E-22
.PARAM      RMIRR       = 0.32
.PARAM      BETA        = 5E-5
```



\*FUNCTIONS FOR THE APPROXIMATIONS OF THE FERMI-DIRAC INTEGRALS

```
.FUNC      C12(X)      {3*SQRT(PI/2)/PWR(X+2.13+PWR(PWR(ABS(X-2.13),12/5)+9.6,5/12),1.5)}
.FUNC      C32(X)      {15*SQRT(PI/2)/PWR(X+2.64+PWR(PWR(ABS(X-2.64),9/4)+14.9,4/9),2.5)}
.FUNC      FD12(X)     {1/(EXP(-X)+C12(X))}
.FUNC      FD32(X)     {1/(EXP(-X)+C32(X))}
```

\*FUNCTIONS FOR THE CARRIER DENSITY AND ITS FERMI ENERGY

```
*.FUNC      NC(TE)      {2*(ME*KB*TE/2/PI/HDASH/HDASH)**1.5}
*.FUNC      NV(TH)      {2*(MH*KB*TH/2/PI/HDASH/HDASH)**1.5}
.FUNC      NC(TE)      {2*(ME*TE*1.7999E14)**1.5}
.FUNC      NV(TH)      {2*(MH*TH*1.7999E14)**1.5}
.FUNC      NE(MUE,TE)   {NC(TE)*FD12(MUE/KB/TE)}
.FUNC      NH(MUH,TH)   {NV(TH)*FD12(MUH/KB/TH)}
.FUNC      MUE(NE,TE)   {KB*TE*(LOG(NE/NC(TE))+CF1*(NE/NC(TE))+CF2*(NE/NC(TE))**2
+
+CF3*(NE/NC(TE))**3+CF4*(NE/NC(TE))**4)}
.FUNC      MUH(NH,TH)   {KB*TH*(LOG(NH/NV(TH))+CF1*(NH/NV(TH))+CF2*(NH/NV(TH))**2
+
+CF3*(NH/NV(TH))**3+CF4*(NH/NV(TH))**4)}
```

\*FUNCTIONS FOR THE CARRIER ENERGY DENSITY

```
.FUNC      UE(NE,TE)   {1.5*NE*KB*TE*FD32(MUE(NE,TE)/KB/TE)
+
+FD12(MUE(NE,TE)/KB/TE)}
.FUNC      UH(NH,TH)   {1.5*NH*KB*TH*FD32(MUH(NH,TH)/KB/TH)
+
+FD12(MUH(NH,TH)/KB/TH)}
.FUNC      PUEPNE(NE,TE) {(UE(NE+NE/1E6,TE)-UE(NE-NE/1E6,TE))/(2*NE/1E6)}
.FUNC      PUHPNH(NH,TH) {(UH(NH+NH/1E6,TH)-UH(NH-NH/1E6,TH))/(2*NH/1E6)}
.FUNC      PUEPTE(NE,TE) {(UE(NE,TE+TE/1E6)-UE(NE,TE-TE/1E6))/(2*TE/1E6)}
.FUNC      PUHPTH(NH,TH) {(UH(NH,TH+TH/1E6)-UH(NH,TH-TH/1E6))/(2*TH/1E6)}
```

\*FUNCTION FOR CONVERSION

```
.FUNC      NOFI(IN)    {IN*TAUN/Q0/VOL}
.FUNC      SOFP(P)     {P*TAUCONF*TAUM/VOL/ELIGHT}
```

\*AVERAGE ENERGY LOSS PER CARRIER

```
.FUNC      RDEINJEP(NE,TE) {TAUEL*DE/PUEPTE(NE,TE)/Q0/VOL}
.FUNC      RDEINJHP(NH,TH) {TAUHL*DH/PUHPTH(NH,TH)/Q0/VOL}
.FUNC      RDESTIMEP(NE,TE) {TAUEL*(PUEPNE(NE,TE)-(ELIGHT-
+
+EG)*MH/(ME+MH))/PUEPTE(NE,TE)/Q0/VOL}
.FUNC      RDESTIMHP(NH,TH) {TAUHL*(PUHPNH(NH,TH)-(ELIGHT-
+
+EG)*ME/(ME+MH))/PUHPTH(NH,TH)/Q0/VOL}
.FUNC      RDEAUGEP(NE,TE) {TAUEL*EG/PUEPTE(NE,TE)/Q0/VOL}
.FUNC      RDEAUGHP(NH,TH) {TAUHL*EG/PUHPTH(NH,TH)/Q0/VOL}
.FUNC      RDEFCAEP(NE,TE) {TAUEL*ELIGHT/PUEPTE(NE,TE)/Q0/VOL}
.FUNC      RDEFCAHP(NH,TH) {TAUHL*ELIGHT/PUHPTH(NH,TH)/Q0/VOL}
```



\*PARAMETERS AND FUNCTIONS FOR LEAKAGE CURRENT

```
.PARAM      TAUE      = 1E-9
.PARAM      TAUH      = 1E-9
.PARAM      LE        = {(DFFE*TAUE)**0.5}
.PARAM      LH        = {(DIFFH*TAUH)**0.5}
.FUNC       NE0(NE,TE) {NC(TE)*EXP(-(DE-MUE(NE,TE))/KB/TE)}
.FUNC       NH0(NH,TH) {NV(TH)*EXP(-(DH-MUH(NH,TH))/KB/TH)}
.FUNC       ILEAKE(NE,TE) {Q0*DFFE*NE0(NE,TE)*LY*LZ/LE/TANH(WN/LE)}
.FUNC       ILEAKH(NH,TH) {Q0*DIFFH*NH0(NH,TH)*LY*LZ/LH/TANH(WP/LH)}
```

\*PARAMETER FOR AUGER RECOMBINATION

```
.PARAM      EA        = {Q0*-0.0404}
```

\*CIRCUIT FOR CARRIER DENSITY

```
VIN         1       3       DC      0V
DN          3       0       DNEQ
.MODEL      DNEQ     D      (IS={ISN} N=2 RS=10)
GDN         0       1       VALUE = {I(VIN)}
GLEAK      1       40      VALUE = {ILEAKE(NOFI(I(VIN)),V(10))+ILEAKH(NOFI(I(VIN)),V(20))}
GSRH1      1       9       VALUE = {Q0*VOL*ASRH *NOFI(I(VIN))}
GSPON1     1       8       VALUE = {Q0*VOL*BSPON*NOFI(I(VIN))**2}
GAUG       1       7       VALUE = {Q0*VOL*CAUG *NOFI(I(VIN))**3*(EXP(-EA*(1/KB/V(10)-
+ 1/KB/300))+EXP(-EA*(1/KB/V(20)-1/KB/300)))}
VGLEAK     40      0       DC      0V
VGAUG      7       0       DC      0V
VGSPON1    8       0       DC      0V
VGSRH1     9       0       DC      0V
GN         1       0       VALUE = {I(VN)}
```

\*DERIVATIVE CIRCUIT FOR DN/DT

```
EN         4       0       VALUE = {I(VIN)}
VN         4       5       DC      0V
CN         5       0       {TAUN}
```

\*CIRCUIT FOR PHOTON DENSITY

```
VGSTIM     6       2       DC      0
GSTIM      1       6       VALUE = {Q0*VOL*VG*(DG*(NOFI(I(VIN))-NTR)-DGDTL*(V(30)-THS)-
+ DGDTE*(V(10)-THS)-DGDTH*(V(20)-HS))*SOFP(LIM(V(2)))/
+ (1+ESHB*SOFP(LIM(V(2))))}
GSPON2     0       2       VALUE = {BETA*Q0*VOL*BSPON*PWR(NOFI(I(VIN)),2)}
RS         2       0       {R_S}
CS         2       0       {C_S}
```

\*CIRCUIT FOR ELECTRON HEATING

GINJTE	0	10	VALUE = {RDEINJEP(NOFI(I(VIN)),V(10))*I(VINJ)}
GSTIME	0	10	VALUE = {RDESTIMEP(NOFI(I(VIN)),V(10))*I(VGSTIM)}
GAUGE	0	10	VALUE = {RDEAUGEP(NOFI(I(VIN)),V(10))*I(VGAUG)/2}
GFCAE	0	10	VALUE = {RDEFCAEP(NOFI(I(VIN)),V(10))*Q0*VOL
+			*VG*SIGMAFCAE*NOFI(I(VIN))*SOFP(LIM(V(2)))}
REL	10	11	1
EEL	11	0	VALUE = {V(30)}
REH	10	12	{TAUEH/TAUEL}
EEH	12	0	VALUE = {V(20)}
CE	10	0	{TAUEL}

\*CIRCUIT FOR HOLE HEATING

GINJTH	0	20	VALUE = {RDEINJHP(NOFI(I(VIN)),V(20))*I(VINJ)}
GSTIMH	0	20	VALUE = {RDESTIMHP(NOFI(I(VIN)),V(20))*I(VGSTIM)}
GAUGH	0	20	VALUE = {RDEAUGHHP(NOFI(I(VIN)),V(20))*I(VGAUG)/2}
GFCAH	0	20	VALUE = {RDEFCAHP(NOFI(I(VIN)),V(20))*Q0*VOL
+			*VG*SIGMAFCAH*NOFI(I(VIN))*SOFP(LIM(V(2)))}
RHL	20	21	1
EHL	21	0	VALUE = {V(30)}
RHE	20	22	{TAUEH/TAUHL}
EHE	22	0	VALUE = {V(10)}
CH	20	0	{TAUHL}

\*CIRCUIT FOR LATTICE HEATING

GEL	0	30	VALUE = {(UE(NOFI(I(VIN)),V(10))-UE(NOFI(I(VIN)),V(30)))
+			/TAUEL/CL0/DENSITY*TAUK}
GHL	0	30	VALUE = {(UH(NOFI(I(VIN)),V(20))-UH(NOFI(I(VIN)),V(30)))
+			/TAUHL/CL0/DENSITY*TAUK}
GSRH2	0	30	VALUE = {V(1)*I(VGSRHI)/VOL/CL0/DENSITY*TAUK}
RL	30	31	1
EL	31	0	VALUE = {THS}
CL	30	0	{TAUK}

\*INPUT AND OUTPUT

VINJ	100	1	DC	0V
IINJ	0	100	DC	20MA
.DC	IINJ	0.01MA	20MA	0.01MA
*IINJ	0	100	PULSE (1E-5MA 100MA 0 0 4NS 8NS)	
*.TRAN	1PS	1.5NS	0NS	1PS
*IINJ	0	100	PWL (0 10MA 1FS 500MA 10PS 10MA)	
*.TRAN	1PS	1NS	0NS	1PS
*IINJDC	0	100	DC	20MA
*IINJAC	0	100	AC	0.1MA
*.AC	DEC	100	100M	30G

.PROBE  
.END

## APPENDIX D: PARAMETERS FOR THE SPICE MODELS

Symbol	SPICE parameter	Value	Unit
$m_0$	M0	$9.1095 \times 10^{-31}$	kg
$q_0$	Q0	$1.60219 \times 10^{-19}$	C
$k_B$	KB	$1.38066 \times 10^{-23}$	J/K
$\hbar$	HDASH	$1.05458 \times 10^{-34}$	J·s
$\pi$	PI	3.14159265358979	
$m_e$	ME	0.067	$m_0$
$m_h$	MH	0.45	$m_0$
$E_g$	EG	1.4225	$q_0$
$n_{i0}$	NI0	$2.045 \times 10^{12}$	$m^{-3}$
$L_x$	LX	$1 \times 10^{-7}$	m
$L_y$	LY	$2 \times 10^{-6}$	m
$L_z$	LZ	$3 \times 10^{-4}$	m
$W_n$	WN	$10 \times 10^{-6}$	m
$W_p$	WP	$2 \times 10^{-6}$	m
$X_c$	XC	0.3	
$E_e$	DE	$0.6 \times 1.247 \times XC$	$q_0$
$E_h$	DH	$0.4 \times 1.247 \times XC$	$q_0$
$\hbar\omega$	ELIGHT	1.45	$q_0$
$v_g$	VG	$6.67 \times 10^7$	m/s
$\Gamma$	TAUCONF	0.35	s

Symbol	SPICE parameter	Value	Unit
$\alpha_{int}$	ALPHINT	$1 \times 10^3$	$m^{-1}$
$\sigma_{fca}^e$	SIGAMAFCAE	$3 \times 10^{-22}$	$m^2$
$\sigma_{fca}^h$	SIGAMAFCAH	$7 \times 10^{-22}$	$m^2$
$R_{mirr}$	RMIRR	0.32	
$\beta$	BETA	$5 \times 10^{-5}$	
$\rho_L$	DENSITY	$5.36 \times 10^3$	$kg/m^3$
$\kappa_L$	KL	50	$W \cdot m^{-1} \cdot K^{-1}$
$c_L$	CL0	$0.35 \times 10^3$	$J \cdot kg^{-1} \cdot K^{-1}$
$T_{HS}$	THS	300	K
$A_{SRH}$	ASRH	$1 \times 10^7$	$s^{-1}$
$B_{spon}$	BSPON	$1 \times 10^{-16}$	$m^3/s$
$C_{Aug}$	CAUG	$4.22 \times 10^{-42}$	$m^6/s$
$\tau_n$	TAUN	$1 \times 10^{-8}$	s
$\tau_{spon}$	TAUSPON	$1 \times 10^{-8}$	s
$\tau_{e-L}$	TAUEL	$2 \times 10^{-12}$	s
$\tau_{h-L}$	TAUHL	$1 \times 10^{-12}$	s
$\tau_{e-h}$	TAUEH	$1 \times 10^{-12}$	s
$\tau_k$	TAUK	$1 \times 10^{-7}$	s
$D_e$	DIFFE	$200 \times 10^{-4}$	$m^3$
$D_h$	DIFFH	$10 \times 10^{-4}$	$m^3$
$g_n$	DG	$4 \times 10^{-20}$	$m^3$
$n_{tr}$	NTR	$2.5 \times 10^{24}$	$m^{-3}$

Symbol	SPICE parameter	Value	Unit
$\epsilon_{shb}$	ESHB	$1 \times 10^{-23}$	$m^3$
$g_{T_e}$	DGDTE	$2.167 \times 10^2$	$m^{-3} \cdot K^{-1}$
$g_{T_h}$	DGDTH	$2.482 \times 10^2$	$m^{-3} \cdot K^{-1}$
$g_{T_L}$	DGDTL	$3.484 \times 10^2$	$m^{-3} \cdot K^{-1}$

## LIST OF PUBLICATIONS

1. C. Y. Tsai, F. P. Shih, C. H. Chen, T. Y. Wu, T. L. Sung, and C.Y. Tsai, "Effects of electron-hole energy transfer on the nonlinear gain coefficients in the small-signal modulation response of semiconductor lasers," *Appl. Phys. Lett.*, vol. 71, pp. 1747-1749, 1997.
2. C. Y. Tsai, F. P. Shih, T. L. Sung, T. Y. Wu, C. H. Chen, and C.Y. Tsai, "A small signal analysis on the modulation response of high-speed quantum-well lasers: effects of spectral hole burning, carrier heating, and carrier diffusion-capture-escape," *IEEE J. Quantum Electron.*, vol. 33, pp. 2084-2096, 1997.
3. F. P. Shih, T. L. Sung, C. H. Chen, T. Y. Wu, C. Y. Tsai, and C. Y. Tsai, "Nonlinear gain coefficient in semiconductor lasers," the *3rd IEEE High Frequency Postgraduate Student Colloquium*, Leeds, UK, Sep. 19, pp. 65-66, 1997.
4. T. Y. Wu, F. P. Shih, T. L. Sung, C. H. Chen, C. Y. Tsai, and C. Y. Tsai, "Effects of hot carriers and hot phonons on the second-order harmonic distortion in CATV semiconductor lasers," *3rd IEEE High Frequency Postgraduate Student Colloquium*, Leeds, UK, Sep. 19, pp. 67-68, 1997.
5. F. P. Shih, T. Y. Wu, C. H. Chen, T. L. Sung, C. Y. Tsai, and C. Y. Tsai, "Effects of nonequilibrium LO phonons on the carrier heating in semiconductor quantum-well lasers," *3rd International Workshop on Thermal Investigation of ICs and Microstructure*, Cannes, France, Sep. 21-23, pp. 192-194, 1997.

6. T. L. Sung, C. H. Chen, C. Y. Tsai, and C. Y. Tsai, "Effects of carrier heating on the frequency chirping of semiconductor lasers," *5th IEEE International Workshop on High Performance Electron Devices for Microwave and Optoelectronic Application*, London, UK, Nov. 24-25, pp. 229-231, 1997.
7. C. Y. Tsai, C. H. Chen, and Tien-Li Sung, "Theoretical modeling of energy transfer processes in semiconductor lasers: The phonon bath sharing of nonequilibrium optical phonons," *Semiconductor and Integrated Optoelectronic Conference, SIOE'98*, Cardiff, UK, Apr. 6-8, 1998.
8. C. Y. Tsai, C. H. Chen, T. L. Sung, C. Y. Tsai, and J. M. Rorison, "Theoretical modeling of the frequency response of the carrier and lattice temperatures with nonequilibrium optical phonons in semiconductor lasers," *Electron. Lett.* vol. 34, pp. 2337-2339, 1998.
9. C. Y. Tsai, F. P. Shih, T. L. Sung, C. H. Chen, T. Y. Wu, and C. Y. Tsai, "Effects of carrier heating, nonequilibrium LO phonons, and lattice heating on the small-signal modulation response of semiconductor lasers," *IEE Proc.-Optoelectronics*, vol. 145, pp. 13-20, 1998.
10. C. Y. Tsai, C. Y. Tsai, C. H. Chen, T. L. Sung, T. Y. Wu, and F. P. Shih, "Theoretical model for intravalley and intervalley free carrier absorption in semiconductor lasers: Beyond the classical Drude model," *IEEE J. Quantum Electron.*, vol. 34, pp. 552-558, 1998.
11. C. Y. Tsai, C. Y. Tsai, C. H. Chen, T. L. Sung, F. P. Shih, and T. Y. Wu, "Theoretical model for studying hot phonon effects and electron energy relaxation in GaN: The roles of A1 mode and E1 mode optical phonons," *Optoelectronic Materials and Devices, Proc. SPIE*, vol. 3419, pp. 310-316, 1998.



12. C. Y. Tsai, F. P. Shih, C. H. Chen, T. L. Sung, T. Y. Wu, and C. Y. Tsai, "Thermal modeling in semiconductor lasers by incorporating the effects of carrier heating, nonequilibrium optical phonons, and thermal conduction of acoustic phonons," *Optoelectronic Materials and Devices, Proc. SPIE*, vol. 3419, pp. 399-421, 1998.
13. C. Y. Tsai, T. Y. Wu, C. H. Chen, T. L. Sung, F. P. Shih and C. Y. Tsai, "Hot-carrier effects on second-order harmonic distortion of directly modulated semiconductor lasers: A theoretical investigation," *Optical Fiber Communication, Proc. SPIE*, vol. 3420, pp. 330-336, 1998.
14. C. H. Chen, C. Y. Tsai, T. L. Sung, and C. Y. Tsai, "Simulating carrier and lattice heating with the effects of nonequilibrium optical phonons in the modulation response of high-speed semiconductor lasers", *6th IEEE International Workshop on High performance Electron Devices for Microwave and Optoelectronic Applications, EDMO'98*, Manchester, UK, pp. 194-199, Nov. 23-24, 1998.
15. C. H. Chen, C. Y. Tsai, and T. L. Sung, "Theoretical modelling of electron energy relaxation and nonequilibrium optical phonons in GaN," *Condensed Matter and Materials Physics, CMMP 98, Institute of Physics, Manchester*, UK, p. 96, 21-23 Dec., 1998.
16. C. Y. Tsai, C. H. Chen, T. L. Sung, C. Y. Tsai, and J. M. Rorison, "Theoretical modeling of carrier and lattice heating effects for frequency chirping in semiconductor lasers," *Appl. Phys. Lett.*, vol. 74, pp. 917-919, 1999.
17. C.Y. Tsai, C. H. Chen, T. L. Sung, C. Y. Tsai, and J. M. Rorison, "Theoretical modeling of the small-signal modulation response of carrier and lattice temperatures with the dynamics of nonequilibrium

optical phonons in semiconductor lasers," *IEEE J. Select. Topics Quantum Electron.*, vol. 5, pp. 596-605, 1999.

18. C. Y. Tsai, Chih-Hsiung Chen, Tei-Li Sung, Chin-Yi Tsai, and J. M. Rorison, "Theoretical modeling of nonequilibrium optical phonons and electron energy relaxation in GaN," *J. Appl. Phys. Lett.*, vol. 85, pp. 1475-1480, 1999.